Vodice (Šibenik) • Croatia •September 30 – October 3, 2025

11th International Congress of Croatian Society of Mechanics

Book of Abstracts

Editors • Marko Čanađija • Leo Škec



ECCOMAS
Special Interest Conference

11th ICCSM

11th International Congress of Croatian Society of Mechanics

Organised by

Croatian Society of Mechanics

Under the Auspices of

Central European Association for Computational Mechanics

Book of Abstracts

Editors

Marko Čanađija, University of Rijeka

Leo Škec, University of Rijeka

CSM
CROATIAN SOCIETY OF MECHANICS
ZAGREB - OSIJEK - RIJEKA - SL. BROD - SPLIT

Vodice (Šibenik), Croatia, September 30 – October 3, 2025

Published by

Croatian Society of Mechanics

Head Office

Croatian Society of Mechanics

Ivana Lučića 5, HR-10000 Zagreb, Croatia

http://www.csm.hr/

Printed in

Grafika Helvetica

Issues: 150 copies

ISSN 2584-7716



Copyright © Croatian Society of Mechanics, Zagreb, Croatia, 2025

General Chairs

Marko ČANAĐIJA, University of Rijeka
Leo ŠKEC, University of Rijeka

Organising Committee

Marino BRČIĆ, University of Rijeka
Vedrana CVITANIĆ, University of Split
Darko DAMJANOVIĆ, University of Slavonski Brod
Antonia JAGULJNJAK-LAZAREVIĆ, University of Zagreb
Gordan JELENIĆ, University of Rijeka
Dražan KOZAK, University of Slavonski Brod
Hrvoje KOZMAR, University of Zagreb
Ivica KOŽAR, University of Rijeka
Lovre KRSTULOVIĆ-OPARA, University of Split
Silva LOZANČIĆ, University of Osijek
Ivica SKOZRIT, University of Zagreb
Jurica SORIĆ, University of Zagreb
Zdenko TONKOVIĆ, University of Zagreb

Scientific Committee

Naida ADEMOVIĆ, University of Sarajevo, BA
Giulio ALFANO, Brunel University London, GB
Vincenzo ARMENIO, University of Trieste, IT
Martin ARNOLD, Martin Luther University Halle-Wittenberg, DE
Ferdinando AURICCHIO, University of Pavia, IT
Frédéric BARLAT, Pohang University of Science and Technology, KR
Raffaele BARRETTA, University of Naples Federico II, IT
Peter BETSCH, Karlsruhe Institute of Technology, DE
Bert BLOCKEN, Heriot-Watt University and KU Leuven, GB/BE
Claudio BORRI, University of Florence, IT
Boštjan BRANK, University of Ljubljana, SI
Günter BRENN, TU Graz, AT
Olivier BRÜLS, University of Liège, BE
Luca CARACOGLIA, Northeastern University, US
Mirco D. CHAPETTI, University of Mar Del Plata, AR
José A.F.O. CORREIA, University of Porto, PT
Laura DE LORENZIS, ETH Zürich, CH
Antonio DE SIMONE, Sant'Anna School of Advanced Studies, IT
Nicholas FANTUZZI, University of Bologna, IT
Marc G.D. GEERS, Eindhoven University of Technology, NL
Johannes GERSTMAYR, University of Innsbruck, AT

Friedrich GRUTTMANN,	TU Darmstadt, DE
Nenad GUBELJAK,	University of Maribor, SI
Adnan IBRAHIMBEGOVIĆ,	University of Technology of Compiègne, FR
Ahsan KAREEM,	University of Notre Dame, US
Gabriel KATUL,	Duke University, US
Sven KLINKEL,	RWTH Aachen, Germany, DE
Jože KORELC,	University of Ljubljana, SI
Sigrid LEYENDECKER,	Friedrich-Alexander University, DE
Wing Kam LIU,	Northwestern University and Co-Founder of HIDENN-AI, LLC, US
János LÓGÓ,	Budapest University of Technology and Economics, HU
Stefan LÖHNERT,	TU Dresden, DE
Herbert A. MANG,	Vienna Technical University, AT
Igor MEZIĆ,	University of California, Santa Barbara, US
Jörn MOSLER,	Technical University Dortmund, DE
Bojan NIČENO,	Paul Scherrer Institute, Villigen, CH
Hiroshi OKADA,	Tokyo University of Science, JP
Marta C. OLIVEIRA,	University of Coimbra, PT
Vikram PAKRASHI,	University College Dublin, IE
Anna PANDOLFI,	Polytechnic University of Milan, IT
Milovan PERIĆ,	University of Duisburg-Essen, DE
Nik PETRINIĆ,	University of Oxford, UK
Jindřich PETRUŠKA,	VUT Brno, CZ
Henryk PETRYK,	Polish Academy of Sciences, PL
Bernhard PICHLER,	Vienna University of Technology, AT
Pavel POLACH,	Research and Testing Institute Plzeň, CZ
Franz G. RAMMERSTORFER,	Vienna Technical University, AT
Stefanie REESE,	RWTH Aachen, DE
Zoran REN,	University of Maribor, SI
Jörg SCHRÖDER,	University of Duisburg-Essen, DE
Sebastian SKATULLA,	University of Cape Town, ZA
Laurent STAINIER,	Ecole Centrale de Nantes, FR
Stanislaw STUPKIEWICZ,	Institute of Fundamental Technological Research, PL
Božidar ŠARLER,	University of Ljubljana, SI
Matej VESENJAK,	University of Maribor, SI
Werner WAGNER,	Karlsruhe Institute of Technology, DE
Peter WRIGGERS,	Leibniz University of Hannover, DE

Congress Secretariat

Travel Agency - PerfectMeetings.hr

URKA d.o.o., Cernička 21, 10000 Zagreb, Croatia

Sponsors:

Silver sponsor

KONČAR

KONČAR, Fallerovo šetalište 22, 10000 Zagreb, Croatia

Bronze sponsors

EAST d.o.o.

EAST d.o.o, Ivana Matrljana 39, 51000 Rijeka, Croatia

SUHA GRADNJA
RIGIPS, KNAUF
SERILIA
d.o.o.
mail: info@serilia.de
www.serilia.de
I OSTALI SISTEMI
mob.: +385 99 7330 214 • tel.: +49 160 9196 0875

SERILIA d.o.o., Brestovice 18 b, 51215 Kastav, Croatia

TOPOMATIKA

TOPOMATIKA d. o. o., Industrijska ulica 3, Novaki, 10431 Sveta Nedelja, Croatia

Preface

Dear Reader,

The Croatian Society of Mechanics has been established as an independent society in 1969, with the goals to promote education, research and application in the field of solid and fluid mechanics. Throughout the decades it has organized many scientific meetings, including the series of triennial International Congress of Croatian Society of Mechanics (ICCSM). The first ICCSM took place in Pula in 1994. The ICCSM has always been an international forum for the presentation and discussion of the latest advances in various areas of theoretical, computational and experimental mechanics. These scientific meetings are also an opportunity for valuable interactions between young and senior researchers, leading to new ideas and promising new research directions.

The 11th ICCSM was held in Vodice, Croatia, from September 30 to October 3, 2025. For the first time, an ICCSM congress was awarded the status of an ECCOMAS Special Interest Conference. This Book of Abstracts presents extended abstracts from 4 plenary and 83 contributed lectures, with 111 participants attending the congress. All contributions are printed directly from the camera-ready extended abstracts submitted by the authors; therefore, the editors do not assume liability for possible errors or copyright issues. The talks were delivered in 3 special and 12 regular sessions, with one additional session dedicated to research by the winner of the 2025 Young Scientist Award of the Croatian Society of Mechanics. Plenary lectures addressed issues in wind engineering, fracture, applications of artificial intelligence in CAE and micromagnetic simulations. Special sessions focused on metamaterials, non-conventional materials and structures, and the dynamic behaviour of materials. A variety of recent accomplishments in the field if inelasticity, damage, fracture and failure mechanics, computational, structural and experimental mechanics, wind engineering and fluid mechanics, finite element method and machine learning in mechanics were presented in regular contributions.

This International Congress has been organised under the auspices of Central European Association for Computational Mechanics. The Croatian Society of Mechanics also kindly acknowledges support from our silver sponsor KONČAR,

Zagreb and bronze sponsors EAST d.o.o., Rijeka, SERILIA d.o.o., Kastav and TOPOMATIKA d.o.o., Sveta Nedelja.

At the end, on behalf of the Organization Committee we would like to give special thanks to Ms. Tina Pintar, administrative secretary of the Croatian Society of Mechanics for her continuous support to CSM and organization of congress. Likewise, we are most grateful for our technical organizer Urka d.o.o. on their contribution to the congress organization and to ECCOMAS and all the other colleagues for promoting the congress in the world-wide mechanics community.

Marko Čanađija

Leo Škec

Table of Contents

Plenary Lectures

Bert Blocken
Pure or Practical? How Some of the Most Stringent Requirements in Numerical Fluid Mechanics can be Relaxed in Practical Case Studies in Urban Physics and Wind Engineering 3

Laura De Lorenzis
Variational Phase-Field Modeling of Fracture: Towards Second-Generation Models 5

Wing Kam Liu, Chanwook Park, Jiachen Guo, Gino Domel, Hantao Zhang
AI-Empowered CAE via Software 3.0: Applications in Digital Twins, Additive Manufacturing, and Electronic Design Automation 7

Jörg Schröder and Maximilian Vorwerk
Micromagnetic Simulations of Strongly Heterogeneous Magnetic Materials 9

Special Sessions

SS01 - Emerging Trends in Mechanical Metamaterials

organized by
Giuseppe Failla and Andrea Russillo
University of Reggio Calabria, Italy

Andrea Burlon, Francesco Lo Iacono, Giacomo Navarra, Giuseppe Failla
A Novel Metamaterial Design Based on a Multiple Beam System with Internal Local Resonance.....15

Giuseppe Failla, Andrea Francesco Russillo
Water-Tank Metabarriers as a Novel Concept of Seismic Metamaterials...17

Janko Morosavljević, Dražan Kozak, Ivan Morosavljević, Wei Li
Optimization of the Boat Ceiling Supports Using Diamond Lattice Structure 19

Aleksej Rikić, Branko Nečemer
Low-Cycle Fatigue Analysis of Different TPMS Metamaterials 21

Raffaella Servadei
Fractional Problems: Theory and Applications.....23

SS02 - Mechanics of Non-Conventional Materials and Structures

organized by
Raffaele Barretta, University of Naples Federico II, Italy
Noël Challamel, Université Bretagne Sud, France
Nicholas Fantuzzi, University of Bologna, Italy
Marzia Sara Vaccaro, University of Naples Federico II, Italy

Domenico Ammendolea, Fabrizio Greco, Lorenzo Leonetti, Paolo Lonetti, Arturo Pascuzzo
A Data-Driven Multiscale Approach for the Numerical Prediction of Damage Evolution in Anisotropic Composite Materials.....27

Marko Čanađija, Stefan Ivić
Carbon Nanotube Nanotrusses as Building Blocks of Advanced Metamaterials: An MD-ML-FE Optimization Framework 29

Andrea Caporale, Valentina Cima, Marzia Sara Vaccaro, Raffaele Barretta, Raimondo Luciano
A FEM Iterative Approach to the Nonlocal Integral Elasticity of Nanoplates 31

Rana Nazifi Charandabi, Julia de Castro Motta, Gerardo Carpentieri, Jordi Bonada Bo, Fernando Fraternali, Ada Amendola
Innovative Tensegrity-Based Roof Structures with Integrated Sun-Tracking Mechanisms.....33

Baidehi Das, Raffaele Barretta, Marko Čanađija
Dynamics of Stress-Driven Nonlocal Beams Using PINN Approach.....35

Fabio De Angelis
Variational Formulations in Plasticity and Viscoplasticity With a Consistent Derivation of Computational Algorithms 37

Rosa Penna, Giuseppe Lovisi, Luciano Feo
Integral Solution of Stress-Driven Nonlocal Model with Morozov Regularization on Different Nonlocal Kernels 39

Rosa Penna, Giuseppe Lovisi, Annavirginia Lambiase, Gerarda Landi, Luciano Feo
Micromechanical Model and Experimental Investigation of the Piezoelectric Response in CNTs - Based Cement Composites 43

Luca Placidi, Anil Misra, Francesco Fabbrocino, Raimondo Luciano
Granular Micromechanics Based Formulation of Damage-Elasto-Plasticity: Hysteric Cycles and Fatigue 47

Giovanni Romano, Raffaele Barretta, Marina Diaco
On Clapeyron Theorem in Linear Elasticity 49

Marzia Sara Vaccaro, Raffaele Barretta, Raimondo Luciano, Francesco Marotti de Sciarra
Stress-Driven Nonlocal Elasticity for Higher-Order Nanobeams 51

Cheng Angelo Yan, Riccardo Vescovini, Nicholas Fantuzzi, Raimondo Luciano
A C2-Finite Element Formulation for Strain Gradient Kirchhoff Nanoplates Using Hierarchical Hermite Basis Functions 53

SS03 - State-of-the-Art on the Dynamic Behaviour of Materials and its Applications

organized by
Borja Erice, Mondragon Unibertsitatea & IKERBASQUE, Spain
Louise Le Barbenchon, Arts et Métiers, I2M, France
Nina Čeh, University of Rijeka, Croatia
Maria Lißner University of Oxford, United Kingdom

Nina Čeh, Ivan Sindičić, Anđela Janković, Leo Škec

Modelling the Dynamic Response of Masonry–Binder Assemblies with Compliant Adhesive Interfaces 57

Damjan Jurković, Leo Škec, Giulio Alfano
Study of the Rate-Dependent Mixed-Mode Adhesive Debonding Using an Efficient Numerical Model 59

Louise Le Barbenchon, Borja Erice, James Lee, Nina Čeh, Maria Lißner
Energy Dissipation in Polymer-Based Mechanical Metamaterials Under Dynamic Loading Rates 61

Mokhtar Tantawi, Daniel B. Merczel, Janos Logo
Long-Term Effects on CLT-Concrete Composite Slabs 63

Žiga Žnidarič, Nejc Novak, Srečko Glodež, Branko Nečemer
High-Cycle Fatigue Behaviour of Gyroid TPMS Metamaterial 65

Contributed Lectures

Tomas Adamec, Frantisek Sebek, Jindrich Petruska
On Limitations of the Chaboche Model in Uniaxial Ratcheting Predictions 69

Petra Adamović, Lovro Matoc, Srećko Sabalić, Janoš Kodvanj
Strength and Stability of Conventional and Variable Locking Screws in Healthy and Osteoporotic Mandibular Angle Fractures: A Finite Element Study & Pre-Study 71

D. G. Andrade, V. Cvitanić, L. Simões da Silva, D. M. Rodrigues
Characterisation of Elastic and Plastic Anisotropy in 316L Austenitic Stainless Steel Produced by WAAM 73

Petra Bagavac, Alen Grebo, Ante Medvidović, Željana Nikolić, Lovre Krstulović-Opara
Automatic Recognition of the Structural Integrity of Buildings in Kaštela Bay Using CNN Models Supported by IR Thermography 75

Dario Ban
On Newly Discovered Hydrostatic Rotation Properties of Immersed Isosceles Triangular Cross-section Pontoon 77

Dario Ban, Jani Barle, Stipe Perišić
On Direct Method for Calculation of Joint CDF of Directional Wind Spectrum Using L1 Norm PRBF 79

Damjan Banić, Goran Turkalj, Domagoj Lanc
Advanced Finite Element Model for Stability Analysis of Laminated Beam-Type Structures 81

Frédéric Barlat
Distortional Plasticity and Associated Thermodynamics 83

Matej Borovinšek, Aljaž Ignatijev, Aleš Belšak, Srečko Glodež
Analysing the Wear Behaviour of Polymer Gears.....85

Andrija Buljac, Petar Škvorc, Wenxian Yang, Ahsan Kareem, Hrvoje Kozmar
Dynamic Response of Floating Wind Turbines Subjected to Wind, Current and JONSWAP Waves 87

Luca Caracoglia, Marko Čanađija
Application of Artificial Neural Networks in Structural Mechanics: Energy Harvesting Problems 89

Carlos Cardoso, Ricardo Sousa, Fábio Fernandes, Afonso Silva
Development and Validation of Sex-Specific Finite Element Head Models.91

Mirco Daniel Chapetti, Nenad Gubeljak
A Fracture Mechanics-Based Approach for Material Defects and Fatigue Assessment: Highlighting the Role of the Intrinsic Fatigue Limit 93

Csaba Gáspár
Solving Biharmonic and Bi-Helmholtz Problems by a Localized Method of Fundamental Solutions.....95

Hrvoje Gotovac, Marin Zelenika
Flow and Transport Karst Modelling: Salt and Heat Tracer Tests in 3-D Laboratory Physical Models.....97

Laura Grbac, Gordan Jelenić
Application of Fixed-Pole Interpolation in Vibration Analysis of 3D Micropolar Continuum 99

Sara Grbčić Erdelj, Gordan Jelenić, Adnan Ibrahimbegović

Geometrically Non-Linear Hexahedral Micropolar Finite Element Enhanced with Incompatible Modes.....101

Gabrijela Grozdanić, Mirela Galić,Vladimir Divić
Different Approaches in Numerical Modelling of LG Structures.....103

Friedrich Gruttmann
A FE2 Model for Thin and Thick Shells with Periodic Boundary Conditions 105

Emina Hadžalić, Leo Škec, Adnan Ibrahimbegović
DCB Test Modelling Using a Beam-on-Foundation Framework with Inelastic DCB Arms and Adhesive 107

Krunoslav Haramina, Nenad Kranjčević, Joško Deur, Ivan Ruškan, Matija Hoić
Mechanical Modelling of Active Seat Suspension System Based on Scott-Russell Mechanism.....109

Antonio Horvat, Tomislav Hercigonja, Nenad Drvar
From 3D Scan to Functional Component: Experimental Redevelopment of a Damaged Component.....111

Mikhail Itskov, Rasul Abdusalamov
Constitutive Modeling of Soft Materials by Deep Symbolic Regression ...113

Darko Ivančević, Jakov Ratković
Phenomenological Modelling of Impact-Induced Delamination in Composite Laminates.....115

Marin Ivanković, Marvin Jentzsch, Anna Friederike Rahel Großmann, Vladimir Zimmermann, Marinos Manolesos, Christian Navid Nayeri, Hrvoje Kozmar
Dynamic Stall Control of Wind-Turbine Blades Equipped with Vortex Generators and Gurney Flaps 117

Boris Jalušić; Tomislav Jarak; Marin Vukovojac; Jurica Sorić; Zdenko Tonković
On the Boundary Conditions in Meshless Collocation Methods for Solving Heat Conduction Problems.....119

Matko Jelašić, Christoph Irrenfried, Günter Brenn, Hrvoje Kozmar
Wind-Driven Natural Ventilation of Elongated Building Structures.....121

Gordan Jelenić, Dragan Ribarić

Pure Bending of Rectangular Prism Including Anticlastic Deformation in Cosserats' Continuum – Analytical Approach.....123

Ante Jurčević, Tomislav Lesičar, Zdenko Tonković, Jurica Sorić
A Multiscale Approach to Damage Modelling in Heterogeneous Materials Using Phase-Field Method.....125

Damir Tin Jurković, Marino Brčić
Numerical Structural Analysis of Steel Frames Used in Belt Conveyors....127

Ivan Kraus, Davide Lavorato, Alessandro Colitta, Petra Olić Miloš
Seismic Response of a Traditional Rammed Earth Sub-Assembly: Experimental and Numerical Study 129

Lucas Lemos, Gabriel Serra, Ricardo Sousa, Fábio Fernandes, Guilherme Sousa
Dynamic Compressive Behavior of Cork Agglomerates Combined with Shear Thickening Fluids: Experimental and Computational Approaches.....131

Željan Lozina, Damir Sedlar, Ivan Tomac
Motion of the Body on Rough Surface Under Random Kinematic Excitation 133

Tanja Mališ, Antonia Jaguljnjak Lazarević, Petar Hrženjak
Modelling of an Underground Quarry of Dimension Stone: the Possibility of Expanding the Excavation.....135

Ivo Marinić-Kragić, Teo Čolović, Marta Nekić
Gurney Flap Effects on Savonius Turbine Performance: Aerodynamic and Structural Insights from Integrated CFD and Wind Tunnel Analysis 137

Benjamin Mihaljec, Goran Vukelić
Experimental Analysis of Marine Environment Effects on the Additively Manufactured Stainless Steel AISI 316L.....139

Ivan Morosavljević, Dražan Kozak, Janko Morosavljević, Pejo Konjatić
Comparison of Analytical and Numerical Calculations of the Steel Shell Silo Reinforced with Thin Rings.....141

Mijo Nikolić, Andjelka Stanic, Noemi Friedman, Hermann G. Matthies
Embedded Discontinuity Dynamic Fracture Model and Bayesian Identification of Parameters.....143

Nejc Novak, Oraib Al-Ketan, Anja Mauko, Matej Vesenjak, Zoran Ren
Assessing Additively Manufactured TPMS Structures Under High-Speed Loading 145

Domen Ocepek, Jure Korbar, Gregor Čepon
On the Use of Sparse Regression for Experimental Joint Identification in Frequency-Based Substructuring 147

Domagoj Opačak, Darko Damjanović, Dražan Kozak, Nenad Gubeljak
Numerical Analysis of the Influence of Pipe Support Stiffness in Pipeline Systems 149

Duje Pavić, Matej Šodan, Noemi Friedman, Mijo Nikolić
Bayesian Approach for Identifying Elastic Parameters and Coefficients for Lattice Element Models 151

Pavel Polach, Michal Hajžman, Luboš Smolík
Design of Helical Springs for Vibratory Sorter Mounting 153

Matej Porubsky, Jan Havelka, Pavel Rychnovsky, Jan Novak
Thymos - A Compact, Open-Hardware Testing Frame for Small-Scale Mechanical Experiments 155

Bjorn Sauren, Sven Klinkel
On the Stabilization of a Low-Order Polytopal Mixed Displacement-Pressure Finite Element Formulation 157

Sophie J. Schmid, Alexandre Ouzia, Markus Königsberger, Bernhard Pichler
Characterization of Early-Age Creep Behavior and Strength of Low Carbon Cement Pastes and Multiscale Strength Modelling 159

Damir Sedlar, Željan Lozina, Ivan Tomac
Integration Scheme with Modal Analysis and Modal Superposition for Non-Linear Problems 161

Ana Marija Šegon, Tomislav Lesičar
A Hybrid Computational Framework for Phase-Field Brittle Fracture Modelling 163

Leo Škec, Damjan Jurković, Giulio Alfano
Simulation of Adhesive Debonding in Fracture-Mechanics Tests Using a Novel Hybrid Analytical-Numerical Model 165

Jerko Škifić, Zoran Čarija
Numerical Simulations of Hydraulic Transients in HPP Zakučac 167

Ante Skoblar, Goranka Štimac Rončević, Roberto Žigulić, Marko Čanađija
Numerical Strategies for Finding Roots of Transcendental Characteristic Equations 169

Ivica Smojver, Darko Ivančević, Fran Ušurić
Constitutive Modelling of FDM Printed Continuous Fibre Composites.....171

Matej Šodan, Vladimir Divić, Noémi Friedman, Mijo Nikolić,
Bayesian Parameter Identification of Non-Standard Aluminum Specimens Using Simple Laboratory Measurements 173

Ivan Sokol, Ivan Ćatipović, Neven Hadžić, Hrvoje Kozmar
Environmental Loads on Offshore Engineering Structures 175

Goranka Štimac Rončević, Ante Skoblar, Sanjin Braut, Roberto Žigulić, Goran Turkalj
Regression-Based Machine Learning for Predicting Natural Frequencies of Thin Beams Supported by Translational Springs 179

Damir Tomerlin, Dražan Kozak, Nenad Gubeljak, Darko Damjanović
Tensile Testing of Welded Joints Using Small-Scale Specimens.....181

Zvonimir Tomičević, Andrija Zaplatić, Benjamin Smaniotto, François Hild
DVC Analysis of Failure Modes in Glass Plain-Weave Fabric Composites Under On- and Off-Axis Loading 183

Balázs Tóth
Mixed hp-Finite Element Framework for Modeling Laser Pulse Heating Processes in Irreversible Thermodynamics 185

Marko Vukasović, Dražen Kustura, Frane Vlak, Radoslav Pavazza, Tomislav Matić
Stress and Displacement Analysis of a Thin-walled Curved Beam Subjected to the Eccentric Uniformly Distributed Line Load.....187

Marin Vukovojac, Boris Jalušić, Tomislav Lesičar, Ivica Skozrit, Zdenko Tonković
Finite Element Modeling of Residual Stress Development and Damage Progression in Welded Components.....189

Martin Zlatić, Marko Čanađija
Recovering Isotropic Energies with Mullins-Type Damage Using Physics-Augmented Neural Networks 191

Author Index 193

Sponsors 199

CSM
CROATIAN SOCIETY OF MECHANICS
ZAGREB - OSIJEK - RIJEKA - SL. BROD - SPLIT

Plenary Lectures

11th International Congress
of Croatian Society of Mechanics
September 30 – October 3 2025
Vodice, Croatia

Pure or practical? How some of the most stringent requirements in numerical fluid mechanics can be relaxed in practical case studies in urban physics and wind engineering

Bert Blocken

Institute of Mechanical, Process and Energy Engineering, School of Engineering & Physical Sciences, Heriot-Watt University, Scotland, UK
E-mail: b.blocken@hw.ac.uk

Keywords: urban, building, computational fluid dynamics, cfd, heat transfer

1. Introduction

Over the past decades, an increasing number of practical case studies in urban physics and wind engineering have been conducted by numerical simulation with computational fluid dynamics (CFD). Examples are air pollution in urban areas, heatwaves in cities and the natural ventilation of buildings and urban areas. These case studies in urban areas are intrinsically based on well-established fluid mechanics theory and the associated rules and requirements in numerical simulations. These include the need to numerically reproduce the von Karman vortex shedding in the wake of buildings, the alternating build-up and collapse of separation bubbles, the spatial and temporal gradients in turbulent diffusivity and the need to include the thin laminar sublayer in the boundary layer to assess surface convective heat transfer. However, it are those rules and requirements that can sometimes make large practical case studies very difficult or even impossible. As a result, many researchers and practitioners in setting up their case studies have relaxed and in some cases even completely violated some of these rules and requirements, often without a clear view on the errors and uncertainties induced by this action. In this presentation, three case studies are outlined in which some rules and requirements have been relaxed or bluntly violated, and some indications of the associated errors and uncertainties are provided by the comparison of the simulation results with either wind tunnel or field measurements.

2. The three case studies

The first case study is pollutant gas dispersion in a street network in a densely built-up area by 3D steady RANS CFD simulation that do not reproduce the von Karman vortex shedding, separation bubble unsteadiness and calculate pollutant concentrations assuming the standard gradient-diffusion hypothesis with a turbulent diffusivity linked to the turbulent viscosity using a spatially and temporally constant turbulent Schmidt number. While reproducing these features is essential for pollutant gas dispersion around isolated buildings or obstructions, in dense street networks von Karman vortex shedding and separation bubble unsteadiness are suppressed by the multitude and proximity of building facades and pretty accurate concentration values can be obtained using a constant turbulent Schmidt number (Fig. 1a,b; [1]).

The second case study is reproducing surface temperatures in a real urban area during part of the 2006 heat wave in Europe. This is performed by 3D steady RANS simulations that use standard momentum and temperature wall functions with y+ values far above 5 that ignore the importance of the viscous sublayer in surface convective heat transfer. It is well-known that the very thin viscous sublayer is the part of the boundary layer that provides the largest resistance to convective heat transfer. However, in urban aerodynamics with Reynolds numbers up to 10^5-10^7, the sublayer thickness can go down to a few millimetre or less. Resolving this sublayer then requires computational cells to be placed within this sublayer, which would be nearly impossible for a large city model with hundreds, maybe thousands of buildings. Because the standard temperature wall

functions can introduce errors in convective heat flux up to 60% and more, adjusted thermal wall functions have been developed in the past [2,3]. But the large case study shows that even with the standard temperature wall functions, surface temperatures can be accurately reproduced. The reason is the relatively low importance of surface convective heat transfer in the overall heat transfer due to the wind shielding effect of upstream on downstream buildings in the dense built-up area(Fig. 1c,d; [4]).

The third case study is the ventilation of a large football stadium to reduce respiratory aerosol particle concentrations in the stadium in the context of the COVID19 pandemic. Here, Large Eddy Simulations (LES) are performed on a fairly high-resolution grid that nevertheless exhibits y+ values that locally exceed 10,000. While the application of wall functions in this case violates the both the concept and the range of the law of the wall, it is shown that this hardly influences the wind velocity field driving the stadium ventilation (Fig. 1e,f).

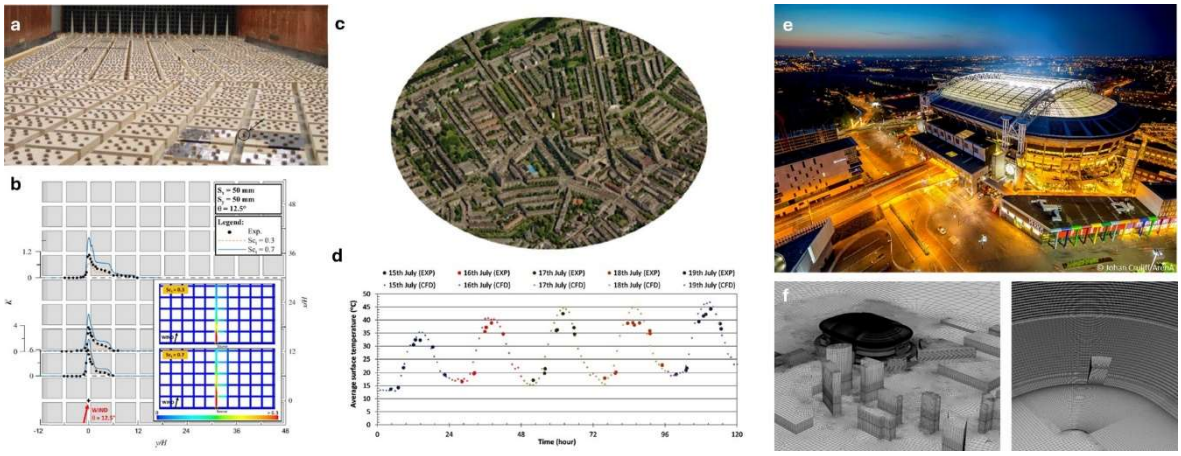


Figure 1. (a) Wind tunnel model; (b) Comparison of dimensionless concentration K by CFD and wind tunnel in the street network; (c) Urban area Bergpolder Zuid; (d) Comparison of surface temperatures by CFD and satellite imagery; (e) Johan Cruijff Football Stadium; (f) Computational grid outside and inside the stadium

3. Conclusions

Three case studies have been presented in which some aspects of well-established fluid mechanics theory and the associated rules or requirements in numerical simulations have been relaxed or even completely ignored. While this relaxation or violation can be far from best practice in numerical fluid mechanics and can lead to major errors and uncertainties in CFD simulations for isolated buildings or small groups of buildings, in these case studies in densely built-up areas, the errors and uncertainties appear rather limited. The reasons for these observations are discussed and are related to the multitude and proximity of building facades/walls in the configuration under study.

References

[1] Blocken, B., Vervoort, R., van Hooff, T., Reduction of outdoor particulate matter concentrations by local removal in semi-enclosed parking garages: a preliminary case study for Eindhoven city center. *Journal of Wind Engineering and Industrial Aerodynamics*, 159, 80-98, 2016.

[2] Defraeye, T., Blocken, B., Carmeliet, J., An adjusted temperature wall function for turbulent forced convective heat transfer for bluff bodies in the atmospheric boundary layer. *Building and Environment* 46(11), 2130-2141, 2011.

[3] Defraeye, T., Blocken, B., Carmeliet, J., CFD simulation of heat transfer at surface of bluff bodies in turbulent boundary layers: evaluation of a forced-convective temperature wall function for mixed convection. *Journal of Wind Engineering and Industrial Aerodynamics* 104-106, 439-446, 2012.

[4] Toparlar, Y., Blocken, B., Vos, P., van Heijst, G.J.F, Janssen, W.D., van Hooff, T., Montazeri, H., Timmermans, H.J.P., CFD simulation and validation of urban microclimate: A case study for Bergpolder Zuid, Rotterdam. *Building and Environment* 83, 79-90, 2015.

11th International Congress
of Croatian Society of Mechanics
September 30 – October 3 2025
Vodice, Croatia

Variational phase-field modeling of fracture: towards second-generation models

Laura De Lorenzis*

*Department of Mechanical and Process Engineering, ETH Zürich, Switzerland
E-mails: l.delorenzis@ethz.ch

Keywords: phase-field modeling, brittle fracture, cohesive fracture, strength surface, nucleation

1. Introduction

In this lecture, we overview some recent developments of variational phase-field modeling of fracture, that have revealed its limited flexibility to reproduce a desired strength surface while still correctly describing crack propagation. We finally present the latest developments: a new variational phase-field modeling framework of cohesive fracture which, while keeping all the desirable properties of the original model, is also able to describe fracture nucleation with a flexibly tunable strength surface.

2. An excursus on the study of fracture nucleation

Over twenty years after its birth, variational phase-field modeling of fracture has achieved a tremendous success, especially in the computational mechanics community, due to the unprecedented flexibility of fracture computations obtainable with this approach. The recognition of the limitations of the model in reproducing crack nucleation is more recent and has prompted a number of investigations (see e.g. [1], [2] among many others, referenced therein). The main obtained insights can be summarized as follows:

- The original variational phase-field model of brittle fracture is usually augmented with an energy decomposition approach in order to prevent interpenetration of the crack surfaces in compression. This can be achieved with the volumetric-deviatoric decomposition, known since 2008, which however is not flexible enough to independently tailor tensile and compressive strength.
- Other energy decompositions are either not sufficiently flexible to enable the independent calibration of tensile and compressive strength, or do not satisfy the requirement of "crack-like" residual stresses, which implies spurious stresses across fully developed crack surfaces [2,3].
- The star-convex energy decomposition proposed in [2] can accommodate the independent calibration of tensile and compressive strength, and at the same time satisfies the requirement of "crack-like" residual stresses. On the other hand, this decomposition produces a strength surface of star-convex shape, which is not a realistic description for strength surfaces of brittle and quasi-brittle materials. Indeed, the model in [2] is to be intended as a means of preventing spurious damage under compression in multiaxial settings (e.g. in the plate with hole under compression where points under tensile and compressive stress states compete for nucleation), and not as a model leading to a realistic strength surface.

In our recent contribution [3], inspired by the variational phase-field model of fracture coupled with plasticity in [4], we propose a new variational phase-field model of cohesive fracture, intended for brittle and quasi-brittle materials, which enables flexible tuning of the (convex) strength surface, while preserving all the desirable properties of the original model.

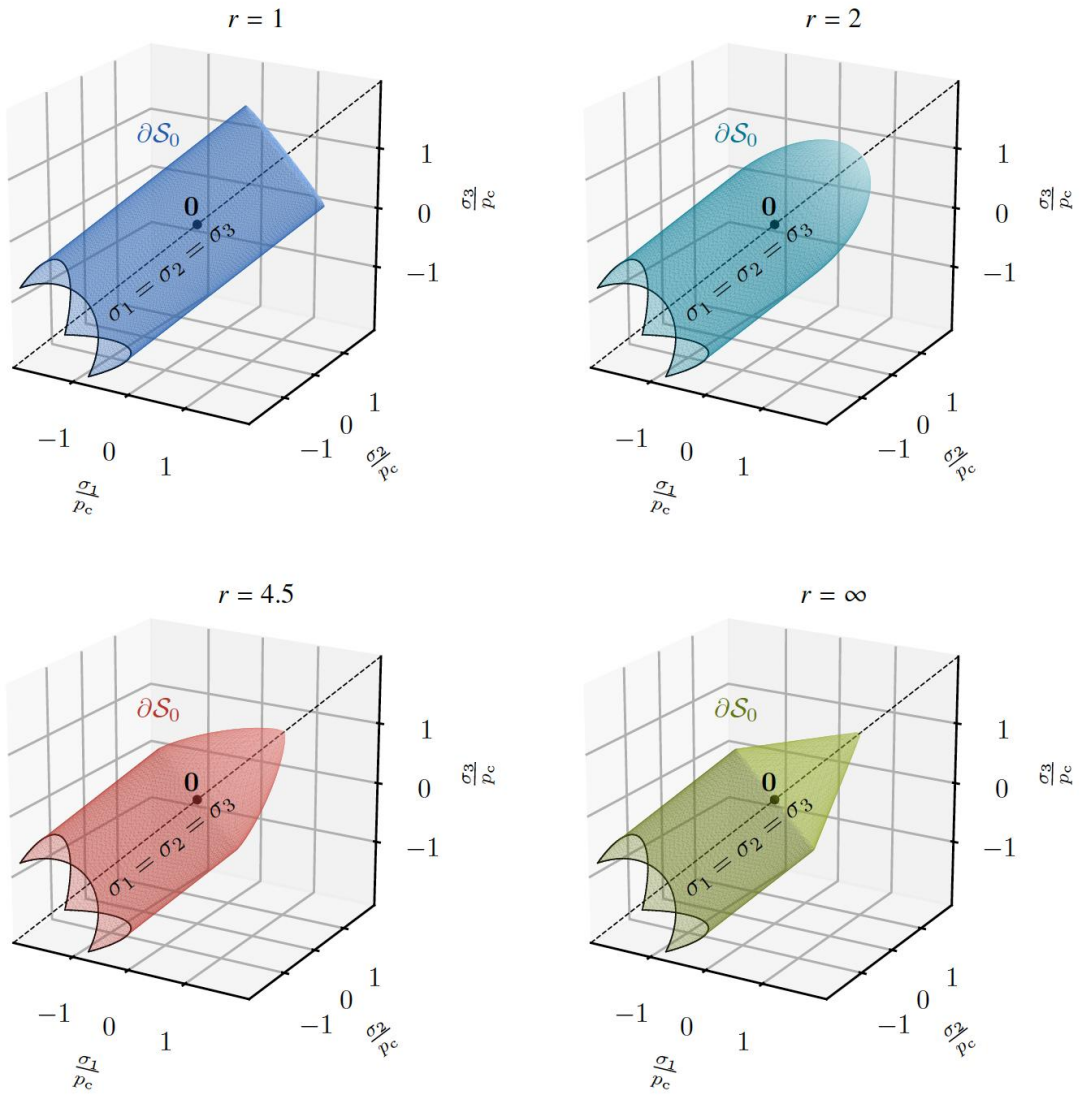


Figure 1. Examples of strength surfaces obtainable with the model in [4].

3. Conclusions

With the novel variational phase-field approach to cohesive fracture, a new spectrum of possibilities is now open to reconcile the description of fracture nucleation and propagation with a significantly enhanced flexibility. The new model can be applied to brittle, ductile, dynamic and anisotropic fracture where several advantages can be envisioned.

References

[1] L. De Lorenzis, C. Maurini, Nucleation under multi-axial loading in variational phase-field models of brittle fracture, *International Journal of Fracture,* 237 (1), 61–81, 2022.

[2] F. Vicentini, C. Zolesi, P. Carrara, C. Maurini, L. De Lorenzis, On the energy decomposition in variational phase-field models for brittle fracture under multi-axial stress states, *International Journal of Fracture*, 247 (3), 291–317, 2024.

[3] F. Vicentini, P. Carrara, L. De Lorenzis, Variational phase-field modeling of cohesive fracture with flexibly tunable strength surface, *submitted*.

[4] R. Alessi, J.-J. Marigo, S. Vidoli, Gradient damage models coupled with plasticity and nucleation of cohesive cracks, *Archive for Rational Mechanics and Analysis*, 214, 575–615, 2014.

11th International Congress
of Croatian Society of Mechanics
September 30 – October 3, 2025
Vodice, Croatia

AI-Empowered CAE via Software 3.0: Applications in Digital Twins, Additive Manufacturing, and Electronic Design Automation

Wing Kam Liu[*], Chanwook Park[+], Jiachen Guo[+], Gino Domel[*], Hantao Zhang[+]

[*]*Northwestern University, HIDENN-AI, LLC*

E-mails: w-liu@northwestern.edu, wingkamliu@gmail.com

[+]*Northwestern University*

E-mail: chanwookpark2024@u.northwestern.edu, jiachenguo2020@u.northwestern.edu, hantaozhang2029@u.northwestern.edu, gino.domel@northwestern.edu

Keywords: Software 3.0, predictive scientific AI, hierarchical neural network finite element, ultra large-scale simulation, additive manufacturing, integrated circuit

1. Introduction

Software development is undergoing a paradigm shift from explicit programming ("Software 1.0") toward software learned from data ("Software 2.0") [1]. This evolution has now progressed to the era of "Software 3.0," in which natural language serves as the programming interface and large pretrained models handle the rest [2]. In this new paradigm, large language models (LLMs) function as versatile general purpose reasoning engines, allowing developers to articulate goals in plain English and have the model generate the corresponding solutions [3]. The impact of this shift extends far beyond computer science: foundation models are already driving advances in biomedical research and healthcare [4], education [5, 6], and high-stakes fields such as finance, consulting, and law [7].

Drawing an analogy from engineering software in computer-aided engineering (CAE), Software 1.0 corresponds to classical finite element analysis (FEA) solvers, where engineers hand-coded numerical formulations (e.g., Ansys, Abaqus, etc.) [8]. Software 2.0 introduced data-driven surrogate modelling, where machine learning was used to approximate high-fidelity simulations [9]. Software 3.0 aims to combine the strengths of both worlds: embedding engineering domain knowledge into LLMs that can understand context, retrieve relevant information from a stack of domain expertise, and generate solutions or insights on demand. While recent uses of LLMs in CAE have automated tasks such as CAD model generation or FEM simulations [10], these applications largely replicate tasks that human experts can already perform. In this talk, we introduce how the Software 3.0 framework can convey transformative advances CAE, highlighting its applications to digital twins, additive manufacturing, and electronic design automation [11].

2. Software 3.0 in CAE

2.1. Agentic AI via model context protocol (MCP) for digital twins

Agentic AI refers to AI systems that move beyond passively assisting engineers and instead act as autonomous collaborators capable of planning, executing, and adapting CAE workflows. Enabled by the Model Context Protocol (MCP), which standardizes communication between LLMs and software tools, such systems can dynamically invoke functions for geometry import, meshing, solver execution, data processing, and surrogate modelling. This workflow supports the creation and operation of digital twins by automating decision-making steps, such as selecting sampling strategies or training models, that are typically problem dependent and reached through trial and error. As MCP tools accumulate

into a scalable knowledge base, annotated by engineers and interpretable by LLMs, agentic AI can leverage this collective expertise to accelerate exploration of parameter spaces, enhance computational efficiency, and deliver adaptive digital twin simulations.

2.2. Automated solver development for intrusive model order reduction (MOR) for space-parameter-time forward and inversed engineering problems

A transformative opportunity for CAE lies in automated solver development for intrusive model order reduction (MOR), which reduces the computational burden of large-scale simulations that prevail in additive manufacturing and electronic design automation while preserving accuracy. Unlike non-intrusive data-driven surrogates, intrusive MOR directly modifies governing equations to create efficient, data-free reduced-order models, but its adoption has been limited by the difficulty of redeveloping complex solvers. Recent advances in LLMs offer a pathway to overcome this barrier by automating algebraic derivations, code restructuring, and solver implementation, enabling engineers to generate high-fidelity reduced-order models with natural language prompts. We demonstrate this capability through Tensor-decomposition-based A Priori Surrogates (TAPS) [12], showing how LLMs can reduce development effort while meeting key performance metrics of accuracy, speed, and efficiency. This workflow holds promise for accelerating digital twin applications in additive manufacturing and electronic design automation, where scalable and adaptive reduced-order models are critical for design and optimization.

References

1. Karpathy, A., *Software 2.0*. 2017.
2. Karpathy, A., *Software 3.0*. 2025.
3. Raiaan, M.A.K., et al., *A review on large language models: Architectures, applications, taxonomies, open issues and challenges.* IEEE access, 2024. **12**: p. 26839-26874.
4. Nazi, Z.A. and W. Peng. *Large language models in healthcare and medical domain: A review*. in *Informatics*. 2024. MDPI.
5. Kasneci, E., et al., *ChatGPT for good? On opportunities and challenges of large language models for education.* Learning and individual differences, 2023. **103**: p. 102274.
6. Jeon, J. and S. Lee, *Large language models in education: A focus on the complementary relationship between human teachers and ChatGPT.* Education and Information Technologies, 2023. **28**(12): p. 15873-15892.
7. Chen, Z.Z., et al., *A survey on large language models for critical societal domains: Finance, healthcare, and law.* arXiv preprint arXiv:2405.01769, 2024.
8. Liu, W.K., S. Li, and H.S. Park, *Eighty years of the finite element method: Birth, evolution, and future.* Archives of Computational Methods in Engineering, 2022. **29**(6): p. 4431-4453.
9. Guo, J., et al., *Interpolating Neural Network-Tensor Decomposition (INN-TD): a scalable and interpretable approach for large-scale physics-based problems.* arXiv preprint arXiv:2503.02041, 2025.
10. Zhang, L., et al., *Large language models for computer-aided design: A survey.* arXiv preprint arXiv:2505.08137, 2025.
11. Guo, J., et al., *AI-Empowered CAE via Software 3.0.* In prep, 2025.
12. Guo, J., et al., *Tensor-decomposition-based A Priori Surrogate (TAPS) modeling for ultra large-scale simulations.* Computer Methods in Applied Mechanics and Engineering, 2025. **444**: p. 118101.

11th International Congress
of Croatian Society of Mechanics
September 30 – October 3 2025
Vodice, Croatia

Micromagnetic simulations of strongly heterogeneous magnetic materials

Jörg Schröder* and Maximilian Vorwerk*

*Institute of Mechanics, University of Duisburg-Essen, Universitätsstr. 14, 45141 Essen, Germany

E-mails: j.schroeder@uni-due.de, maximilian.vorwerk@uni-due.de

Keywords: Magnetic materials, micromagnetism, phase-field

1 Introduction

State-of-the-art permanent magnetic materials, such as neodymium-iron-boron (NdFeB) magnets, are essential for maximizing the efficiency of energy conversion systems, including wind turbines, sensors, and electric motors. Efficient and robust simulation techniques can help to reveal potential for improvements. Hence, this work gives a brief excursion into micromagnetic theory and introduces afterwards a computationally efficient approach for the numerical description of time-varying magnetic fields.

2 Micromagnetic simulations

The magneto-mechanically coupled system of equations is derived from the field equations

$$\operatorname{div}\boldsymbol{\sigma} = 0, \qquad \operatorname{div}\boldsymbol{B} = 0 \qquad \text{and} \qquad \dot{\boldsymbol{m}} = -\gamma_0\mu_0\,\boldsymbol{m}\times\boldsymbol{H}^{\text{eff}} + \alpha\,\boldsymbol{m}\times\dot{\boldsymbol{m}} \tag{1}$$

which are the mechanical balance of momentum, the magnetic Gauss law and Gilbert's equation. The mechanical Cauchy stress tensor is given as $\boldsymbol{\sigma}$, the magnetic induction is denoted as $\boldsymbol{B}$, the magnetization is indicated as $\boldsymbol{m}$ and the effective field is presented as $\boldsymbol{H}^{\text{eff}}$. The gyromagnetic ratio and the vacuum permeability are given as γ_0 and μ_0, while α indicates a material dependent damping coefficient. The stresses, the induction and the effective field

$$\boldsymbol{\sigma} = \mathbb{C} : \boldsymbol{\varepsilon}, \quad \boldsymbol{B} = \mu_0\,(\boldsymbol{H} + M_s\,\boldsymbol{m}) \quad \text{and} \quad \boldsymbol{H}^{\text{eff}} = \frac{-1}{\mu_0 M_s}\left[\partial_{\boldsymbol{m}}\mathscr{H} - \operatorname{div}\left(\partial_{\nabla\boldsymbol{m}}\mathscr{H}\right)\right] \tag{2}$$

follow the constitutive relations respectively. The material tensor is denoted as $\mathbb{C}$, the strains as $\boldsymbol{\varepsilon}$ and the magnetic field is given as $\boldsymbol{H}$. To precisely capture the magnetic behavior, all magnetic fields $\boldsymbol{H}$ evolving around the magnet itself have to be considered in simulations as well. Efficient methods to capture these effects are proposed in [1] and [2]. The enthalpy is

$$\mathscr{H}(\boldsymbol{\varepsilon},\boldsymbol{H},\boldsymbol{m},\nabla\boldsymbol{m}) = \mathscr{H}^{\text{ela}}(\boldsymbol{\varepsilon}) + \mathscr{H}^{\text{mag}}(\boldsymbol{H},\boldsymbol{m}) + \mathscr{H}^{\text{exc}}(\nabla\boldsymbol{m}) + \mathscr{H}^{\text{ani}}(\boldsymbol{m}), \tag{3}$$

with contributions to mechanics, magnetostatics, magnetic exchange and the crystal lattice orientation (anisotropy). The micromagnetic theory involves an important constraint $\|\boldsymbol{m}\| = 1$ which limits the length of the magnetization vectors to the unit length. This constraint is enforced in this work by introducing a perturbed Lagrange multiplier method

$$g_\lambda = \int_{\mathscr{B}} \left(\lambda\left[\|\boldsymbol{m}\|^2 - 1\right] - \frac{\lambda^2}{2\kappa_L}\right) \mathrm{dv}, \tag{4}$$

where λ indicates the Lagrange parameter and $\kappa_L \approx 10^5$ the perturbation parameter. The Lagrange parameter is subsequently condensed on element level and thus enables more efficient simulations, compared to the non-condensed version, cf. [3]. To discretize the equations

introduced above the finite element method (FEM) is considered. Compared to other established discretization methods as the finite difference method it is not that computationally efficient, but allows for very flexible and exact approximations of microstructures, cf. [4].

3 Analysis of a polycrystalline structure

In this section, the material behavior of a polycrystalline magnetic cube is analyzed. Within the grains, the material consists of ferromagnetic neodymium-iron-boron ($Nd_2Fe_{14}B$). Surrounding these grains, a neodymium-rich paramagnetic layer forms the grain boundaries. This structure is essential for achieving magnetic decoupling between the ferromagnetic grains. All grains have a different orientation of the C-axes, which leads to different nucleation times and individual reversal, as demonstrated in Fig. 1 in the individual magnetization states. This behavior can be tracked within the demagnetization path by means of kinks. The more kinks the better the grains are decoupled. Without the decoupling layer, premature reversal of the grains is possible, which means that the performance of the magnet is reduced, cf. [5].

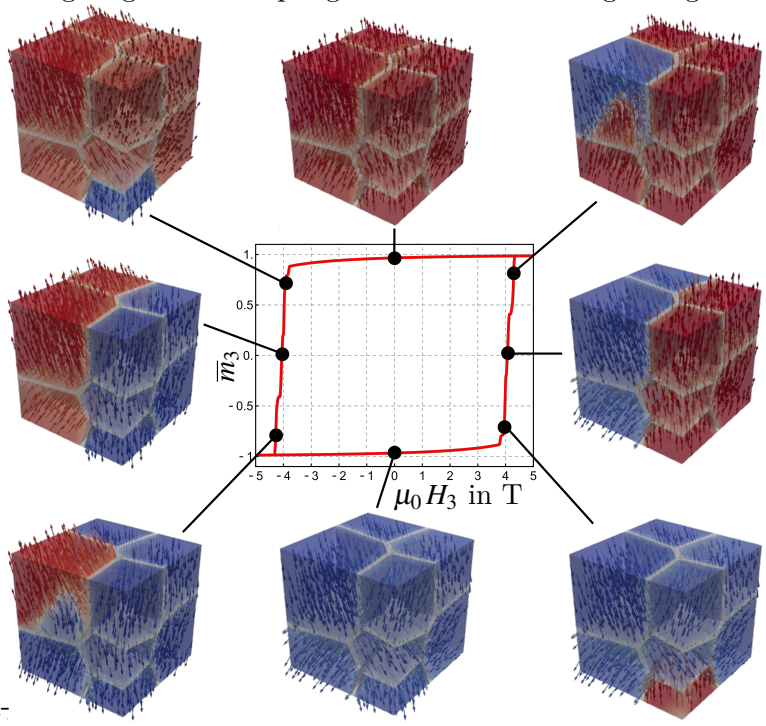


Figure 1. The hysteresis loop of the considered polycrystalline microstructure with its corresponding switching states a)-h).

4 Conclusion

This work deals with a micromagnetic-mechanically coupled material model that incorporates the magnetization unit constraint by means of a perturbed and subsequently condensed Lagrange parameter. This material model is consequently applied to the simulation of a heterogeneous permanent magnetic cube. Future work will deal with the analysis of further heterogeneous structures with significantly more magnetic grains.

References

[1] Birk, C., Reichel, M., Schröder, J., Magnetostatic simulations with consideration of exterior domains using the scaled boundary finite element method. Computer Methods in Applied Mechanics and Engineering, 399, 115362, 2022.

[2] Schröder, J., Reichel, M., Birk, C., An efficient numerical scheme for the FE-approximation of magnetic stray fields in infinite domains. Computational Mechanics, 70, 141-153, 2022.

[3] Reichel, M., Niekamp, R., Schröder, J., Efficient micromagnetic simulations based on a perturbed Lagrangian function. Journal of Applied Physics, 134, 103901, 2023.

[4] Vansteenkiste, A., Leliaert, J., Dvornik, M., Helsen, M., Garcia-Sanchez, F., Van Waeyenberge, B., The design and verification of MuMax3. AIP Advances, 4:10, 107133, 2014.

[5] Soderžnik, M., Sepehri-Amin, H., Sasaki, T.T., Ohkubo, T., Takada, Y., Sato, T., Kaneko, Y., Kato, A., Schrefl, T., Hono, K., Magnetization reversal of exchange-coupled and exchange-decoupled Nd-Fe-B magnets observed by magneto-optical Kerr effect microscopy. Acta Materialia, 135, 68–76, 2017.

Special Sessions

CSM
CROATIAN SOCIETY OF MECHANICS
ZAGREB - OSIJEK - RIJEKA - SL. BROD - SPLIT

SS01 - Emerging Trends in Mechanical Metamaterials

organized by

Giuseppe Failla and Andrea Russillo

University of Reggio Calabria, Italy

Special Sessions

11th International Congress
of Croatian Society of Mechanics
September 30 – October 3 2025
Vodice, Croatia

A novel metamaterial design based on a multiple beam system with internal local resonance

Andrea Burlon*, Francesco Lo Iacono+, Giacomo Navarra+, Giuseppe Failla*

*Department of Civil, Energy, Environmental and Materials Engineering (DICEAM) University of Reggio Calabria, Via Zehender, Località Feo di Vito, 89124 Reggio Calabria, Italy
E-mails: andrea.burlon@unirc.it, giuseppe.failla@unirc.it

+Department of Engineering and Architecture, Kore University of Enna, Cittadella Universitaria, Enna, Italy
E-mail: francesco.loiacono@unikore.it, giacomo.navarra@unikore.it

Keywords: Metamaterials, Finite element analyses, 3D Printing process, Experimental analyses

1 Introduction

Metamaterials have increasingly attracted attention in the field of structural dynamics due to their ability to influence wave propagation by means of engineered substructures arranged in periodic patterns [1, 2]. These artificially engineered materials offer new possibilities for vibration mitigation and control, enabling strategies that go beyond conventional approaches. Potential applications include vibration-isolating foundations (metafoundations), wave-blocking barriers (metabarriers), engineered surfaces (metasurfaces), as well as structural elements such as beams, rods, and plates with embedded metamaterial features. These developments rely on the band gap concept and represent meaningful progress toward more efficient and targeted vibration mitigation techniques. In this broad landscape, locally resonant metamaterials play a predominant role [1, 2, 3, 4]. Unlike phononic or periodic materials, which rely on Bragg scattering mechanism to induce forbidden gaps for elastic waves, locally resonant metamaterials can induce band gaps thanks to the presence of embedded resonant elements. These internal resonators interact with the host structure by absorbing and trapping vibrational energy, giving rise to local resonance phenomena that lead to effective wave attenuation. As a result, such metamaterials offer a powerful and compact solution for controlling elastic or acoustic waves, especially in applications where size constraints or low-frequency operation are critical.

2 Proposed study

This work introduces an original metamaterial concept, designed as an assembly of parallel beams interconnected by periodic arrays of internal resonators. Each resonator consists of a solid block connected to neighboring beams through slender rods. These resonators act as energy absorbers capable of inducing local resonances, which in turn give rise to wide and well-defined band gaps in the dispersion characteristics of the beam ensemble. A key advantage of the proposed configuration lies in the integration of the resonators within the structure itself, rather than attaching them as external components, as commonly seen in other locally resonant beam designs reported in the literature. This structural arrangement lends itself to practical realization while improving robustness and overall applicability.

The analysis and design process is structured into three main phases. First, an effective analytical model is formulated under simplifying assumptions regarding the beam and resonator dynamics, allowing the preliminary prediction of wave dispersion behavior. Next, comprehensive dynamic simulations are performed using a three-dimensional finite element model developed in ABAQUS with solid elements, enabling an accurate description of the mechanical response of the system. The model assumes the entire structure to be made of a resin-based material, whose elastic properties have been determined through experimental characterization.

Finally, physical prototypes of the metamaterial structure are fabricated at the mesoscale using high-resolution resin 3D printing technology. Experimental tests are carried out on these samples to validate the numerical predictions and assess the practical feasibility of the design.

3 Conclusion

Theoretical, numerical, and experimental results confirm the effectiveness of the proposed metamaterial concept in generating substantial band gaps and attenuating elastic wave propagation.

References

[1] Hussein, M.I., Leamy, M.J., and Ruzzene, M., Dynamics of Phononic Materials and Structures: Historical Origins, Recent Progress and Future Outlook, *Applied Mechanics Reviews*, 66 (4), 040802, 2014.

[2] Contreras, N., Zhang, X., Hao H., Hernandez F. Application of elastic metamaterials/meta-structures in civil engineering: A review, *Composite Structures*, 327, 117663, 2024.

[3] Xiao, Y., Wen, J., Yu, D., Wen, X., Flexural wave propagation in beams with periodically attached vibration absorbers: band-gap behavior and band formation mechanisms. *Journal of Sound and Vibration* 332, 2013.

[4] Liu, Z.Y., Zhang, X.X., Mao, Y.W., Zhu, Y.Y., Yang, Z.Y., Chan, C.T., et al. Locally resonant sonic materials. *Science* 289 (5485), 1734–1736, 2000.

11th International Congress
of Croatian Society of Mechanics
September 30 – October 3 2025
Vodice, Croatia

Water-tank Metabarriers as a Novel Concept of Seismic Metamaterials

Giuseppe Failla*, Andrea Francesco Russillo*

*Department of Civil, Environmental, Energy and Materials Engineering (DICEAM), University of Reggio Calabria, Via R. Zehender, 89124 Reggio Calabria, Italy
E-mails: giuseppe.failla@unirc.it, andreaf.russillo@unirc.it

Keywords: Water-tank Metabarriers, Seismic Metamaterials, Rayleigh waves propagation

Research on seismic protection of buildings and infrastructures recently focused on the very promising concept of seismic metamaterial. The term metamaterial broadly refers to an engineered material with exotic properties not obtainable in nature, which arise from a tailored design of its architecture. Within this framework, early studies on seismic metamaterials proposed to modify the properties of the soil surrounding the structure to be protected by appropriate structuring. In a pioneering work, Brulé and coworkers [1] showed theoretically and via large-scale experimental tests on soft soils that periodic arrangements of vertical boreholes with a spacing of about one meter induce Bragg band gaps for Rayleigh waves at frequencies around 50 Hz. Later, Miniaci et al. [2] proposed different periodic structures embedded in soil, consisting of cross-shaped, hollow and locally resonant (with rubber, steel and concrete) cylinders to attenuate both Rayleigh and bulk waves in the 1-10 Hz frequency range. Building on these works [1, 2], many other studies were developed in the last few years [3]. In this study, an innovative concept of resonant metabarrier to control Rayleigh waves propagation in soil is presented. It consists in an array of water tanks embedded in soil, whose resonance associated to sloshing phenomena ensures Rayleigh wave attenuation at very low frequency ranges. The concept is validated by extensive numerical simulations in COMSOL Multiphysics, applying Floquet-Bloch theory on the unit cell to obtain the band structure of the infinite array and computing transmission properties in corresponding 3D finite arrays.

References

[1] S. Brûlé, E.H. Javelaud, S. Enoch, S. Guenneau, 2014, Experiments on Seismic Metamaterials: Molding Surface Waves, Physical Review Letters, 112, 133901.

[2] M. Miniaci, A. Krushynska, F. Bosia, N.M. Pugno, 2016, Large Scale Mechanical Metamaterials as Seismic Shields, New Journal of Physics, 18, 083041.

[3] A. Colombi, R. Zaccherini, G. Aguzzi, A. Palermo, E. Chatzi, 2020, Mitigation of Seismic Waves: Metabarriers and Metafoundations Bench Tested, Journal of Sound and Vibration, 485, 115537.

11th International Congress
of Croatian Society of Mechanics
September 30 – October 3 2025
Vodice, Croatia

Optimization of the boat ceiling supports using diamond lattice structure

Janko Morosavljević*, Dražan Kozak*, Ivan Morosavljević*, Wei Li+

*University of Slavonski Brod, Mechanical Engineering Faculty, Slavonski Brod, Croatia
E-mails: {jmorosavljevic,dkozak, imorosavljevic}@unisb.hr

+School of Mathematics and Statistics, Xidian University, Xi'an 710071, China
E-mail: liweilw@mail.xidian.edu.cn

Keywords: structural optimization, boat ceiling, lattice structure, diamond lattice cell

1. Introduction

For larger boats, repairs are typically conducted in shipyards and marinas, where the boat is taken for service. The objective is always to complete repairs as quickly as possible to ensure the boat can return to operation. However, unexpected issues may arise, and sometimes all the necessary replacement parts have not been anticipated. Given that boat parts can be quite specific, waiting for their availability can take a considerable amount of time. In such cases, the ability to rapidly produce replacement parts is invaluable, particularly with the use of 3D printing technology [1].

In boats, ceilings are often adorned with decorative panels made from plywood, which are then covered with fabric in the cabin area. These ceilings are designed in such a way that the supports are not visible, and they are typically constructed from polymer materials. In this instance, it was needed to manufacture ceiling lining supports for the ceiling made from birch plywood, measuring 2000 x 600 x 12 mm. It was decided to create these supports using FDM 3D printing technology with PLA material.

2. Optimisation of the boat ceiling support

According to the dimensions of the ceiling, six supports were foreseen for installation. Before proceeding, it was important to design a support that could fit the installation location, and to create a 3D model. To minimize material consumption and reduce the weight of the support, a model featuring a diamond lattice cell structure was opted [2], while maintaining a wall thickness of 1 mm. Figure 1. shows the created model along with cross-sections that illustrate the internal structure.

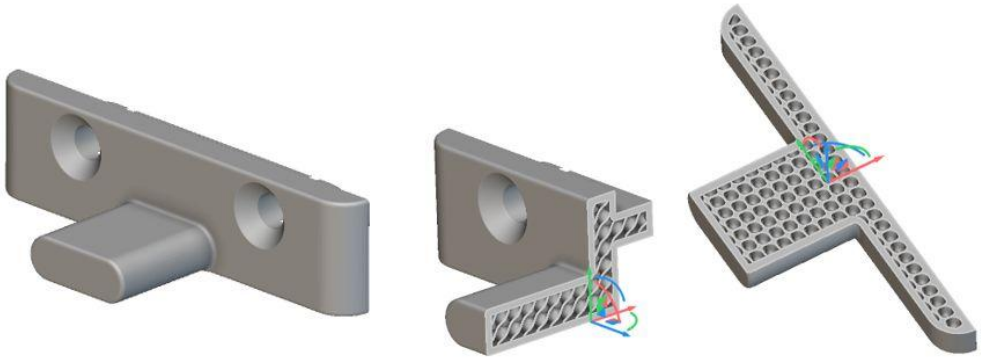


Figure 1. Model of the boat ceiling support along with cross-sections

To accurately determine the dimensions of the diamond lattice structure, specifically of the defined parameter Wall thickness and the optimal porosity of the structure, optimization is necessary.

The load was calculated based on the mass of the plywood with previously specified dimensions, incorporating a safety factor of 3 to account for dynamic loads during the boat's movement. The resultant force is 52.97 N and is applied perpendicular to the protruding surface on which the plywood is intended to rest. The support is secured with two screws, and a clamping boundary condition was applied at those surfaces.

Optimization was conducted in software nTopology by generating a total of six structures, with the wall thickness parameter varying from 0.25 mm to 1.25 mm in increments of 0.25 mm, ultimately including full support. A static analysis was performed for each structure, correlating the maximum equivalent stress, deflection, and required printing time with the porosity of the structure. All designs met the established strength requirements. The maximum tensile strength of 3D-printed PLA for this application is 62.4 MPa [3]. The maximum equivalent stress for the structure with 0.25 mm wall thickness is 17.36 MPa, significantly lower than the maximum tensile strength.

Based on the generated diagrams, the optimal solution in terms of equivalent stress corresponds to a support structure with a porosity of 68%. The correlation between the maximum equivalent stress and the porosity of the structure is shown in the Figure 2.

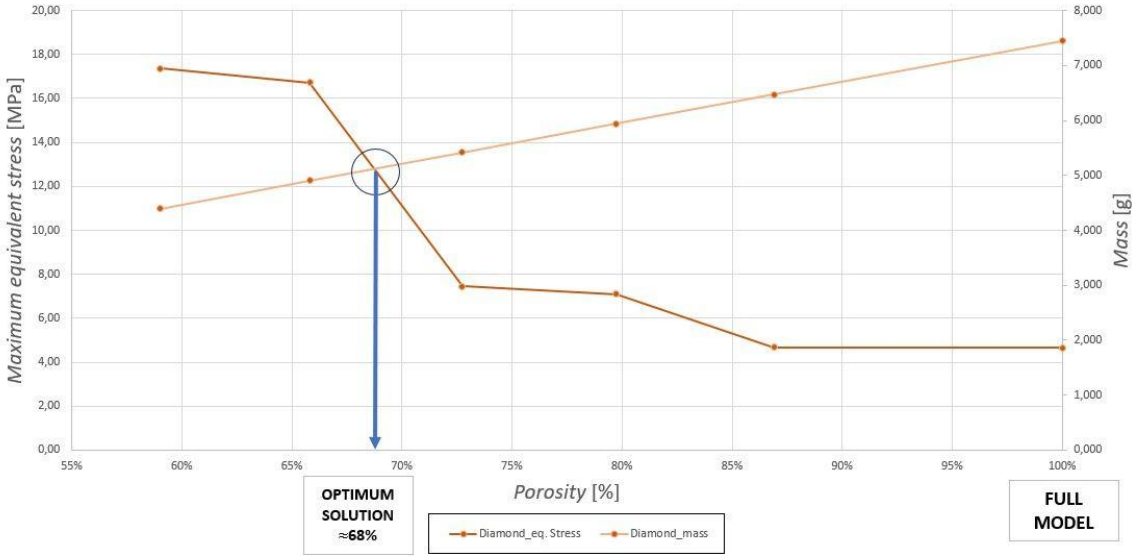


Figure 2. The correlation between the maximum equivalent stress and the porosity of the structure

3. Conclusions

In conclusion, the analysis conducted demonstrates that 3D printing is a highly beneficial technology. However, to produce parts of the highest quality and meet specific requirements, it is essential to perform numerical analysis and implement an optimisation process. This approach benefits by minimising the printing time and reducing material consumption, ultimately maximising cost savings and ensuring financial profitability.

References

[1] Maconachie, T., Leary, M., Lozanovski, B., Zhang, X., Qian M., Faruque, O., & Brandt, M. (2019). SLM lattice structures: Properties, performance, applications and challenges. Materials & Design, 183, 108137. https://doi.org/10.1016/j.matdes.2019.108137

[2] Marco, M., Belda, R., Henar Miguélez, M., & Giner, E. (2021). Numerical analysis of mechanical behaviour of lattice and porous structures. Composite Structures, 261, 113292-113307. https://doi.org/10.1016/j.compstruct.2020.113292

[3] Chacón, J. M., Caminero, M. A., García-Plaza, E., & Núñez, P. J. (2017). Additive manufacturing of PLA structures using fused deposition modelling: effect of process parameters on mechanical properties and their optimal selection. Materials & Design, 124, 143-157. https://doi.org/10.1016/j.matdes.2017.03.065

11th International Congress
of Croatian Society of Mechanics
September 30 – October 3 2025
Vodice, Croatia

Low-cycle fatigue analysis of different TPMS metamaterials

Aleksej Rikić*, Branko Nečemer*

*University of Maribor, Faculty of Mechanical Engineering, Smetanova 17, SI-2000 Maribor, Slovenia
E-mails: {aleksej.rikic, branko.necemer}@um.si

Keywords: low-cycle fatigue, computational analysis, TPMS, aluminium alloy

1. Introduction

Cellular structures are increasingly used in modern engineering practice due to their favourable combination of mechanical and physical properties. Their advantages are lightweight construction, high sound insulation, damping capacity, and high mechanical energy absorption. A computational fatigue study was conducted on selected triply periodic minimal surfaces (TPMS) metamaterials. The research also aimed to analyse the influence of unit cell shape and load level on the fatigue life of the analysed TPMS metamaterials.

2. Computational model

The computational model developed in this study focused on analysing three different Triply Periodic Minimal Surface (TPMS) structures: Gyroid, Diamond, and Primitive topologies. Finite Element (FE) analyses were conducted on sheet-based lattice configurations, with each model consisting of 2×2×4 unit cells. Symmetry boundary conditions were applied to replicate the mechanical behaviour of a larger 4×4×4 unit cell structure. The material properties used in the simulations corresponded to aluminium alloy 5083-H111, as reported in the literature [1]. Since the study concentrated on large deformation amplitudes, plastic deformations were expected. Therefore, the Strain-Life approach was chosen for its ability to capture material behaviour in the plastic regime. An isotropic elasto-plastic material model with kinematic hardening was implemented and calibrated based on experimental data [2], ensuring an accurate representation of the material response under cyclic loading. All models were subjected to strain-controlled loading conditions with a fully reversed loading ratio (R = –1), as illustrated in Figure 1. The analysis accounted for material and structural nonlinearities to ensure realistic simulation outcomes.

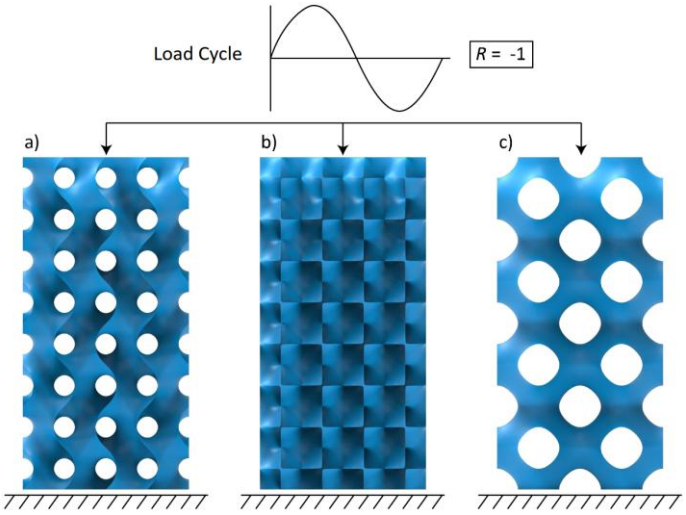


Figure 1: Boundary conditions for the computational model [3]

3. Results and Discussion

Only the central region of the models was considered in the evaluation to eliminate the potential influence of boundary condition placement on the computed fatigue life. The computational results were summarised using three fatigue life curves. Figure 2 illustrates the strain amplitude versus the number of cycles to fatigue crack initiation. Based on the results presented in Figure 2, the Primitive topology exhibits the longest fatigue life, requiring the highest number of cycles before crack initiation occurs. In contrast, the Diamond topology shows the shortest fatigue life, with cracks initiating after the fewest cycles. These findings are consistent with the reaction force analysis, which indicates that the Diamond topology demonstrates the highest stiffness while the Primitive topology exhibits the lowest stiffness. [3]

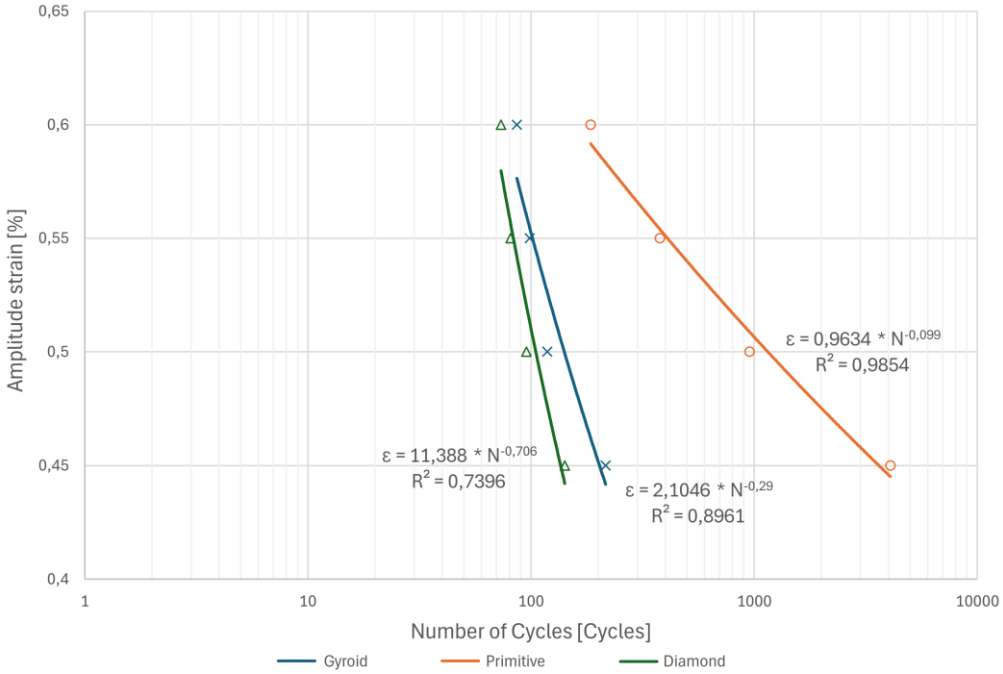


Figure 2: Strain – Life curves

4. Conclusions

This research offers valuable insight into the fatigue performance of various Triply Periodic Minimal Surface (TPMS) structures, specifically Gyroid, Diamond, and Primitive topologies. The findings reveal a clear trade-off between stiffness and fatigue life: while the Diamond structure exhibits the highest stiffness, it demonstrates the shortest fatigue life. Conversely, the Primitive structure, despite having the lowest stiffness, endures the highest number of loading cycles before fatigue crack initiation, indicating superior durability under cyclic loading. These results highlight the potential for tailoring TPMS structures to specific application requirements, whether prioritising mechanical strength or long-term fatigue resistance. Such adaptability is particularly relevant in engineering fields such as aerospace, automotive, and biomedical design, where optimising material performance for a given use case is critical.

References

[1] B. Nečemer, F. Zupanič, D. Gabriel, E. A. Tarquino, M. Šraml, and S. Glodež, "Low cycle fatigue behaviour of ductile aluminium alloys using the inelastic energy approach," *Mater. Sci. Eng. A*, vol. 800, no. October 2020, 2021, doi: 10.1016/j.msea.2020.140385.

[2] Nečemer, B., Klemenc, J., Zupanič, F., Glodež, S., Modelling and predicting of the LCF-behaviour of aluminium auxetic structures, *International Journal of Fatigue*, 156, 106673, 2022.

[3] Rikić, A., Nečemer, B., *Analiza utrujanja TPMS struktur*, Fakulteta za strojništvo Univerza v Mariboru, Maribor, 2024.

11th International Congress
of Croatian Society of Mechanics
September 30 – October 3 2025
Vodice, Croatia

Fractional problems: theory and applications

Raffaella Servadei*

**Università degli Studi di Urbino Carlo Bo, Dipartimento di Scienze Pure e Applicate, Piazza della Repubblica, 13, Urbino (Italy)*
E-mail: raffaella.servadei@uniurb.it

Keywords: fractional operators, nonlocal phenomena, nonlinear analysis

1 Introduction

A very interesting area of nonlinear analysis lies in the study of elliptic equations involving fractional operators. Recently, a great attention has been focused on these problems, both for the pure mathematical research and in view of concrete real-world applications.

Indeed, this type of operators arises in a quite natural way in different contexts, such as, among the others, the thin obstacle problem, optimization, finance, phase transitions, stratified materials, anomalous diffusion, crystal dislocation, soft thin films, semipermeable membranes, flame propagation, conservation laws, ultra-relativistic limits of quantum mechanics, quasi-geostrophic flows, multiple scattering, minimal surfaces, materials science, water waves, chemical reactions of liquids, population dynamics, geophysical fluid dynamics, mathematical finance (American options), jump Lévy processes in probability theory. In all these cases, the nonlocal effect is modeled by the singularity at infinity. For more details and applications, see [1, 2, 3, 4, 5, 6, 7, 8, 9, 10, 11] and the references therein.

The current literature on nonlocal fractional operators and on their applications is, therefore, very interesting and, up to now, quite large.

Motivated by this increasing interest on these subjects, this talk deals with some classes of fractional problems, widely investigated by the mathematical community, as well as their applications in different fields.

More precisely, during the talk we consider problems modeled by

$$\begin{cases} (-\Delta)^s u - \lambda u = |u|^{q-2}u & \text{in } \Omega \\ u = 0 & \text{in } \mathbb{R}^n \setminus \Omega, \end{cases} \tag{1}$$

where $s \in (0,1)$ is fixed, $\Omega \subset \mathbb{R}^n$, $n > 2s$, is open, bounded, $\lambda > 0$, and $(-\Delta)^s$ is the fractional Laplace operator defined as

$$-(-\Delta)^s u(x) = \frac{1}{2}\int_{\mathbb{R}^n} \frac{u(x+y)+u(x-y)-2u(x)}{|y|^{n+2s}}\,dy, \quad x \in \mathbb{R}^n,$$

$2_s^* = 2n/(n-2s)$ is the fractional critical Sobolev exponent and $2 < q \le 2_s^*$, that is problems with subcritical ($q < 2_s^*$) and critical growth ($q = 2_s^*$). In problem (1) the Dirichlet datum is given in $\mathbb{R}^n \setminus \Omega$ and not simply on $\partial\Omega$, consistently with the nonlocal character of the operator $(-\Delta)^s$.

Problem (1) represents the nonlocal counterpart of the following nonlinear elliptic equation

$$\begin{cases} -\Delta u - \lambda u = |u|^{q-2}u & \text{in } \Omega \\ u = 0 & \text{on } \partial\Omega, \end{cases}$$

with $2 < q \le 2^*$, where $2^* = 2n/(n-2)$ and $n > 2$.

Aim of this talk is to present some existence and multiplicity results for nonlocal fractional problems modeled by (1). All these results may be seen as the extension of some classical nonlinear analysis theorems to the case of fractional operators.

References

[1] D. Applebaum, *Lévy processes and stochastic calculus*, Second edition. Cambridge Studies in Advanced Mathematics, 116. Cambridge University Press, Cambridge, 2009.

[2] J. Bertoin, *Lévy processes*, Cambridge Tracts in Mathematics, 121. Cambridge University Press, Cambridge, 1996.

[3] C. Bucur and E. Valdinoci, em Nonlocal diffusion and applications. Lecture Notes of the Unione Matematica Italiana, Springer Cham, 2016.

[4] L. Caffarelli, *Nonlocal equations, drifts and games*. *Nonlinear Partial Differential Equations*, Abel Symposia, 7: 37–52, 2012.

[5] L. Caffarelli and L. Silvestre, *An extension problem related to the fractional Laplacian*. *Comm. Partial Differential Equations*, 32: 1245–1260, 2007.

[6] R. Cont, P. Tankov, *Financial modelling with jump processes*, Chapman & Hall/CRC Financial Mathematics Series. Boca Raton, Fl, 2004.

[7] A. Majda, E Tabak, *A two-dimensional model for quasigeostrophic flow: comparision with the two-dimensional Euler flow*, Nonlinear phenomena in ocean dynamics (Los Alamos, NM, 1995). Phys. D 98 (1996), no. 2-4, 515–522.

[8] E. Valdinoci, *From the long jump random walk to the fractional Laplacian*, Bol. Soc. Esp. Mat. Apl. Se MA, **49** (2009), 33–44.

[9] J.L. Vázquez, Nonlinear Diffusion with Fractional Laplacian Operators. *Nonlinear partial differential equations*, Abel Symp., 7: 271–298, 2012.

[10] J.L. Vázquez, Recent progress in the theory of nonlinear diffusion with fractional Laplacian operators. *Discrete Contin. Dyn. Syst. Ser. S*, 7, no. 4: 857–885, 2014.

[11] L. Vlahos, H. Isliker, Y. Kominis, K. Hizonidis, *Normal and anomalous Diffusion: a tutorial. In Order and chaos*, 10th volume, T. Bountis (ed.), Patras University Press, 2008.

CSM
CROATIAN SOCIETY OF MECHANICS
ZAGREB - OSIJEK - RIJEKA - SL. BROD - SPLIT

SS02 - Mechanics of Non-Conventional Materials and Structures

organized by

Raffaele Barretta, University of Naples Federico II, Italy

Noël Challamel, Université Bretagne Sud, France

Nicholas Fantuzzi, University of Bologna, Italy

Marzia Sara Vaccaro, University of Naples Federico II, Italy

Special Sessions

11th International Congress
of Croatian Society of Mechanics
September 30 – October 3 2025
Vodice, Croatia

A data-driven multiscale approach for the numerical prediction of damage evolution in anisotropic composite materials

Domenico Ammendolea*, Fabrizio Greco*, Lorenzo Leonetti*, Paolo Lonetti*, Arturo Pascuzzo+

*Department of Civil Engineering, University of Calabria, Via Pietro Bucci, 87036 Rende, Italy
E-mails: {domenico.ammendolea,fabrizio.greco,lorenzo.leonetti,paolo.lonetti}@unical.it

+Department of Engineering, Pegaso University, Centro Direzionale Isola F2, 80143 Naples, Italy
E-mail: arturo.pascuzzo@unipegaso.it

Keywords: data-driven multiscale models, anisotropic damage models, micromechanics, nanocomposites, nonlinear finite elements

1. Introduction

Nowadays, several reinforced and/or lightweight microstructured materials are usually employed in many engineering fields, such as aerospace, civil construction, automotive and medical equipment. Indeed, such materials, which also include nanocomposites and bioinspired materials, offer enhanced properties and/or additional functionalities induced by their microstructural arrangements [1–3].

Nevertheless, the design of such materials can be difficult, due to presence of extremely complex microstructural patterns. Indeed, such materials may experience strong fracture-induced anisotropy as well as multiple failure mechanisms [4]. Consequently, numerical modelling and simulation are crucial tools for optimizing the mechanical design of these heterogeneous materials.

Despite numerous advancements in the development of sophisticated models, a universally recognized approach that ensures both high accuracy and computational efficiency for simulating failure in composite structures under general loading conditions remains elusive. Among existing numerical strategies for accurately and efficiently predicting failure in anisotropic microstructures, multiscale approaches are the most common in recent literature due to their versatility in practical applications involving damage, fracture, instability, and other failure mechanisms.
Nevertheless, multiscale approaches based on first-order homogenization are unsuitable for strain localization. To address this, refined computational homogenization schemes have been developed in the recent literature, including higher-order [5] and continuous-discontinuous homogenization [6]. To significantly accelerate these computational homogenization methods, especially for realistic 3D problems, several approaches have been proposed, including those involving data-driven and machine learning techniques. Many of these utilize artificial neural networks (ANN) for the training phase of the homogenized model. A wide variety of data-driven approaches have been employed to accurately predict the evolution of fracture and damage in many classes of composite materials [7].

2. Description of the data-driven multiscale approach

This work proposes a novel and efficient data-driven multiscale strategy for investigating complex failure phenomena in anisotropic heterogeneous structures. This strategy employs a parametrically homogenized continuum damage mechanics (PHCDM) framework [8], being able to explicitly integrate microstructural evolution into macroscopic constitutive models, in combination with a deep neural network (DNN) approach for calibrating the associated surrogate damage model.

The proposed multiscale strategy consists of two computational stages. In the first stage, a discrete state database is constructed by performing micromechanical analyses on a Representative Volume Element along various macrostrain paths to cover the entire macrostrain space. Once this database is built, a DNN surrogate model for macroscopic damage evolution is fitted using the obtained sample

points. In the latter stage, macroscale finite element computations are performed using the calibrated surrogate model to simulate anisotropic damage evolution in general heterogeneous structures.

The main application of this multiscale approach, termed as data-driven multiscale model (DDMM), is the investigation of failure in porous nanomaterials with periodically arranged holes and in nacre-like composites with periodically arranged nanoplatelets. All numerical results have been validated against a conventional numerically homogenized model (HM) serving as the reference, for different macrostrain paths, as shown in Figure 1.

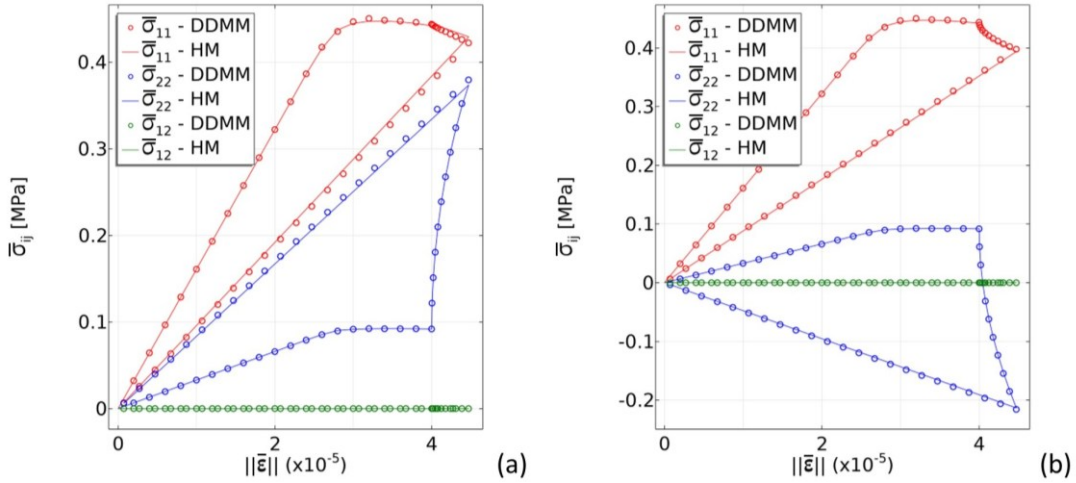


Figure 1. Comparison of stress-strain responses for a perforated microstructure between the data-driven multiscale model (DDMM) and the homogenized model (HM), for different macrostrain paths.

3. Conclusions

The principal advantages of the present data-driven multiscale model (DDMM) are:

- High numerical accuracy in predicting the failure response of damaging composites.
- Excellent computational efficiency also for highly nonlinear computations.
- Capability of dealing with both proportional and nonproportional macrostrain histories and correctly capturing the effect of unloading processes on the macroscopic damage evolution.

References

[1] Ko, S., Yang, J., Tuttle, M.E., Salviato, M., Effect of the platelet size on the fracturing behavior and size effect of discontinuous fiber composite structures. *Composite Structures*, 227, 111245, 2019.

[2] Orrego, S., Chen, Z., Krekora, U., Hou, D., Jeon, S.-Y., Pittman, M., Montoya, C., Chen, Y., Kang, S.H., Bioinspired materials with self-adaptable mechanical properties. *Advanced Materials*, 32, 1906970, 2020.

[3] Chiang, C.-C., Brelin, J., Weeks, S., Meng, Z., Dynamic mechanical behaviors of nacre-inspired graphene-polymer nanocomposites depending on internal nanostructures. Extreme Mechanics Letters, 49, 101451, 2021.

[4] Huang, W., Restrepo, D., Jung, J., Su, F.Y., Liu, Z., Ritchie, R.O., McKittrick, J., Zavattieri, P., Kisailus, D., Multiscale toughening mechanisms in biological materials and bioinspired designs. *Advanced Materials*, 31, 1901561, 2019.

[5] Kouznetsova, V.G., Geers, M.G.D., Brekelmans, W.A.M., Multi-scale second-order computational homogenization of multi-phase materials: a nested finite element solution strategy. *Computer Methods in Applied Mechanics and Engineering*, 193, 5525–5550, 2004.

[6] Belytschko, T., Song, J., Coarse-graining of multiscale crack propagation. International Journal for Numerical Methods in Engineering, 81, 537–563, 2010.

[7] Chafia, Z., Yvonnet, J., Bleyer, J., A Data-Driven-based homogenization method to simulate the anisotropic damage of brittle heterogeneous structures. *Computer Methods in Applied Mechanics and Engineering*, 437, 117747, 2025.

[8] Zhang, X., O'Brien, D.J., Ghosh, S., Parametrically homogenized continuum damage mechanics (PHCDM) models for composites from micromechanical analysis. *Computer Methods in Applied Mechanics and Engineering*, 346, 456–485, 2019.

11th International Congress
of Croatian Society of Mechanics
September 30 – October 3 2025
Vodice, Croatia

Carbon Nanotube Nanotrusses as Building Blocks of Advanced Metamaterials: An MD-ML-FE Optimization Framework

Marko Čanađija*, Stefan Ivić*

*University of Rijeka, Faculty of Engineering, Vukovarska 58, 51000 Rijeka, Croatia
E-mails: marko.canadija@riteh.uniri.hr, stefan.ivic@riteh.uniri.hr

Keywords: Carbon nanotubes, Nanotrusses, Convex neural networks, Metamaterials

1 Introduction

The focus of the present research is on the mechanical performance of hypothetical metamaterials composed of configurations built from single-walled carbon nanotubes (SWCNTs). Specifically, we examine nanotrusses made of SWCNTs, which combine the classical structural efficiency of trusses with the outstanding mechanical properties of carbon nanotubes (CNTs).

Truss-based structures have previously been considered as the basis for novel metamaterials. Analyses of mechanical performance are typically conducted using molecular dynamics (MD) and, occasionally, finite element methods. For the present purpose, it is convenient to categorize such analyses into non-CNT-based materials [1] and CNT-based materials [2]. The usual goal is to enhance certain mechanical or thermal properties [3]. For instance, this could involve designing a material with a negative Poisson's ratio [3, 4, 5].

The research cited above shares a common feature: in all cases, an intuitive approach to nanotruss design is employed. Due to the high computational cost associated with MD simulations, iterative procedures such as those used in optimization are prohibitively expensive. On the other hand, molecular structural mechanics [6], which relies on beam finite elements (FE) to model interatomic connections, is less computationally demanding but may struggle to achieve MD-level accuracy.

This research bridges MD and FE approaches by employing neural networks (NNs) as surrogate constitutive models. The NNs are trained on a comprehensive dataset obtained from MD simulations of tensile tests on SWCNTs with all possible configurations having diameters less than 4 nm. The trained NNs are then coupled with rod elements in Abaqus, resulting in a practical numerical tool. Finally, this framework is integrated with Indago [11], an open-source optimization code, to design metamaterials with targeted mechanical properties. Details of this procedure are documented in [7, 8, 9, 10].

2 MD simulations, NN training & FE

To train a neural network (NN), a suitable dataset is required. In the present study, uniaxial tensile and compression molecular dynamics (MD) simulations of 818 SWCNTs with various configurations were conducted using LAMMPS. All simulations were performed at room temperature (300 K). For each test, a stress-strain curve was generated and used as part of the dataset. Although a plain feedforward NN can be readily applied to such data, the resulting model is unsuitable for use as a constitutive model in finite element (FE) analysis. This is primarily because, at room temperature, the stress-strain curves exhibit non-monotonic behavior, and the strain energy is not convex with respect to strain due to stochastic thermal noise.

To address this issue, physical constraints are incorporated into the NN. Specifically, a partially input convex integrable neural network (PICINN) is employed to enforce convexity of the strain energy with respect to strain. Convexity is not required for the additional input variables n and m, which define the chirality of a SWCNT. Training is carried out using a Sobolev-type approach, meaning the NN is trained on the derivatives of stress-strain data. Further differentiation of the trained model yields the tangent modulus.

The trained PICINN is then coupled to the Abaqus FE code via the UMAT subroutine. Each nanotube is modeled using a T3D2 truss/rod finite element and assembled into a nanotruss structure. Both geometric and material nonlinearities are considered.

3 Optimization

This MD-NN-FE framework is then integrated into the nanotube truss design optimization procedure. Several optimization methods available in the Indago module are tested to identify the most efficient approach for addressing the global optimization of nanotube truss structures used to design novel nano-materials. Specifically, the following algorithms were considered: the Nelder–Mead method (NM), Particle Swarm Optimization (PSO), Artificial Bee Colony (ABC) optimization, the Squirrel Search Algorithm (SSA), and the Bat Algorithm (BA). Each method was evaluated over a larger sample of runs to ensure the reliability and statistical justification of the results.

The optimization aims to minimize the mass of the nanotube truss while simultaneously achieving desired macro-elastic properties, such as stiffness and compliance, under specific loading conditions. These objectives are pursued while strictly satisfying structural constraints to ensure mechanical integrity and manufacturability. The combination of the MD-NN-FE framework with global optimization techniques provides a powerful tool for the rational design of high-performance nano-materials with tailored mechanical characteristics.

4 Conclusion

Finally, the accuracy of the MD-NN-FE framework was evaluated against benchmark cases computed directly using MD. The results demonstrate that the proposed framework retains the accuracy of MD simulations while requiring only a fraction of the computational cost. This significant reduction in cost makes optimization feasible.

In summary, this paper presented a computationally efficient tool for optimizing the shape of nanotrusses to design metamaterials with targeted properties. The effectiveness of the framework is demonstrated through a representative example.

Acknowledgments: This work has been supported by the University of Rijeka, project numbers uniri-iskusni-tehnic-23-37 and uniri-iskusni-tehnic-23-52. This support is gratefully acknowledged.

References

[1] L. Meza, A. Zelhofer, N. Clarke, A. Mateos, D. Kochmann, J. Greer, Resilient 3D hierarchical architected metamaterials, *Proceedings of the National Academy of Sciences of the United States of America*, 112 (Sep. 2015).

[2] C. Zhang, A. Akbarzadeh, W. Kang, J. Wang, A. Mirabolghasemi, Nano-architected metamaterials: carbon nanotube-based nanotrusses, *Carbon* 131 (2018) 38–46.

[3] J. Cai, A. Akbarzadeh, Hierarchical kirigami-inspired graphene and carbon nanotube metamaterials: Tunability of thermo-mechanic properties, *Materials & Design*, 206 (2021) 109811.

[4] J. Cai, H. Chen, Y. Li, A. Akbarzadeh, Lessons from nature for carbon-based nanoarchitected metamaterials, *Small Science*, 2 (12) (2022) 2200039.

[5] J. Cai, B. Shahryari, A. Akbarzadeh, Tunable auxeticity in hydrogenated carbon nanotube origami metamaterial, *MRS Bulletin*, (2023) 1–11.

[6] C. Li, T.-W. Chou, A structural mechanics approach for the analysis of carbon nanotubes, *International Journal of Solids and Structures*, 40 (10) (2003) 2487 – 2499.

[7] M. Čanađija, Deep learning framework for carbon nanotubes: Mechanical properties and modeling strategies, *Carbon*, 184 (2021) 891–901.

[8] V. Košmerl, I. Štajduhar, M. Čanađija, Predicting stress–strain behavior of carbon nanotubes using neural networks, *Neural Computing and Applications*, (2022) 1–16.

[9] M. Čanađija, V. Košmerl, M. Zlatić, D. Vrtovšnik, N. Munjas, A computational framework for nanotrusses: Input convex neural networks approach, *European Journal of Mechanics-A/Solids*, 103 (2024) 105195.

[10] M. Čanađija, S. Ivić, Carbon nanotubes as a basis of metamaterials and nanostructures: Crafting via design optimization. *Mechanics of Materials*, 197 (2024): 105105.

[11] S. Družeta, S. Ivić, Indago-Python module for numerical optimization, 2020.

11th International Congress
of Croatian Society of Mechanics
September 30 – October 3 2025
Vodice, Croatia

A FEM iterative approach to the nonlocal integral elasticity of nanoplates

Andrea Caporale[*], Valentina Cima[*], Marzia Sara Vaccaro[**], Raffaele Barretta[**],

Raimondo Luciano[***]

[*]*Department of Civil and Mechanical Engineering, University of Cassino and Southern Lazio*
E-mails: {a.caporale,valentina.cima}@unicas.it

[**]*Department of Structures for Engineering and Architecture, University of Naples Federico II*
E-mails: {rabarret,marziasara.vaccaro}@unina.it

[***]*Department of Engineering, University of Naples Parthenope*
E-mail: {raimondo.luciano}@uniparthenope.it

Keywords: nanoplates, nonlocal integral elasticity, stress-driven, FEM, geometric nonlinearity.

1. Introduction

The behavior of small structures (e.g., NEMS) exhibits size effects that need to be considered in the theoretical modeling. To this end, many theories have been proposed in the last decades. Among the generalized continuum mechanics theories, the nonlocal continuum theory [1] considers that the stress at a point depends on an integral over the whole region occupied by the body (strain-driven approach). The relevant integro-differential equations governing the problem of nonlocal continua admit an equivalent differential formulation, which is constituted of only differential equations accompanied by appropriate constitutive boundary conditions [2]. Not considering the constitutive boundary conditions can lead to paradoxes in nonlocal nanobeams [3]. In one-dimensional nanostructures such as nanobeams and nanorods, exact closed-form solutions can be obtained from both the integro-differential and the differential formulation [4]. In two-dimensional nanostructures such as nanoplates, obtaining closed-form solutions is not straightforward, and numerical methods help treat the nonlocal problem. Romano et al. [5] introduced numerical iterative methods to solve nonlocal nanostructures and applied them to obtain numerical solutions of nanobeams in static bending. Later, Ussorio et al. [6] proposed an iterative analytical solution procedure to address the geometrically nonlinear problem of soft nanobeams.

2. Formulation

This work applies an iterative method to determine the nonlocal elastic solution of thin nanoplates in static bending. The adopted nonlocal continuum theory assumes that the elastic curvature vector $\boldsymbol{\chi}^{\mathrm{nl}}$ (strain) at a point depends on an integral convolution of the moment vector $\boldsymbol{M}$ (stress) over the whole region occupied by the body (stress-driven approach). The adopted iterative method is based on the solution of a sequence of linear problems solved using the finite element method (FEM). The finite element solution automatically guarantees that the strain-displacement equations and the equilibrium equations are satisfied through a local constitutive relationship between elastic curvature and moment. In nanoplates, a nonlocal constitutive law exists between elastic curvature $\boldsymbol{\chi}^{\mathrm{nl}}$ and moment $\boldsymbol{M}$. Therefore, the nonlocality of the $\boldsymbol{\chi}^{\mathrm{nl}}$-$\boldsymbol{M}$ constitutive law is imposed through the iterative method. Specifically, the nonlocal elastic curvature $\boldsymbol{\chi}^{\mathrm{nl}}$ is the integral convolution of the moment vector $\boldsymbol{M}$: in the FEM framework, the evaluation of the integral convolution is straightforward using Gauss quadrature. At a given iteration, the difference between the nonlocal and local elastic curvatures is a residual that is imposed in the next iteration. The iterations end when the residual is smaller than a given tolerance.

The proposed method is first applied to nonlocal nanoplates within the infinitesimal strain theory and then to the geometrically nonlinear problem of soft nanoplates. In the latter case, the von Kármán theory models the nonlinearity, characterized by small strains and moderate rotations. The FEM solves the incremental analysis; at each increment, the above-mentioned iterative method applies to make the $\boldsymbol{\chi}^{\mathrm{nl}}$-$\boldsymbol{M}$ constitutive law convergent to the nonlocality.

3. Conclusions

An iterative method is applied to determine the nonlocal elastic state of thin nanoplates in static bending. Two different formulations are presented, one within the infinitesimal strain theory and the other assuming geometric nonlinearity. In both formulations, the adopted iterative method requires the solution of a sequence of linear problems solved using the FEM. Gauss quadrature evaluates the integral convolution of the moment vector required by the iterative procedure and is also used to check the convergence of the method. Many numerical examples complete the presented work.

4. Acknowledgement

The research leading to these results has received funding from Project “2022ZW2NMJ - Nonlocal Mechanics of Innovative Soft Nanostructures (NoMISN)” CUP H53D23001410006 funded by European Union in NextGenerationEU plan, Mission 4, Component 2, Investment 1.1 through the Italian "Bando Prin 2022 - D.D. 104 del 02-02-2022" by MUR.

References

[1] Eringen, A.C., On differential equations of nonlocal elasticity and solutions of screw dislocation and surface waves. *Journal of Applied Physics*, 54, 4703-4710, 1983.

[2] Romano G., Barretta R., Stress-driven versus strain-driven nonlocal integral model for elastic nano-beams. *Composites Part B: Engineering*, 114, 184-188, 2017.

[3] Romano, G., Barretta, R., Diaco, M., Marotti de Sciarra, F., Constitutive boundary conditions and paradoxes in nonlocal elastic nanobeams. *International Journal of Mechanical Sciences*, 121, 151-156, 2017.

[4] Caporale A., Luciano R., Scorza D., Vantadori S., Local–nonlocal stress-driven model for multi-cracked nanobeams. *International Journal of Solids and Structures*, 273, art. no. 112230, 2023.

[5] Romano G., Barretta R., Diaco M., Iterative methods for nonlocal elasticity problems. *Continuum Mechanics and Thermodynamics*, 31, 669-689, 2019.

[6] Ussorio D., Vaccaro M.S., Barretta R., Luciano R., Marotti de Sciarra F., Large deflection of a nonlocal gradient cantilever beam. *International Journal of Engineering Science*, 206, art. no. 104172, 2025.

11th International Congress
of Croatian Society of Mechanics
September 30 – October 3 2025
Vodice, Croatia

Innovative Tensegrity-Based Roof Structures with Integrated Sun-Tracking Mechanisms

Rana Nazifi Charandabi[1], Julia de Castro Motta[2], Gerardo Carpentieri[2], Jordi Bonada Bo[3], Fernando Fraternali[2], Ada Amendola[2]

[1] *Department of Information Engineering, Electrical Engineering and Applied Mathematics (DIEM), University of Salerno, Via Giovanni Paolo II, 132 - 84084 Fisciano (SA), Italy.*
E-mail: rnazificharandabi@unisa.it

[2] *Department of Civil Engineering (DICIV), University of Salerno, Via Giovanni Paolo II, 132 - 84084 Fisciano (SA), Italy.*
E-mails: jdecastromotta@unisa.it, gcarpentieri@unisa.it, f.fraternali@unisa.it, adaamendola1@unisa.it

[3] *Department of Strength of Materials and Structural Engineering, Universitat Politècnica de Catalunya, Avinguda Diagonal 647 09028, Barcelona, Spain*
E-mail: jordi.bonada@upc.edu

Keywords: Tensegrity, Sun-tracking, Prestress, Minimal mass

1 Introduction

In recent years, the demand for sustainable and energy-efficient architectural solutions has grown significantly, particularly in the context of large-scale public infrastructures such as sports stadiums. These venues, due to their size and energy consumption, present both a challenge and an opportunity for innovation in structural design and renewable energy integration. Among the various strategies explored to address these challenges, deployable and modular systems have gained prominence for their adaptability, cost-effectiveness, and reduced environmental footprint.

This study introduces a novel approach to stadium roofing through the development of a modular, deployable structure that incorporates sun-tracking photovoltaic (PV) panels. The design is grounded in the principles of tensegrity—a structural concept based on a synergy between tensioned and compressed components—which enables the creation of lightweight yet stable and resilient systems [1, 2, 3]. Central to the design presented in this work is the V-Expander module, a newly engineered unit specifically optimized for minimal mass. This optimization not only improves structural efficiency but also enhances the system's ability to align with the sun, thereby maximizing the energy yield of the integrated PV panels.

To validate the proposed concept, a comprehensive analysis was carried out, encompassing both kinematic and mechanical investigations [3]. Particular attention was paid to the system's vibrational behavior, which was assessed through numerical simulations, as well as to the role of cable pre-tension in influencing the overall performance and stability of the structure. The results demonstrate that the proposed design achieves a favorable balance between mechanical efficiency and energy adaptability.

The findings of this research highlight the broader potential of tensegrity-based structures in the context of sustainable architecture. In particular, they showcase the adaptability of the V-Expander module for integration into a wide range of existing stadium roofing systems, offering a versatile solution that aligns with current goals in environmental performance, renewable energy utilization, and architectural innovation.

2 Deployable tensegrity-based roof structure

We examine the V-Expander cell proposed in [3], which is illustrated in Fig. 1. The upper roof panels in this structure are deployed by activating two struts positioned beneath each panel, a motion

achieved by altering the rest length of a looped cable connected to the struts' lower ends. This deployment mechanism operates by winding the bus cable around an external winch, allowing the struts to rise and rotate the panels until they reach a predefined maximum tilt angle.

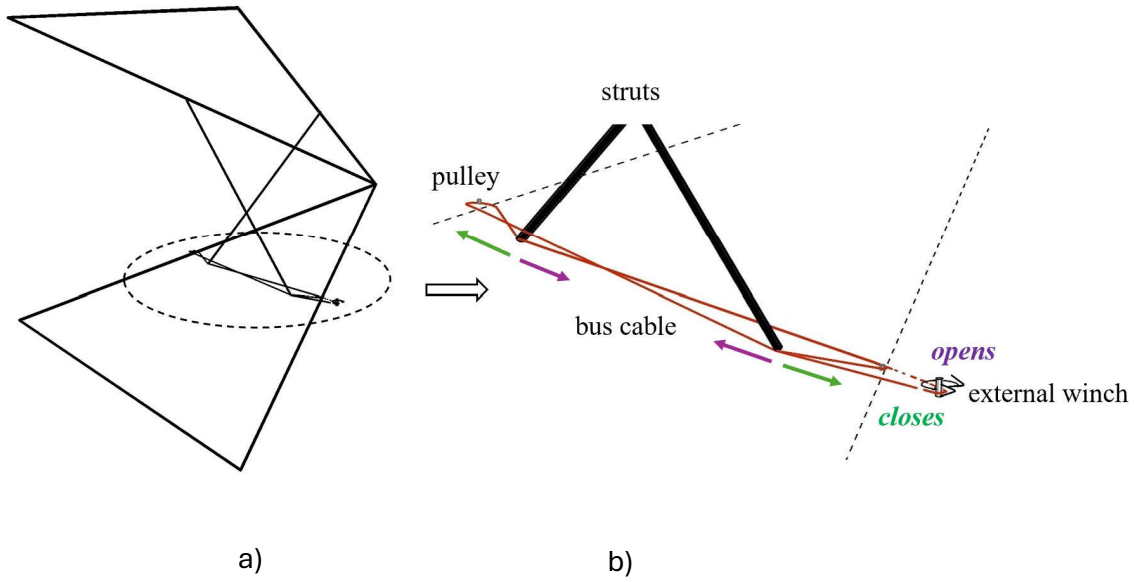


Figure 1. Deployable V-Expander roof unit. (Reproduced from [3], CC BY-NC-ND 4.0)

A minimal-mass design procedure for the system illustrated in Fig. 1 was presented in [1], along with a detailed structural analysis of a configuration employing this module to form a grandstand section of a sports stadium, under the action of dead loads, wind, and seismic forces. We refer the reader to that reference for the full details of the study.

3 Conclusions

The innovation introduced in the present study lies in the generalization of the original roof concept presented in [3], making it adaptable for integration with a wide range of existing roof structures. This enhancement significantly increases the versatility and practical relevance of the system, making it a viable solution for both new constructions and retrofitting applications in various architectural contexts. The proposed design is firmly rooted in the principles of tensegrity, which are particularly advantageous in deployable structures, where material efficiency, ease of transportation, and structural integrity are critical.

At the core of the design is the V-Expander module, a novel unit specifically engineered to minimize mass while maintaining structural performance. This mass optimization contributes directly to reduced material usage and lower energy demands during deployment and operation. Furthermore, the geometric configuration of the module enhances the dynamic adaptability of the structure, allowing the integrated photovoltaic panels to align optimally with the sun throughout the day. This feature leads to increased solar exposure and improved energy harvesting, as confirmed by prior analysis in Ref. [3].

References

[1] Fraternali, F., de Castro Motta, J., Germano, G., Babilio, E., Amendola, A., Mechanical response of tensegrity-origami solar modules. *Applications in Engineering Science*, 17, 100174, 2024.

[2] Fraternali, F., Babilio, E., Charandabi, R. N., Germano, G., Luciano, R., Spagnuolo, G., Dynamic origami solar eyes with tensegrity architecture for energy harvesting Mashrabiyas. *Applications in Engineering Science*, 19, 100190, 2024.

[3] R. N. Charandabi, R.N., Babilio, E., Carpentieri, G., Spagnuolo, G., Amendola, A., Fraternali, F., A tensegrity structure for a solar stadium roof with sun-tracking capability, *Thin-Walled Structures* 113033, 2025.

11th International Congress
of Croatian Society of Mechanics
September 30 – October 3 2025
Vodice, Croatia

Dynamics of stress-driven nonlocal beams using PINN approach

Baidehi Das[a], Raffaele Barretta[b], Marko Čanađija[c]

[a]*Department of Civil Engineering and Architecture, University of Catania, Viale Andrea Doria 6, Catania 95125, Italy*
E-mail: baidehi.das@phd.unict.it

[b]*Department of Structures for Engineering and Architecture, University of Naples Federico II, Via Claudio 21, Naples 80125, Italy*
E-mail: rabarret@unina.it

[c]*Department of Engineering Mechanics, University of Rijeka, Faculty of Engineering, Vukovarska 58, Rijeka 51000, Croatia*
E-mail: marko.canadija@riteh.uniri.hr

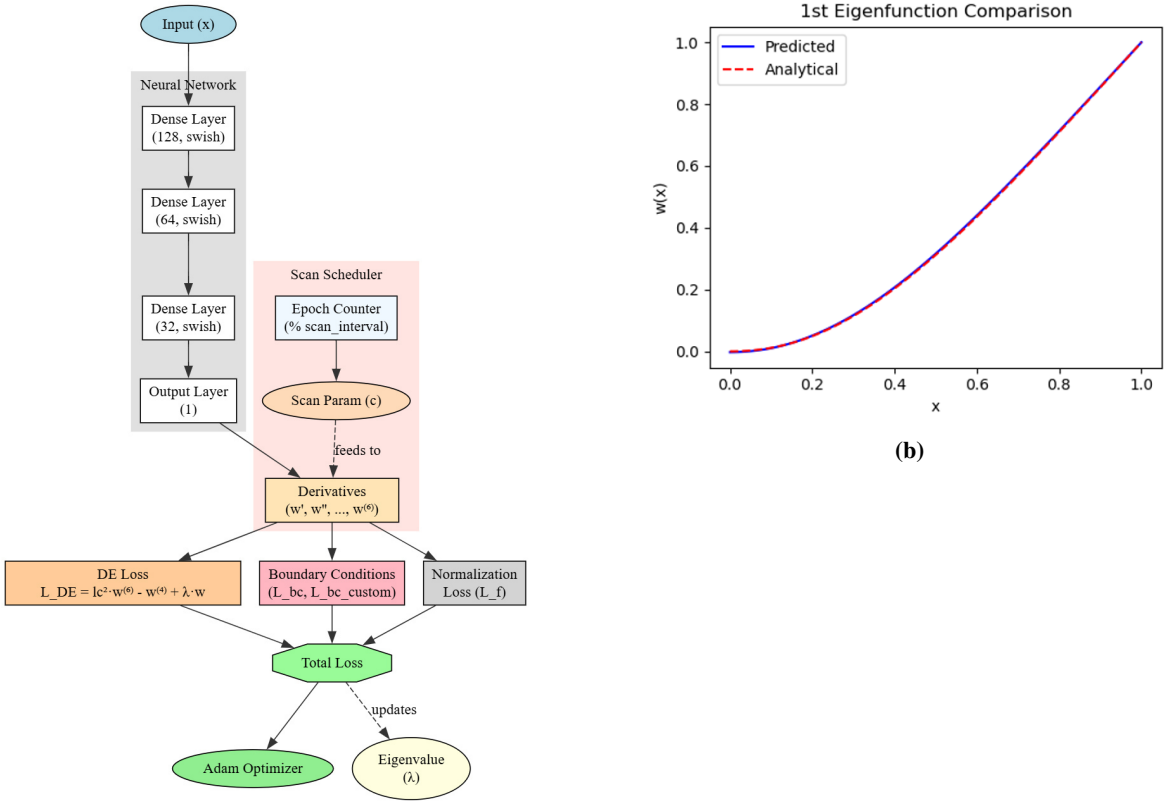
Keywords: Nonlocal elasticity, Nanobeams, Stress-driven nonlocal model, Physics-Informed Neural Networks (PINN)

1 Introduction

Nanotechnology in recent days is a grown interest amongst scientific community and undoubtedly, the design and fabrication of ultrasmall devices like the Micro-Electro-Mechanical systems (MEMS) and Nano-Electro-Mechanical systems (NEMS) in this realm having diverse applications, is worth mentioning. Studying nanostructural behavior of these micro and nanodevices, the effect of molecular and interatomic interactions cannot be overlooked leading to the proposal of several atomistic theories [1] to capture the behaviors at micro and nanoscales. However, these simulations are computationally intensive, prompting the use of nonlocal continuum theories like Eringen's nonlocal elasticity to model size-dependent behavior [2]. Although, it was implemented to address several engineering formulations but was proved to be ill-posed in case of structural mechanics problems[3]. Therefore, to tackle this issue in nonlocal continua, an effective stress-driven integral approach [4] was proposed that consistently solved this problem and was later implemented in solving several static and dynamic problems [5]. To address the complexity of analytical solutions for higher-order differential equations, a Physics-Informed Neural Networks (PINNs) approach [6, 7] offers a computationally efficient and accurate solution. The present study investigates the free vibration of a stress-driven nonlocal cantilever beam, comparing the results of robust PINN approach with benchmark analytical solutions, showing strong agreement and could be very useful to solve further complex problems related to the optimization and design of nanodevices.

2 Methodology

A PINN approach is proposed to investigate the dynamics of nonlocal cantilever beams using Stress-Driven Nonlocal Method. The constitutive and kinematic boundary conditions are defined in terms of respective losses as shown in Fig. 1a. The total loss calculated by training gives an idea about how accurate the predicted model is to that of the analytical results. The analytical formulation has been previously conducted in Wolfram Mathematica that provides the reference to our neural network model. The predicted model shows very promising coherence with the analytical result with minimization of total loss, as shown in Fig. 1b.



(a)

(b)

Figure 1. (a) PINN Architecture (b) Predicted vs Analytical Eigenfunction

3 Conclusion

The proposed Physics Informed Neural Network is able to predict the analytical first eigenfunction and also the predicted eigenvalue obtained is quite close to the analytical one (2.5 % deviated). This approach could be further implemented to solve more complex computational problems, particularly in capturing size-dependent structural responses of smaller and smaller wires, curved beams, plates and shells of current interest in Nano-Engineering.

References

[1] Mojtaba Shariati, Babak Azizi, Mohammad Hosseini, and Mohammad Shishesaz. On the calibration of size parameters related to non-classical continuum theories using molecular dynamics simulations. *International Journal of Engineering Science*, 168:103544, 2021.

[2] A Cemal Eringen. On differential equations of nonlocal elasticity and solutions of screw dislocation and surface waves. *Journal of applied physics*, 54(9):4703–4710, 1983.

[3] Giovanni Romano, Raffaele Barretta, Marina Diaco, and Francesco Marotti de Sciarra. Constitutive boundary conditions and paradoxes in nonlocal elastic nanobeams. *International Journal of Mechanical Sciences*, 121:151–156, 2017.

[4] Giovanni Romano and Raffaele Barretta. Nonlocal elasticity in nanobeams: the stress-driven integral model. *International Journal of Engineering Science*, 115:14–27, 2017.

[5] Marzia Sara Vaccaro, Francesco Pinnola, Francesco Marotti de Sciarra, and Raffaele Barretta. Dynamics of stress-driven two-phase elastic beams. *Nanomaterials*, 11:1138, 04 2021.

[6] Liam Harcombe and Quanling Deng. Physics-informed neural networks for discovering localised eigenstates in disordered media. *Journal of Computational Science*, 73:102136, 2023.

[7] Henry Jin, Marios Mattheakis, and Pavlos Protopapas. Physics-informed neural networks for quantum eigenvalue problems. *International Joint Conference on Neural Networks (IJCNN)*, 2022.

11th International Congress
of Croatian Society of Mechanics
September 30 – October 3 2025
Vodice, Croatia

Variational formulations in plasticity and viscoplasticity with a consistent derivation of computational algorithms

Fabio De Angelis*

*Department of Structures for Engineering and Architecture,
University of Naples Federico II, via Claudio 21, Naples 80125, Italy
E-mail: fabio.deangelis@unina.it

Keywords: plasticity, viscoplasticity, variational formulations, computational algorithms.

1. Introduction

In this work a multifield variational formulation is addressed for solids and structures. The variational framework encompasses solids and structures with plasticity and viscoplasticity constitutive behaviour. The treatment is capable to include problems characterized by singularities and non-smooth functions. A multifield variational potential is derived and the corresponding multifield variational principle is formulated. The procedure allows the derivation of a consistent set of variational principles in the different combination of the unknown variables. Furthermore, the procedure is complemented with the definition of variationally consistent computational algorithms for finite element applications in the analysis of inelastic behaviour of solids and structures. The presented algorithmic procedure reduces the solution of the local constitutive equation to a single variable algebraic equation in the plastic rate parameter. The analytical solution of the algebraic equation can be found in exact closed form.

2. A procedure for deriving variational formulations in plasticity and viscoplasticity with a consistent derivation of computational algorithms

In the present analysis a variational formulation for viscoplasticity is considered and applied to problems of solids and structures, see e.g. Perzyna [1], Skrzypek and Hetnarski [2], Oden and Reddy [3]. A strategy is illustrated for the derivation of variational principles by including the nonlinear field equations and the constitutive multivalued equations into a viscoplastic operator governing the structural problem, see e.g. De Angelis [4]. A consistent procedure is illustrated for deriving a multifield potential in all the unknown variables of the viscoplastic structural problem and accordingly the relevant multifield variational principle is presented.

The proposed procedure shows to be appropriate for the consistent derivation of variational principles in viscoplasticity suitable to deal with problems characterized by singularities and non-smooth functions, see De Angelis [5][6]. The presented treatment provides the support for a variationally consistent development of numerical algorithms for finite element applications in the inelastic analysis of solids and structures. An implicit numerical scheme is adopted. The procedure has the advantage of being applicable to different constitutive models by suitably specializing the viscoplastic flow function, see De Angelis and Cancellara [7]. The computational approach is also enhanced by deriving a tangent operator which can be adopted for different constitutive models.

The present procedure reduces the local constitutive equation to the solution of a single variable algebraic equation in the plastic rate parameter. The analytical solution of the algebraic equation in the plastic rate parameter can be found in exact closed form, see De Angelis and Taylor [8][9]. A remarkable feature of the present approach is that no iterative solution method is needed to solve the local constitutive equations of three-dimensional problems with nonlinear kinematic hardening rules. Computational results and examples are presented to illustrate the effectiveness of the proposed approach for different types of cyclic and complex loading conditions in solids with nonlinear kinematic hardening rules, see e.g. De Angelis and Taylor [8][9].

3. Conclusions

Variational formulations are investigated, and a suitable procedure is discussed for deriving a multifield variational formulation for solids and structures. The variational formulation includes the plasticity and viscoplasticity constitutive behaviour of solids. The formulation is presented within the framework of convex analysis and subdifferential calculus and is capable to include the treatment of problems characterized by singularities and non-smooth functions.

From the multifield variational principle a consistent set of variational principles is derived in the different combinations of the unknown variables. Accordingly, a complete set of variational principles is presented in plasticity and viscoplasticity problems of solids and structures.

The presented variational formulation can provide a suitable framework for the derivation of consistent computational algorithms for finite element applications in the plastic and viscoplastic analysis of solids and structures. At this regard a proper algorithmic procedure is applied in which the solution of the local constitutive inelastic problem reduces to a single variable algebraic equation in the plastic rate parameter. The analytical solution of the algebraic equation can be found in exact closed form by avoiding the necessity of iterative procedures for the solution of the local constitutive problem with nonlinear kinematic hardening rules.

References

[1] Perzyna, P., The constitutive equations for rate sensitive materials, *Quart. Appl. Math.*, Vol. 20, pp. 321-332, 1963.

[2] Skrzypek, J.J., Hetnarski, R.B., *Plasticity and Creep*, Begell House CRC Press, Boca Raton, 1993.

[3] Oden, J.T., Reddy, J.N., *Variational Methods in Theoretical Mechanics*, Springer, New York, 1983.

[4] De Angelis, F., An internal variable variational formulation of viscoplasticity, *Computer Methods in Applied Mechanics and Engineering*, Vol. 190, pp. 35-54, 2000.

[5] De Angelis, F., A multifield variational formulation of viscoplasticity suitable to deal with singularities and non-smooth functions, *Int. Journal of Engineering Science*, Vol. 172, Art. 103616, pp. 1-16, 2022.

[6] De Angelis, F., An internal variable treatment of evolutive problems in hardening plasticity and viscoplasticity with singularities, *Continuum Mechanics and Thermodynamics*, Vol. 35, pp. 1807-1819, 2023.

[7] De Angelis, F., Cancellara, D., Multifield variational principles and computational aspects in rate plasticity, *Computers and Structures*, Vol. 180, pp. 27-39, 2017.

[8] De Angelis, F., Taylor, R.L., An efficient return mapping algorithm for elastoplasticity with exact closed form solution of the local constitutive problem, *Engineering Computations*, Vol. 32, Issue 8, pp. 2259-2291, 2015.

[9] De Angelis, F., Taylor, R.L., A nonlinear finite element plasticity formulation without matrix inversions, *Finite Elements in Analysis and Design*, Vol. 112, pp. 11-25, 2016.

11th International Congress
of Croatian Society of Mechanics
September 30 – October 3 2025
Vodice, Croatia

Integral solution of Stress-Driven Nonlocal Model with Morozov regularization on different nonlocal kernels

Rosa Penna, Giuseppe Lovisi and Luciano Feo

University of Salerno,Department of Civil Engineering, Fisciano (SA), 84084

E-mails: {rpenna@unisa.it, glovisi@unisa.it, lfeo@unisa.it}

Keywords: nonlocal, nanobeam, Morozov discrepancy principle, Stress-Driven nonlocal model, boundary effects.

1. Introduction

In this work, we present a comprehensive analysis of the nonlocal Stress-Driven Model (SDM) in its integral formulation [1], focusing on the bending behavior of Bernoulli-Euler nanobeams. Unlike traditional approaches - which typically reformulate the original integro-differential problem into an equivalent differential equation via the Helmholtz kernel [2] - this study introduces and implements a rigorous numerical strategy to directly solve the integral equation across a broad class of nonlocal kernels. Specifically, we investigate six distinct convolution kernels: Helmholtz, Gaussian, Lorentzian (Cauchy), Triangular, Bessel, and Hyperbolic Cosine (Figure 1).

These kernels are examined in terms of their mathematical properties (Table 1) - including symmetry, regularity, support, and decay - and their influence on the model's solutions.

Kernel	Symmetry	Decay Rate	Support	Smoothness
Helmholtz	Yes	Exponential (fast)	Infinite	C^∞
Gaussian	Yes	Exponential (moderate)	Infinite	C^∞(smooth)
Lorentzian	Yes	Exponential (moderate)	Infinite	C^∞
Bessel	Yes	Power-law (slow)	Infinite	C^∞
Triangular	Yes	Linear (fast)	Finite	C^1
Hyperbolic Cosine	Yes	Intermediate	Infinite	C^∞

Table1. Mathematical properties of various types of nonlocal kernels.

A major computational challenge stems from the ill-posed nature of the integral operators associated with many of the nonlocal kernels, particularly in the presence of long-range interactions. To address this issue, we adopt Morozov's discrepancy principle, a well-established regularization technique for handling ill-posed problems. This method enables the adaptive selection of an optimal regularization parameter through a bisection approach, ensuring a balance between numerical stability and physical fidelity. Furthermore, the spatial domain discretization and the optimization of nodal point density are carried out adaptively, guided by criteria aimed at minimizing the normalized residual of the regularized system. Special attention is given to boundary effects, which are often neglected in theoretical studies but play a critical role in numerical implementations over finite domains [3]. To mitigate the asymmetry and loss of normalization of kernels near the domain boundaries, we propose a

systematic local clipping and renormalization procedure. This approach preserves the weighted averaging property of the kernel, even in proximity to the edges a correction particularly vital for kernels with infinite support or slow decay. The proposed methodology is validated through numerical comparisons with known analytical solutions for the Helmholtz kernel [4]. Results show that the method delivers accurate and stable solutions, with errors consistently below 1% relative to reference values. A comparative study across different kernels reveals a general stiffening effect of the nonlocal model as the nonlocal parameter increases, with the intensity of this effect depending on the specific kernel shape. In the absence of renormalization, significant deviations from the local behavior are observed - especially for kernels other than Helmholtz - while the proposed strategy ensures correct convergence to the local limit as the nonlocal parameter approaches zero.

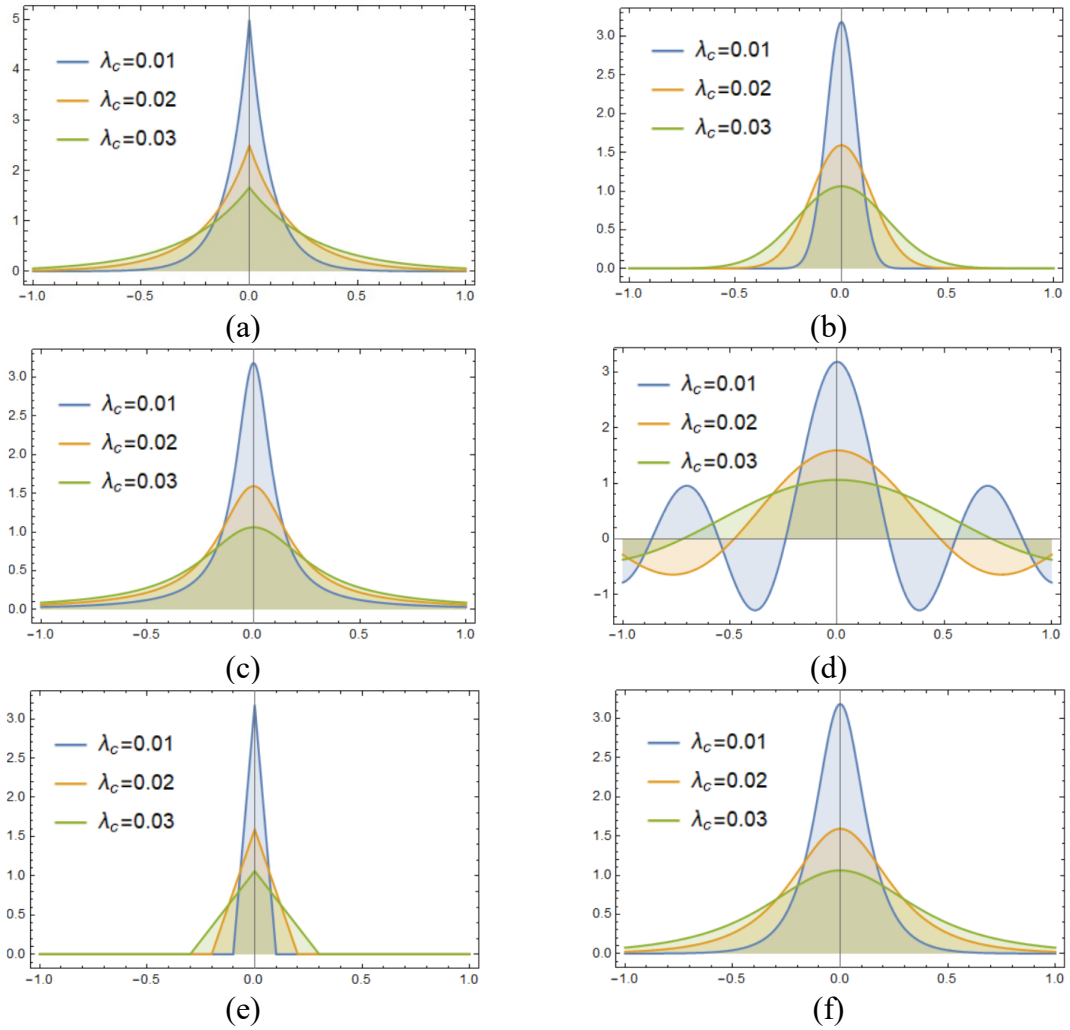


Figure 1. Nonlocal kernels: (a) Helmholtz kernel, (b) Gaussian kernel, (c) Lorentzian kernel, (d) Bessel kernel, (e) Triangular kernel, (f) Hyperbolic Cosine kernel

2. Conclusions

In conclusion, this work advances a robust and general integral formulation of the Stress-Driven Model, expanding the range of kernels that can be treated numerically and providing effective tools for managing boundary effects. These contributions are particularly relevant for applications in nanostructures and advanced material mechanics.

This work was supported by the National Recovery and Resilience Plan (NRRP), Mission 4, Component 2, Investment 1.1 (Call No. 104, 2.2.2022), funded by the European Union – NextGenerationEU – under the project "Intelligent Systems for Infrastructural Diagnosis in Smart Concrete (ISIDE)" (Grant No. 2022S88WAY, CUP: D53D23008820006). Additional support was provided by the PRIN 2020 Research Grant No. 2020EBLPLS, titled "Opportunities and Challenges of Nanotechnology in Advanced andGreen Construction Materials."

References

[1] Giovanni Romano, Raffaele Barretta, Nonlocal elasticity in nanobeams: the stress-driven integral model, International Journal of Engineering Science, Volume 115, 2017, Pages 14-27, ISSN 0020-7225,https://doi.org/10.1016/j.ijengsci.2017.03.002.

[2] Rosa Penna, Luciano Feo, Giuseppe Lovisi, Hygro-thermal bending behavior of porous FG nanobeams via local/nonlocal strain and stress gradient theories of elasticity, Composite Structures, Volume 263, 2021, 113627, ISSN 0263-8223, https://doi.org/10.1016/j.compstruct.2021.113627.

[3] Sansit Patnaik, Sai Sidhardh, Fabio Semperlotti, Displacement-driven approach to nonlocal elasticity, European Journal of Mechanics - A/Solids, Volume 92, 2022, 104434, ISSN 0997-7538,https://doi.org/10.1016/j.euromechsol.2021.104434.

[4] Raffaele Barretta, Marko Canadija, Luciano Feo, Raimondo Luciano, Francesco Marotti de Sciarra, Rosa Penna, Exact solutions of inflected functionally graded nano-beams in integral elasticity, Composites Part B: Engineering, Volume 142, 2018, Pages 273-286, ISSN 1359-8368, https://doi.org/10.1016/j.compositesb.2017.12.022.

11th International Congress
of Croatian Society of Mechanics
September 30 – October 3 2025
Vodice, Croatia

Micromechanical model and experimental investigation of the piezoelectric response in CNTs – based cement composites

Rosa Penna, Giuseppe Lovisi, Annavirginia Lambiase, Gerarda Landi and Luciano Feo

University of Salerno,Department of Civil Engineering, Fisciano (SA), 84084

E-mails: {rpenna@unisa.it, glovisi@unisa.it, annalambiase@unisa.it, gelandi@unisa.it, lfeo@unisa.it}

Keywords: micromechanical model, CNT cement matrix-composites, piezoelectric material, self-sensing, structural health monitoring.

1. Introduction

This study presents an integrated micromechanical and experimental investigation into the piezoelectric and piezoresistive behavior of cement-based composites reinforced with Multi-Walled Carbon Nanotubes (MWCNTs), aimed at developing advanced multifunctional materials for Structural Health Monitoring (SHM) applications [1]. A novel micromechanical model is introduced, based on methodologies established for polymer matrix materials [2,3], to predict the electrical conductivity and piezoelectric properties of MWCNT-reinforced cement composites. The model accounts for key parameters such as nanotube geometry, concentration, waviness, tunneling potential barrier height, and introduces an innovative quantum-mechanics-based approach to estimate the inter-nanotube matrix thickness (Figure 1).

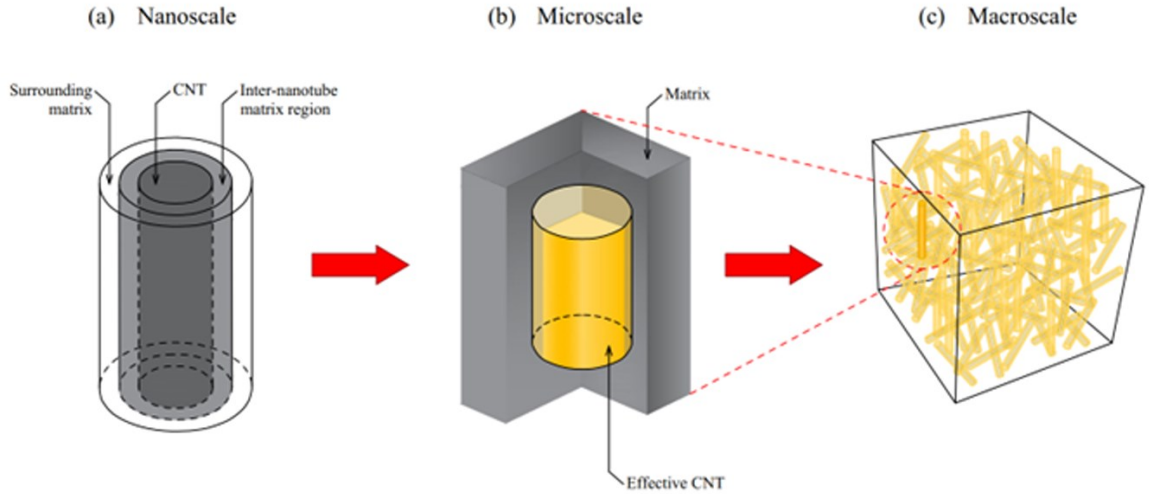


Figure 1. Schematic illustration of the micromechanical modeling of a cement-based composite at the (a) nanoscale, (b) microscale and (c) macroscale.

Validation against literature data confirms [4-6] its reliability and effectiveness in exploring structure–property relationships in cementitious matrices (Figure 2).
Complementing the modeling, a series of preliminary experiments were carried out at the University of Salerno's Materials and Structures Testing Laboratory to assess the mechanical and piezoresistive behavior of these nanocomposites. Specimens using Ordinary Portland Cement (42.5R) and varying MWCNT contents were fabricated, with dispersion improved

through ultrasonic agitation and Sodium Dodecyl Sulfate (SDS) surfactant treatment. The experimental results demonstrated good strain-sensing capabilities and confirmed the feasibility of using MWCNT-reinforced composites as self-sensing materials. This combined theoretical and experimental approach offers a robust framework for the design of cementitious materials that overcome the limitations of conventional SHM systems - such as vulnerability to environmental conditions and limited spatial coverage - by enabling the material itself to act as an integrated sensor.

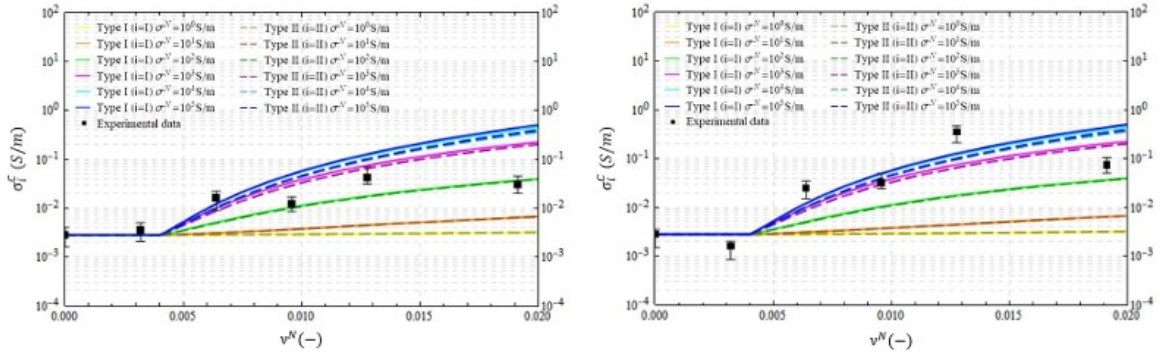


Figure 2. Comparison between modeling results and experimental for the cement pastes data available in the literature [4,5,6].

2. Conclusions

The new model was validated by comparing analytical predictions with experimental data already available in the literature, revealing strong consistency between the obtained results. Furthermore, the comparison between the obtained analytical results and experimental data for various cementitious materials - including cement pastes, mortars, and concretes - demonstrates the reliability of the proposed model and its accuracy in reproducing the reported conductivity values. Finally, to gain a better understanding of the factors influencing the electrical behavior of CNT-cement composites, a sensitivity analysis was conducted, followed by a detailed parametric study. The developed analytical model, characterized by simplicity and efficiency, represents a valuable tool for investigating the relationship between structure and properties in CNT- cement-matrix composites. This methodology lays a foundation for designing new multifunctional cementitious materials with promising applications in Structural Health Monitoring, where they can be employed as smart sensors for real-time structural monitoring.

This work was supported by the National Recovery and Resilience Plan (NRRP), Mission 4, Component 2, Investment 1.1 (Call No. 104, 2.2.2022), funded by the European Union – NextGenerationEU – under the project “Intelligent Systems for Infrastructural Diagnosis in Smart Concrete (ISIDE)” (Grant No. 2022S88WAY, CUP: D53D23008820006). Additional support was provided by the PRIN 2020 Research Grant No. 2020EBLPLS, titled “Opportunities and Challenges of Nanotechnology in Advanced andGreen Construction Materials.”

References

[1] Han, B., Ding, S., and Yu, X. (2015a). “Intrinsic self-sensing concrete and structures: A review.”Measurement, 59, 110–128.

[2] Deng F, Zheng QS. An analytical model of effective electrical conductivity of carbon nanotube composites. Appl Phys Lett 2008;92:071902.

[3] Takeda T, Shindo Y, Kuronuma Y, Narita F. Modeling and characterization of the electrical conductivityof carbon nanotube-based polymer composites. Polymer 2011;52:3852-6.

[4] Li H, Xiao H, Yuan J, Ou J. Microstructure of cement mortar with nano-particles. Compos B Eng 2004;35:185–9. 57.

[5] E. García-Macías, A. D'Alessandro, R. Castro-Triguero, et al., Micromechanics modeling of the uniaxial strain-sensing property of carbon nanotube cement- matrix composites for SHM applications, Compos. Struct. 163 (2017) 195–215. 58.

[6] Enrique García-Macías, Antonella D'Alessandro, Rafael Castro-Triguero, Domingo Pérez-Mira, Filippo Ubertini, Micromechanics modeling of the electrical conductivity of carbon nanotube cement-matrix composites, Composites Part B: Engineering, Volume 108, 2017, Pages 451-469, ISSN 1359-8368, https://doi.org/10.1016/j.compositesb.2016.10.025.

11th International Congress
of Croatian Society of Mechanics
September 30 – October 3 2025
Vodice, Croatia

Granular micromechanics based formulation of damage-elasto-plasticity: hysteric cycles and fatigue

Luca Placidi*, Anil Misra+, Francesco Fabbrocino**, Raimondo Luciano++

*Università Telematica Internazionale Uninettuno
E-mails: lplacidi@gmail.com

+Florida International University
E-mails: anmisra@fiu.edu

**Pegaso University
E-mail: francesco.fabbrocino@unipegaso.it

++Parthenope University of Naples
E-mail: raimondo.luciano@uniparthenope.it

Keywords: Hemivariational approach, plasticity, hysteric cycles, fatigue, granular micromechanics

1 Extended abstract

In this presentation we report a new framework for plasticity, that was developed in [1] for the 1D axial case. It is based on a hemivariational procedure, similar to that developed in damage mechanics in [2], where a damage variable is assumed to have a mono lateral behaviour by imposing positive sign of damage velocity. In order to do this, the plastic displacement u^{pl} of an elasto-plastic spring is decomposed as the difference between two plastic multipliers: the accumulated plastic tension λ^t and the accumulated plastic compression λ^c,

$$u^{pl} = \lambda^t - \lambda^c. \tag{1}$$

Each of the two accumulation variables have the same mono-lateral property of the damage in [2]. We show, in this hemivariational approach, the derivation of the phenomenology of standard perfect plasticity, of linear (see e.g. [3]) and isotropic hardening. Besides, by insertion of proper coupling between damage and plastic variables, also the derivation of fatigue's effect, with the inclusion of the Whöler diagram, is possible. We end this first part with the derivation of an elasto-plastic Euler-Bernoulli beam. The 3D generalization is not easy with this approach. However, in granular micromechanics the pair interaction is of the same nature of the spring developed in the first part of the presentation and the plastic part of the normal displacement u_η is decomposed in the same way of 1,

$$u_\eta^{pl} = \lambda_\eta^t - \lambda_\eta^c. \tag{2}$$

We will show that the density U of the elastic internal energy

$$U = \frac{1}{2}\mathbb{C}_{ijab}G_{ij}G_{ab} + \mathbb{P}_{ij}G_{ij}, \tag{3}$$

has not only a standard quadratic term with respect to the strain tensor G but also a linear term, with the identification of the following pre-stress tensor,

$$\mathbb{P}_{ij} = -L\int_{\mathscr{S}^1} k_\eta u_\eta^{pl}\hat{c}_i\hat{c}_j d\theta, \tag{4}$$

where the integration is done over all the orientations (represented by the unit vector $\hat{c}$, which is also parameterized by an angle θ in the present 2D context) and where L represents the inter-granular

distance. It is worth to note the k_η is the normal stiffness. The energy functional $\mathscr{E}$ is defined as the sum of the elastic internal strain part U with the inclusion of the external one, and of the dissipation potential W energy densities,

$$\mathscr{E}\left(\chi, \lambda_\eta^t, \lambda_\eta^c\right) = \int_{\mathscr{B}} \left[U + W - b_i^{ext}\chi_i\right] dV - \int_{\partial_N \mathscr{B}} \left[t_i^{ext}\chi_i\right] dV. \tag{5}$$

b^{ext} represents the external distributed body force acting on the surface $\mathscr{B}$, while t^{ext} denotes the external distributed force applied to the portion $\partial_N \mathscr{B}$ of the boundary $\partial\mathscr{B}$ where the placement χ is not prescribed (i.e., where Dirichlet boundary conditions of placement type are not enforced) and Neumann boundary conditions of force type are applied. In strain gradient materials the set of possible external action prescription is larger than that considered for the sake of simplicity in (5) and includes concentrated and double forces at specific and different portions of the boundary $\partial\mathscr{B}$. However, for the sake of simplicity we consieder only the external energy terms included in (5).

Thus, in the second part of the presentation we will derive, according to [4], the desired 3D generalization of the present approach to plasticity. Finally, we will show applications in geotechnics [5] and in ultra high performance fiber-reinforced concrete (uhp frc) [6].

References

[1] Placidi, L. (2016). A variational approach for a nonlinear one-dimensional damage-elasto-plastic second-gradient continuum model. *Continuum Mechanics and Thermodynamics*, 28, 119-137.

[2] Francfort, G. A., Marigo, J. J. (1998). Revisiting brittle fracture as an energy minimization problem. *Journal of the Mechanics and Physics of Solids*, 46(8), 1319-1342.

[3] Placidi, L., Misra, A., Kandalaft, A., Nayeban, M. M., Yilmaz, N. (2024). Analytical results for a linear hardening elasto-plastic spring investigated via a hemivariational formulation. *Constructive Mathematical Analysis*, 7(Special Issue: AT&A), 50-75.

[4] Placidi, L., Barchiesi, E., Misra, A., Timofeev, D. (2021). Micromechanics-based elasto-plastic–damage energy formulation for strain gradient solids with granular microstructure. *Continuum Mechanics and Thermodynamics*, 33(5), 2213-2241.

[5] Yilmaz, N., Yildizdag, M. E., Fabbrocino, F., Placidi, L., Misra, A. (2024). Emergence of critical state in granular materials using a variationally-based damage-elasto-plastic micromechanical continuum model. International *Journal for Numerical and Analytical Methods in Geomechanics*, 48(13), 3369-3391.

[6] Placidi, L., Dell'Isola, F., Kandalaft, A., Luciano, R., Majorana, C., Misra, A. (2024). A granular micromechanic-based model for ultra high performance fiber-reinforced concrete (uhp frc). *International Journal of Solids and Structures*, 297, 112844.

11th International Congress
of Croatian Society of Mechanics
September 30 – October 3 2025
Vodice, Croatia

On Clapeyron Theorem in Linear Elasticity

Giovanni Romano[1], Raffaele Barretta[2], Marina Diaco[2]

[1]*Alma Mater and past professorship: University of Naples Federico II, Naples, Italy.*
[2]*Department of Structures for Engineering and Architecture, University of Naples Federico II, via Claudio 21, Naples, 80125, Italy.*
E-mails: gromano1941@gmail.com, rabarret@unina.it, diaco@unina.it

Keywords: Standing structural models, Virtual power and work principles, CLAPEYRON*'s theorem.*

1 Introduction

During the early 1830s, two pioneering papers concerning internal equilibrium problems were proposed by Benoît Paul Émile CLAPEYRON and Gabriel LAMÉ in [1,2]. In the middle of the XIX century LAMÉ [3] provided the following essential description of a brilliant theorem provided by Émile CLAPEYRON expressing the energy stored in a linearly elastic structure which is standing during the dynamic process of loading from an initial to a final state of static equilibrium.

In 1927, a further proof of the formula was given by Augustus Edward Hough LOVE in [4, p.173] and in 1946 CLAPEYRON's theorem was so stated by Ivan Stephan SOKOLNIKOFF in [5]:
"If a body is in equilibrium under a given system of body forces and surface forces, then the strain energy of deformation is equal to one-half the work that would be done by the external forces (of the equilibrium state) acting through the displacements from the unstressed state to the state of equilibrium." The *work that would be done* here has to be intended as the *virtual work* done.

The topic was again discussed by Roger Lee FOSDICK and Lev TRUSKINOWSKI in [6] where it is claimed that the stored elastic energy represents only half of the work done by the external forces, the remaining half being lost somewhere in achieving the equilibrium state, and labeled the result as paradoxical and incomplete. Therefore, FOSDICK and TRUSKINOWSKI suggested adoption of dissipative constitutive models to account for thermo-viscous phenomena in the material, thus bringing the structure out of the elastic range. Their analysis was seriously flawed in two main respects: Firstly, in CLAPEYRON's theorem what is compared to the elastic energy is the product (or better the virtual work) between incremental forces and displacement and not the work performed by the applied force. Moreover, no dissipation in the material is needed to be assumed. On physical ground what plays the decisive role is the dispersion of kinetic energy in the fluid surrounding the elastic structure. The same dispersion occurs when any elastic structure is loaded and this fact is at the very basis of the engineering computation of elastic structures.

With their improper analysis, FOSDICK and TRUSKINOWSKI have unconsciously concluded that elastic structural design performed in the last two centuries should be discarded as paradoxical and incomplete, despite physical evidence of the contrary, documented by countless engineering successes. The present contribution is aimed at providing a correct formulation of CLAPEYRON's theorem and at clarifying the alleged paradox without leaving the framework of linear elasticity.

2 Clapeyron's theorem

The transition of an elastic structure from an initial state to a final state of static equilibrium requires the dispersion of the kinetic energy involved in the dynamic process.

Notably, the kinetic energy is dispersed by the contact of the elastic structure with its surrounding fluid environment. Without dispersion, the motion imparted to the elastic structure by the loading process would never come to a stop, contradicting physical evidence.

Treatments of CLAPEYRON's theorem in literature consider the loading process under investigation to start from a ground-state with vanishing stress and elastic-state fields.

The present formulation refers to a standing linear elastic structure, undergoing small displacements and deformations, and a loading process which may induce dynamic effects, while evolving from an initial to a final state of static equilibrium. Exploiting the Incremental Virtual Work Principle [7, 8], the following equality can be proven

$$\langle \Delta\ell, \mathbf{u} \rangle_\Omega = \int_\Omega \langle \mathbf{E}(\mathbf{D}(\mathbf{u})), \mathbf{D}(\mathbf{u}) \rangle \mathbf{m} = 2 \int_\Omega \varphi(\mathbf{D}(\mathbf{u})) \mathbf{m}, \tag{1}$$

where $\Delta\ell$ is the incremental external loading, $\mathbf{D}(\mathbf{u})$ is the linearised geometric deformation generated by the displacement field $\mathbf{u} \in T_\Omega S$ (based on the configuration Ω and tangent to EUCLID space S), $\mathbf{E}$ is the linear elastic stiffness and φ is a quadratic elastic potential such that $d\varphi = \mathbf{E}$.

Eq. (1) is the statement of CLAPEYRON's theorem in incremental form [9]:

"In an elastic structure loaded from an initial to a final state, both in static equilibrium, the incremental elastic energy is independent of the loading process set out and, as long as the structure evolves in a linear elastic regime of small displacements, it is equal to half the virtual work of the load increment for the induced displacement."

3 Conclusion

CLAPEYRON's theorem, formulated nearly two centuries ago, provides a simple formula for expressing the energy stored in a linearly elastic structure which is standing during the dynamic process of loading from an initial to a final state of static equilibrium. A careful formulation of the theorem is here presented to clarify assumptions and range of validity. Beauty and power of CLAPEYRON's theorem are recovered, showing that the formula, as equality based on variational conditions of equilibrium and on linear elasticity, is independent of the way dispersion occurs and of its amount, provided that the dynamic process of the structure evolves in a linear elastic range for the stress field in the material.

Acknowledgments

Financial support from the Italian Ministry of University and Research (MUR) in the framework of the Project PRIN 2022 PNRR code P20223PLC2 "Nonlocal modelling of nano-coatings" are gratefully acknowledged.



References

[1] Lamé, G., Clapeyron, B.: "Mémoire sur l'équilibre intérieur des corps solides homogènes. (Suite)." Journal für die reine und angewandte Mathematik **7**, 381–413 (1831) `http://eudml.org/doc/146751`.

[2] Lamé, G., Clapeyron, É.: Mémoire sur léquilibre intérieur des corps solides homogénes. Mém. Divers Savants **IV**, 463–562 (1833)

[3] Lamé, G.: Leçons sur la théorie mathématique de l'élasticité des corps solides. Bachelier, Paris (1852)

[4] Love, A.E.H.: A Treatise on the Mathematical Theory of Elasticity. 4th ed. Cambridge University Press (1927). Reprint by Dover Publications, New York (1944)

[5] Sokolnikoff, I.S.: Mathematical Theory of Elasticity. McGraw-Hill Company, first ed. 1946, 2nd ed. 1956.

[6] Fosdick, R.L., Truskinowsky, L.: About Clapeyron's Theorem in Linear Elasticity. Journal of Elasticity **72**, 145–172 (2003)

[7] Romano, G.: Continuum Mechanics and Electrodynamics: Geometric Foundations. About 1800 pages (in completion) (2024) posted in `https://gioprof1941.web.app`

[8] Romano, G., Barretta, R.: Advancements in Continuum Mechanics and Electrodynamics by a spacetime geometric approach. Acta Mech. **235**, 4357–4399 (2024)

[9] Romano, G., Barretta, R., Diaco, M.: Genesis, degeneracy and progress of Clapeyron theorem in linear elasticity. Journal of Applied and Computational Mechanics. To appear (2025)

11th International Congress
of Croatian Society of Mechanics
September 30 – October 3 2025
Vodice, Croatia

Stress-driven nonlocal elasticity for higher-order nanobeams

Marzia Sara Vaccaro*, Raffaele Barretta*, Raimondo Luciano+, Francesco Marotti de Sciarra*

*Department of Structures for Engineering and Architecture, University of Naples Federico II, via Claudio 21, Naples, 80125, Italy.
E-mails: marziasara.vaccaro@unina.it, rabarret@unina.it,marotti@unina.it

+Department of Engineering, University of Naples Parthenope, via Amm. F. Acton 38, Naples, 80133, Italy.
E-mail: raimondo.luciano@uniparthenope.it

Keywords: Higher-order beam theory; Stress-driven integral elasticity; Nanobeams.

1 Introduction

The size dependent behavior of higher-order nanobeams is addressed by exploiting the stress-driven nonlocal approach. Several shear deformation beam theories are adopted, eliminating the need for shear correction factors that is a crucial point in the framework of nonlocal elasticity. By combining higher-order shear deformation theories with the stress-driven integral model, a consistent nonlocal methodology is derived. Exemplar case studies are solved and commented upon to show the effectiveness of the proposed approach.

2 Modeling and analysis

Innovative nanotechnological applications increasingly involve small-scale structures and advanced materials [1–3] requiring accurate modeling of scale effects, as conventional theories of Continuum Mechanics fail to capture size-dependent behavior. The work extends the stress-driven nonlocal approach [4] to higher-order shear deformable beams, avoiding the need for shear correction coefficients. To provide an innovative and comprehensive framework for modeling the bending behavior of nanobeams, the stress-driven integral model is combined with higher-order beam theories, id est Reddy third-order [5,6], sinusoidal [7], hyperbolic [8] and exponential shear deformation theory [9]. The nonlocal structural problem of a higher-order nanobeam of length L is presented. A Cartesian coordinate system is adopted where the x-axis coincides with the locus of geometric centroid of cross sections, y is the bending axis and z is orthogonal to the bending plane xy. The beam kinematics is described as follows

$$\begin{cases} s_x(x,y,z) = -\Psi(y)\, v'(x) + \Phi(y)\, \varphi(x) \\ s_y(x,y,z) = v(x) \\ s_z(x,y,z) = 0 \end{cases} \tag{1}$$

where s_x, s_y and s_z are, respectively, the $x-$, $y-$ and $z-$components of the displacement vector field $\mathbf{u}$, v is the transverse displacement of the centroidal axis and φ is the rotation of the cross section about the z axis. The apex denotes the first derivative along the beam axis x. Different higher-order beam theories can be considered by properly selecting the functions Ψ and Φ to get third-order, sinusoidal, hyperbolic and exponential shear deformation theories. Scale effects are modeled exploiting the nonlocal stress-driven approach, according to which the nonlocal elastic strain vector $\mathbf{q}$ is spatial convolution between an averaging kernel ϕ depending on the characteristic length parameter c and the local elastic strain vector $\mathbf{q}^l$, id est $\mathbf{q}(x) = \int_0^L \phi(x-\xi, c)$.

The relevant nonlocal elastic equilibrium problem is formulated and exploited to perform parametric analyses of higher-order nanobeams. A cantilever nanobeam of length $L = 50\,nm$ under a distributed transverse loading $q = 10^{-2}\,nN/nm$ is considered. The geometric and material properties are: height $h = 0.2L$, width $b = 0.5h$, elastic modulus $E = 380\,GPa$, Poisson's ratio $\nu = 0.3$. The

non-dimensional nonlocal parameter $\lambda = c/L$ is $\{0^+, 0.02, 0.05, 0.10, 0.20, 0.30, 0.40\}$. Parametric plots of the transverse stress field are depicted in Figure 1 for the third-order shear deformation theory.

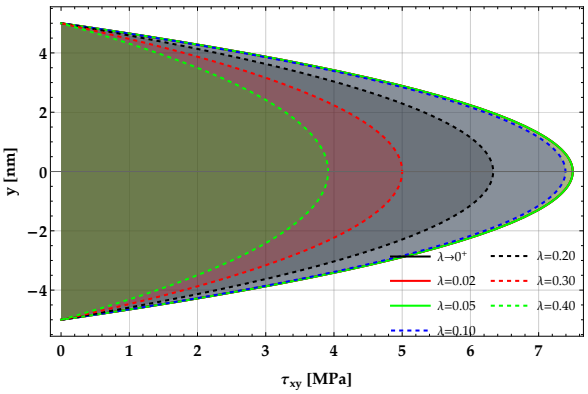


Figure 1. Nanocantilever: transverse stress field $\tau_{xy}(y)$ at $x = L/2$.

3 Conclusion

The stress-driven nonlocal methodology is generalized to capture the size dependent behavior of higher-order beams. The governing nonlocal elastic equilibrium problem is derived and parametric analyses are performed to highlight the effect of the nonlocal parameter on structural responses. By combining the stress-driven nonlocal approach with refined beam theories, the needing of shear correction coefficients is bypassed. A comprehensive and innovative framework for accurately modeling size-dependent behavior in shear deformable nanobeams is provided.

Acknowledgments

Financial supports from the Italian Ministry of University and Research (MUR) in the framework of the Project PRIN 2022 code 2022ZW2NMJ "Nonlocal Mechanics of Innovative Soft Nanostructures" and in the framework of the Project PRIN 2022 PNRR code P20223PLC2 "Nonlocal modelling of nano-coatings" are gratefully acknowledged.

References

[1] Gabrelian, A., Miikkulainen, V., Ross, G., Paulasto-Kröckel, M., Scaling of piezoelectric in-plane NEMS: Towards nanoscale integration of AlN-based transducer on vertical sidewalls. *Materials & Design*, 244, 113116, 2024.

[2] Guo, Y., Maalla, A., Habibi, M., Moradi, Z., Electroelastic wave dispersion in the rotary piezoelectric NEMS sensors/actuators via nonlocal strain gradient theory. *Mechanical Systems and Signal Processing*, 216, 111453, 2024.

[3] Penna, R., Lovisi, G., Surface and nonlocal effects in piezoelectric nanobeams. *European Journal of Mechanics - A/Solids*, 113, 105715, 2025.

[4] Romano, G., Barretta, R., Nonlocal elasticity in nanobeams: the stress-driven integral model. *Int. J. Eng. Sci.*, 115, 14–27, 2017.

[5] Vaccaro, M. S., Barretta, R., Marotti de Sciarra, F., Reddy, J. N., Nonlocal integral elasticity for third-order small-scale beams. *Acta Mech*, 233, 2393–2403, 2022.

[6] Reddy, J. N., A simple higher-order theory for laminated composite plates. *J. Appl. Mech.*, 51(4), 745–752, 1984.

[7] Touratier, M., An efficient standard plate theory. *Int. J. Eng. Sci.*, 29(8), 901–916, 1991.

[8] Soldatos, K. P., A transverse shear deformation theory for homogeneous monoclinic plates. *Acta Mech.*, 94(3), 195–220, 1992.

[9] Karama, M., Afaq, K. S., Mistou, S., Mechanical behaviour of laminated composite beam by the new multi-layered laminated composite structures model with transverse shear stress continuity. *Int. J. Solids Struct.*, 40(6), 1525–1546, 2003.

11th International Congress
of Croatian Society of Mechanics
September 30 – October 3 2025
Vodice, Croatia

A C^2-Finite Element Formulation for Strain Gradient Kirchhoff Nanoplates Using Hierarchical Hermite Basis Functions

C.A. Yan*, R. Vescovini*, N. Fantuzzi+, R. Luciano⋆

*Politecnico di Milano, Via La Masa 34, 20156, Milan, Italy
E-mails: chengangelo.yan@polimi.it, riccardo.vescovini@polimi.it

+Università di Bologna, Viale del Risorgimento 2, 40136, Bologna, Italy
E-mail: nicholas.fantuzzi@unibo.it

⋆Università degli Studi di Napoli Parthenone, Centro Direzionale ISOLA C4, 80133, Naples, Italy
E-mail: raimondo.luciano@uniparthenone.it

Keywords: Finite elements, Strain gradient theory, Kirchhoff nanoplates, Hermite shape functions

1 Introduction

Classical continuum theories are widely used in mechanics to efficiently model solid behavior via field variables like displacement, strain, and stress. However, they inherently neglect microstructural effects, making them inadequate for capturing size-dependent phenomena that arise at nanoscales.

Strain gradient elasticity addresses this limitation by incorporating size effects into the continuum framework, while retaining the advantages of field-based modeling [1]. Nevertheless, its practical use in Finite Element (FE) analysis remains limited due to the higher inter-element continuity required by the governing equations – specifically, C^2-continuity is required in the case of Kirchhoff strain gradient elasticity. This poses significant challenges, as standard FEs are formulated to accommodate only C^0-continuity.

This work introduces a novel FE formulation based on hierarchical Hermite polynomials that explicitly enforce C^2-continuity. The method is applied to isotropic Kirchhoff nanoplates and benchmarked against the conventional C^2-Hermite formulation.

2 Methodology

To illustrate the proposed FE formulation, we study the bending of a Kirchhoff-type strain gradient nanoplate. The governing equation is derived via the Principle of Virtual Work:

$$\begin{aligned}\int_\Omega \Bigg\{ &-D\left[\frac{\partial^2\delta w}{\partial x^2}\frac{\partial^2 w}{\partial x^2}+\frac{\partial^2\delta w}{\partial y^2}\frac{\partial^2 w}{\partial y^2}+2(1-\nu)\frac{\partial^2\delta w}{\partial x\partial y}\frac{\partial^2 w}{\partial x\partial y}+\nu\left(\frac{\partial^2\delta w}{\partial x^2}\frac{\partial^2 w}{\partial y^2}+\frac{\partial^2\delta w}{\partial y^2}\frac{\partial^2 w}{\partial x^2}\right)\right]+\\ &-Dl^2\left[\frac{\partial^3\delta w}{\partial x^3}\frac{\partial^3 w}{\partial x^3}+\frac{\partial^3\delta w}{\partial y^3}\frac{\partial^3 w}{\partial y^3}+(3-2\nu)\left(\frac{\partial^3\delta w}{\partial x^2\partial y}\frac{\partial^3 w}{\partial x^2\partial y}+\frac{\partial^3\delta w}{\partial x\partial y^2}\frac{\partial^3 w}{\partial x\partial y^2}\right)+\right.\\ &\left.+\nu\left(\frac{\partial^3\delta w}{\partial x\partial y^2}\frac{\partial^3 w}{\partial x^3}+\frac{\partial^3\delta w}{\partial x^3}\frac{\partial^3 w}{\partial x\partial y^2}+\frac{\partial^3\delta w}{\partial x^2\partial y}\frac{\partial^3 w}{\partial y^3}+\frac{\partial^3\delta w}{\partial y^3}\frac{\partial^3 w}{\partial x^2\partial y}\right)\right]\Bigg\}\mathrm{d}\Omega+\int_\Omega \delta w q\,\mathrm{d}\Omega=0\end{aligned}\tag{1}$$

where $D=\frac{Eh^3}{12(1-\nu^2)}$ is the bending rigidity with Young's modulus E, thickness h and Poisson ratio ν; w is the deflection; l is the nonlocal parameter; q is an external pressure acting on the plate domain Ω.

The variational statement in Equation 1 involves third-order derivatives. As result, C^2-continuity is required across element boundaries to have a well-posed FE approximation. This requirement is met here by employing a hierarchical Hermite function space, S^p, defined as:

$$\begin{aligned} f_k(\xi) &= a_{k0}+a_{k1}\xi+a_{k2}\xi^2+a_{k3}\xi^3+a_{k4}\xi^4+a_{k5}\xi^5 && \text{for} && k=1,\dots,6\\ f_{i+1}(\xi) &= \sqrt{\frac{2i-1}{2}}\iiint_{-1}^{\xi} P_{i-3}(\xi')\mathrm{d}\xi' && \text{for} && i=6,5,\dots,p \end{aligned}\tag{2}$$

where p denotes the order of the polynomial space, the functions f_1-f_6 are the conventional C^2-Hermite polynomials of order five which ensure continuity of displacement and its first two derivatives [2]. The higher-order functions, f_{i+1}, are constructed from the triple integrals of Legendre polynomials P_{i-3}, yielding shape functions of order i.

The function space defined by Equation 2 represents a C^2-extension of the hierarchical series first proposed in [3], and previously applied in [4] within a C^0-continuous finite element framework for composite shells. It retains the favorable properties of the original series, including hierarchical structure, good numerical stability of the stiffness matrix, and spectral convergence of the FE solution.

3 Results

To evaluate the convergence of the proposed FE formulation, we consider a simply supported square nanoplate ($b/a = 1$) subjected to uniform pressure $q = q_0$. The mesh configuration is shown in Figure 1a. In the convergence analysis, shown in Figure 1b, two approaches are employed to refine the FE model: (I) h-refinement, where the element size h is reduced while keeping the polynomial order fixed at $p = 5$; (II) p-refinement, where the mesh is fixed and the polynomial order p is increased. The former is the refinement approach typically employed in C^2-Hermite elements [2], while the latter is adopted for the present hierarchical C^2-Hermite formulation.

Convergence is assessed using the dimensionless central deflection $\alpha = Dw_{\max}/(q_0 a^4)$ computed from the FE solution and exact solutions from [5]. The results demonstrate that the proposed method achieves significantly faster convergence than the conventional C^2-Hermite approach.

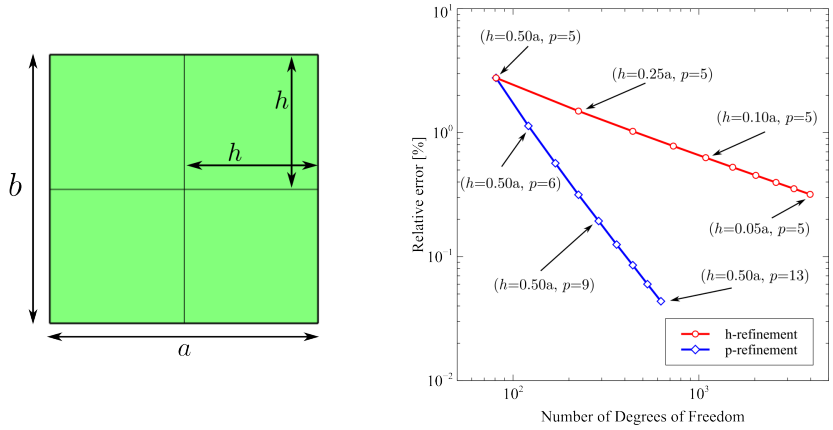


Figure 1. (a) Finite element mesh; (b) Convergence study using h- and p-refinements.

4 Conclusion

This work introduced a FE formulation based on hierarchical Hermite shape functions for modeling Kirchhoff-type strain gradient nanoplates. The formulation enforces C^2-continuity, enabling to handle the high-order governing equations inherent to gradient elasticity. Numerical results demonstrate superior convergence rates compared to the conventional C^2-Hermite formulation, confirming the effectiveness of the approach for nanoscale structural analysis of thin plates. Future work will focus on extending the proposed formulation to the analysis of strain gradient nanoshells.

Acknowledgements

This work has been supported by the Ministry of University Research (MUR) PRIN 2020 project 2020F23HZ7_003 (CUP: J35F22000640001), PRIN 2022 project 2022YLNJRY (CUP: J53D23002500006) which is funded by the European Union - NextGenerationEU.

References

[1] Aifantis, E.C., On the role of gradients in the localization of deformation and fracture. *International Journal of Engineering Science*, 30(10), 12791299, 1992.

[2] Bacciocchi, M., Fantuzzi, N., Ferreira, A.J.M., Conforming and nonconforming laminated finite element Kirchhoff nanoplates in bending using strain gradient theory. *Computers & Structures*, 239, 106322, 2020.

[3] Babuška, I., Szabó, B. A., and Katz, I. N., The p-version of the finite element method. *SIAM Journal on Numerical Analysis*, 18(3), 515-545, 1981.

[4] Yan, C.A., Vescovini, R., Application of the ps-Version of the Finite Element Method to the Analysis of Laminated Shells. *Materials*, 16(4), 515-545, 1395.

[5] Babu, B., Patel, B.P., Analytical solution for strain gradient elastic Kirchhoff rectangular plates under transverse static loading. *European Journal of Mechanics-A/Solids*, 73, 101–111, 2019.

CSM
CROATIAN SOCIETY OF MECHANICS
ZAGREB - OSIJEK - RIJEKA - SL. BROD - SPLIT

SS03 - State-of-the-Art on the Dynamic Behaviour of Materials and its Applications

organized by

Borja Erice, Mondragon Unibertsitatea & IKERBASQUE, Spain

Louise Le Barbenchon, Arts et Métiers, I2M, France

Nina Čeh, University of Rijeka, Croatia

Maria Lißner University of Oxford, United Kingdom

Special Sessions

11th International Congress
of Croatian Society of Mechanics
September 30 – October 3 2025
Vodice, Croatia

Modelling the Dynamic Response of Masonry–Binder Assemblies with Compliant Adhesive Interfaces

Nina Čeh*, Ivan Sindičić*, Anđela Janković*, Leo Škec*

*University of Rijeka, Faculty of Civil Engineering, Radmile Matejčić 3, 51000 Rijeka
E-mails: nina.ceh@uniri.hr, sindicicivan2@gmail.com, ajankovic@student.uniri.hr, leo.skec@uniri.hr

Keywords: seismic response, masonry structures, elastic adhesives, nonlinear interface modelling

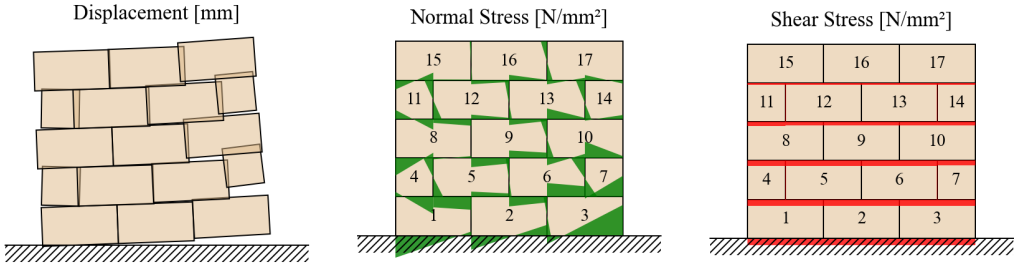
1 Introduction

Masonry remains common in low- and mid-rise buildings, yet unreinforced masonry with brittle joints performs poorly under seismic loads due to limited ductility. Elastic binders, especially polyurethane foams [1], offer improved energy absorption and damage delay. However, their complex rate-dependent behavior under dynamic loading cannot be captured by linear models. This study builds on a validated rigid block model [2, 3] and extends it with nonlinear adhesive interface behavior to better simulate seismic response.

2 Methodological Framework and Preliminary Results

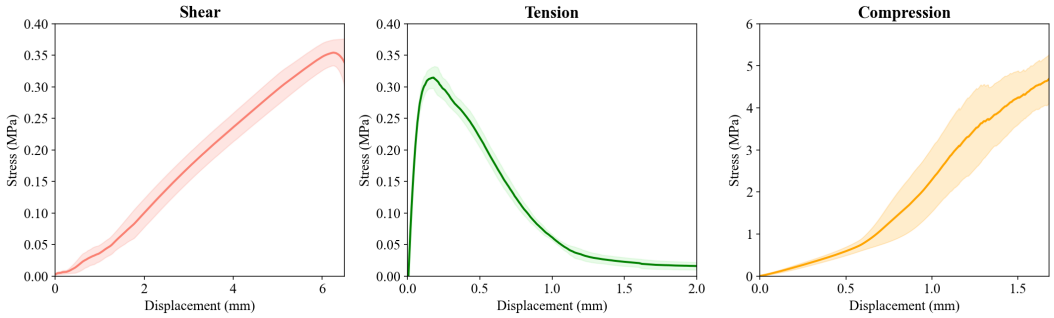
The approach integrates three levels: adhesive material properties (experimentally characterized), joint behavior (modeled as elastic interfaces), and global structural response (simulated via a rigid block model). The numerical model solves equations of motion for rigid blocks using interface stiffness and damping calibrated from free-vibration tests.

The model (Figure 1) is calibrated using experimental data, including stiffness parameters (Figure 2) and damping ratios derived from free-vibration decay. Validation is carried out through dynamic testing of small-scale wall models with silicone adhesive joints, tested under harmonic excitation at different frequencies.

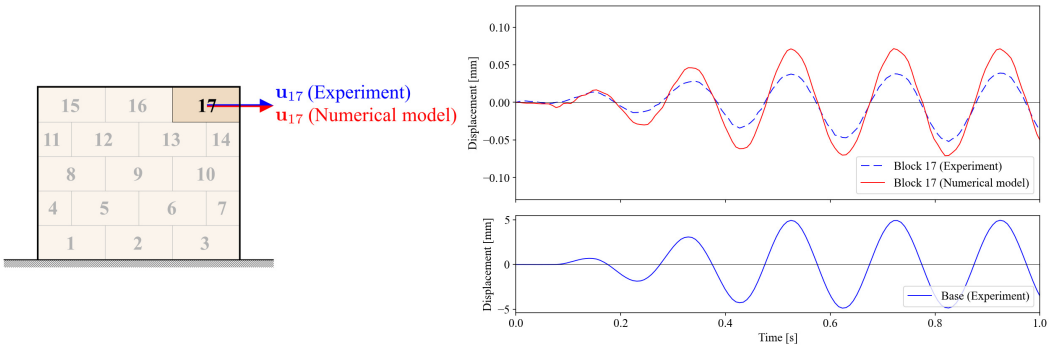


Slika 1. Deformed configuration and stress distribution on a masonry wall model with elastic contacts [3]

Initial results show good agreement between experimental and numerical responses under harmonic excitation (Figure 3), confirming the model's capability to simulate dynamic behavior of adhesive-bonded masonry in the linear regime. Displacement patterns, amplitude distributions, and resonance effects observed in testing are well reproduced in simulations, supporting the validity of the current contact model.



Slika 2. Adhesive material properties obtained from preliminary tests [3]



Slika 3. Validation of dynamic response at a frequency of 10 Hz during the first second of testing [3]

Although the current version employs linear elastic assumptions, the framework is designed for modular extension toward nonlinear contact behavior, rate-sensitive stiffness, and progressive interface damage, reflecting the actual viscoelastic and degradation-prone nature of polyurethane adhesives. This methodology lays the groundwork for evaluating the structural implications of new adhesive formulations and non-standard masonry construction practices.

3 Discussion and Future Work

The next phase of development will focus on enhancing the numerical model with nonlinear interface laws, strain-rate dependent stiffness degradation, and damage evolution mechanisms. The research will extend to capture more realistic and irregular bonding scenarios, particularly those found in rubble masonry used in post-disaster reconstruction. In such conditions, adhesive joints may feature variable thickness, discontinuities, and non-planar contacts. These complexities affect local interface mechanics and global dynamic behavior, requiring tailored numerical strategies. Incorporating these irregularities will enable the model to simulate not only idealized lab specimens but also masonry systems encountered in field applications where construction quality, geometry, and contact integrity vary significantly. Ultimately, the model will serve as a predictive tool for both conventional design and innovative, resource-conscious construction using next-generation elastic adhesives.

4 Acknowledgements

This research has been supported by the University of Rijeka under the project “Dynamic Characterization of Rigid Blocks with Cohesive Contacts” (UNIRI-iskusni 2024), and is further connected to the ongoing international collaboration within the DYMAT project.

References

[1] Gams, M., Triller, P., Jager, A. In-plane seismic behaviour of URM and confined masonry built from vertically perforated blocks and polyurethane glue. *Structures*. Vol. 58, p. 105528, 2023

[2] Sindičić, I. Numerical and Experimental Analysis of Seismic Response of Masonry Structures With Elastic Binder *(master thesis)*, University of Rijeka, Faculty of Civil Engineering, 2024.

[3] Janković, A. Numerical and Experimental Analysis of the Dynamic Response of a Block Portal With Elastic Contacts *(bacchelor thesis)*, University of Rijeka, Faculty of Civil Engineering, 2024.

11th International Congress
of Croatian Society of Mechanics
September 30 – October 3 2025
Vodice, Croatia

Study of the rate-dependent mixed-mode adhesive debonding using an efficient numerical model

Damjan Jurković*, Leo Škec*, Giulio Alfano+

*University of Rijeka, Faculti of Civil Engineering
E-mails: damjan.jurkovic@gradri.uniri.hr, leo.skec@gradri.uniri.hr

+Brunel University London, College of Engineering, Design and Physical Sciences
E-mail: giulio.alfano@brunel.ac.uk

Keywords: Adhesive joints, mixed-mode debonding, cohesive-zone model, rate-dependent effects, experiments

1 Introduction

Response of adhesive joints at varying loading speeds is a topic that has recently gathered significant attention. This is due to the use of adhesive joints in industrial applications, often as a part of high performance structures, together with the dependence of their mechanical performance on the loading speed. To address this problem, an efficient beam-based numerical model capable of capturing rate-dependent effects is developed and verified against experimental data.

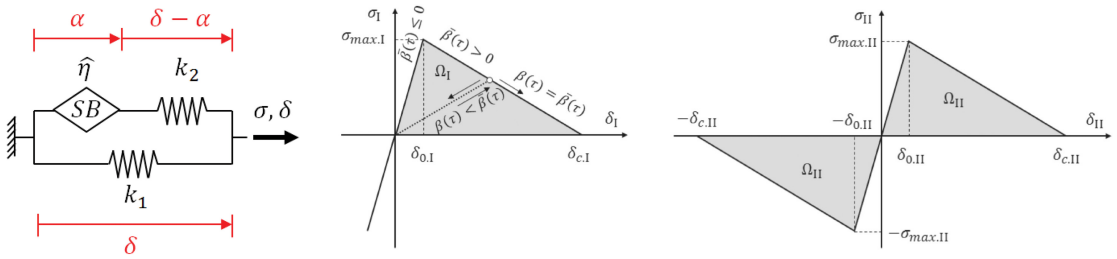
2 Rate-dependent effects in mode-II and mixed-mode adhesive debonding

Rheological representation of the fractional viscoelastic material model of the adhesive presented in [1] is shown in Figure 1(a). The so-called *Scott Blair element* in the viscous arm of the rheological model represents the response of the adhesive based on fractional viscoelasticity and is defined as:

$$\sigma_{SB} = \hat{\eta} \frac{\mathrm{d}^{\nu} \alpha}{\mathrm{d}t^{\nu}}, \tag{1}$$

where $\hat{\eta}$ is the viscosity coefficient, α is the relative displacement and $0 < \nu < 1$ is the order of fractional derivative with respect to time, which becomes an additional material parameter.

The cohesive-zone model is used to model the damage evolution in the adhesive. Bi-linear traction-separation laws for mode-I and mode-II are shown in Figures 1(b) and 1(c), respectively. The model assumes that the rate-dependent effects are contained just in the undamaged response of the interface, while the damage evolution is rate-independent. This formulation is integrated into the iterative procedure [2], used to calculate the contribution of the interface to the overall structural behaviour. Here, bulk material is modelled using Timoshenko beam elements and the interface is assumed to act upon them as a distributed load. Since this is generalised to a mixed-mode loading condition, this



(a) **(b)** **(c)**

Figure 1. Elements of the adhesive model: (a) viscoelastic rheological model, traction-separation laws for (b) mode-I and (c) mode-II

distributed load has both a vertical and a horizontal component. The damage initiation parameter [3] is computed by coupling the contributions produced in two independent modes as:

$$\beta = \sqrt{\frac{\delta_{0,\mathrm{I}}}{\delta_{c,\mathrm{I}}} + \frac{\delta_{0,\mathrm{II}}}{\delta_{c,\mathrm{II}}}} - 1, \tag{2}$$

where $\delta_{0,i}$ and $\delta_{c,i}$ are interfacial relative displacements at the initiation of damage and at full damage for mode-i (where $i = \mathrm{I}, \mathrm{II}$), respectively. These interface displacements are calculated as a difference in displacements of adjacent beam edges.

3 Adhesive debonding experiments

In order to verify the presented model, the end-notch flexure (ENF) and the mixed-mode bending (MMB) tests were carried out with varying loading speeds. Together with the double-cantilever beam (DCB) test previously used to assess the mode-I rate-dependent behaviour of the adhesive [4], these tests form a complete experimental set of the structural adhesive Araldite® 2015. The test specimens consist of two aluminium plates bonded together by the adhesive. The following loading speeds were used for both tests: 0.1 mm/s, 1 mm/s, 10 mm/s, 100 mm/s, 1000 mm/s and 5000 mm/s.

A significant amount of scatter in the load-displacement curve can be seen for specimens tested at the same loading speed. Unlike for the DCB test, averaging of the load-displacement curves for mode-II and mixed-mode tests is not trivial. Using the standard approach of averaging the load-displacement curves for these tests leads to average curves that cannot be used for an accurate identification of the material properties of the adhesive. Hence, in this work, the load-displacement curves are parametrised and the average curve for each speed is constructed based on the average values of these parameters. The response of the adhesive at different loading speeds is quantified and compared with the numerical model capable of capturing rate-dependent effects.

It is assumed that the friction in the area of fully damaged interface causes the scattering in the load-displacement curves. With this in mind, the friction effects are added to the numerical model.

4 Conclusion

The developed model is computationally efficient, robust and accurate, and is therefore suitable for parameter identification based on debonding test results. In addition, the model will be used to assess the accuracy of the standard mixed-mode delamination formulation and investigate alternative formulations (such as [5]) that take into account the influence of friction on the mode-II fracture resistance. For this purpose, the interface of the tested specimens will be laser-scanned in order to investigate the topology of the fracture plane.

Acknowledgements

This work was financially supported by the Croatian Science Foundation research project "Fixed-Pole Concept in Numerical Modelling of Cosserat Continuum" (IP-2018-01-1732) and the University of Rijeka research grant "An efficient and robust computational modelling of delamination of spatial layered structures" (uniri-iskusni-tehnic-23-300).

References

[1] Musto, M., Alfano, G., A fractional rate-dependent cohesive-zone model. *International Journal For Numerical Methods In Engineering*, 103(5), 313-341, 2015.

[2] Škec, L., Jelenić, G., Lustig, N., Mixed-mode delamination in 2D layered beam finite elements. *International Journal For Numerical Methods In Engineering*, 104(8), 767-788, 2015.

[3] Alfano, G., Crisfield, M. A., Finite element interface models for the delamination analysis of laminated composites: mechanical and computational issues. *International Journal for Numerical Methods in Engineering*, 50(7), 1701-1736, 2001.

[4] Škec, L., Alfano, G., Experimental and numerical study of rate-dependent mode-I failure of structural adhesive. *The Journal Of Adhesion*, 99(8), 1323-1355, 2023.

[5] Serpieri, R., Alfano, G., Sacco, E., A mixed-mode cohesive-zone model accounting for finite dilation and asperity degradation. *International Journal of Solids and Structures*, 67-68, 102-115, 2015.

11th International Congress
of Croatian Society of Mechanics
September 30 – October 3 2025
Vodice, Croatia

Energy Dissipation in Polymer-Based Mechanical Metamaterials Under Dynamic Loading Rates

Louise Le Barbenchon[1], Borja Erice[2,3], James Lee[4], Nina Ceh[5], Maria Lißner[4]

[1]*Arts et Metiers Institute of Technology, University of Bordeaux, CNRS, Bordeaux INP, Hesam Universite, I2M, UMR 5295, F-33400 Talence, France*
Email: louise.le_barbenchon@ensam.eu
[2]*Mechanical and Industrial Production Department, Mondragon University, Loramendi 4, 20500, Mondragón, Spain*
[3]*IKERBASQUE, Basque Foundation for Science, Bilbao, Spain*
Email: berice@mondragon.edu
[4]*Department of Engineering Science, University of Oxford, Parks Road, Oxford OX1 3PJ, England, United Kingdom*
Email: james.lee@eng.ox.ac.uk , maria.lissner@eng.ox.ac.uk
[5] *Faculty of Civil Engineering, University of Rijeka, Croatia*
Email: nina.ceh@uniri.hr

Keywords: Rate dependence, Additive Manufacturing, Viscoelastic Materials, Impact

1. Introduction

There is growing interest in low-impedance materials with superior energy-dissipation capabilities to develop lightweight structures with enhanced mechanical performance for demanding environments, such as those involving impact and crash events commonly encountered in aerospace, automotive, and sports applications [1,2]. Additive manufacturing (AM) plays an important role, offering the ability to create bespoke unit cell geometries and minimize material usage leading ultimately to lightweight. When combined with advanced polymers, AM enables tailoring of material properties to meet requirements for vibration damping, protective systems, and resilience to high dynamic loadings. Among the materials considered, elastomeric polyurethanes (EPUs) have attracted particular attention due to their exceptional mechanical properties, which are well-suited for high-performance applications. Motivated by these promising characteristics, the present work investigates mechanical metamaterials based on EPUs and explores their capacity to dissipate increasing amounts of energy as a function of loading rate. Consequently, it is essential to exploit the interplay between mechanical instabilities to unlock novel functionalities [3]. To this end, the mechanical response of both dense and architectured EPU specimens was experimentally and numerically studied across a range of strain rates, from quasi-static to high-rate loading conditions.

2. Methods and Materials

Four distinct unit-cell geometries were selected to investigate their influence on energy dissipation performance under varying loading rates. The chosen architectures are Octet-Truss (OC), Rhombic Dodecahedron (RD), Iso-Truss (IT) (all strut-based lattices), and Gyroid (a sheet-based Triply Periodic Minimal Surface lattice) – see Figure 1. They were designed using Ntop software. Samples were fabricated as 5×5×5 arrays of unit cells, each measuring 6 mm, resulting in overall sample dimensions of 30×30×30 mm³. Both truss- and surface-based metamaterials were designed with a relative density of $\rho* = 0.25$ to promote different strain mechanisms, specifically stretching- and bending-dominated deformation modes.

Two elastomeric polyurethane (EPU) materials, EPU41 and EPU45 from Carbon3D, were utilized for additive manufacturing by Erpro using Direct Light Synthesis (DLS). The viscoelastic behaviour of dense specimens was characterized using Dynamic Mechanical Analysis (DMA) in tension. To extend the investigation to finite strains, solid compression specimens were tested under

various strain rates: quasi-static loading was applied with an electromechanical test machine, while dynamic loading was performed using a flywheel apparatus for intermediate strain rates and a Direct Split Hopkinson Bar for high strain rates. Both dense and architected specimens were subjected to compression testing at quasi-static (QS, 0.017 s^{-1}), medium-rate (MR, 200 s^{-1}) and high-rate (HR, 1000 s^{-1}) conditions.

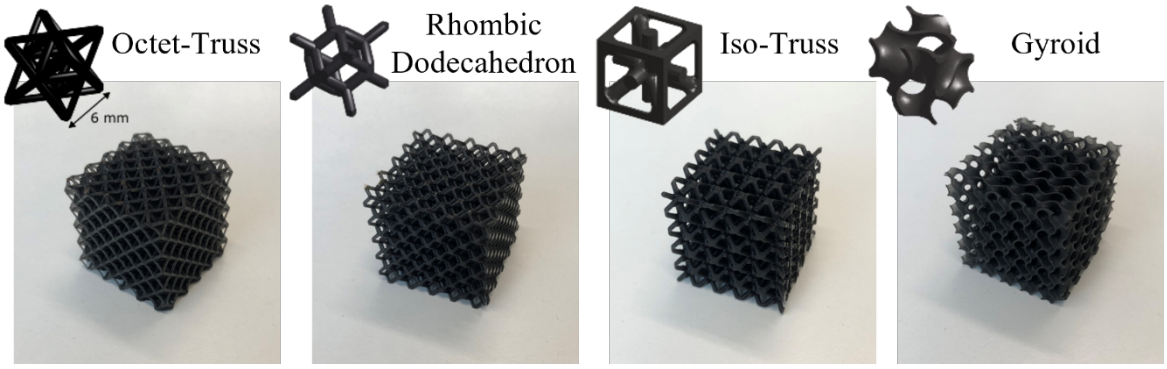


Figure 1. Mechanical metamaterials and their corresponding unit-cell geometries.

3. Results and Discussion

A comparison of the rate-dependent compressive responses of dense EPU materials reveals that EPU45 exhibits a more pronounced strain-rate dependence than EPU41 at room temperature [4]. This behaviour aligns with their viscoelastic properties, as demonstrated by DMA results. EPU41, with a glass transition temperature of −10°C, remains in its rubbery state at room temperature, demonstrating minimal hysteresis under compression and primarily elastic behaviour. In contrast, EPU45, which has a glass transition temperature of 40°C, is tested within its transition region at room temperature, displaying significant hysteresis indicative of heightened viscoelasticity.

This distinction in viscoelastic response directly affects the mechanical behaviour of architected structures under varying loading rates. In particular, EPU45 metamaterials exhibit a substantially stronger strain-rate dependency compared to EPU41 metamaterials. This is reflected in a 1208% increase in Young's modulus for EPU45 metamaterials with increasing strain rate, whereas EPU41 metamaterials show a comparatively lower increase of 483%.

4. Conclusions

This study emphasizes the importance of understanding how the strain-rate dependency of the base constitutive material and the architecture of the metamaterial together influence energy dissipation capabilities. Central to this approach is the use of specialized equipment capable of testing low-impedance materials across a range of loading rates, thereby enabling detailed mechanical characterization under both quasi-static and dynamic conditions. In parallel, a finite element modelling framework has been developed that incorporates viscoelastic material behaviour, allowing simulation and validation of responses at various strain rates. Together, these methods provide comprehensive insight into the interplay between constitutive material properties and unit-cell geometry in loading rate-dependent environments.

References

[1] Brechet, Y., Embury, J. D., and Embury, J. D. (2013). *Architectured materials: Expanding materials space*. Scripta Materialia.

[2] Jiang, H., Le Barbenchon, L., Bednarcyk, B. A., Scarpa, F., and Chen, Y. (2020). *Bioinspired multilayered cellular composites with enhanced energy absorption and shape recovery*. Additive Manufacturing

[3] Dykstra, D., Janbaz, S. and Coulais, C. (2022). *The extrem mechanics of viscoelastic metamaterials*. APL Materials

[4] Le Barbenchon, L. and Lißner, M. (2024). *On the dynamic performance of additively manufactured visco elastic meta-materials*. Materials Letters.

11th International Congress
of Croatian Society of Mechanics
September 30 – October 3 2025
Vodice, Croatia

LONG-TERM EFFECTS ON CLT-CONCRETE COMPOSITE SLABS

Mokhtar Tantawi[*], Daniel B. Merczel[+], Janos Logo[*]

[*]*Department of Structural Mechanics, Budapest University of Technology and Economics, Műegyetem rkp.3. Budapest, HUNGARY*
E-mails: logo.janos@emk.bme.hu mokhtar.tantawi@edu.bme.hu

[+] *ARC-S Innovation & Technology Ltd. H-1113 Budapest, Ulászló str. 51., HUNGARY*
E-mails: tantawi.mokhtarl@arcs.hu daniel.merczel@arcs.hu

Keywords: Cross-laminated timber, CLT-Concrete, Composite, Slip stiffness, parametric

Increasingly stringent sustainability-focused building regulations are motivating designers and investors to adopt mass timber load-bearing structures. In such buildings, cross-laminated timber (CLT) panels are commonly used for walls and slabs. However, when designing CLT slabs, various performance limitations—such as high or low vibration frequencies, deflection issues, or high costs—can restrict their practical use. A promising way to overcome these challenges is by adding a concrete topping to the CLT panel, enabling structural interaction between the materials. This creates a timber-concrete composite (TCC) slab, which offers improved performance and greater cost efficiency compared to using CLT alone.

Various researchers have investigated the design of TCC slabs in ultimate and serviceability states [1]. Usually, since TCC slabs are applied in the span range between 7-11 meters, the design is governed by serviceability limit states, such as deflections and vibration. Short-term deflections can be controlled by selecting appropriate slab thicknesses, CLT-to-concrete ratio, and the efficiency of the connection between the two materials. However, long-term deflections are influenced by additional factors. For example, the creep behavior of concrete differs from that of timber. Concrete creeps more rapidly, resulting in composite behavior distinct from either material alone. Concrete shrinkage also induces additional stresses that act as loads on the composite slab, increasing deflections. Furthermore, connectors also creep with time, leading to a lower connection efficiency over time.

Because of the logistical challenges of conducting empirical long-term studies, and to better isolate the influence of each of those factors on the long-term deflection of TCC slabs, numerical models using the finite element method (FEM) were used. Different models were used to capture the different kinematic effects in the numerical model. Creep and shrinkage of concrete were estimated using the formulas in EN1992-1-1 section 3.1.4. To capture the rheological components of timber, Toratti's model [2, 3] has been employed to capture the rheological components of timber, but has been simplified to account for only viscoelastic creep. Since the study only investigates indoor wood samples, mechano-sorptive and hygro-expansion behaviors are neglected. As for the creep of connections with time, Eurocode 5 recommends a reduction of the stiffness with a proportional ratio to the creep coefficient of timber K_{def}.

A parametric study was conducted using these models implemented into a previously validated FEM model where both CLT and concrete slabs are shell elements based on the Mindlin plate theory. The mesh consisted of six nodded serendipity elements. Moreover, the layers are connected using spring elements, accounting for the stiffness of the connection. The variables were the shrinkage of concrete,

creep of concrete and timber, and the connection stiffness. The study was performed on composite slabs that are loaded uniformly. Several slab configurations with different CLT to concrete ratios were investigated.

Results of the parametric study show that the shrinkage of concrete has the most significant impact on increasing the deflections of CLT-concrete composites. Controlling the shrinkage by using low-shrinkage concrete mixes proves to minimize the deflections. Figure 1 illustrates the magnitude of this influence. For a slab with a CLT layer configuration of 120-3s and an 80 mm concrete topping, deflections were recorded under various shrinkage loads, expressed in terms of relative humidity (RH) for easier comparison. These deflections were then normalized to those of the TCC slab with the lowest deflection (RH 90%), yielding percentage values for better comparability. In this context, shrinkage loads can increase deflections by up to 30%. The study also reveals that deflections caused by shrinkage are governed more by the total slab thickness than by the thickness of the concrete layer alone. This translates to the increased distance from the concrete centroid to the neutral axis of the slab. The larger the distance, the higher the effect of shrinkage is.

In contrast, the effect of concrete creep on long-term deflection is less significant. Increasing the concrete creep coefficient from 1.5 to 3 results in only a 5–10% increase in deflections, depending on the slab configuration and support conditions.

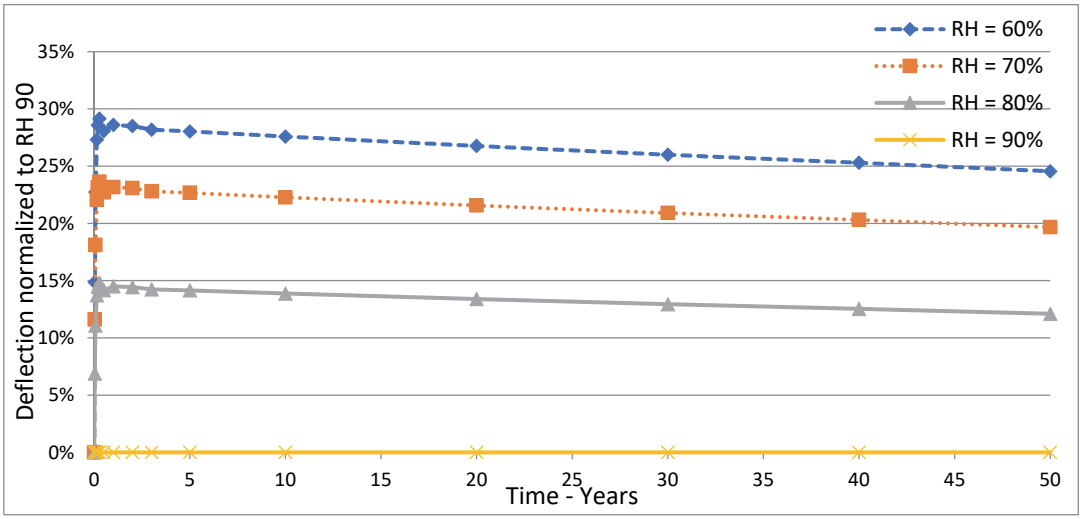


Figure 1: Shrinkage effect - Normalized deflection (CLT 120-3s-Conc-80-mm)

ACKNOWLEDGEMENT: KDP-IKT-2023-900-I1-00000957/0000003 has been implemented with the support provided by the Ministry of Culture Innovation of Hungary from the National Research, Development and Innovation Fund, financed under the C2316739 and OTKA K138615.

REFERENCES:

1. A. Dias, J. Schänzlin, P. Dietsch, Design of Timber-Concrete Composite Structures: A State-of-the-Art Report by COST Action FP1402/WG 4. Aachen: Shaker Verlag, 2018.
2. Shi, B.; Zhou, X.; Tao, H.; Yang, H.; Wen, B. Long-Term Behavior of Timber–Concrete Composite Structures: A Literature Review on Experimental and Numerical Investigations. *Buildings* **2024**, *14*, 1770. https://doi.org/10.3390/buildings14061770.
3. Yeoh, D., Fragiacomo, M., De Franchesci, M., & Boon, K. State of the Art on Timber-Concrete Composite Structures: Literature Review. Journal of Structural Engineering, 137, 10, 2011, October. https://doi.org/10.1061/(ASCE)ST.1943-541X.0000353

11th International Congress
of Croatian Society of Mechanics
September 30 – October 3 2025
Vodice, Croatia

High-cycle fatigue behaviour of Gyroid TPMS metamaterial

Žiga Žnidarič*, Nejc Novak*, Srečko Glodež*, Branko Nečemer*

* *University of Maribor, Faculty of Mechanical Engineering, Smetanova ulica 17, SI-2000 Maribor, Slovenia*
E-mails: {ziga.znidaric, srecko.glodez, n.novak, branko.necemer}@um.si

Keywords: high-cycle fatigue, experimental testing, TPMS metamaterials,

1. Introduction

Cellular structures have gained significant attention in modern engineering due to their unique ability to combine low density with favourable mechanical and physical properties [1]. These architected materials offer clear advantages over traditional solid materials, particularly in applications where lightweight design, vibration damping, sound insulation, and high energy absorption capacity are critical. Among these, metamaterials based on Triply Periodic Minimal Surfaces (TPMS) have emerged as a promising class of structures due to their smooth, continuous surfaces and tunable mechanical behaviour. One of the most studied TPMS configurations is the Gyroid topology, known for its balanced stiffness-to-weight ratio, isotropic mechanical response, and excellent manufacturability via additive manufacturing techniques. Additionally, the microstructure of polycrystalline materials inspires the design approach of stochastic sheet-based TPMS metamaterials. They consist of several grains within which lattices are randomly oriented [2]. While numerous computational studies have explored the static and dynamic behaviour of TPMS structures, experimental validation, especially under fatigue behaviour, remains limited [3]. This research addresses that gap by experimentally investigating the fatigue performance of implicit-based stochastic Gyroid-based TPMS metamaterials under high-cycle fatigue (HCF) loading regimes. The primary objective is to evaluate the fatigue life of the Gyroid structure and understand how its cellular geometry responds to prolonged cyclic loading. In addition, the study aims to assess the influence of unit cell design and loading amplitude on fatigue resistance. These findings contribute to a deeper understanding of the mechanical durability of TPMS metamaterials and support their integration into applications where long-term performance under repeated loading is essential, such as aerospace, automotive, and biomedical components.

2. Experimental testing

The experimental investigation aimed to evaluate the high-cycle fatigue (HCF) behaviour of Gyroid-based TPMS metamaterials. The tested geometry, illustrated in Figure 1, was manufactured using the Powder Bed Fusion (PBF) additive manufacturing process [4]. AlSi10 aluminium alloy was selected as the base material owing to its favourable combination of low density, good mechanical strength, and high suitability for fatigue-critical lightweight applications.



Figure 1. Specimen geometry

The fatigue tests were conducted on an electrodynamic pulsating testing machine Vibrophore 100 (Zwick/Roell), which enables high-frequency cyclic loading under controlled conditions. All tests were performed under uniaxial compressive loading with a stress ratio of R = 0.1. The experimental tests were performed at different loading levels, where multiple tests were performed at each level. The obtained experimental results were presented using the fatigue life curves (Figure 2). The presented results offer valuable insights into the fatigue performance of the Gyroid TPMS structure and serve as a reference for comparison with corresponding numerical simulations. These results contribute to a deeper understanding of the durability and failure mechanisms in architected metallic metamaterials manufactured by additive technologies.

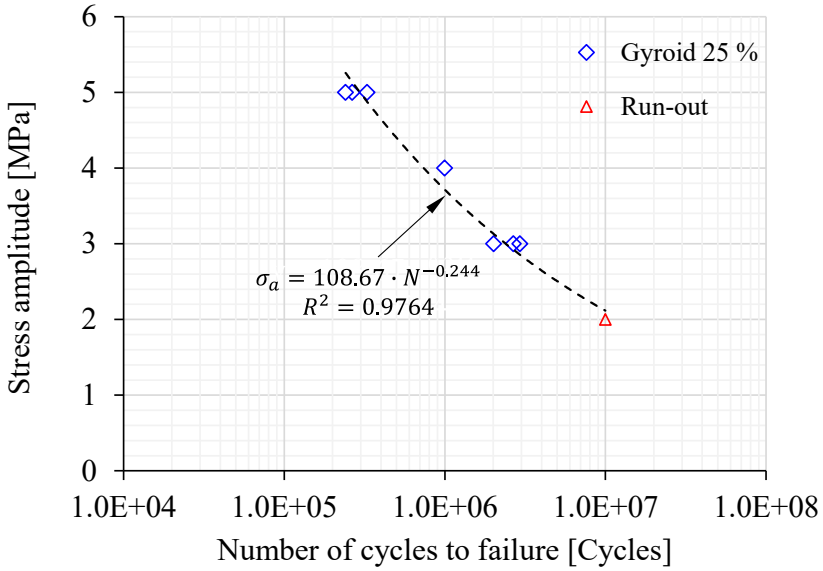


Figure 2. Experimental results

3. Conclusions

The proposed study experimentally investigated the high-cycle fatigue performance of Gyroid-based TPMS metamaterials manufactured using Powder Bed Fusion with AlSi10 alloy. The obtained experimental results will serve as a basis for validating the corresponding numerical model, ensuring its reliability in predicting the fatigue behaviour of architected materials. In future work, the validated numerical model will be employed as a design tool for the optimisation of such metamaterials, with the aim of tailoring their structural performance for specific engineering applications.

Overall, the research contributes to a deeper understanding of the mechanical durability of TPMS metamaterials and supports their future integration into high-performance engineering systems, particularly in fields such as aerospace, automotive, and military engineering.

References

[1] Nečemer, B., Vesenjak, M., Glodež, S., F Fatigue of Cellular Structures – a Review. *Journal of Mechanical Engineering*, 9, 525-536, 2019.

[2] Al-Ketan, O., Lee, R., Abu Al-Rub, Rashid K., Mechanical properties of additively-manufactured sheet-based gyroidal stochastic cellular materials. *Additive Manufacturing*, PA, 102418, 2021.

[3] Žnidarič, Ž., Nečemer, B., Novak, N., Glodež, S., Fatigue Analysis of Axisymmetric Chiral Cellular Structures Made out of 316L Stainless Steel. *Materials*, 24, 6152, 2024.

[4] Al-Ketan, O., Singh, A., Karathanasopoulos, N., Strut and sheet metal lattices produced via AM-assisted casting and powder bed fusion: A comparative study. *Additive Manufacturing Letters*, 100118, 2022.

Contributed Lectures

11th International Congress
of Croatian Society of Mechanics
September 30 – October 3 2025
Vodice, Croatia

On limitations of the Chaboche model in uniaxial ratcheting predictions

Tomáš Adamec*, František Šebek*, Jindřich Petruška*

*Brno University of Technology, Faculty of Mechanical Engineering, Institute of Solid Mechanics, Mechatronics and Biomechanics, Technická 2896/2, 616 69 Brno, Czech Republic
E-mails: Tomas.Adamec@vutbr.cz, sebek@fme.vutbr.cz , petruska@fme.vutbr.cz

Keywords: Cyclic behaviour, Low-cycle fatigue, Parameter evolution, Strain memory surface

1 Introduction

The tendency of the Chaboche model to over-predict the ratcheting behaviour is widely recognized. However, it can provide reasonable predictions for certain materials. In this study, the Chaboche model is calibrated on data from uniaxial tests of stainless steel 304 [1] and the resulting simulations are analysed to identify the limitations of the Chaboche model.

2 Model calibration and simulations

A small strain theory along with an additive decomposition of strain is used for the constitutive modelling. The plasticity is described using the von Mises yield criterion, associative flow rule and combined hardening, consisting of Voce isotropic hardening and Chaboche kinematic hardening. Additionally, the evolution of material parameters is governed by the strain memory surface with isotropic and kinematic components and the evanescent term according to [2] in order to better describe the cyclic hardening. The evolution of the material parameters γ_{1-3} as functions of the radius of the strain memory surface q is given as follows

$$\mathrm{d}\gamma_i = D_{\gamma_i}\left(a_{\gamma_i} + b_{\gamma_i}\mathrm{e}^{-c_{\gamma_i}q} - \gamma_i\right)\mathrm{d}p, \tag{1}$$

where D_{γ_i}, a_{γ_i}, b_{γ_i} and c_{γ_i} are the material parameters and $\mathrm{d}p$ is the increment of the accumulated plastic strain. In total, the model consists of 28 parameters, including elastic constants, yield stress, Voce hardening parameters, Chaboche hardening parameters, parameters governing the evolution and the strain memory surface parameters. The calibration process consists of two steps. First, the material parameters are roughly estimated and then all parameters are refined using differential evolution, except for the elastic constants. The error function evaluates the differences between the results of the experiments and simulations for every set of material parameters. The following tests are considered for the calibration: a single-amplitude uniaxial strain-controlled test with a strain amplitude of 0.01 and six uniaxial stress-controlled tests with mean stress $\pm$ stress amplitude in MPa being 19 ± 236, 36 ± 220, 36 ± 236, 36 ± 250, 36 ± 268 and 47 ± 236. The error function is focused primarily on the stabilized loop of the strain-controlled test and the stabilized ratcheting rates of the stress-controlled tests. A minor focus is placed on the evolution of the loop shape in the strain-controlled test and the stabilized loop shapes in the stress-controlled tests.

Left Fig. 1 shows a simulation of strain-controlled test, where both the shape of stabilized loop and the evolution of loop shape are captured well. In contrast, the monotonic response is not fitted well, because it is significantly different from the cyclic response in the case of the considered material. Right Fig. 1 shows simulated last loops of stress-controlled tests with a good agreement compared to experiments. Figure 2 shows simulated tensile peaks of plastic strain for six stress-controlled tests. It can be seen that the Chaboche model was able to fit the stabilized ratcheting rate decently for all experiments. However, the bad fit of the monotonic response resulted in a large difference in the experimental and simulated plastic strains. Furthermore, the monotonic response is largely controlled by γ_4 after saturation of the first three backstresses, which is set primarily to fit the stabilized ratcheting rate of individual stress-controlled tests, as it affects them greatly and therefore is overloaded.

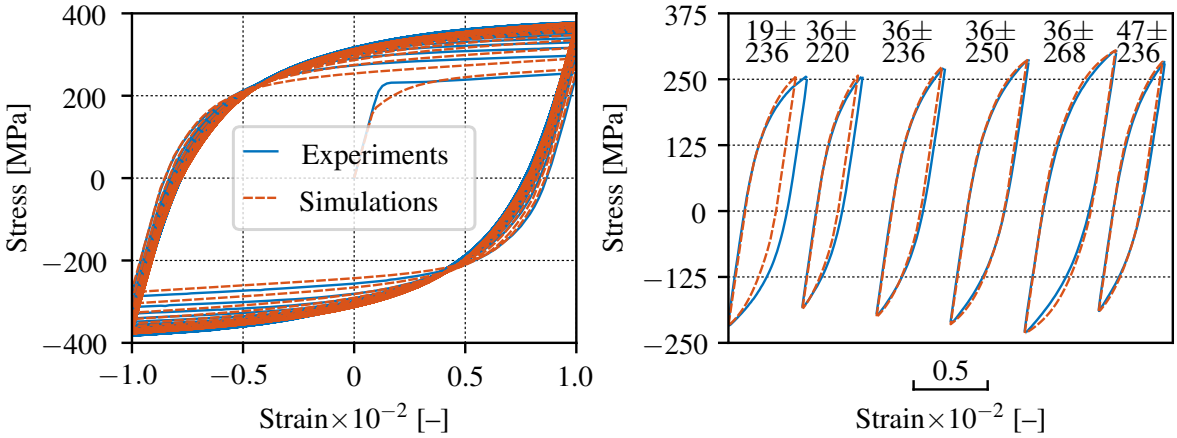


Figure 1. Strain-controlled test (left) and the last loops of stress-controlled test (right)

Another reason for a poorer prediction of strains is the transient behaviour, which is a specific feature of the Chaboche model characterized by a rapid decay of the ratcheting rate due to stabilization of mean values of individual backstresses. Figure 2 also shows that transient behaviour decreases with increasing stress amplitude. Transient behaviour may not seem that influential in predicting correct plastic strains compared to the goodness of fit of the monotonic response, however, the transient may reoccur each time the stress amplitude changes.

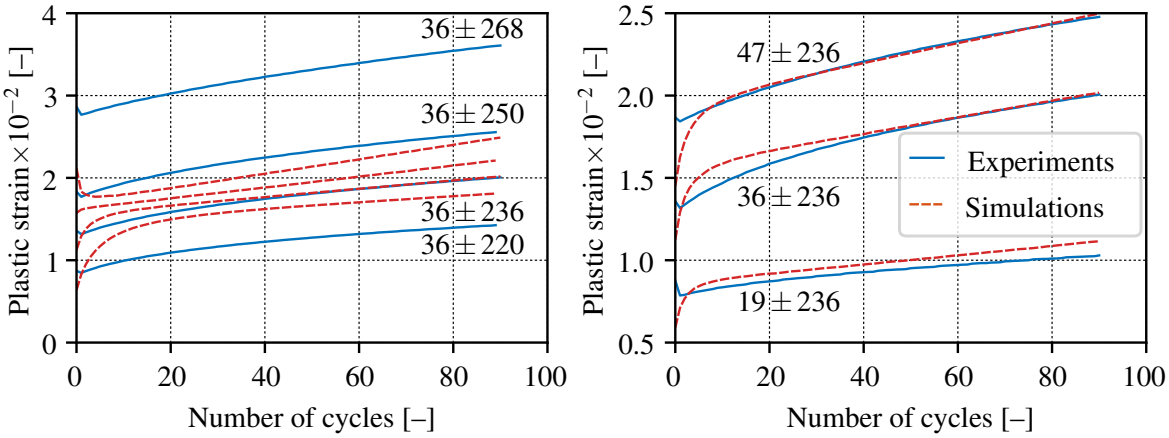


Figure 2. Tensile peaks of plastic strain for stress-controlled tests

3 Conclusion

The Chaboche model demonstrates the ability to predict the stabilized ratcheting rate to a certain extent. However, its accuracy is limited by the excessive constraint of γ_4, which affects both the monotonic response and the ratcheting rate. The material parameter also influences the transient behaviour, leading to poor prediction of the plastic strain peaks in stress-controlled simulations.

References

[1] Hassan, T., Kyriakides, S., Ratcheting of cyclically hardening and softening materials: I. Uniaxial behavior. *International Journal of Plasticity*, 10, 2, 149–184, 1994.

[2] Nouailhas, D., Cailletaud, G., Policella, H., Marquis, D., Dufailly, J., Lieurade, H. P., Ribes, A., Bollinger, E., On the description of cyclic hardening and initial cold working. *Engineering Fracture Mechanics*, 21, 4, 887–895, 1985.

11th International Congress
of Croatian Society of Mechanics
September 30 – October 3 2025
Vodice, Croatia

Strength and Stability of Conventional and Variable Locking Screws in Healthy and Osteoporotic Mandibular Angle Fractures: A Finite Element Study & Pre-Study

Petra Adamović*, Lovro Matoc+, Srećko Sabalić‡, Janoš Kodvanj*

*Faculty of Mechanical Engineering and Naval Architecture, Ivana Lučića 5, 10000 Zagreb
E-mails: {petra.adamovic,janos.kodvanj}@fsb.unizg.hr

+Department of Maxillofacial Surgery, University Hospital Centre Zagreb, Kišpatićeva Ulica 12, 10000 Zagreb, Croatia
E-mail: lovro.matoc@gmail.com

‡Department of Traumatology, Sestre Milosrdnice University Hospital Center, Draškovićeva 19, 10000 Zagreb, Croatia
E-mail: ssabalic@gmail.com

Keywords: mandible fractures, variable locking screws, finite element method, medical implants

1. Introduction

Approximately 33% of all types of mandible fractures occur in the mandibular angle as a result of interpersonal violence, sports, falls and motor vehicle accidents. Treatment is often problematic due to the mandible's complex bone geometry resulting in post-treatment complications in 20 to 26% of patients [1]. Most common used osteosynthesis procedure is (often) less than 1 mm thick, bendable plate combined with screws. Finite element analysis is used in many studies to determine factors that affect the biomechanical stability of the bone – implant system such as plate shapes, thickness and geometry. Although several studies describing various biomechanical impacts of screw's thread on bone have been conducted, there isn't much information about screws' behaviour on a human mandible. Therefore, the aim of this study is two-fold. First, to determine the difference of biomechanical stability between four types of screw head thread definitions in Abaqus simulations on a human mandible with a favourable fracture using conventional locking plate system (Figure 1). The results from this pre-study can be used as a guidance in other similar studies. Second, to determine the biomechanical properties of novel osteosynthesis implants presented in [2] in treating of healthy and osteoporotic favourable mandibular angle fractures.

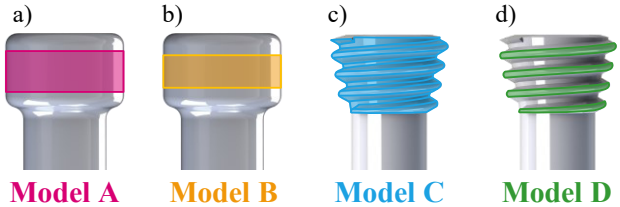


Figure 1. Pre-study models: a) 86% tie engagement (*smooth cylinder*), b) 65% tie engagement (*smooth cylinder*), c) all surfaces are tied (*thread*), d) less than half are surfaces tied (*thread*)

2. Materials and methods

A mandible of an 83-year-old male was reconstructed using computer tomography and Mimics software (Materialise NV, Belgium). The model was imported in SolidWorks software (SolidWorks, Dassault Systèmes, USA) where it was integrated in an assembly with a bendable 1.25 mm thick plate and four 2 mm screws. Each pair of the screws was on one side of the fracture. The *bone – implant* assembly was then imported into Abaqus software (version 6.14-5, Dassault Systèmes,

France) where a total of 48 simulations were conducted. One-plate technique as suggested by Champy, was selected as control sample, while the testing sample was the variable locking screw system introduced in [2]. Load cases are displayed in Figure 2.

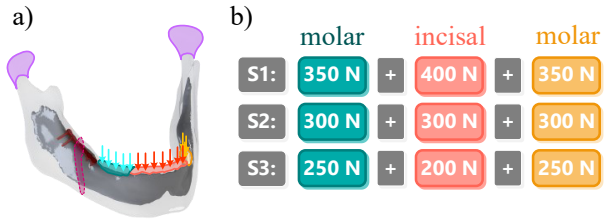


Figure 2. Boundary conditions on fractured mandible, b) load cases

Elastic modulus for healthy cortical bone was set to 13.7 GPa, while for trabecular bone 0.793 GPa. For osteoporotic cortical bone, modulus was 7.54 GPa, while for trabecular bone 0.436 GPa. Screws and plates for conventional locking system had the modulus of 110 GPa, while the plate for the new system was 98.66 GPa, and for screws 101.5 GPa. Friction between screws and plate in conventional system was set to 0.35, while it was tied it the variable locking system. Friction between fracture surfaces was set to 0.4. All Poisson's ratios were set to 0.3.

3. Results

The results of pre-study simulations are presented in Table 2, while the main study's results are presented in Table 3 and Table 4.

Table 2. Maximum von Mises stress and displacement for models of pre-study

Load case (Fig. 2)	Forces [N]		Maximum von Mises stress [MPa] Model				Maximum displacement [mm] Model			
	Molar	Incisal	A	B	C	D	A	B	C	D
S3	500	200	1754	1340	7946	9710	3.061	2.617	2.622	3.072
S2	600	300	1921	1766	8552	10716	3.407	3.411	3.418	3.419
S1	700	400	2397	2204	12097	12592	4.214	4.219	4.227	4.230

Table 3. Maximum von Mises stress and displacement for conventional locking system

Load case	Forces [N]		Maximum von Mises stress [MPa]		Maximum displacement [mm]	
	Molar	Incisal	Healthy bone	Osteoporotic bone	Healthy bone	Osteoporotic bone
S3	500	200	505.2	491.1	2.809	5.044
S2	600	300	670.2	653.4	3.742	6.719
S1	700	400	833.3	814.4	4.671	8.391

Table 4. Maximum von Mises stress and displacement for variable locking system

Load case	Forces [N]		Maximum von Mises stress [MPa]		Maximum displacement [mm]	
	Molar	Incisal	Healthy bone	Osteoporotic bone	Healthy bone	Osteoporotic bone
S3	500	200	262.4	301.3	2.691	4.910
S2	600	300	359.5	413.8	3.584	6.539
S1	700	400	455.2	524.5	4.474	8.166

3. Conclusions

There are no significant displacements differences of the four models which indicates safe use of smooth cylinders instead of threaded ones for much faster simulations. Displacements and stresses of the new locking systems shows promising results for the upcoming experimental validation.

References

[1] Ayali, A., Erkmen, E. *Biomechanical evaluation of different plating methods used in mandibular angle fractures with 3-dimensional finite element analysis: favorable fractures*. Journal of Oral and Maxillofacial Surgery, 2017;75:1464–74, doi:10.1016/j.joms.2017.02.028.

[2] Adamović, P., Matoc, L., Knežević, P., Sabalić, S., Kodvanj, J. *Biomechanical analysis of a novel screw system with a variable locking angle in mandible angle fractures*. Medical & Biological Engineering & Computing, 2023;61(11):2951-2961, doi: 10.1007/s11517-023-02895-y.

11th International Congress
of Croatian Society of Mechanics
September 30 – October 3 2025
Vodice, Croatia

Characterisation of elastic and plastic anisotropy in 316L austenitic stainless steel produced by WAAM

D. G. Andrade[*], V. Cvitanić[+], L. Simões da Silva[*], D. M. Rodrigues[**]

[*]*University of Coimbra, ISISE, ARISE, Department of Civil Engineering, Coimbra, Portugal*
E-mails: david.andrade@uc.pt, luisss@dec.uc.pt

[+]*Faculty of Electrical Engineering, Mechanical Engineering and Naval Architecture, University of Split, R. Boškovića 32, HR-21000 Split, Croatia*
E-mail: vcvit@fesb.hr

[**]*University of Coimbra, ISISE, ARISE, Department of Mechanical Engineering, Coimbra, Portugal.*
E-mails: dulce.rodrigues@dem.uc.pt

Keywords: WAAM, 316L Stainless Steel, Elastic Anisotropy, Plastic Anisotropy, Lankford Coefficient

1. Introduction

Additive manufacturing (AM) technologies, particularly Wire Arc Additive Manufacturing (WAAM), are increasingly employed to fabricate large-scale metallic components with high material efficiency. However, the directional nature of WAAM's layer-by-layer deposition induces thermal gradients and microstructural heterogeneities that often lead to pronounced anisotropy in mechanical properties [1–3]. For austenitic stainless steels such as 316L, this anisotropy affects both the elastic and the plastic behaviour, influencing components performance and making numerical modelling more complex. Therefore, understanding and accurately characterising the anisotropic response is essential for reliable design, simulation, and structural integrity assessment of WAAM-fabricated parts [4,5]. While prior studies have explored directional strength variations, few have provided a combined evaluation of the elastic and plastic anisotropy, including strain path analysis and constitutive modelling. This work investigates the in-plane mechanical anisotropy of thin-walled 316L components, produced by WAAM, using tensile testing in three orientations and strain data acquisition by digital image correlation (DIC).

2. Experimental Procedure

Thin-walled samples of 316L austenitic stainless steel were fabricated using Cold Metal Transfer (CMT) based Wire Arc Additive Manufacturing. Tensile specimens were extracted in three orientations (0°, 45° and 90°) relative to the deposition direction. Prior to testing, surfaces were machined to remove as-built roughness. Quasi-static tensile tests were performed on three samples for each orientation at room temperature according to ISO 6892-1. Longitudinal strain was recorded using a mechanical extensometer, while full-field strain data were acquired via DIC to assess anisotropic deformation behaviour and compute strain paths and strain ratios.

2. Results and Discussion

As shown in **Figure 1,** the tensile tests revealed significant anisotropy in both elastic and plastic responses of the WAAM-fabricated 316L stainless steel. Young's modulus varied notably with orientation, with the 45° samples exhibiting the highest mean stiffness (~193 GPa), followed by 0° samples (~144 GPa) and 90° samples (~117 GPa). Poisson's ratio also displayed strong directional dependence, with mean value ranging from ~0.14 (45°) to ~0.43 (0°). Plastic behaviour followed a

similar pattern. The mean yield stresses for the 45° and 90° samples had almost equal value (~443 MPa) higher than for the 0° samples (~397 MPa). All samples exhibited strain hardening, with tensile strengths exceeding 870 MPa. The mean Lankford's coefficients, derived from DIC strain paths considering the whole strain hardening range, for the 0° and 90° samples were very close (~1.7) and much higher than for the 45° samples (~0.34), indicating distinct deformation mechanisms. Regarding stress anisotropy, the observed trends were consistent across both extensometer and DIC measurements.

The combination of stress-strain curves and DIC-based strain mapping allowed for a detailed assessment of anisotropy. These results provide a robust basis for the calibration and validation of orthotropic elasto-plastic constitutive models, including those based on the Hill'48 stress function.

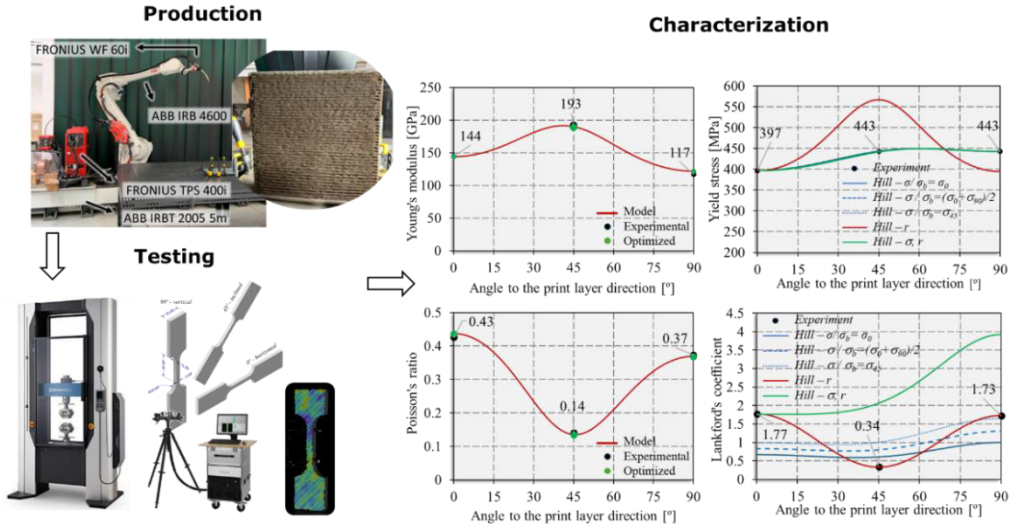


Figure 1. Overview of the experimental setup and material characterisation.

3. Conclusions

This study confirmed that 316L stainless steel produced by CMT-based WAAM exhibits marked elastic and plastic anisotropy. Tensile testing and DIC analysis revealed direction-dependent Young's modulus, Poisson's ratio, yield stress and Lankford's coefficient. The lowest stiffness occurred along the 90° direction, while the 45° samples showed the highest strength and most distinct strain behaviour. These results validated the use of orthotropic constitutive models and supported the application of plasticity models based on non-associated flow rule for accurately predicting the anisotropic response of WAAM components.

Acknowledgement

This article is a result of the Innovation Pact "R2UTechnologies | modular systems" (C644876810-00000019), by "R2UTechnologies" Consortium, co-financed by NextGeneration EU, through the Incentive System "Agendas para a Inovação Empresarial" ("Agendas for Business Innovation"), within the Recovery and Resilience Plan (PRR).

References

[1] Kyvelou P, Hong W, Zhang R, Gardner L. Mechanical properties and microstructure of wire laser metal deposited austenitic stainless steel. Mater Des 2025;250:113558. https://doi.org/10.1016/j.matdes.2024.113558.

[2] Laghi V, Palermo M, Gasparini G, Veljkovic M, Trombetti T. Assessment of design mechanical parameters and partial safety factors for Wire-and-Arc Additive Manufactured stainless steel. Eng Struct 2020;225:111314. https://doi.org/10.1016/j.engstruct.2020.111314.

[3] Hadjipantelis N, Weber B, Buchanan C, Gardner L. Description of anisotropic material response of wire and arc additively manufactured thin-walled stainless steel elements. Thin-Walled Struct 2022;171:108634. https://doi.org/10.1016/j.tws.2021.108634.

[4] Andrade DG, Tankova T, Zhu C, Branco R, Simões da L, Rodrigues DM. Mechanical properties of 3D printed CMT-WAAM 316 LSi stainless steel walls 2024;215. https://doi.org/10.1016/j.jcsr.2024.108527.

[5] Tankova T, Andrade D, Branco R, Zhu C, Rodrigues D, Simões da Silva L. Characterization of robotized CMT-WAAM carbon steel. J Constr Steel Res 2022;199. https://doi.org/10.1016/j.jcsr.2022.107624.

11th International Congress
of Croatian Society of Mechanics
September 30 – October 3 2025
Vodice, Croatia

Automatic recognition of the structural integrity of buildings in Kaštela bay using CNN models supported by IR thermography

Petra Bagavac*, Alen Grebo*, Ante Medvidović*, Željana Nikolić+, Lovre Krstulović-Opara*

*FESB, University of Split, R. Boškovića 32, Split, Croatia
E-mails: {petra.bagavac,agrebo,opara,ante.medvidovic.00}@fesb.hr

+FGAG, University of Split, Ul. Matice hrvatske 15, Split, Croatia
E-mail: zeljana.nikolic@gradst.hr

Keywords: structural integrity, IR thermography, CNN model

1. Introduction

This research represents one of the key outcomes of the ongoing project STRategies for assessing climate change risks, increasing resilience against ENvironmental hazards, and promoting territorial GrowTH (INTERREG IT CRO STRENGTH; https://www.italy-croatia.eu/web/strength). One of the project's specific objectives, in which FESB and FGAG are primarily involved, is the development of a digital strategy for the monitoring and detection of structural damage, enabling automatic recognition of structural integrity and reliable seismic vulnerability analysis.

In the first phase of the project, our research team collected infrared (IR) images using a FLIR E96 thermal camera in the area of Kaštela Bay, Fig.1. For each building, approximately ten thermograms were captured to ensure full coverage from all sides. In addition to thermal imaging, GPS coordinates, azimuth data, building floor plans, and building heights were recorded. These serve as the input parameters for each location (i.e., structure), and were used to create a comprehensive database. Based on the collected IR images, a custom-developed algorithm identifies structural elements and construction types with a certain degree of probability. Using this information, key parameters for seismic vulnerability analysis are calculated. These results will be used to generate a seismic hazard map for the surveyed area. A similar evaluation of building structures was previously conducted manually as part of the PMO GATE Interreg project [4]. As a next step, an AI-based approach is being introduced to accelerate the thermographic survey process and eliminate the influence of subjective interpretation by the thermographer.

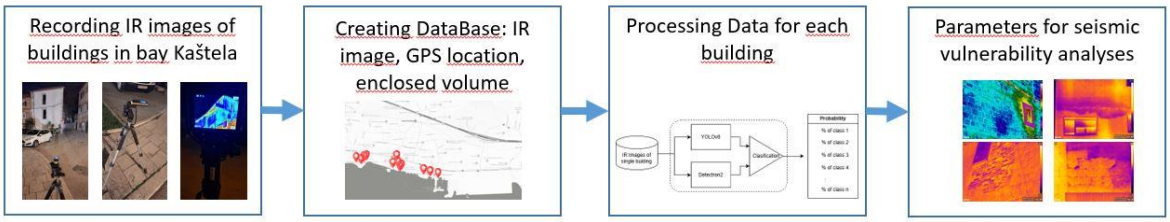


Figure 1. Key steps for automatic recognition of the structural integrity of buildings

2. Methodology

An advanced convolutional neural network (CNN)-based artificial intelligence (AI) system is being developed to enable the identification and classification of load-bearing walls in civil engineering structures. Particular emphasis is placed on construction typologies commonly found in the Dalmatian region, where reinforced concrete and masonry dominate. Due to the limited prevalence of wood as a structural material in these buildings, wooden elements are deliberately

excluded from the training process. This exclusion facilitates the optimization of detection performance and allows the system to be tailored to the region's most relevant construction practices.

A large and continuously expanding dataset is required to support the training process. To improve the reliability and accuracy of structural element detection, infrared (IR) imaging technology is employed in place of conventional RGB imaging. IR imaging provides enhanced analytical depth by revealing material-specific thermal signatures, structural integrity variations, moisture content, and subtle density differences—all critical features for the accurate identification of load-bearing components. This approach represents a significant improvement over traditional visual inspection methods, particularly in the assessment of historical buildings or structures lacking detailed documentation.

The system architecture is based on two classification networks, each designed to classify input images according to specifications related to the Vulnerability Index. The classification output represents the probability that a given structural feature corresponds to one of the predefined classes in the training dataset, Fig.2. If both networks assign a high probability to the same class, the image is assigned to the corresponding Vulnerability Index category.

To support the training and deployment of the CNN models, two open-source AI frameworks—Detectron2 [2, 3] and YOLOv8 [4] — are utilized. Detectron2 is selected for its modular architecture, robustness, and effectiveness in segmentation tasks, which are critical for the precise identification of structural components in complex image datasets. Concurrently, YOLOv8 is employed for its high-speed inference capabilities and efficiency in real-time object detection, particularly valuable during on-site assessments. By leveraging the strengths of these state-of-the-art frameworks, a comprehensive and efficient solution is being developed to address the structural inspection needs specific to buildings in the Dalmatian region.

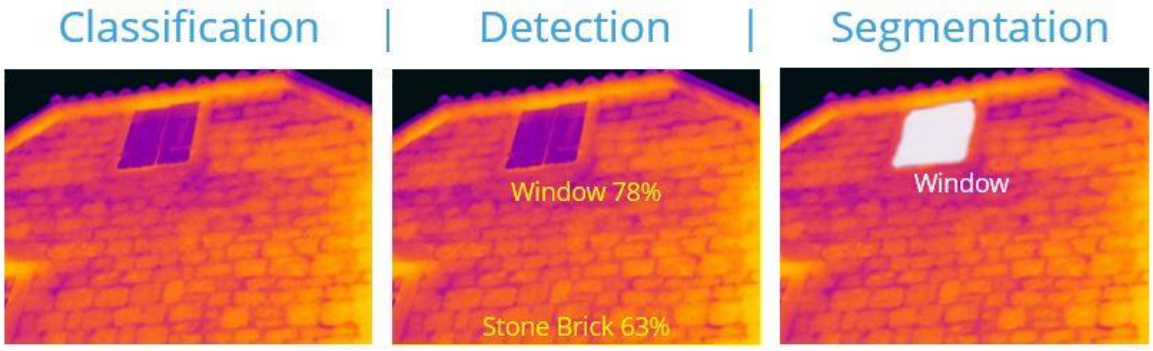


Figure 1. Export of the classification; probability that the given artifact or shape corresponds to the classes from training set

3. Conclusions

The proposed AI-based system, leveraging infrared imaging and state-of-the-art deep learning frameworks, offers a robust and efficient approach for the automated detection and classification of structural components in Dalmatian buildings. By enabling accurate seismic vulnerability assessments, this methodology supports the development of targeted strategies for structural resilience and disaster risk reduction.

References

[1] L. Krstulović-Opara, Utvrđivanje sastava zida ispod fasade u cilju određivanja potresne otpornosti, 9. stručni skup termografista HUICTa, Terme Sv. Martin, 2022.

[2] Wu Y, Kirillov A, Massa F, Lo WY, Girshick R. Detectron2. GitHub. https://github.com/facebookresearch/detectron2. Accessed Jan 29, 2025.

[3] Facebook AI Research. Detectron2 Projects. GitHub. https://github.com/facebookresearch/detectron2/tree/main/projects. Accessed Jan 29, 2025.

[4] Reis D, Kupec J, Hong J, Daoudi A. Real-Time Flying Object Detection with YOLOv8. arXiv preprint arXiv:2305.09972. 2023. https://arxiv.org/abs/2305.09972

11th International Congress
of Croatian Society of Mechanics
September 30 – October 3 2025
Vodice, Croatia

On Newly Discovered Hydrostatic Rotation Properties of Immersed Isosceles Triangular Cross-section Pontoon

Dario Ban *

*Faculty of Electrical Engineering, Mechanical Engineering and Naval Architecture, University of Split, R. Boškovića 32, 21000 Split, Croatia
E-mail: dario.ban@fesb.hr

Keywords: hydrostatic, rotation, kinematics, isosceles triangle, additional cusp discontinuity

1. Introduction

In this paper, the newly discovered hydrostatic rotation properties of the immersed pontoon in the shape of an isosceles triangle are examined for the additional extreme cusp discontinuities of the metacentric locus curve for all coordinate system quadrants.

2. Additional extreme cusp discontinuity angle definitions for isosceles triangle

For the case of the static, two-dimensional problem of the hydrostatic immersion of isosceles triangular cross section observed here, similar to that for rectangles in [1,2], the cusp discontinuities for triangles are divided into two types only in this paper, with

– *Extreme type cusp discontinuities*, E, with constant heel angle values for draughts d

$$\phi_{\mathrm{E},k}(d) = const., k = 1, \ldots, 6 \tag{1}$$

– *Vertex type cusp discontinuities*, V, with variable occurrence heel angles for draughts d

$$\phi_{\mathrm{V},j}(d) \neq const., j = 0, \ldots, 6 \tag{2}$$

For the cuspidal Lamé equations of the six metacentric locus M-curve segments in Cartesian parametric form

$$z'_M = a'_j cos^3(\phi'_j) \qquad y'_M = b'_j sin^3(\phi'_j) \tag{3}$$

the local extremes of the of the metacentric locus M-curve components $X_{\mathrm{M}} \equiv \{y'_{\mathrm{M}}, z'_{\mathrm{M}}\}$ occur in the local coordinate systems $y' - z'$, as shown in Figure 1 below (showing centre of buoyancy B-curve components $X_{\mathrm{B}} \equiv \{y'_{\mathrm{B}}, z'_{\mathrm{B}}\}$ and centre of floatation F-curve, too).

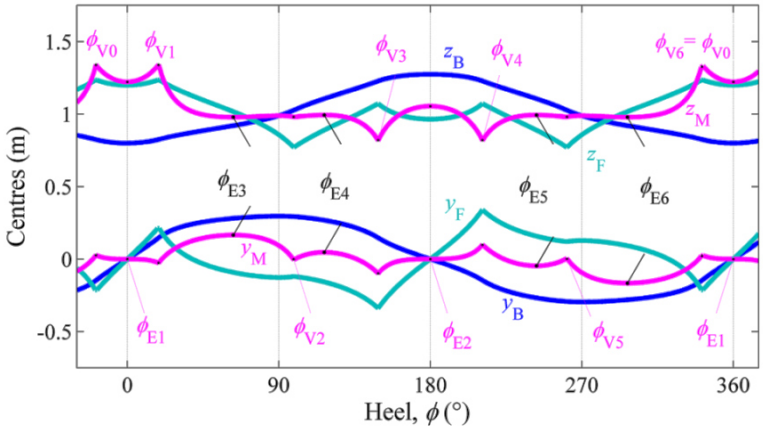


Figure 1. Hydrostatic centres components diagram for example of triangular isosceles cross section

Now, regarding additional extreme cusp discontinuity ϕ_{E3} existence in the first coordinate system quadrant, it occurs between two neighbour vertex cusp discontinuities ϕ_{V1} and ϕ_{V2}

$$\phi_{E3}: \frac{dX_M}{d\phi} = 0, \phi_{V1} \leq \phi_{E3} \leq \phi_{V2} \tag{4}$$

Above extreme cuspidal heel angle ϕ_{E3} value is different than 45° for a rectangular cross section, [3], and it is found that it depends on the isosceles triangle side angle β with

$$\phi_{E3} = 90 - \beta/2 \tag{5}$$

And when it depends on the isosceles triangle's symmetry angle α, the equation for it is

$$\phi_{E3} = 45 + \alpha/4 \tag{6}$$

Belonging formula for the calculation of the additional extreme cusp discontinuity heel angle pairs for all four coordinate system quadrants can be set now with

$$\phi_{Ek,k+1} = k \cdot 90° \mp \beta/2 \tag{7}$$

where $k = 2i + 1$, $i = 1, 2$ are the coordinate system half-planes, with results shown in Figure 2.

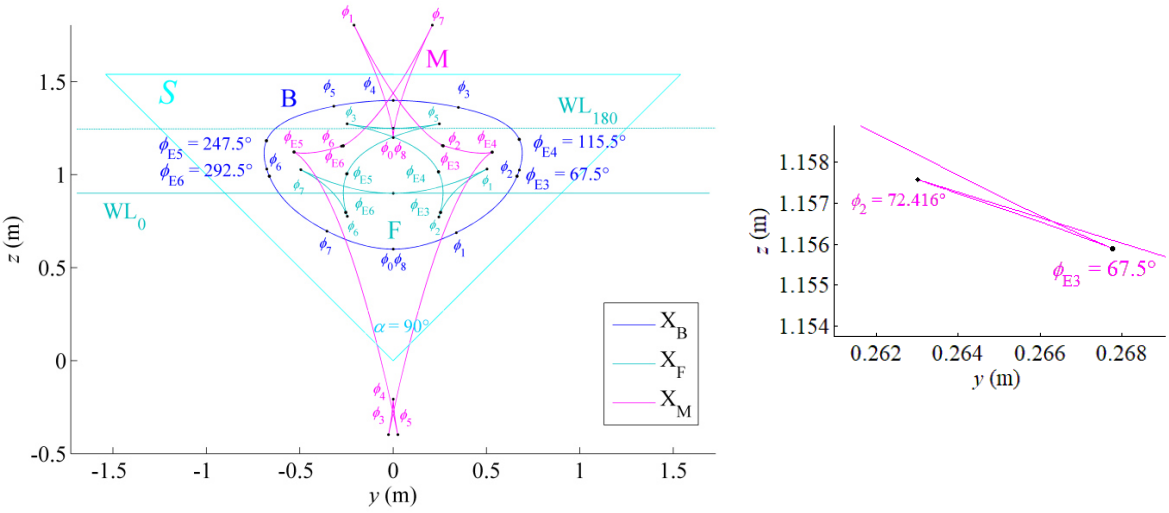


Figure 2. Hydrostatic centres curves diagram example for $\alpha = 90°$ ($\beta = 45°$)

3. Conclusions

The additional extreme cusp discontinuities of the metacentric locus curve in the first c.s. quadrant occurs for the heel angles equal to 45° + $\alpha/4$, depending on the symmetry angle α, or equal to 90° – $\beta/2$, in the symmetry of the isosceles triangle side angle β. Additional main result of the paper is the theorem about the general extreme cusp discontinuities existence in the symmetry of the isosceles triangle side angles that corresponds to similar theorem for rectangles from Zeeman. Except that, the formula for their calculation for all four c.s. quadrants is given also, showing no difference in their occurrence for upright or downward isosceles triangle.

Finally, since the additional extreme cusp discontinuities do not always occur, their existence bound can be determined, and that will be done in the future work of the author.

References

[1]Ban, D., Re-examination of centre of buoyancy curve and its evolute for rectangular cross-section, Part 1: Swallowtail discontinuity bounds. *Brodogradnja*, 74(2), 1-19, 2023. https://doi.org/10.21278/brod74201

[2]Ban, D., Re-examination of centre of buoyancy curve and its evolute for rectangular cross-section, Part 2: using quadratic functions. *Brodogradnja*, 74(3), 17-46, 2023. https://doi.org/10.21278/brod74302

[3]Zeeman, E. C., A Catastrophe Model for Stability of Ships. *Geometry and Topology: III Latin American School of Mathematics*, I.M.P.A., Rio de Janeiro, Brazil, 775-827, 1976.

11th International Congress
of Croatian Society of Mechanics
September 30 – October 3 2025
Vodice, Croatia

On Direct Method for Calculation of Joint CDF of Directional Wind Spectrum using L1 norm PRBF

Dario Ban [*], Jani Barle [*], Stipe Perišić [*]

[*] *Faculty of Electrical Engineering, Mechanical Engineering and Naval Architecture, University of Split, R. Boškovića 32, 21000 Split, Croatia*
E-mails: dario.ban@fesb.hr; jani.barle@fesb.hr; stipe.perisic@fesb.hr

Keywords: directional wind spectrum, joint CDF, L1 norm PRBF, direct calculation

1. Introduction

One of the main goals of the signal processing methods is to obtain a directional wind spectrum suitable for further calculations based on the measured wind data. The wind "Bora" data, [1], obtained from the in-situ measurements on the wind-turbines farm site in the coastal Croatia, is used here to show the integration method for direct determination of its Joint Cumulative Distribution Function (Joint CDF), [2], based on the Directional Wind Spectrum description using L_1 norm Polynomial Radial Basis Functions (L1 PRBF), [2].

2. Joint Cumulative Distribution Function Calculation using L1 norm PRBF

The method for the Joint Cumulative Distribution Function (CFD) determination, shown here, enables its direct calculation by solving double integral below the measured Directional Wind Spectrum, described by surrogate description using some of Radial Basis Functions (RBF) types.

Instead of usually used L_2 norms, this paper deals with polynomial type RBFs with L_1 norm, [2], showing their advantages and disadvantages in their usage for Joint CDF calculation. The general polynomial type of RBF with L_1 norm is here written in the form of the Multiquadric Radial Basis Function (MQRBF) equation with main function exponent β from the space of real numbers as

$$f(x,y) = \sum_{i=1}^{O} w_i \left(|x - t_{xi}| + |y - t_{yi}|\right)^{\beta} + c; \beta \in \mathbb{R} \tag{1}$$

where c is shape parameter, and $X \equiv \{x_j, y_j\}$, j = 1, ..., N, is input data set with $N \ll N_M$, where N_M are measured data set points, and $t \equiv \{t_{xi}, t_{yi}\}$, i = 1, ..., O, are RBF approximation/interpolation development centers.

The integral form that must be solved for a direct calculation of Joint CDF for a directional wind spectrum defined for the wind speed vector $v = [0, v_{max}]$ and directions $\phi = [0, 2\pi]$ is then

$$0 \le I \equiv F(v,\phi) = \int_0^{\varphi}\int_0^{v}\left(\sum_{i=1}^{O} w_i (|v - v_i| + |\phi - \phi_i|)^{\beta} + c\right) d\phi dv \le 1 \tag{2}$$

While the solution of above double integral I, in (2), is given for the minimal value of the main function exponent $\beta = 2$ in [2], belonging general solution, having interchanging ± signs, is given in this paper, for L_1 norm PRBFs with the main function exponent from the space of integer numbers, as

$$I = \frac{\sum_{j=1}^{4}\sum_{i=1}^{N} w_i [sign(x - t_{xi}) \pm 1]\left[sign\left(y - t_{yi}\right) \pm 1\right]\left(-y + t_{yi} - x + t_{xi}\right)^{\beta+2}}{4(\beta+1)(\beta+2)}, \beta \in \mathbb{N} \tag{3}$$

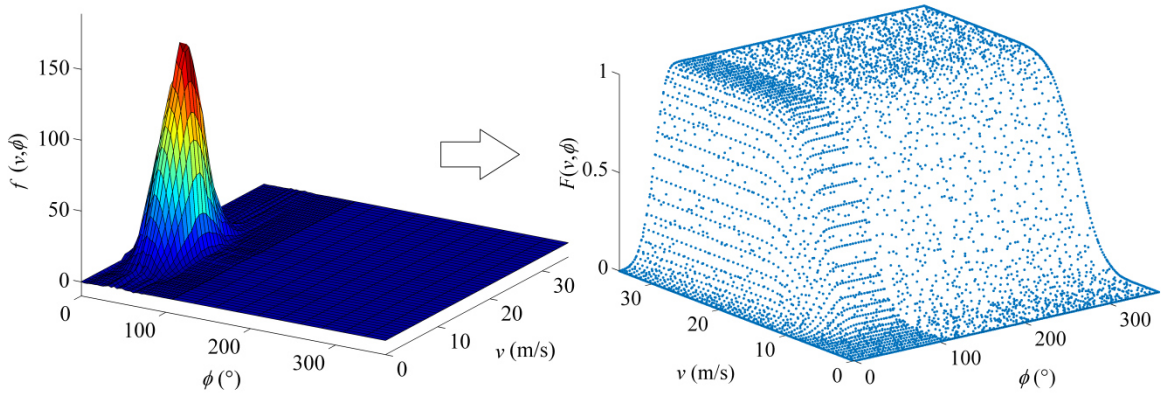


Figure 1. Joint CDF calculation from "Bora" Directional Wind Spectrum using L1 PRBF with $\beta = 2$

The example of a Joint CDF calculation, obtained using solution (3) for $\beta = 2$, in Figure 1 above, shows good smoothness results inside required function range $F \in [0, 1]$.

Advantages

- The main advantage of L_1 norm RBFs surface description (opposite to those for RBFs with L_2 norm) is that they don't have fill distance between points $h_{X,\Omega}$ limitation in data site X points arrangement, with their mutual distance $h_{X,\Omega} \to 0$. In other words, the only necessary condition to avoid singularity being that all input points should be different to each other with

$$X_1 \neq X_2 \neq X_3 \neq \cdots X_{N-1} \neq X_N \tag{4}$$

- High precision in comparison to RBFs with L_2 norm.
- Direct solution of double integral below surface is known for L_1 norm PRBFs, i.e. for the integer main function exponents.

Disadvantages

- The main disadvantage of the L_1 norm RBF directional wind spectrum description in (1) is that it is hard to achieve that all the results have the values above zero, i.e. $f(x, y) > 0$. This problem can be solved by boundary tension of the surface description using boundary points N_B added to the directional wind spectrum N_S input points, [2], obtaining total number of points

$$N = N_S + N_B \tag{5}$$

- Another disadvantage of the L_1 norm RBF surrogate description is quasi-smooth quality of obtained surface that can have several peaks.
- The final disadvantage is that the solution of the double integral in (2) is not known for non-integer main exponents of L_1 norm RBFs that can give smoother Directional Wind Spectrum and Joint CDF description results.

3. Conclusions

The L1 PRBF integration method for determination of the volume below Directional Wind Spectrum surface represents a direct method for the calculation of a Joint Cumulative Distribution Function (CDF) required in the wind data analysis, with advantages and belonging disadvantages of its application shown in this paper. While its solution for the integer main exponent value of the L_1 norm PRBF is shown here, the general solution of the double integral below directional wind spectrum for arbitrary main exponent is to be found in the future work of the authors.

References

[1] Barle, J., Đukić, P., Ban, D., Reliable model of Maximum Wind Load Amplitude, *30th Danubia-Adria Symposium on Advances in Experimental Mechanics,* Primošten, Croatia, 2013.

[2] Ban, D., Directional Wind Spectrum Description using Bivariate L1 Norm RBFs. *International Journal for Engineering Modelling*, Vol. 36, No. 1 Regular Issue, 2023.

11th International Congress
of Croatian Society of Mechanics
September 30 – October 3 2025
Vodice, Croatia

Advanced finite element model for stability analysis of laminated beam-type structures

Damjan Banić*, Goran Turkalj*, Domagoj Lanc*

*University of Rijeka, Faculty of Engineering, Vukovarska 58 Rijeka Croatia
E-mails: {dbanic,goran.turkalj,domagoj.lanc}@riteh.uniri.hr

Keywords: thin-walled, composite cross-section, shear deformable beam model, stability analysis

1. Introduction

Since load-bearing composite structures typically feature slender beam elements with thin-walled cross-sections, their response to external loads is significantly more complex. These structures have a higher propensity for stability loss and exhibit a more pronounced risk of buckling and deformation [1,2]. In the design process, it is crucial to carefully determine the stability limits of deformation forms. Analytical solutions are only applicable in simpler scenarios [1,2], which makes the development and implementation of numerical methods essential [3,4].

The goal of this study is to perform a nonlinear analysis of large displacements for thin-walled beam-type structures, taking into account shear deformation effects. The cross-section is subdivided into multiple rectangles, with each rectangle consisting of orthotropic layers arranged in a symmetric and balanced laminate. The analysis will rely entirely on a numerical model developed by the authors, with the results being compared to those from other relevant sources.

2. Methods

To incorporate shear deformation effects into the formulation, Timoshenko's theory for non-uniform bending and the modified Vlasov's theory for non-uniform or warping torsion are utilized. Additionally, this work presents an enhanced shear-deformable beam formulation that accounts for bending-bending and bending-warping torsion coupling shear deformation effects [3,4]. These effects occur in an asymmetric cross-section where the principal bending and shear axes do not align [5]. The beam is assumed to be prismatic and straight, with external loads considered as conservative and static. The element's geometric stiffness is derived using the updated Lagrangian (UL) incremental formulation [6], along with the nonlinear displacement field of a cross-section, which includes second-order displacement terms due to large rotation effects. This approach leads to the determination of the incremental geometric potential for the semitangential moment, representing internal bending and torsion moments. This ensures the preservation of moment equilibrium at the frame joints where beam members with different spatial orientations are connected [7].

By employing cubic interpolation for deflections and twist rotation, and a quadratic interpolation for slopes and the warping parameter, which accounts for shear-deformable effects, a locking-free beam element is achieved. This element, often referred to as a super-convergent element, does not require reduced integration techniques to avoid the shear-locking phenomenon [8].

To address material inhomogeneity in the composite cross-section, a separate numerical model is employed to calculate the cross-sectional properties. These properties are then weighted using three distinct reference moduli, effectively replacing the inhomogeneous cross-section with an equivalent homogeneous one [5]. The three reference moduli used are the longitudinal modulus Q_{11R}, shear modulus Q_{66R}, and coupling modulus Q_{16R}. Each modulus is responsible for handling specific cross-sectional properties. The properties related to the coupling between normal stress forces and normal strains are weighted by the referent longitudinal modulus Q_{11R} and are associated with the area, moments of inertia, area moments, sectorial inertial moments, and sectorial area moments. The torsional moment of inertia and shear coefficients are weighted by the referent shear modulus Q_{66R}.

Lastly, the coupling expressions that link normal forces with shear strains, and vice versa, are weighted with the referent coupling modulus Q_{16R}.

3. Results

A computer program called THINWALL v.17 was developed based on the procedures outlined in the previous section. To examine the impact of shear effects on the stability behavior of the analyzed structural members, two model comparisons are conducted. The first model ignores shear deformability (denoted as "SR"), while the second incorporates shear deformation effects using the procedure presented in this paper (denoted as "SD"). The material being analyzed is graphite-epoxy (AS4/3501), with properties of E_1 = 144 GPa, E_2 = 9.65 GPa, G_{12} = 4.14 GPa, and ν_{12} = 0.3. The cross-section branches are constructed with a symmetric and balanced laminate following a $[\theta/-\theta]_{2S}$ stacking sequence. Figure 1 displays the load-deflection curves for the free end of the cantilever column for different numbers of finite elements along the column length. The results obtained are consistent with the NX Nastran laminate shell eigenvalue solution, which gives F_{cr} = 40.5 kN for θ = 0° and Fcr = 44.5 kN for θ = 15°.

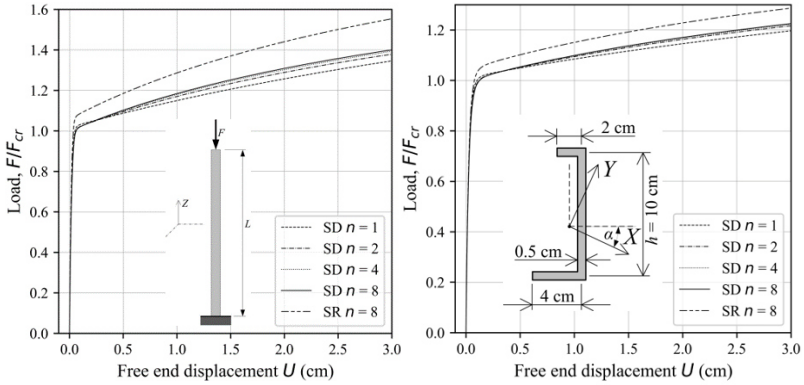


Figure 1. Cantilever U-profile column, L = 50 cm: θ = 0° (left), θ = 15° (right), buckling load vs free end displacement in the direction of X axis

4. Conclusions

A refined shear-deformable beam formulation has been developed for the geometrically nonlinear stability analysis of composite frames. The shear deformation effects are considered due to the non-uniform bending and torsion of thin-walled beams with asymmetric cross-sections. A benchmark example has been provided to validate the model. The significance of incorporating shear deformations into the formulation is evident from the substantial reduction in stability strength. Various material configurations have been analyzed, and their impact on the critical load has been presented and verified through a selected example.

References

[1] Cortínez, V.H., Piovan, M.T. Vibration and buckling of composite thin-walled beams with shear deformability. *Journal of Sounds and Vibrations*, Vol. 258, Issue 4, 2002.

[2] Kollár, L.P, Springer, G.S., *Mechanics of Composite Structures*. New York: Cambridge University Press; 2003.

[3] Turkalj, G., Lanc, D., Banić, D., Brnić, J., Vo, T.P., A shear-deformable beam model for stability analysis of orthotropic composite semi-rigid frames. *Composite Structures*, Vol. 189, 2018.

[4] Kim, N.I., Kim, M.Y., Exact dynamic/static stiffness matrices of non-symetric thin-walled beams considering coupled shear deformation effects. *Thin-Walled Structures*, Vol. 43, 2005.

[5] Pilkey, W.D., *Analysis and Design of Elastic Beams: Computational Methods*. John Wiley & Sons, INC., 2002.

[6] Lanc, D., Vo, T.P., Turkalj, G., Lee, J., Buckling analysis of thin-walled functionally graded sandwich box beams. *Thin-Walled Struct*, Vol. 86, 2015.

[7] Lanc, D., Turkalj, G., Vo, T.P., Brnic, J., Nonlinear buckling behaviours of thin-walled functionally graded open section beams. *Compos Struct*, Vol. 152, 2016.

[8] Reddy, J.N., *Energy principles and variational methods in applied mechanics*. Hoboken: Wiley, 2002.

11th International Congress
of Croatian Society of Mechanics
September 30 – October 3 2025
Vodice, Croatia

Distortional Plasticity and Associated Thermodynamics

Frédéric Barlat[*+]

[*]*IRDL, University of South Brittany, Lorient, France*
E-mails: frederic.barlat@univ-ubs.fr

[+]*Pohang University of Science and Technology, Republic of Korea*
E-mail: f.barlat@postech.ac.kr

Keywords: distortional, plasticity, hardening, Bauschinger, thermodynamics

1. Introduction

The effect of non-linear strain paths on the material constitutive response can be described effectively with distortional hardening. However, this comes at the expense of several state variables with their evolution equations. This makes this approach more complex than isotropic hardening for practical applications. Moreover, the classical continuum thermodynamics concepts are not suitable to obtain an accurate description of the material behavior. This work describes a recent distortional plasticity model and a non-conventional thermodynamics approach that circumvent the drawbacks explained above.

2. Distortional plasticity

During non-linear strain paths, the resulting stress-strain curve is subject to large fluctuations compared with the monotonic curve. For instance, the Bauschinger effect occurs at reversal with a flow stress much lower at reloading than at unloading. Cross-loading contraction, latent hardening and permanent softening are among other effects that may be observed. Classically, the Bauschinger effect has been modelled using kinematic hardening. However, recent works [1], [2] have shown that distortional hardening only (no back-stress) is a viable alternative to kinematic hardening to model the Bauschinger and other effects.

The yield condition in [1] writes

$$\bar{\sigma}(\boldsymbol{\sigma}) = \frac{1}{g}\left\{\bar{\xi}^q + f_1^q\langle \hat{\mathbf{h}} : \boldsymbol{\sigma}'\rangle^q + f_2^q\langle -\hat{\mathbf{h}} : \boldsymbol{\sigma}'\rangle^q\right\}^{\frac{1}{q}} \leq \sigma_r(\bar{\varepsilon}), \tag{1}$$

where g, f_1, f_2 and $\hat{\mathbf{h}}$ are state variables, and $\bar{\xi}$ an anisotropic effective stress. $\langle\cdot\rangle$ represents the Macauley brackets. $\hat{\mathbf{h}}$ indicates the distortion direction. Other state variables are hidden in Eq. (1) because they are arguments of $\bar{\xi}$, f_1 and f_2. When $g = 1$ and $f_1 = f_2 = 0$, the model reduces to isotropic hardening, with isotropic or anisotropic plasticity. In [2], the yield condition is similar but more than one $\hat{\mathbf{h}}$ are defined.

As an application, Fig. 1 corresponds to the tension-compression-tension (TCT) stress-strain curve of a TRIP 1180 advanced high strength steel sheet. Fig. 1(a) indicates that the distortional model is suitable to capture the material behavior successfully. In fact, the identification was mostly done with trial-and-error, showing that the coefficients are easily calculated despite the model relative complexity. The reason is that, by design, the coefficients are uncoupled by subsets and their physical meaning are known. Thus, four identification steps are needed: 1) Monotonic stress-strain curve; Anisotropy coefficients in the yield function; 3) Reverse loading coefficients and; 4) Cross-loading coefficients. It is worth noting that after each identification process, the corresponding coefficients are final. Of course, these coefficients might be optimized with a suitable algorithm. In

that sense, the uncoupling between coefficient subsets and the accuracy of the manually determined initial values guarantee a successful optimization.

Fig. 1(b) shows yield locus shapes before any deformation occurs (initial), after the first tension step (T1), the compression step (C) and the second tension step (T2).

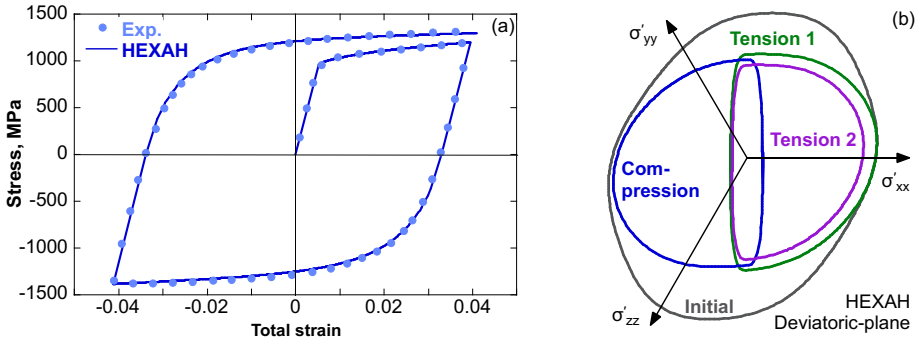


Figure 1. Tension-Compression-Tension for TRIP 1180 advanced high strength steel (AHSS). (a) Experimental and HEXAH-predicted stress-strain curve; (b) Yield loci in pi-plane at the end of different loading segments.

3. Continuum thermodynamics

In classical continuum thermodynamics [3], a postulated free energy potential ψ, function of several state variables, is postulated and leads to the definition of the thermodynamics forces. Moreover, a dissipation potential allows the definition of the state variable evolutions. If the model is strictly developed following this approach, the Clausius-Duhem inequality leads to a mechanical dissipation

$$\mathcal{D}_m = \boldsymbol{\sigma} : \dot{\boldsymbol{\varepsilon}}_p - \rho\dot{\psi}_p \geq 0 \tag{2}$$

which is always positive. In the above equation, ρ is the material density and ψ_p the plastic part of the free energy density. However, this method requires generalized normality, e.g., not only the normality of the strain rate to the dissipation potential but also normality of all the state variable rates. As a result, there is not much freedom for the choice of the evolution equations, and it is difficult to describe experimental results involving strain paths changes.

For distortional plasticity, it is proposed to find a free energy potential such that $\rho\dot{\psi}_p = 0$. In this case, although generalized normality is not required, Eq. (2) indicates that $\mathcal{D}_m$ is positive if only the plastic strain rate $\dot{\boldsymbol{\varepsilon}}_p$ is normal to the dissipation potential. In fact, by using a free energy based on the yield condition, it is possible to achieve $\rho\dot{\psi}_p = 0$ through the consistency condition. Since it is possible to prove that all the different yield loci are positive and contain the origin, as illustrated in Fig. 1(b), this demonstrates that the mechanical dissipation is positive. Note that all the intermediate yield loci during the evolution are also convex and contain the origin.

4. Conclusions

The use of distortional plasticity only (no back-stress) allows an accurate description of the Bauschinger effect in reversals and other non-proportional loading effects on the stress-strain behavior. A non-conventional, but more restrictive, thermodynamics approach was developed to insure the positivity of the mechanical dissipation.

References

[1] Barlat, F., et al., Distortional plasticity framework with application to advanced high strength steel. *Int. J. Sol. Struct.* 202, 947–962, 2020.

[2] Reyne, B., Barlat, F., HEXAH, an extension of the homogeneous anisotropic hardening framework. *Int. J. Plasticity* 155, 103303, 1-20, 2022.

[3] Lemaitre, J., Chaboche, J.L., Mechanics of Solid Materials. Cambridge University Press, 1990.

11th International Congress
of Croatian Society of Mechanics
September 30 – October 3 2025
Vodice, Croatia

Analysing the Wear Behaviour of Polymer Gears

Matej Borovinšek*, Aljaž Ignatijev*, Aleš Belšak*, Srečko Glodež*

*University of Maribor, Faculty of Mechanical Engineering, Smetanova 17, SI-2000 Maribor, Slovenia

E-mails: {matej.borovinsek, aljaz.ignatijev, ales.belsak, srecko.glodez}@um.si

Keywords: Polymer gears, Wear modelling, Finite element analysis, PrePoMax, Contact mechanics

1. Introduction

The wear behaviour of polymer gears is critical for their application in lightweight and noiseless drive systems [1,2]. Traditional analytical methods, such as those based on VDI 2736 [3], cannot capture the evolving gear geometry under rolling-sliding contact. In this work, we developed a computational model within the open-source PrePoMax environment, using the CalculiX solver, to predict the wear in spur gears with a polymer-steel pair. The model includes contacts, nonlinear material behaviour and geometry updates after the selected number of wear cycles, offering a more accurate prediction than the existing standards.

2. Methods

The Archard wear model [4] was used in its integral form to evaluate the wear depth per cycle:

$$h_i = \int \frac{k}{H} \cdot p_i \cdot \mathrm{d}s, \tag{1}$$

where h_i represents the depth of the wear in the i-th wear cycle, k is a dimensionless wear coefficient, H is the surface hardness of contacting faces, and p_i and ds are nodal contact pressure and differential sliding distance, respectively. Geometry was updated after a selected number of increments using a boundary displacement method and Laplacian mesh smoothing to ensure numerical stability and mesh quality. The computational model (Figure 1) incorporated five teeth on the polymer pinion (POM) and three teeth on the steel gear (16MnCr5).

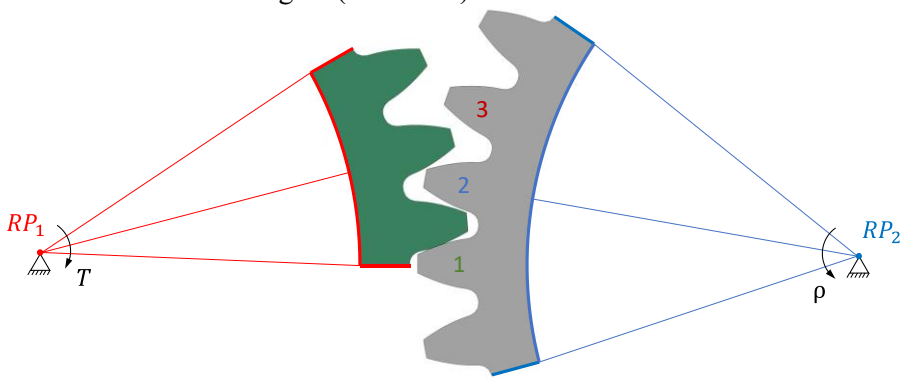


Figure 1: Computational model of a gear pair

An in-house developed test rig was used to evaluate wear experimentally at 20 Nm torque and 1000 rpm. Tooth flank wear was scanned optically after 1,000,000 cycles. Experimental results were compared to computational predictions for validation.

3. Results and Discussion

Simulation results converged when geometry was updated every 100,000 cycles. Figure 2 illustrates the strong correlation between the computed and experimental wear profiles, especially in the tooth root and tip regions. Analytical results based on VDI 2736 deviated significantly due to the assumption of constant geometry and the absence of multi-tooth contact.

The simulation showed that a hyperplastic material model significantly increases the predicted wear near the tooth root due to higher contact stress concentrations. Wear profiles indicated extended contact paths and redistributed pressure over multiple teeth, leading to a more realistic prediction of contact behaviour.

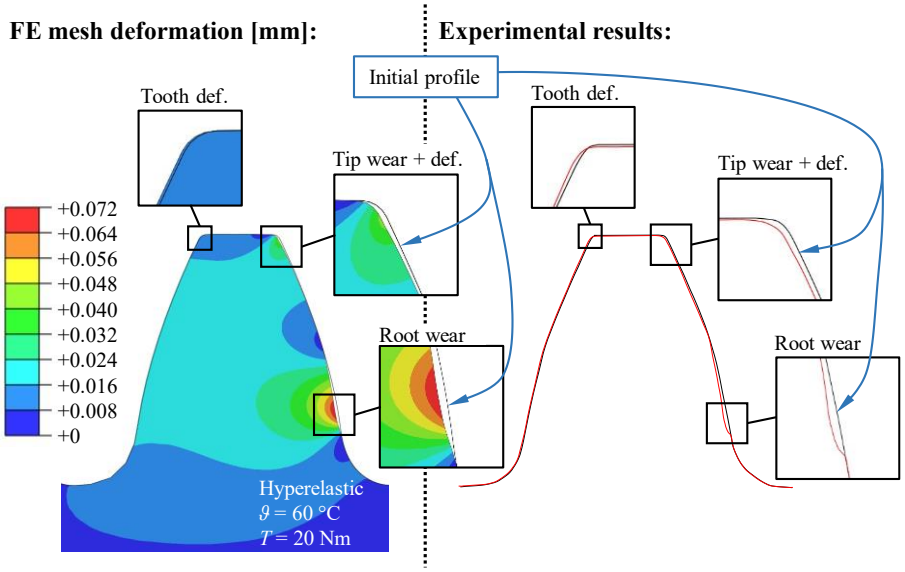


Figure 2: Comparison between numerical and experimental results at 1,000,000 load cycles

4. Conclusions

The proposed computational model enables accurate prediction of wear behaviour in polymer gears under realistic operating conditions. Including tooth deflection and mesh updates due to wear provides a comprehensive analysis tool validated against experimental data. Integrating an open-source tool (PrePoMax) facilitates broader use in research and industry.

References

[1] Ignatijev, A., Borovinšek, M., Glodež, S., A computational model for analysing the dry rolling/sliding wear behaviour of polymer gears made of POM. Polymers. *Polymers*, 16, 1073, 2024.

[2] Ignatijev, A., Glodež, S., Kramberger, J., Computational model for analysing the tooth deflection of polymer gears. *Polymers*, 16, 677, 2024.

[3] *VDI 2736 Part 2. Thermoplastic Gear Wheels - Cylindrical Gears - Calculation of the Load-Carrying Capacity*, Verein Deutscher Ingenieure, 2016.

[4] Archard, J.F., Contact and rubbing of flat surfaces. *Journal of Applied Physics*, 24, 981–988, 1953.

11th International Congress
of Croatian Society of Mechanics
September 30 – October 3 2025
Vodice, Croatia

Dynamic response of floating wind turbines subjected to wind, current and JONSWAP waves

Andrija Buljac[1], Petar Škvorc[2], Wenxian Yang[3], Ahsan Kareem[4], Hrvoje Kozmar[2]

[1] *Fractal d.o.o., Kupreška 37, 21000 Split, Croatia*
E-mail: andrija.buljac@fractal-res.com

[2] *Faculty of Mechanical Engineering and Naval Architecture, University of Zagreb, Ivana Lučića 5, 10000 Zagreb, Croatia*
E-mails: petar.skvorc@fsb.unizg.hr, hrvoje.kozmar@fsb.unizg.hr

[3] *School of Computing and Engineering, University of Huddersfield, Huddersfield, HD1 3DH, United Kingdom*
E-mail: W.Yang@hud.ac.uk

[4] *NatHaz Modeling Laboratory, University of Notre Dame, Notre Dame, IN 46556, USA*
E-mail: Ahsan.Kareem.1@nd.edu

Keywords: Floating offshore wind turbine, concurrent wind, wave and current loads, dynamic response, JONSWAP waves

1. Introduction

Horizontal-axis wind turbines can operate efficiently under steady wind conditions, which makes them well-suited for offshore environments. These locations typically offer more stable wind patterns, with lower turbulence intensity and more consistent wind direction compared to onshore sites. However, despite these advantages, offshore wind turbines (OWTs) face significant engineering challenges. They must withstand harsh marine conditions, including the combined dynamic loading from wind, waves, and ocean currents. These factors complicate both their structural design and long-term operational reliability. This study aims to experimentally investigate the dynamic response of an OWT supported by a tension-leg platform (TLP), using a scaled model subjected to simultaneous wind, wave, and currents loading.

2. Laboratory experiments

Experiments were conducted in the Wind-Wave-Current (WWC) Tank at Newcastle University, UK, which is capable of generating wind, waves, and currents. A scaled model of a TLP OWT was used in the study. The model included a buoyancy cylinder designed to maintain tension in the four mooring lines anchoring the platform to the seabed. This configuration helps prevent slack and snapping loads under dynamic environmental conditions [1], see Figure 1.

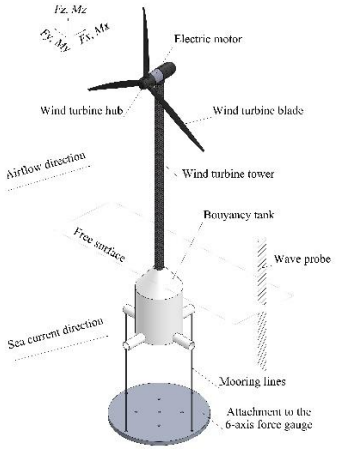


Figure 1. Floating OWT model placed in the WWC Tank test section

Data were recorded at a sampling rate of 200 Hz over a duration of 60 s. Wave heights were measured using a wave probe. To capture six-degree-of-freedom displacements of the OWT model, Qualisys motion capture cameras were employed. These devices tracked the relative positions of reflective markers attached to the OWT model. The displacement measurements were conducted only for configurations without airflow. Waves were generated in the WWC Tank using a wave generator, following the JONSWAP wave spectrum. The displacements of the OWT model in the surge and sway directions are presented in Figure 2 for two cases: a) waves only, and b) waves and currents.

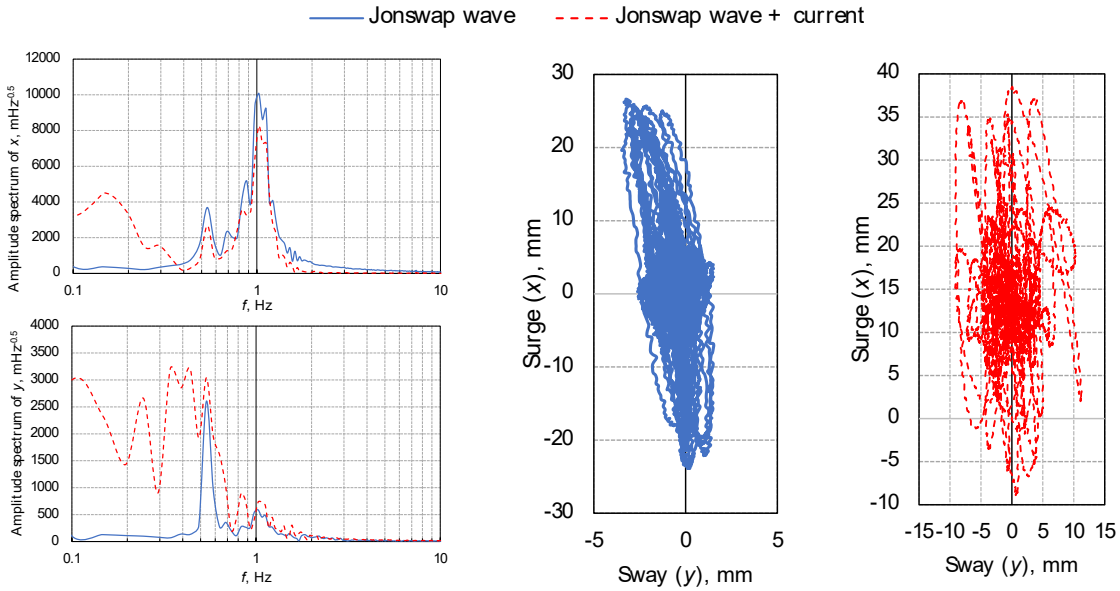


Figure 2. Surge and sway displacements and spectra for: a) waves only and b) currents with waves

The trajectory of the OWT model exhibits increased displacement in both the surge and sway directions when subjected to combined wave and currents loading. In the wave-only scenario, the trajectory forms an elliptical pattern, with surge motion being the dominant component. The peak displacement frequency aligns with the peak frequency of the wave spectrum as expected. However, the introduction of currents yields an amplification of low-frequency components in both surge and sway motions. The presence of currents also decreases the amplitude of spectral peak in the surge motion. This study builds upon previous work reported in [2], which focused on monopile-supported offshore wind turbines.

3. Conclusions

The dynamic behavior of a floating OWT subjected to combined wind, wave, and currents loading was investigated experimentally using a small-scale model mounted on a TLP. Under JONSWAP wave conditions, the model exhibited significant surge displacement at the peak wave frequency. The introduction of currents led to an increase in the low-frequency displacement. In the sway motion spectrum, the natural frequency remained the dominant feature in both loading scenarios. However, the presence of currents introduced additional displacement in the lower frequency range, indicating a shift in the system's dynamic response under combined loading.

ACKNOWLEDGEMENTS

This work was supported by the Croatian Science Foundation under the project number HRZZ-IP-2022-10-9434. Special thanks are extended to the WWC technical staff for their help with preparing the experiments.

References

[1] Hsu, W., Thiagarajan, K. P., Manuel, L., Extreme mooring tensions due to snap loads on a floating offshore wind turbine system, *Marine Structures*, 55, 182-199, 2017.

[2] Buljac, A., Kozmar, H., Yang, W., Kareem, A., Concurrent wind, wave and current loads on a monopile-supported offshore wind turbine, *Engineering Structures*, 255, 113950, 1-17, 2022.

11th International Congress
of Croatian Society of Mechanics
September 30 – October 3 2025
Vodice, Croatia

Application of Artificial Neural Networks in Structural Mechanics: Energy Harvesting Problems

Luca Caracoglia*, Marko Čanađija+

*Dept. of Civil & Envir. Engr., Northeastern University, 360 Huntington Av., Boston, MA 02115, USA
E-mail: lucac@coe.neu.edu

+University of Rijeka, Vukovarska 58, 51000 Rijeka, Croatia
E-mail: marko.canadija@riteh.hr

Keywords: Structural mechanics, surrogate modeling, Artificial Neural Networks (ANNs), wind-based energy harvesting, critical flutter condition

1 Introduction

Machine Learning methods have been rapidly expanding in science and engineering as efficient frameworks for the analysis, simulation and interpretation of complex physical phenomena. ANNs have emerged in recent years as modeling techniques that enable the generation of "surrogates" to approximate the behavior of mechanical and dynamical systems. The ANN is a computer algorithm that imitates the behavior of brain synapses through interconnected "neurons" to reconstruct the nonlinear relationship between a set of independent input variables and output variables. ANN neurons are organized in an input layer (variables x_i, $i = 1,\ldots,n$), one or more hidden layer(s), and an output layer (variables y_j, $i = 1,\ldots,m$). Each neuron in each layer is connected to each node of an adjacent layer. Hidden layers result from calculations using the input layer; outcomes are propagated between adjacent layers by a transfer or "activation" function. An ANN model requires calibration of the hyper-parameters, which is carried out using a set of input-output data. The objective of this study is to document recent research activity in the field of structural mechanics, in which ANN surrogates are used to replicate complex nonlinear solutions of a harvesting device.

2 Example: dynamic analysis of a torsional-flutter wind harvester

The increasing demand for renewable energy sources has promoted the use of innovative wind-based methods for electric power extraction. Apart from macro-scale systems, i.e., large wind turbines, and micro-scale miniature sensors, "meso-scale" devices at the scales of a few meters are important technology solutions. To bridge this gap, a meso-scale system that exploits torsional flutter to extract and convert kinetic energy from the wind airflow, has been proposed by the first author [1]. The torsional flutter converter concept originates from pioneering studies in 1970. Energy conversion is achieved by eddy currents [1].

The apparatus (Fig. 1a) is composed of a rigid blade-airfoil of chord-wise length $2b$ (with $0.5 \leq b \leq 1.0\,\text{m}$) and span-wise length ℓ. The blade-airfoil is a NACA0012 streamlined profile of aspect ratio $\text{AR} = \ell/b$. The blade-airfoil is attached to a support mast using a flexible plate-like interface component, shown as "torsional-rotational" mechanism in Fig. 1a. This interface is flexible and allows for a nonlinear, elastic torsional restoring moment about pivot "O". The pivot position, measured the from mid-chord point "C", is designated as ab with dimensionless $a = -1$ corresponding to the windward position at the apex of the airfoil. Apart from the range of positions $-1 \leq a < -0.75$ [1], a recent study considered positioning the pivot and support mast at a greater upwind distance $ab < -b$ from C ($a < -1.0$) to increase the moment arm of loads. Incipient torsional flutter solution under smooth, uniform wind speed U is found from Eq. (1a)-(1b) below [1]. In these equations, $\gamma = \omega_\alpha/\omega$ is the frequency ratio between the still-air angular frequency of the system (ω_α) and the incipient torsional flutter frequency at harmonic motion (ω); $\varepsilon = \pi\rho b^4\ell(I_{0,\alpha})^{-1}$ is a dimensionless inertia

parameter; $I_{0\alpha}$ is the total polar mass moment of inertia with respect to pivot O; $F(k)$ and $G(k)$ are the real and imaginary parts of the Theodorsen function with reduced frequency $k = \omega b/U > 0$; $\eta_{3D} = \mathrm{AR}/(2+\mathrm{AR})$ accounts for three-dimensional lift loads.

$$\gamma^2 = 1 + \varepsilon\eta_{3D}\left[(0.125+a^2) + k^{-2}(2a+1)F(k) + k^{-1}(2a^2-0.5)G(k)\right] \tag{1a}$$

$$-G(k)(2a+1) + k(0.5-a) + kF(k)(2a^2-0.5) = 0 \tag{1b}$$

The reduced frequency at incipient flutter k^* is found from Eq. (1b). Then, k^* is substituted into Eq. (1a) to derive the frequency ratio at flutter γ^* and the critical flutter wind speed $U_r^* = (k^*\gamma^*)^{-1}$, which depends on ε and η_{3D}. The operational range of the harvester must be restricted to $\gamma^* > 0$ only, i.e., the solution exists if and only if Eq. (1a) is positive. Notably, the range of suitable ε values yielding $\gamma^* > 0$ reduces as the moment arm of the loads (a) increases [1].

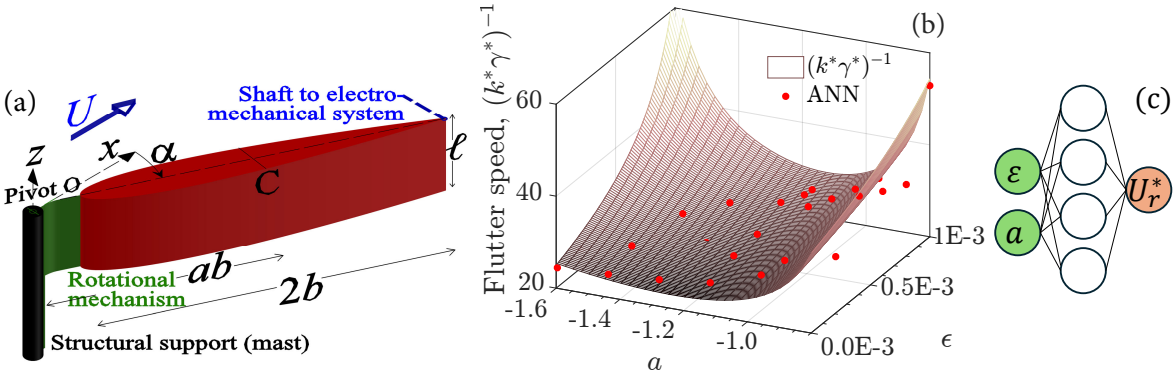


Figure 1. Analysis of a wind harvester with aspect ratio $\mathrm{AR} = 4$ ($\eta_{3D} = 0.67$)**: (a) 3D geometry (not to scale), (b) dimensionless flutter speed *vs.* pivot position a and inertia parameter ε, (c) ANN schematics**

Fig. 1b examines the dimensionless flutter U_r *vs.* a and ε. The pivot position varies as $-1.6 \le a \le -0.8$, while the inertia parameter is $1\mathrm{E}-4 \le \varepsilon \le 1\mathrm{E}-3$. The data set of analytical solutions is found from Eqs. (1a)-(1b). The analytical solution is depicted by a continuous surface.

An ANN-based surrogate model with two inputs ($x_1 = a$, $x_2 = \varepsilon$), one output ($y_1 = U_r^*$) and one hidden layer with 10 neurons is considered to replicate the analytical solutions; the ANN schematics in Fig. 1c is for illustration purposes only. The log-sigmoid application function is employed. The ANN hyper-parameters are determined by Levenberg–Marquardt back propagation algorithm; training, calibration and testing are carried out by splitting the data set as 70%, 15% and 15%.

The surrogate model approximates the analytical solution surface for most values of a and ε, except for large upwind values of the pivot ($a \approx -1.6$). Nevertheless, the tuning of the harvester in this range of a and ε is less important; the design solution is not very promising since the flutter speed $U_r^* = (k^*\gamma^*)^{-1}$ rapidly increases, thus reducing the power efficiency. Increasing the number of neurons in the hidden layer or utilizing two or three hidden layers does not lead to relevant improvement. Possibly, the ANN model could be improved by considering input-convex neural networks or by splitting the regression into sub-models, defined over a narrower range of inputs.

3 Remarks and conclusions

The final research will present other examples of wind energy applications, i.e., to predict the performance of harvesting devices and small turbines with various configurations. The aim of these comparisons is to demonstrate the versatility of ANN-based surrogate modeling in the various fields, to highlight advantages and to examine potential limitations.

4 Acknowledgments

L. Caracoglia acknowledges support from USA Natl. Science Foundation, Award CMMI-2020063.

References

[1] Caracoglia, L., Modeling the Coupled Electro-Mechanical Response of a Torsional-Flutter-Based Wind Harvester with a Focus on Energy Efficiency Examination. *J. Wind Eng. Ind. Aerodyn.*, 174, 437–450, 2018.

11th International Congress
of Croatian Society of Mechanics
September 30 – October 3 2025
Vodice, Croatia

Development and validation of Sex-specific finite element head models

Carlos Cardoso*, Ricardo Sousa* , Fábio Fernandes+, Afonso Silva*

* *TEMA - Centre for Mechanical Technology and Automation, Department of Mechanical Engineering, University of Aveiro, Campo Universitário De Santiago, Aveiro, 3810-193, Portugal.*
E-mail: rsousa@ua.pt

+ *LASI—Intelligent Systems Associate Laboratory, Portugal*

Keywords: Compression, Dynamic Behaviour, Cork, Numerical Simulation, Experimental tests

1. Introduction

Traumatic brain injury (TBI) remains a significant public health concern, exhibiting considerable variation in outcomes based on several demographic factors, including injury severity, genetic factors and sex [1]. Recent studies have elucidated notable sex differences in the incidence and consequences of TBI, underscoring that females may exhibit distinct physiological responses compared to their male counterparts [1-2]. Additionally, sex differences, including variations in brain morphology and material properties, may significantly affect biomechanical responses to head impacts. For instance, a study utilising sex-specific axonal models found that female axons exhibited substantially higher peak strains and associated neurofilament failures compared to male axons, attributed to differences in microtubule configurations [3]. Finite element head models (FEHMs) have become indispensable tools for studying these differences, offering detailed insights into stress and strain distributions during impact scenarios. In this study, we utilised validated female and male FEHMs incorporating different material properties and anthropometric characteristics. Both models were subjected to identical simulation setups replicating one soccer heading scenario, with accelerations applied to the head's centre of gravity (COG). The analysis and comparison of the resulting strain and stress distributions aims to elucidate the impact of sex-specific factors on brain injury mechanisms, thereby contributing to more personalised and effective TBI prevention and treatment strategies.

2. Methods

The simulation setup presented in this study was based on the work of Wahlquist *et al.* [4], in which data from youth soccer heading sessions were retrieved from Triax SIM-G sensors positioned within the player's headbands. The sensor data was derived from repetitive head impacts exposures involving 27 female youth soccer players over 2 playing seasons. The data obtained was subjected to a selection process based on the severity, including the peak linear acceleration (PLA) and peak rotational velocity (PRV), totalling 81 headers over 30 games and 1506 headers over 41 practices. For this study, it was selected one of the highest g impact cases. In Abaqus environment, the accelerations and velocities were established as tabular amplitudes with increments for each millisecond, for a total of 61 ms. These were used as boundary conditions (BCs), which were applied to the COG of the head models. The models employed in this study were the YEAHM [5] and the FeFEHM [6], for the male and female head models, respectively. Both represent subjects of the same age (65 years old), with each Finite Element Head Model (FEHM) exhibiting distinct material properties. The YEAHM employs homogeneous brain material properties derived from Rashid *et al.* [7], while the FeFEHM utilises the parameters from Menichetti *et al.* [8] for the soft tissues. The cerebrospinal fluid (CSF) properties in both models were adapted from Gilchrist M. [9], though the parameter values differ between the models. Regarding the interaction between structures, a tangential behaviour friction coefficient (μ=0.2) was considered for both models, to limit unrealistic

brain motion. Both models were meshed with elements with reduced integration and hourglass stabilization (C3D8R) for the skull and brain tissues. Injury assessment was conducted by selecting injury criteria, such as the Maximum Principal Strain (MPS), von Mises stress, and pressure. Additionally, the volume fraction of total brain exceeding a predetermined strain threshold, Cumulative Strain Damage Model (CSDM), was calculated to assess TBI probability [10]. Each lobe of the head models was analysed, and the selected perimeter for data extraction is demonstrated in Figure 1D, including a wide range of finite elements between the sulci and gyri regions.

Acknowlegments: The authors acknowledge the support given by Fundação para a Ciência e a Tecnologia (FCT) through the projects PTDC/EME-EME/1239/2021 (BAFHTA). Afonso Silva acknowledges the grant FCT 2024.00600.BDANA while Marcos Gomes acknowledges grant FCT 2024.04271.BDANA.

References

[1] Gupte, R., *et al.*, J. of Neurotrauma, 2019.
[2] Munivenkatappa, A., *et al.*, Inj. Science, 2016.
[3] Zhang, C., *et al.*, J. of Neurotrauma, 2023.
[4] Wahlquist, V., *et al.*, Sports Medicine, 2021.
[5] Fernandes, F., *et al.*, Eng Computations, 2018.
[6] Carmo, G., *et al.*, Comp Meth & Prog Biomed, 2023.
[7] Rashid, B., et al., J. of the Mech Beh. of Biomed. Mat., 2012.
[8] Menichetti, A., *et al.*, Int. J. of Eng. Science, 2020.
[9] Gilchrist, M., Key Eng. Materials, 2003.
[10] Takhounts, E., *et al.*, Stapp Car Crash J., 2003.

11th International Congress
of Croatian Society of Mechanics
September 30 – October 3 2025
Vodice, Croatia

A Fracture Mechanics-Based Approach for Material Defects and Fatigue Assessment: Highlighting the Role of the Intrinsic Fatigue Limit

Mirco D. Chapetti*, Nenad Gubeljak+

*Research Institute for Material Science (INTEMA). National University of Mar del Plata, CONICET, Av. Colón 10850 (B7606BWV) Mar del Plata, Argentina.
E-mails: mchapetti@fi.mdp.edu.ar

+Faculty of Mechanical Engineering, University of Maribor, Smetanova ul. 17, 2000 Maribor, Slovenia
E-mail: nenad.gubeljak@um.si

Keywords: fatigue resistance, fracture mechanics, defect assessment, estimation

1. Introduction

Certain manufacturing processes, particularly additive manufacturing, often produce intrinsic defects that can bypass or significantly shorten the crack initiation phase. Consequently, fatigue damage in such components is primarily governed by crack propagation from pre-existing flaws until final failure occurs.

Fracture mechanics plays an important role in developing robust fatigue predictive models. When combined with improved understanding of small-crack behaviour, this has established damage tolerance design as the most effective strategy for ensuring the structural integrity of mechanical components. However, applying fracture mechanics to materials with inherent defects requires an estimation of the material's resistance in the absence of flaws, namely, its intrinsic fatigue limit.

This study outlines fundamental concepts and assumptions related to fatigue limits and fracture mechanics, supported by experimental evidence linking intrinsic fatigue resistance to naturally-arrested, non-propagating cracks. Additionally, two straightforward equations are proposed to estimate the intrinsic fatigue resistance of metallic alloys.

2. The fracture mechanics' approach and the minimum threshold for crack growth associated to the intrinsic fatigue limit, ΔK_{dR}

Currently it is considered that the high cycle fatigue limit is not a critical stress for crack initiation but the one below which an initiated micro-crack cannot propagate, that is to say, the fatigue limit is in fact a threshold stress for micro-crack growth. This concept was clearly illustrated by Miller in by using a Kitagawa-Takahashi diagram [1] that shows the threshold stress range for crack propagation as a function of crack length (see Figure 1).

Here we investigate the importance of distinguishing between the intrinsic fatigue limit of the material, given by $\Delta\sigma_{eR}$ or ΔK_{dR}, and the fatigue limit of a material containing small cracks or defects larger than the microstructural size d (see Figure 1). In these materials, what is being experimentally measured or estimated, for instance, using the Murakami-Endo model [2] is the fatigue limit of the matrix-defect ensemble. In this case, it is not possible to experimentally measure the intrinsic fatigue limit of the matrix, so it becomes necessary to estimate it appropriately.

Let's now analyse two formulas proposed here to estimate the intrinsic fatigue limit, $\Delta\sigma_{eR}$, or alternatively the associated propagation threshold, ΔK_{dR}, that according to the model proposed by Chapetti is defined as [3]:

$$\Delta K_{dR} = Y\,\Delta\sigma_{eR}\,\sqrt{\pi\,d} \tag{1}$$

One of them can be inferred using the Murakami-Endo model [2] and the microstructural size *d*, in the following manner:

$$\Delta K_{dR} = 0{,}00356\ (H_V + 120)\ d^{1/3} \quad (2)$$

Where *d* is in μm and H_V in kgf/mm^2, given ΔK_{dR} in MPa.m$^{1/2}$. On the other hand, Chapetti has proposed the following expression to estimate ΔK_{dR} for steels as a function of H_V hardness and the microstructural size *d* [4]:

$$\Delta K_{dR} = 1 + 0.5\ H_V \sqrt{\pi\ d} \quad (3)$$

Figure 2 shows the ΔK_{dR} values given equation (1), along with the corresponding estimations obtained using equations (2) and (3) for the steels data reported in literature [5].

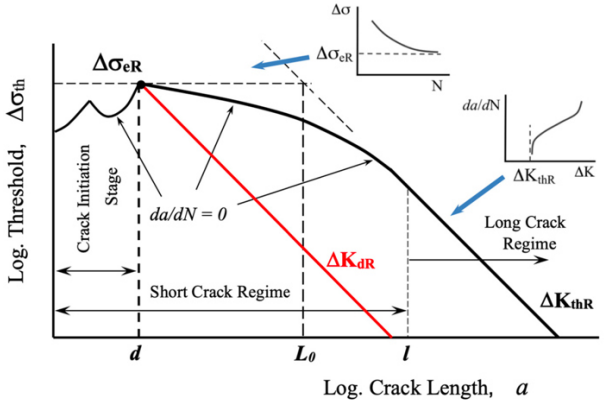


Figure 1. Kitagawa-Takahashi diagram showing the transition between the intrinsic fatigue limit and the threshold for long cracks

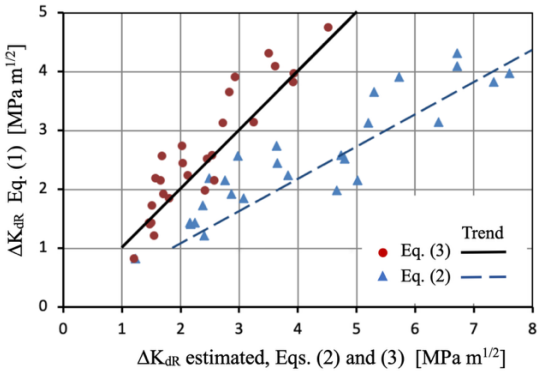


Figure 2. Comparison between ΔK_{dR} values given by equation (1) for experimental data [5] and estimations using equations (2) and (3)

3. Conclusions

Black line in Figure 2 represents the equality between the values obtained from equation (1) and the estimations, indicating the satisfactory performance of equation (3) to estimate ΔK_{dR}.

References

[1] Miller, K.J. The two thresholds of fatigue behaviour. Fat Fract Engng Mater Sruct 16(9):931–9, 1993.

[2] Murakami, Y, Endo, M. Effects of defects, inclusions and inhomogeneities on fatigue strength. Int J Fatigue 16(3):163-182, 1994

[3] Chapetti, M.D. Fatigue propagation threshold of short cracks under constant amplitude loading. Int J Fatigue 25:1319–26, 2003.

[4] Chapetti, M.D. Hardness as a tool for the estimation of the microstructural threshold. Procedia Structural Integrity 7: 229–234, 2017.

[5] Chapetti, M.D., Gubeljak, N., Kozak, D. Intrinsic fatigue limit and the minimum fatigue crack growth threshold. Materials 16:5874, 2023.

11th International Congress
of Croatian Society of Mechanics
September 30 – October 3 2025
Vodice, Croatia

Solving Biharmonic and Bi-Helmholtz Problems by a Localized Method of Fundamental Solutions

Csaba Gáspár*

*Széchenyi István University, Egyetem tér 1, H-9026 Győr, Hungary
E-mail: gasparcs@math.sze.hu

Keywords: Method of Fundamental Solutions, biharmonic equation, bi-Helmholtz equation, localization, Schwarz overlapping method

Abstract

Many engineering problems are described by the biharmonic equation defined in a sufficiently regular domain Ω:

$$\Delta\Delta u = f, \tag{1}$$

where Δ denotes the Laplace operator. Eq. (1) appears, for instance, in plate bending problems in linear elasticity, or in fluid mechanics (e.g., Stokes flow). Note that since Eq. (1) is of fourth order, two independent boundary conditions should be imposed, e.g., a Dirichlet boundary condition:

$$u|_\Gamma = u_0, \qquad \frac{\partial u}{\partial n}|_\Gamma = v_0, \tag{2}$$

or Navier boundary condition:

$$u|_\Gamma = u_0, \qquad (\Delta u)|_\Gamma = w_0, \tag{3}$$

where Γ denotes the boundary of the domain Ω, and u_0, v_0 and w_0 are prescribed, sufficiently regular boundary functions.

The traditional solution techniques such as the Finite Difference Method or the Finite Element Method require a more or less sophisticated grid or element structure inside the domain Ω, and introduce a high number of unknowns. In contrast to this, meshless methods do not require any grid or mesh structure, only a set of scattered domain and boundary points, so that they exhibit some advantageous properties from a computational point of view.

Similar problems also appear in elasticity when the governing equation is the modified bi-Helmholtz equation:

$$(\Delta - c^2 I)^2 u = f, \tag{4}$$

where c is a given constant (I denotes the identity operator). Note, however, that Eqs. (1) and (4) do not arise only in real-life engineering problems, but also in completely different areas, e.g. in scattered data interpolation problems based on the biharmonic (or even bi-Helmholtz) equation [1]. In this case, the boundary conditions are completed by pointwise interpolation conditions at some predefined interpolation points defined in the domain Ω. Another source of such problems is when the Laplace equation is approximated by a singularly perturbed fourth-order Laplace-Helmholtz equation.

The Method of Fundamental Solution (MFS, see e.g. [2]) is a well-established meshless method. For the 2D homogeneous biharmonic problem, the approximate solution of the problem is expressed in the following form:

$$u(x) = \sum_{j=1}^{N} \alpha_j \Phi(x - s_j) + \sum_{j=1}^{N} \beta_j \Psi(x - s_j), \tag{5}$$

where $s_1, s_2, \ldots, s_N$ are predefined external *source points*. The functions Φ and Ψ denote the 2D

harmonic and biharmonic fundamental solution, respectively:

$$\Phi(x) = \frac{1}{2\pi} \log ||x||, \qquad \Psi(x) = \frac{1}{8\pi} \cdot ||x||^2 \cdot \log ||x||,$$

where $||.||$ denotes the familiar Euclidean norm in $\mathbf{R^2}$.

The a priori unknown coefficients $\alpha_1, ..., \alpha_N$, $\beta_1, ..., \beta_N$ can be calculated by enforcing the boundary conditions at some predefined $x_1, x_2, ..., x_M$ *boundary collocation points*. This results in an algebraic linear system of equations. The numbers N and M do not necessarily need to be equal. If they differ, this system can be solved in the sense of least squares, or using the Singular Value Decomposition. It is worth noting that the expression in Eq. (5) can be simplified by omitting the first sum, that is, the approximate solution is sought as a linear combination of only the biharmonic fundamental solution Ψ shifted to the source points, provided that a double set of the source points located along two different closed curves around the domain are used. For details, see [3].

The greatest computational advantage of the MFS is that it is truly meshless, easily programmable, and the number of introduced unknowns is moderate. However, the resulting algebraic system is ill-conditioned in general. The proper choice of source points is also a nontrivial problem [4]. If the function in the right-hand side of Eq. (1) or Eq. (4) differs from zero, i.e. the problem is nonhomogeneous, then the idea of the Method of Particular Solutions (MPS) should be used. However, this needs a scattered data interpolation for the function f, which significantly increases the number of introduced unknowns.

To reduce the above computational problems, *localization techniques* have been introduced, which split the original problem into several subproblems. These subproblems are defined in small local subdomains which cover the original domain. The matrices of the subproblems can be assembled into a global sparse matrix [5], which makes it possible to apply numerically efficient solution techniques. The idea remains applicable also to inhomogeneous problems [6].

In this paper, a different type of localization is presented. In this approach, the local subdomains are strongly overlapped; the local subproblems are solved separately, using the MFS, and the computed values within a local subdomain serve as boundary values for the neighboring subproblems. This results in a Seidel-like iterative method, which mimics the classical Schwarz overlapping method, see [7]. See also [8] for the Laplace equation. In [1], the same idea was applied to the biharmonic scattered data interpolation. Here the technique is extended to the case of the bi-Helmholtz equation as well. It is also possible to simplify the computations when the governing equation is inhomogeneous. The applied localization technique avoids the problems associated with large, dense and ill-conditioned linear systems. The method is illustrated via numerical examples.

References

[1] Gáspár, C., Biharmonic Scattered Data Interpolation Based on the Method of Fundamental Solutions. In: J. Mikyška, C. Mulatier, M. Paszynski, V.V. Krzhizhanovskaya, J.J. Dongarra, P.M.A. Sloot, eds, *Computational Science - ICCS 2023*, 485-499. LNCS 10476, Springer, Cham, 2023.

[2] Golberg, M.A. The method of fundamental solutions for Poisson's equation. *Eng. Anal. Bound. Elem.* 16, 205-13, 1995.

[3] Gáspár, C., Karageorghis, A., Method of fundamental solutions formulations for biharmonic problems. *Eng. Anal. Bound. Elem.* 175, 106180, 2025.

[4] Chen, C.S., Karageorghis, A., Li, Y., On choosing the location of the sources in the MFS. *Numer. Algorithms* 72, 107-30, 2016.

[5] Fan, C.M., Huang, Y.K., Chen, C.S., Kuo, S.R., Localized method of fundamental solutions for solving two-dimensional Laplace and biharmonic equations. *Eng. Anal. Bound. Elem.* 101, 188-97, 2019.

[6] Zhang, J., Yang, C., Zheng, H., Fan, C.M., Fu, M.F., The localized method of fundamental solutions for 2D and 3D inhomogeneous problems. *Math. Comput. Simulat.* 200, 504-524, 2022.

[7] Lions, P.L., On the Schwarz alternating method I. In: R. Glowinski, G.H. Golub, G.A. Meurant, J. Périaux, eds., *First International Symposium on Domain Decomposition Methods for Partial Differential Equations*, 1-42. SIAM, Philadelphia, PA, 1988.

[8] Gáspár, C., A Localized Version of the Method of Fundamental Solutions in a Multi-level Context. *Periodica Polytechnica Civil Engineering*, https://doi.org/10.3311/PPci.21535, 2023.

11th International Congress
of Croatian Society of Mechanics
September 30 – October 3 2025
Vodice, Croatia

Flow and transport karst modelling: Salt and heat tracer tests in 3-D laboratory physical models

Hrvoje Gotovac*, Marin Zelenika+

*Faculty of Civil Engineering, Architecture and Geodesy, University of Split, Matice hrvatske 15, 21000 Split, Croatia.
E-mails: hrvoje.gotovac@gradst.hr

+Promark gradnja d.o.o., Mostarska 12, Metković.
E-mail: marin.zela@gmail.com

Keywords: flow and transport modelling, karst aquifers, physical models, tracer tests, control volume isogeometric analysis

1. Introduction

Flow and transport modelling in karst aquifers is faced by many challenging issues, especially due to absence of validation and verification of models. In this paper, we will present salt and heat tracer tests under strongly laboratory conditions. In large 3-D physical model, that consists of porous matrix and conduits, tracer tests are performed measuring piezometric head, flow rates separately in porous matrix and conduits as well as concentration and/or temperature of the injected tracers. In order to verify appropriate numerical karst model with tracer experiments, we develop new hybrid model based on Control Volume IsoGeometric Analysis [1,2,3]. Comparison between numerical and laboratory simulations proves that hybrid distributed numerical model are needed to adequately describe complex tracer tests in karst aquifers.

2. Experimental setup

Figures 1 and 2 present geometrical setup of 3-D physical model with dimensions 4*2.55*2 m, filled with gravel, fine and coarse quartz sand and three conduits: smaller C1 (d=12 mm), larger C2 (d=44 mm) and C3 (d=12 mm) with branches [see 1].

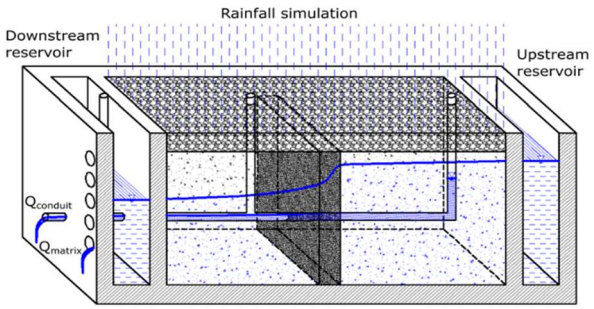


Figure 1. Scheme of 3-D physical model.

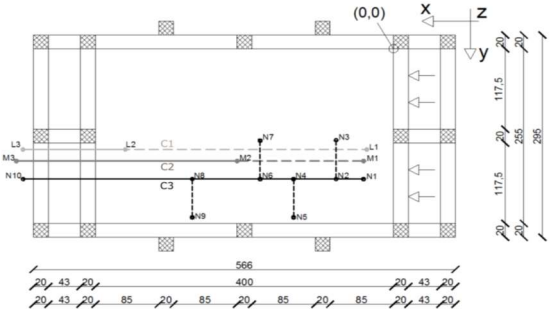


Figure 2. Dimensions of 3-D physical model in x-y plane with conduit setup.

3-D model is equiped with ranfall simulator with eight fields, water level regulations/wiers in upstream and downstream resorvoir, 44 lower piezometers for measurements of piezometric head, 2 flowmeters for matrix and conduit flow rates and 20 uper piezometers measurements of salt concentration and temperature.

3. Tracer tests

In the new Laboratory for Water Resources and Environmental Engineering in Žrnovnica (Split), over than 36 salt and heat tracer tests are performed including the different options for tracer injection position, flow setup between resoirvors, conduit setup or rainfall intensity. For illustration properties, in Figure 3, salt tracer test 9 is presented including comparison with developed hybrid model CV-IGA (Gotovac et al., 2021; Kamber et al., 2022). Tracer test 9 includes open conduit C2, flow rate in matrix of 0.74 m^3/h, flow rate in C2 of 2.39 m^3/h, tracer injection in B20 of 1 kg of salt in 200 litre of fresh water, and after that rainfall intensity of 3 $l/min/m^2$ during the 60 minutes. Comparison proves abiliy of CV-IGA hybrid model to adequately describe tracer tests. This study reveals that relatively complex hybrid CV-IGA model, based on mathematical foundations of 3-D Richards and 1-D diffusive wave equations for flow and advection-dispersion equation for transport, is needed to accurately describe flow and transport exhange and interplay between 3-D matrix and 1-D conduits. Flux flow exchange is described by first order flux based on unknown calibration parameter and head difference between conduits and matrix. Transport exchange is simply presented by advective exchange term without any aditional parameter.

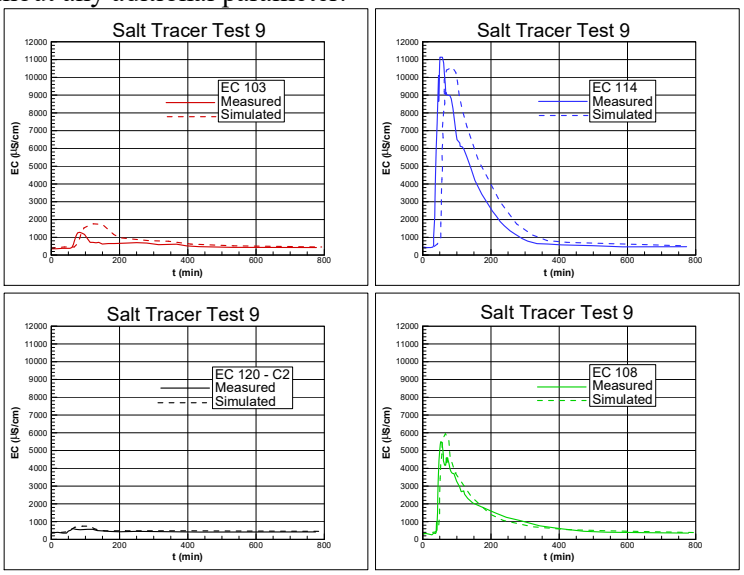


Figure 3. Comparison between numerical and experimental simulations for four selected EC sensors for salt tracer test 9.

3. Conclusions

Salt and heat tracer tests are performed in large 3-D karst physical model. This study reveals that relatively complex hybrid CV-IGA model, is needed to accurately describe flow and transport flux exhange between 3-D matrix and 1-D conduits.

References

[1] Malenica, Luka, et al. "Groundwater flow modeling in karst aquifers: Coupling 3d matrix and 1d conduit flow via control volume isogeometric analysis—Experimental verification with a 3D physical model." *Water* 10.12 (2018): 1787.

[2] Gotovac, Hrvoje, Luka Malenica, and Blaž Gotovac. "Control Volume Isogeometric Analysis for groundwater flow modeling in heterogeneous porous media." *Advances in water resources* 148 (2021): 103838.

[3] Kamber, Grgo, et al. "2-D local hp adaptive isogeometric analysis based on hierarchical Fup basis functions." *Computer methods in applied mechanics and engineering* 398 (2022): 115272.

11th International Congress
of Croatian Society of Mechanics
September 30 – October 3 2025
Vodice, Croatia

Application of Fixed-Pole Interpolation in Vibration Analysis of 3D Micropolar Continuum

Laura Grbac*, Gordan Jelenić*

* *Faculty of Civil Engineering, University of Rijeka, Radmile Matejčić 3, Rijeka, Croatia*
E-mails: laura.grbac@uniri.hr, gordan.jelenic@uniri.hr

Keywords: Cosserats' theory, fixed-pole approach, finite element method, micropolar continuum, vibration analysis

1 Introduction

The micropolar (Cosserats') theory of elasticity represents one of the possible generalisations of the classical (Cauchy) theory, developed to describe more accurately the behaviour of materials with pronounced microstructure, and therefore also to capture the *size-effect* phenomenon. In addition to the Cauchy stress tensor, the theory includes a couple-stress tensor, which implies an additional rotational field in addition to the displacement field already present. As a consequence, we need to know the values of six independent material parameters in order to define a centrosymmetric, linear-elastic and isotropic micropolar material [1]. However, the lack of reliable procedures for their experimental determination presents a major obstacle to the broader application of the theory. Therefore, the development of high-quality micropolar finite elements is essential for the future progress of the theory — both in engineering simulations and in virtual experiments aimed at parameter identification through inverse analysis. For this purpose, the authors developed micropolar finite elements using the *enhanced fixed-pole interpolation* (*EFP*) for the linear static analysis of a micropolar continuum. These elements demonstrated improved convergence compared to conventional finite elements [2], which motivated further investigation into the use of *EFP* interpolation in the dynamic analysis of a 3D micropolar continuum.

2 Enhanced *fixed-pole* interpolation

To approximate the unknown displacement field $\mathbf{u}$ of a micropolar continuum within the finite element method, the so-called *fixed-pole* interpolation has been used, which arises from the concept introduced by Bottasso and Borri [3] in their analysis of geometrically exact 3D beams. This approach reformulates the stress-couple resultants with respect to a unique fixed reference point and introduces a unified kinematic field $\boldsymbol{\rho}$, combining displacements and rotations. In [4], the application of fixed-pole interpolation in the linear static analysis of a Timoshenko beam (as a 1D micropolar continuum) and of the micropolar continuum has been investigated. It has been shown that the use of the linearised form of fixed-pole interpolation ultimately yields the same stiffness matrix as that obtained using standard Lagrangian interpolation. To improve this, a coefficient n has been introduced into the enriched part of the displacement interpolation field, where $n = 1$ corresponds to the original formulation (*OFP*), while in the enhanced version (*EFP*), it is equal to the number of element nodes along the coordinate axis. This modification has been derived from a comprehensive study [2] of the interdependence between fixed-pole interpolation and the linked interpolation [5] which is known to provide exact solutions for arbitrary polynomial loading given a sufficient number of nodes. As a result, the enhanced fixed-pole interpolation emerges in its general form as:

$$\mathbf{u} = \sum_{i=1}^{m} N_i \left(\boldsymbol{\rho}_i - \frac{1}{n} \widehat{\mathbf{r}}_o \boldsymbol{\phi} \right), \tag{1}$$

for an arbitrary number m of finite element nodes, where N_i are Lagrangian polynomials of order $m-1$, and $\mathbf{r}_0 = \sum_{i=1}^{n} N_i \mathbf{r}_{0,i}$ denotes the initial position vector of the reference axis. The operator $\widehat{\bullet}$ represents the antisymmetric matrix equivalent to the vector cross product, such that $\boldsymbol{\phi} \times \mathbf{r}_0 = \widehat{\mathbf{r}}_0 \boldsymbol{\phi}$. The rotation field is interpolated using standard Lagrangian interpolation: $\boldsymbol{\phi} = \sum_{i=1}^{m} N_i \boldsymbol{\phi}_i$. In static analysis, this formulation eliminates the shear-locking problem in beams and generally yields faster convergence to the exact solution compared to Lagrangian elements. In the vibration analysis of a Timoshenko beam, it has also been shown that the *OFP* interpolation has a favourable effect, leading to faster convergence of natural frequencies. This motivated further investigation into the use of both types of fixed-pole interpolation in vibrational analysis of a 3D micropolar continuum.

2.1. Numerical examples - vibrational analysis of 3D micropolar continuum

Hexahedral finite elements with 8 nodes, using the original *Hex8OFP* and the enhanced *Hex8EFP* fixed-pole interpolation, have been developed for the vibration analysis of a 3D micropolar continuum and implemented into the program FEAP. The fully clamped and cantilever plates were discretised using both types of elements, with all geometric and material properties defined in [2, 6]. The results are compared with those obtained using standard Lagrangian elements (*Hex8L*), and Figure 1 demonstrates faster convergence for the *Hex8EFP* formulation, whereas the *Hex8OFP* interpolation does not exhibit any improved performance in the 3D analysis.

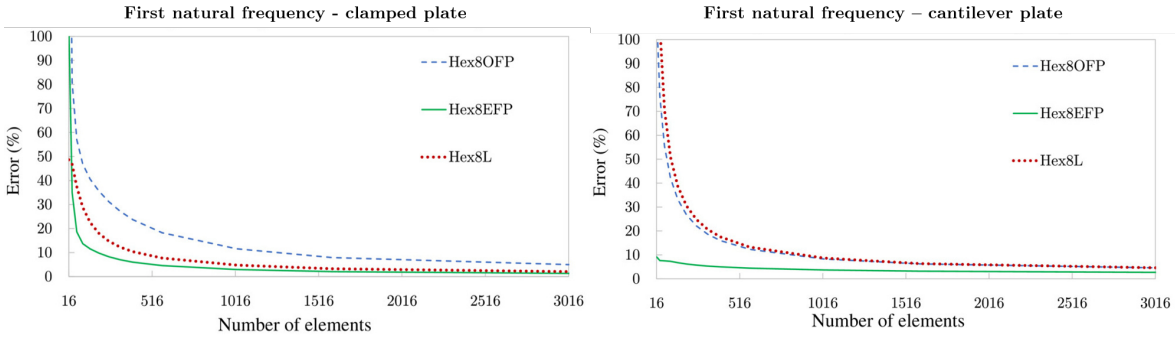


Figure 1. Convergence study of the 1^{st} natural frequencies of the fully clamped and cantilever plates.

3 Conclusion

The fixed-pole interpolation, in both its original and enhanced forms, has been used in the vibration analysis of a 3D micropolar continuum. Results from the conducted numerical examples show that the *EFP* interpolation exhibits faster convergence towards the solution than the conventional interpolation. Further details on the formulation of the *Hex8EFP* element, as well as additional numerical examples, can be found in [2].

Acknowledgments

The presented research has been financially supported by the CSF projects (HRZZ-IP-2018-1732, HRZZ-DOK-2018-09-8806 and HRZZ-IP-2024-05-9904) as well as the grant (uniri-tehnic-18-248 1415).

References

[1] Eringen, A. C., *Microcontinuum Field Theories: I. Foundations and Solids*. Springer Verlag, NY, 2012.

[2] Grbac, L., *et al.*, Hexahedral finite elements with enhanced fixed-pole interpolation for linear static and vibration analysis of 3D micropolar continuum. *Int. J. Numer. Methods Eng.*. 125(8),1-27, 2024.

[3] Bottasso, C., Borri, M., Integrating finite rotations. *Comput. Methods Appl. Mech. Eng.*, 164 (3-4), 307-331, 1998.

[4] Grbac L. *Finite Elements for Linear Analysis of the Micropolar Continuum and the Relationship between the Linked Interpolation and Interpolations on Lie Groups in Linear Form*. PhD Thesis. UNIRI, 2023.

[5] Jelenić G, Papa E. Exact solution of 3D Timoshenko beam problem using linked interpolation of arbitrary order. *Arch. Appl. Mech.* 81(2), 171-183, 2011.

[6] Kohansal. M. V., Ansari R. Quadratic tetrahedral micropolar element for the vibration analysis of 3D micro-structures. *Thin Wall Struct*. 167, 108-152, 2021.

11th International Congress
of Croatian Society of Mechanics
September 30 – October 3 2025
Vodice, Croatia

Geometrically non-linear hexahedral micropolar finite element enhanced with incompatible modes

Sara Grbčić Erdelj*, Gordan Jelenić*, Adnan Ibrahimbegović+

*University of Rijeka, Faculty of Civil Engineering, Croatia
E-mails: sara.grbcic@uniri.hr, gordan.jelenic@uniri.hr

+Université de Technologie Compiègne, France
E-mail: adnan.ibrahimbegovic@utc.fr

Keywords: micropolar elasticity, geometrical nonlinearity, incompatible modes, large 3D rotations

1 Introduction

Discrepancies observed between the widely adopted classical continuum theory and experimental results have highlighted the ongoing need for alternative continuum models. One such extended model is the so-called micropolar (or Cosserat) continuum model where, in addition to the displacement field known from the classical theory, an independent microrotation field is introduced, which accounts for an independent orientation of a material point. This theory is capable of capturing the size-effect phenomenon, manifested as an increase in stiffness in smaller specimens, as experimentally observed in materials with specific microstructures. Within the scope of geometrically nonlinear elasticity, a hexahedral micropolar finite element enhanced with the incompatible modes is presented and tested against the analytical solution of the pure bending problem and a genuine 3D problem for both regular and irregular meshes. The element performance is additionally compared against available Lagrangian elements of first and second order.

2 Equilibrium, kinematic and constitutive equations of the non-linear micropolar model

In the geometrically non-linear regime, a body exhibits large displacements and large rotations. The strong form of equilibrium equations in the material description is obtained as [2]

$$\mathrm{DIV}(\mathbf{QB})+\mathbf{P}_\mathrm{V}=\mathbf{0} \quad \text{and} \quad \mathrm{DIV}(\mathbf{QG})+\mathrm{ax}(\mathbf{QBF}^\mathrm{T}-\mathbf{FB}^\mathrm{T}\mathbf{Q}^\mathrm{T})+\mathbf{M}_\mathrm{V}=\mathbf{0}, \tag{1}$$

together with the corresponding boundary conditions

$$(\mathbf{QB})\mathbf{N}=\mathbf{P}_\mathrm{S} \ \text{ and } \ (\mathbf{QG})\mathbf{N}=\mathbf{M}_\mathrm{S}, \tag{2}$$

where $\mathbf{Q}=\exp\widehat{\boldsymbol{\varphi}}$ represents the microrotation tensor belonging to the so-called special orthogonal Lie group SO(3) ($\mathbf{Q}^{-1}=\mathbf{Q}^\mathrm{T}$, $\det(\mathbf{Q})=+1$) where $\widehat{\boldsymbol{\varphi}}$ is a skew-symmetric tensor belonging to the Lie algebra so(3). Tensor $\mathbf{F}$ represents the deformation gradient tensor, while tensors $\mathbf{B}$ and $\mathbf{G}$ represent the Biot-like stress and couple-stress tensor, respectively. Vectors $\mathbf{P}_\mathrm{V}$, $\mathbf{M}_\mathrm{V}$, $\mathbf{P}_\mathrm{S}$, $\mathbf{M}_\mathrm{S}$ represent body and surface loadings per unit of undeformed volume/area. The non-linear kinematic equations are derived by enforcing the equivalence between the strong form of the equilibrium equations and the principle of virtual work, leading to

$$\mathbf{E}=\mathbf{Q}^\mathrm{T}\mathbf{F}-\mathbf{I} \quad \text{and} \quad \mathbf{K}=-\frac{1}{2}\boldsymbol{\varepsilon}:\left(\mathbf{Q}^\mathrm{T}\mathrm{GRAD}\mathbf{Q}\right), \tag{3}$$

where $\mathbf{E}$ and $\mathbf{K}$ are referred to as Biot-like strain and curvature tensors, respectively, and $\boldsymbol{\varepsilon}$ is the Ricci's alternation tensor. In this work we focus on geometrically non-linear effects and keep the constitutive equations linear, which, in the tensor form read

$$\mathbf{B} = \lambda(\operatorname{tr}\mathbf{E})\mathbf{I} + (\mu+\nu)\mathbf{E} + (\mu-\nu)\mathbf{E}^{\mathrm{T}} \quad \text{and} \quad \mathbf{G} = \alpha(\operatorname{tr}\mathbf{K})\mathbf{I} + (\beta+\gamma)\mathbf{K} + (\beta-\gamma)\mathbf{K}^{\mathrm{T}}, \tag{4}$$

with λ and μ as the Lame constants and ν, α, β and γ as the additional material parameters taking place in micropolar elasticity. For more detail considering the geometrically non-linear micropolar model, together with the additional micropolar material parameters and their relation with technical parameters see [2].

3 Numerical examples

The enhanced Hex8NLIM element is tested against the analytical solution of a micropolar pure bending problem [1] and its performance, robustness and accuracy are compared against available standard Lagrangian elements of first and second order (Hex8NL and Hex27NL). For a thin cantilever beam subject to pure bending, it is observed that both the enhanced element and the second order element reproduce the analytical solution, but with a significantly lower computational time needed for the Hex8NLIM element, as presented in [2]. Hex8NL, however, gives poor results for the chosen finite element mesh due to the existence of the shear locking effects, which is illustrated in representative deformed configurations in Figure 1. A genuine three-dimensional problem consisting of a curved cantilever beam with out-of-plane loading is also analysed and the obtained numerical solution for all three elements is compared against a reference solution in classical elasticity, for small micropolar effects. Again, it is observed that Hex8NL gives poor results, while Hex8NLIM and Hex27NL are very close to the reference solution, with a significantly lower computational time for Hex8NLIM. The incompatible-mode method gives impressive performance for regular (rectangular) meshes, but this is not the case for irregularly shaped elements, where the enhanced element is shown to be very sensitive to mesh distortion.



(a) Hex8NL **(b) Hex8NLIM** **(c) Hex27NL**

Figure 1. Numerical solution for a thin cantilever beam subject to pure bending [2]

4 Conclusion

The solution obtained using the enhanced element with incompatible modes [2] requires significantly lower computational time than the second-order element, with the same precision. The enhanced finite element is fast convergent, more robust and more accurate than the available Lagrangian elements. However, for irregular meshes the enhanced element is shown to be error-prone.

Acknowledgements

This work has been financially supported by the Croatian Science Foundation research project "Analytical, Numerical and Experimental Methods for Identification of Cosserats' Parameters of Materials" (HRZZ-IP-2024-05-9904).

References

[1] Jelenić, G., Pure bending in non-linear micropolar elasticity. *International Journal of Mechanics and Materials in Design*, 18, 243-265, 2022.

[2] Grbčić Erdelj, S., Ibrahimbegović, A., Jelenić, G., Incompatible-mode geometrically non-linear finite element for micropolar elasticity. *International Journal of Solids and Structures*, 289, 112647, 2024.

11th International Congress
of Croatian Society of Mechanics
September 30 – October 3 2025
Vodice, Croatia

Different Approaches in Numerical Modelling of LG Structures

Gabrijela Grozdanić[1], Mirela Galić[1] and Vladimir Divić[1]

[1]*Faculty of Civil Engineering Architecture and Geodesy, Split Croatia*
E-mails: {mgalic@gradst.hr; ggrozdanic@gradst.hr; vdivic@gradst.hr)

Keywords: *laminated glass structures; numerical modelling, fracture and post-fracture simulation*

1. Introduction

The use of glass as a structural material has grown significantly in recent years, becoming increasingly prominent in a wide range of architectural and structural applications. These structural components are subjected to various static and dynamic loads. Laminated glass (LG) meets the requirements for structural safety and has thus become a widely adopted solution in contemporary structural glass applications. Due to the distinct physical, chemical, and mechanical properties of glass and polymer interlayers, LG is a highly complex composite system. Accordingly, numerical modelling of such systems must account for multiple limit states: the Serviceability Limit State (SLS), Ultimate Limit State (ULS), Fracture Limit State (FLS), and Post-Fracture Limit State (PFLS). A reliable numerical model must incorporate current scientific understanding while capturing key phenomena such as fracture initiation, crack propagation, and post-fracture response under both static and dynamic loading. The following sections explore the different aspects of numerical modelling strategies used in the analysis and design of LG structures.

2. Numerical methods for the structural analysis of LG: Capabilities and Limitations

Numerical simulations have been implemented using a range of computational methods, including the Finite Element Method (FEM) [1][2], the Extended Finite Element Method (X-FEM)[3][4], the Discrete Element Method (DEM)[5], the Smoothed Particle Hydrodynamics (SPH) method [6], and the Cohesive Zone Modelling (CZM)[7][8]. Each of these modelling strategies offers distinct advantages, but also presents limitations that currently hinder their broader application in systematic analyses of LG structures.

In commercial software, the FEM is most commonly employed. These models can simulate the fracture using smeared crack models, where fracture initiation is defined by a failure criterion based on Rankine's theory [9]. This allows simulation of cracking without explicitly modelling discrete cracks. Additionally, FEM-based simulations in explicit dynamics often incorporate the element deletion method to represent the failure [10][11]. However, the major drawback of FEM in this context is its strong dependence on mesh topology, which limits its effectiveness in simulating local fracture behaviour and accurate representation of fragmentation. Another approach within FEM is an Embedded Discontinuity method (ED-FEM) that simulates the occurrence of cracks in solids on local element level. Using the ED-FEM, a multi-scale model has been developed that can simulate the load-bearing capacity of LG elements exposed to static load but without simulating a detailed fracture pattern [12]. These FE models are appropriate for simulating LG in SLS and ULS under static and dynamic loads.

The CZM allows crack propagation along the contact surfaces of elements without the need for an initial crack. The CZM represent the fracture process zone as a line or surface between elements in which the cohesive traction occurs. Fracture in such models occurs as a gradual separation in small zones of damage, specifically at the crack tip. This separation is defined by the traction-separation law that can be defined with the macroscopic stress criterion. There are two types of traction-separation laws: the intrinsic [8] and the extrinsic [7], which differ in behaviour before the fracture. A reported limitation of this method is that CZM-based analyses often fail to achieve the expected

level of fragmentation. Instead, only a reduction in the element's stiffness is observed, resulting in a coarse approximation of post-fracture behaviour. These CZ models are mostly appropriate for simulating LG in FLS for dynamic load.

The DEM is based on discontinuity and models LG as assemblies of discrete particles. For the DEM used in the simulation of the behaviour of glass under impact load, a realistic fracture pattern is shown, but the authors notice a deviation in energy dissipation caused by parameter calibration [5]. The method gives satisfactory results for high-speed impacts as well as for low-speed impacts, with the note that the discretisation is mostly achieved with shell elements, which are computationally very demanding due to the need to discretise each layer in LG. The DEM is mostly appropriate for simulating LG in FLS and PFLS under dynamic load.

The X-FEM is extension of FEM by applying additional enrichment functions (jump functions) used for approximating the displacement field. This method enables the appearance of cracks which are inserted independently of the mesh, ensuring that crack propagation is independent of the mesh. The method is used in simulations of the LG exposed to the impact load [3] and a static load [4]. This method is comparable to ED-FEM, but the difference is in the simulation of failure. In X-FEM, the failure occurs globally, while ED-FEM simulates localised failure by introducing a discontinuity in displacement or the deformation field (keeping the additional unknowns at the local element level). TX-FEM is mostly appropriate for simulating LG in FLS in both static and dynamic loads.

3. Conclusions

Laminated glass, as a complex multilayer material with different mechanical properties of its constituent parts, presents a special challenge in numerical modelling. This work provides an overview of the most commonly used numerical methods for simulating the behaviour of LG under static and dynamic loads. Each of the presented methods has specific advantages in terms of the ability to model certain aspects of glass behaviour, however, no method currently manages to fully capture all relevant phases of behaviour. For the reliable and safe use of LG in structures, further improvement of numerical models is necessary to achieve the prediction of all limit states.

References

[1] A. Saputra, R. Behnke, W. Xing, C. Song, J. Schneider, and M. Kaliske, "Numerical representation of fracture patterns and post-fracture load-bearing performance of thermally prestressed glass with polymer foil," *Engineering Structures*, vol. 226, no. October 2020, 2021,

[2] A. K. Gupta, Y. Lin, S. Pesek, N. McDougal, R. Kent, and L. Dietsche, "Predictive Analysis of Laminated Glass Performance Under Static and Dynamic Loading Conditions," *Challenging Glass Conference Proceedings*, vol. 9, no. June, pp. 1–27, 2024

[3] X. Xu, J. Xu, J. Chen, P. Li, B. Liu, and Y. Li, "Investigation of dynamic multi-cracking behavior in PVB laminated glass plates," *International Journal of Impact Engineering*, vol. 100, pp. 62–74, 2017

[4] K. Rodacki and K. Furtak, "Numerical analysis of crack development of timber-glass composite I-beams in the extended finite element method (XFEM)," *Composite Structures*, vol. 209, pp. 349–361, 2019

[5] X. Wang, J. Yang, Q. Liu, Y. Zhang, and C. Zhao, "A comparative study of numerical modelling techniques for the fracture of brittle materials with specific reference to glass"*Engineering Structures*,vol.152, pp.493-505,2017

[6] Z. Wang, Y.Li, D. Ma *et al.*, "Experimental and numerical investigation on the ballistic performance of aluminosilicate glass with different nosed projectiles,"*Ceramics International*,v.49, no.11,pp.17729–17745,2023

[7] D. Wang, S. Chen, W. Xu, M. Zang, and S. Yoshimura, "A computational framework for impact fracture analysis of laminated glass: An extrinsic cohesive shell approach," *Computers and Structures*, vol. 233, 2020

[8] X. Xu, D. Wang, M. Zang, and S. Chen, "Development of an intrinsic solid-shell cohesive zone model for impact fracture of windshield laminated glass," *International Journal of Impact Engineering*, vol. 163, 2021

[9] Z. Wang, D. Ma, and F. Qin, "Smeared fixed crack model for quasi-static and dynamic biaxial flexural response analysis of aluminosilicate glass plates," *Thin-Walled Structures*, vol. 205, no. PB, p. 112533, 2024

[10] Y. Peng, W. Ma, S. Wang, K. Wang, and G. Gao, "Investigation of the fracture behaviors of windshield laminated glass used in high-speed trains," *Composite Structures*, vol. 207, no. August 2018, pp. 29–40, 2019,

[11] X. Zhang and H. Hao, "Experimental and numerical study of boundary and anchorage effect on laminated glass windows under blast loading," *Engineering Structures*, vol. 90, pp. 96–116, 2015

[12] G. Grozdanic, A. Ibrahimbegovic, M. Galic, and V. Divic, "Multiscale beam model for simulating fracture in laminated glass structures," *Engineering Fracture Mechanics*, vol. 292, 2023

11th International Congress
of Croatian Society of Mechanics
September 30 – October 3 2025
Vodice, Croatia

A FE2 model for thin and thick shells with periodic boundary conditions

Friedrich Gruttmann

Institute for Mechanics, Technical University of Darmstadt, Franziska-Braun-Straße 7, 64287 Darmstadt, Germany
E-mail: gruttmann@mechanik.tu-darmstadt.de

Keywords: FE2 modeling, Reissner–Mindlin shell theory, periodic boundary conditions, inhomogeneous shell problems

1 Introduction

In this contribution a FE2 model for thin and thick shells is discussed. We propose a first order homogenization formulation for Reissner-Mindlin shells that couples the boundary value problems at the coarse and fine scale in a variational setting. The associated weak form is consistently linearized whereby the resulting nonlinear finite element equations of both scales can be solved in different ways. As effective alternative to a nested iteration a simultaneous iteration can be applied which also preserves quadratic convergence of Newton's method [1]. The initially linear formulation is extended to finite strain problems introducing transformation relations for the stress resultants and the material matrix. The transformations are performed at each Gauss point on macro level. The considered linear and non-linear examples prove that the developed two-scale model is able to effectively analyze the mechanical behavior of heterogeneous shell structures [2].

2 Variational formulation of the two–scale problem

When applying periodic boundary conditions to representative volume elements (RVEs) in three-dimensional bodies rigid body movements are generally prevented by prescribed displacements of the corner nodes. This is not possible in present case as it causes localized distortions at the corners of the RVE, which extend through the total thickness of the shell. Stress boundary conditions are located at the bottom and top surfaces of the RVEs with coordinates $z = h^-$ and $z = h^+$, whereas at the lateral surfaces periodic boundary conditions are used. Appropriate constraints $\mathbf{g} = \mathbf{0}$ are developed which prevent both rigid body movements and the dependency of the transverse shear stiffness on the RVE length. The side conditions are fulfilled applying the Lagrange multiplier method.

The shell is loaded statically by loads $\bar{\mathbf{p}}$ on the reference surface Ω and by boundary forces $\bar{\mathbf{t}}$ on the boundary Γ_σ. The macro displacements $\bar{\mathbf{v}} = [\bar{\mathbf{u}}_0, \bar{\varphi}]^T$ with displacements $\bar{\mathbf{u}}_0$ and rotations $\bar{\varphi}$ of the reference surface, the displacements $\mathbf{u}$ of the micro problem and the Lagrange parameters Λ are summarized in the vector $\theta = [\bar{\mathbf{v}}, \mathbf{u}, \Lambda]^T$. With admissible variations $\delta\theta = [\delta\bar{\mathbf{v}}, \delta\mathbf{u}, \delta\Lambda]^T$ the variational equation reads

$$g(\theta, \delta\theta) = \int_{(\Omega)} (\boldsymbol{\sigma} \cdot \delta\boldsymbol{\varepsilon} - \bar{\mathbf{p}} \cdot \delta\bar{\mathbf{u}}_0)\, \mathrm{d}A - \int_{(\Gamma_\sigma)} \bar{\mathbf{t}} \cdot \delta\bar{\mathbf{u}}_0\, \mathrm{d}s + \sum_{e=1}^{numel} \sum_{i=1}^{NGP} \int_{(\Omega_i)} \int_{h^-}^{h^+} [\mathbf{S} : \delta\mathbf{E} + \delta(\Lambda \cdot \mathbf{g})]\, \mathrm{d}z\, \mathrm{d}A = 0\,. \quad (1)$$

The first two terms refer to the macro problem (shell), whereas the third term describes the contribution of the $numel \times NGP$ micro problems. Here, $numel$ denotes the total number of shell elements and NGP the number of Gauss points for each element. Furthermore, $\boldsymbol{\sigma}$ and $\delta\boldsymbol{\varepsilon}$ denote the vectors of stress resultants and nonlinear virtual shell strains, respectively. On micro scale the internal virtual work is formulated with the Second Piola-Kirchhoff stress tensor $\mathbf{S}$ and the virtual Green-Lagrange strain tensor $\delta\mathbf{E}$.

3 Example: Square plate with spherical inclusions

We consider an inhomogeneous square plate according to Figure 1 with constant loads $\bar{p} = \lambda \cdot 0.15 \cdot 10^{-2}$ kN/cm^2 acting half on the upper and half on the lower surface. The span of the plate is $L = 1000$ cm and the thickness is $h = 50$ cm. It is simply supported (soft support) at all boundaries.

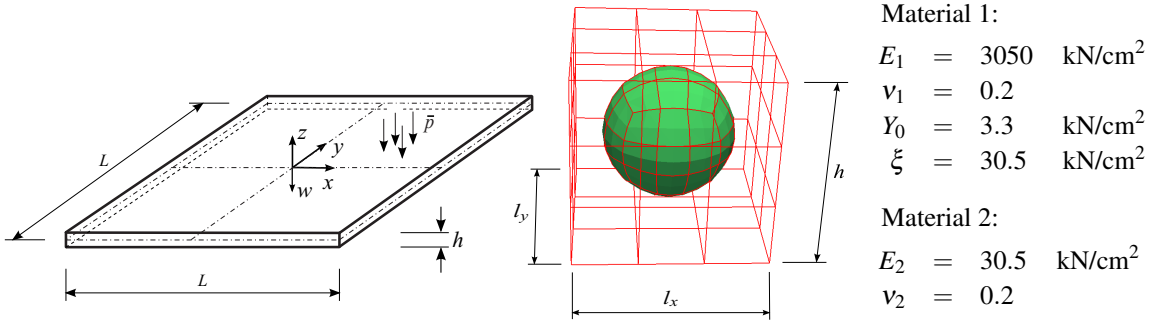


Figure 1. Square plate with spherical inclusions, unit cell and material parameters

The plate consists of 20×20 evenly distributed unit cells with spherical inclusions, see Figure 1. The dimensions are $l_x = l_y = h = 50$ cm and the diameter of the sphere is 35 cm. The outer material of a cell (Material 1) behaves elasto-plastic with linear isotropic hardening, whereas the soft inner material (Material 2) is linear elastic. Hereby, E_α and ν_α $(\alpha = 1,2)$ denote the respective Young's modulus and Poisson's ratio as well as Y_0 and ξ denote the yield stress and the hardening parameter. A small strain material law is used to describe the J_2 elastoplastic behavior. Considering symmetry one quarter of the plate is discretized with 10×10 4-node shell elements with one point integration and stabilization HW-RI [3]. The used RVE corresponds to the unit cell depicted in Fig. 1. It is discretized with 4462 nodes and 351 27-noded solid elements. Considering symmetry conditions as well a full 3D discretization of one quarter of the plate is carried out to compute a comparative solution. A mesh of 11200 27-noded solid elements with 165862 nodes is used. The geometrical linear computation of the loading and unloading path is performed applying an arclength method with displacement control and increments $\Delta w = 2.5$ cm. The computed load factors λ are plotted versus the center displacement w in Figure 2. There is good agreement of the FE2 results with the elaborate 3D reference solution.

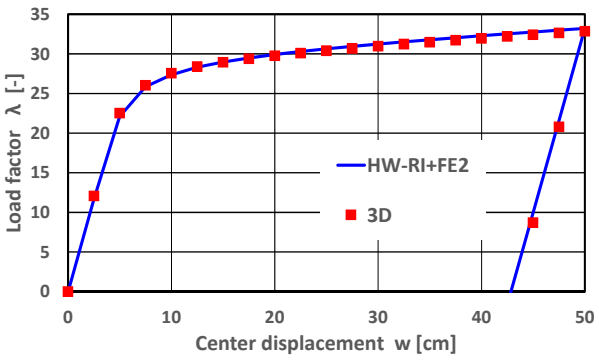


Figure 2. Load factor λ versus displacement w

References

[1] Gruttmann, F., Wagner, W., A coupled two-scale shell model with applications to layered structures, *International Journal for Numerical Methods in Engineering*, 94, 1233-1254, 2013.

[2] Gruttmann, F., Wagner, W., A FE2 shell model with periodic boundary conditions for thin and thick shells, *International Journal for Numerical Methods in Engineering*, 125 (11), e7433, 2024.

[3] Gruttmann, F., Wagner, W., A nonlinear 4-node shell element with one point quadrature and stabilization based on a Hu-Washizu variational formulation, *Computational Mechanics*, https://doi.org/10.1007/s00466-025-02616-2, 2025.

11th International Congress
of Croatian Society of Mechanics
September 30 – October 3 2025
Vodice, Croatia

DCB Test Modelling Using a Beam-on-Foundation Framework with Inelastic DCB Arms and Adhesive

Emina Hadzalic*, Leo Škec*, Adnan Ibrahimbegovic+,×

*University of Rijeka, Faculty of Civil Engineering, 51000 Rijeka, Croatia
E-mails: emina.hadzalic@uniri.hr, leo.skec@uniri.hr

+University of Technology of Compiègne, 60200 Compiègne, France
E-mail: adnan.ibrahimbegovic@utc.fr

×Institut Universitaire de France, 75231 Paris CEDEX 05, France

Keywords: DCB test, delamination, beam-on-foundation, softening, plasticity

1 Introduction

Delamination is among the most severe failure modes in adhesively bonded structures. Depending on the loading conditions, crack propagation may occur in mode I (opening mode), mode II (sliding mode), or mode III (tearing mode). The double cantilever beam (DCB) test is a standard experimental method for assessing mode I fracture behaviour in such structures. This test is primarily designed to determine the properties of the adhesive, including stiffness, strength, and fracture energy, assuming that the DCB arms remain elastic throughout the test. This allows a straightforward interpretation of the energy dissipation associated with damage and separation within the adhesive. However, in practice, plastic deformation in the beam arms may unintentionally occur, mainly due to the suboptimal experimental setup. These irregularities are generally treated as experimental errors, and the corresponding data is usually discarded. Nonetheless, these off-nominal test results can still be used to identify adhesive properties when interpreted through appropriate numerical modelling.

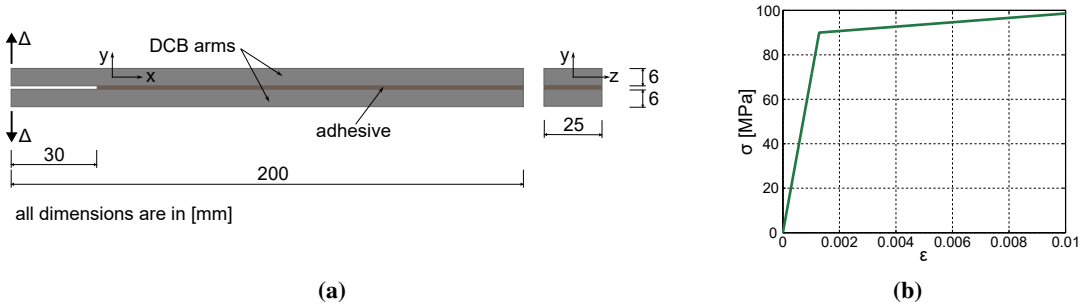
Traditional modelling approaches for the DCB test often involve cohesive zone models (CZM) to represent the adhesive layer, capturing the initiation and evolution of damage through traction–separation laws [1]. These laws vary in complexity, from simple bilinear formulations to more refined exponential laws. Meanwhile, the DCB arms are typically modelled as linear elastic using either two-dimensional plane strain finite elements or beam finite elements.

Given the symmetry of the DCB test setup, which permits modelling only half of the specimen, we propose a monolithic modelling approach for the DCB test based on a beam-on-foundation framework [2, 3]. The main advantage of the proposed model lies in its unified formulation, where the entire bonded structure is modelled using only a single type of finite element. Specifically, the adhesive layer is represented as a spring foundation, with its contribution directly embedded into the beam finite element formulation of the DCB arm. This eliminates the need to model the adhesive separately, as the enriched beam finite element accounts for both the response of the DCB arm and the behaviour of the adhesive. This integrated approach reduces modelling complexity while preserving the ability to capture both adhesive degradation and arm deformation with a single element type.

Within the proposed framework, Timoshenko beam finite elements are adopted and enriched with embedded nonlinear springs to account for the adhesive layer. The springs follow a linear elastic law up to a failure threshold, after which exponential softening governs the progressive degradation of the bond during delamination. To move beyond the standard assumption of linear elastic DCB arms, the proposed formulation extends the behaviour of Timoshenko beam finite elements to include plastic bending, thereby enabling the simulation of both ideal and non-ideal test conditions where plasticity may influence the results. The plastic behaviour is described using a plasticity model with linear isotropic hardening.

2 Numerical results

The geometry of a simulated DCB test with a prescribed displacement is shown in Figure 1a. The DCB arms are made of aluminium with material behaviour described by the stress-strain curve in Figure 1b. The material properties for the aluminium are specified as: Young's modulus $E = 70\,\text{GPa}$, Poisson's ratio $\nu = 0.33$, yield limit $\sigma_y = 90\,\text{MPa}$, and hardening modulus $H = 1\,\text{GPa}$. The adhesive layer is assigned the following properties: failure threshold $\sigma_{max} = 7.5\,\text{MPa}$, relative displacement at the failure limit $\delta_0 = 0.0026\,\text{mm}$, and fracture energy $G_f = 1\,\text{N/mm}$.



(a) **(b)**

Figure 1. (a) Geometry of the DCB (b) stress-strain diagram of the aluminium

Two scenarios are simulated: one assuming linear elastic behaviour of the DCB arm, and the other allowing for plastic bending. The computed responses are presented in Figure 2. The results indicate that the plastic behaviour of the DCB arm leads to a reduction in peak load capacity and a more gradual post-peak softening.

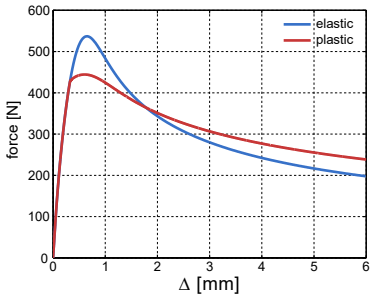


Figure 2. Computed responses for elastic and plastic bending scenarios

3 Conclusion

We have presented a novel monolithic numerical modelling approach for the DCB test, built on a beam-on-foundation framework that accounts for both elastic and plastic bending of the DCB arms, as well as the exponential degradation of the adhesive. The computed results indicate that plastic deformation in the DCB arms reduces the peak load capacity and leads to a more gradual post-peak response. The model will be further validated through comparison with experimental data [4], including the identification of adhesive parameters. The proposed model can be further extended to accommodate other constitutive laws for the DCB arms, different traction–separation laws for the adhesive, and to account for mode II and mode III crack propagation by adding horizontal springs.

References

[1] Škec, L., Alfano, G., Jelenić, G., Complete analytical solutions for double cantilever beam specimens with bi-linear quasi-brittle and brittle interfaces. *International journal of fracture*, 215, 1-37,2019.

[2] Hadzalic, E., Hajdo, E., Ibrahimbegovic, A., Seismic assessment of multi-story steel frame structure on pile foundation. In: Proceedings of the 1st International Conference on Synergy between Multi-physics/Multi-scale Modeling and Machine Learning, June 19-21, 2024, Prague. Editors: Adnan Ibrahimbegovic, Anna Kučerová.

[3] Ibrahimbegović, A., *Nonlinear solid mechanics: theoretical formulations and finite element solution methods*. Springer Science & Business Media, 2009.

[4] Hlača, I., Experimental and numerical analysis of delamination of layered glued plate structures with variable width. *Diss. University of Rijeka. Faculty of Civil Engineering*, 2024.

11th International Congress
of Croatian Society of Mechanics
September 30 – October 3 2025
Vodice, Croatia

Mechanical Modelling of Active Seat Suspension System Based on Scott-Russell Mechanism

K. Haramina*, N. Kranjčević*, J. Deur*, I. Ruškan*, M. Hoić*

*University of Zagreb, Faculty of Mechanical Engineering and Naval Architecture
Ivana Lučića 5, HR-10002 Zagreb, Croatia
E-mails: {krunoslav.haramina, nenad.kranjcevic, josko.deur, ivan.ruskan, matija.hoic}@fsb.unizg.hr

Keywords: active seat suspension, modelling, Scott-Russell mechanism, dynamics

1. Introduction

Active suspension systems can significantly enhance ride comfort in passenger vehicles. While these systems are predominantly applied to and researched for wheel suspension, they can also be highly effective when implemented for passenger seat suspension. To be practical, such system must be both compact, allowing it to fit beneath the seat and sufficiently stiff to support the passenger in both longitudinal and lateral directions, while simultaneously reducing vertical vibrations and thus providing riding comfort. In this work, a mathematical model of a proposed active seat suspension system is presented.

2. Simulation model

The Scott-Russell mechanism is selected for active seat suspension system as shown in Figure 1a [1]. It enables vertical movement of seat supports, and by employing two identical mechanisms it ensures that seat remains parallel to the chassis. The system is actuated by an electric motor and a spindle which drives H-frame. H-frame connects front and rear sections of the mechanism and transmits horizontal force F_{act}. A simulation model of this system is developed to compute seat vertical displacement (z_s) based on two inputs: chassis vertical movement (z_c) and motor torque (T_M). The primary inertias considered include i) motor's rotational inertia, ii) the mass of the H-frame and iii) combined mass of the seat and passenger. These inertias are interconnected by components of negligible elasticity and can therefore be reduced to an equivalent inertia at the motor axis using lumped inertia model as illustrated in Figure 1b.

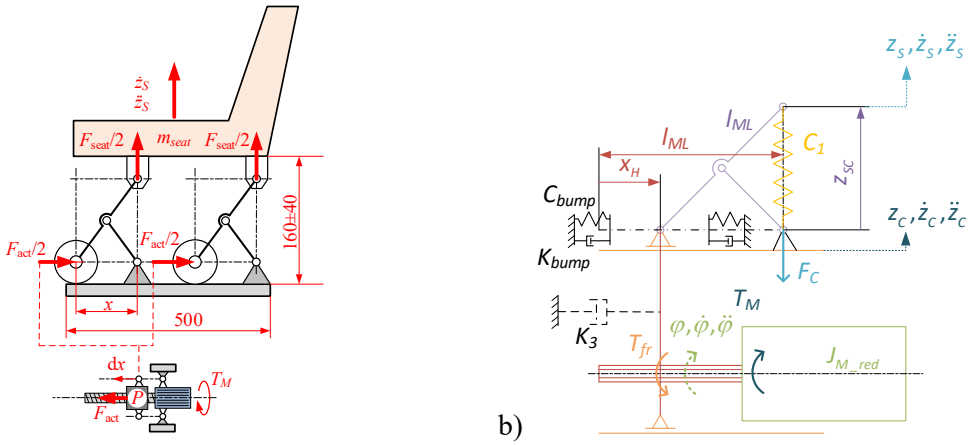


Figure 1. Mechanical scheme of an active seat suspension mechanism (a) and lumped inertia model (b)

The Scott-Russell mechanism is inherently nonlinear; therefore, reduced inertia is not constant but depends on current mechanism displacement.

Friction in the system arises from several sources including bearings, ball spindle, linear guides of the H-frame, and seals. The most significant contribution comes from rolling friction of ball bearings which exhibits dynamic behaviour. This behaviour is modelled using the dynamic Dahl friction model. Stabilized Coulomb friction is also considered and is calculated based on seat force.

Block diagram of the whole simulation model is shown in Figure 2. The rotational dynamics about the motor axis (φ) is presented in green, dynamics of H-frame (x_H) in red and seat dynamics (x_S) in purple, while model inputs ($T_M, z_C, \dot{z}_C$ and $\ddot{z}_C$) are indicated in dark blue while model outputs and seat force ($F_C, z_S, \dot{z}_S, \ddot{z}_S$ and F_{seat}) in light blue colour. The influence of main support springs (C_1) is represented in yellow and dynamic friction model in orange.

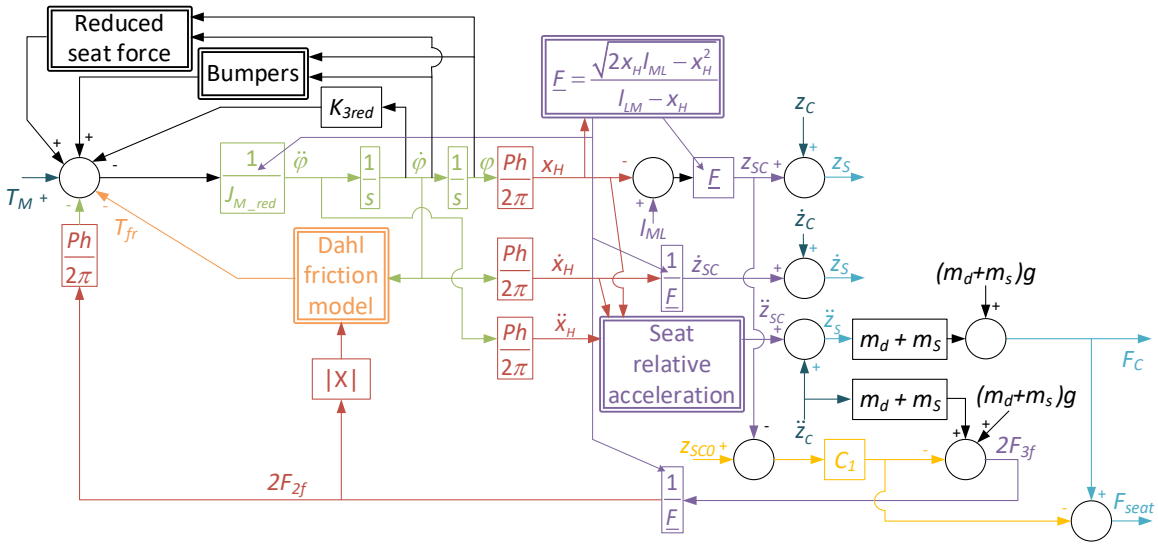


Figure 2. Block diagram of active seat suspension system

The model is tested for sinusoidal reference signal for feedback-controlled seat position. Initial results for various excitation frequencies are presented in Figure 3. The ideal relationship between seat vertical position and motor torque is calculated for purely kinematic case (neglecting inertia and friction). This reference curve, shown as a dashed line, illustrates the inherent nonlinearity of the mechanism. At low frequencies, the influence of friction is prominent, resulting in noticeable hysteresis around the ideal curve. At higher frequencies, inertia becomes more dominant, altering the shape of the response curve. In this case, the electric motor must generate additional torque which accelerates the system's inertias. Due to nonlinearity, the motor must produce significantly higher torque for the same seat movement at lower seat vertical positions than at higher ones.

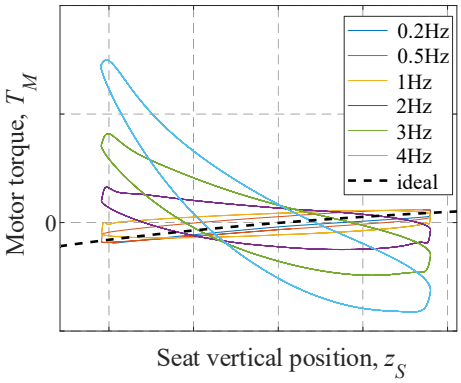


Figure 3. Dynamic characteristic for different frequencies

3. Conclusions

A dynamic model of active seat suspension system has been proposed. All inertias are reduced to the motor axis and model includes nonlinear Scott-Russell mechanism, dynamic friction model, support springs and bumpers. Simulation results demonstrate the expected system behaviour, indicating that the model is suitable for further development of control strategies.

References

[1] Hoić, M., Kranjčević, N., Birt, D., Design of an active seat suspension based on a Scott- Russell mechanism, *20TH IEEE/ASME International Conference on Mechatronic and Embedded Systems and Applications, MESA 2024*, 2024-01-01 2024

11th International Congress
of Croatian Society of Mechanics
September 30 – October 3 2025
Vodice, Croatia

From 3D scan to functional component: experimental redevelopment of a damaged component

Antonio Horvat*, Tomislav Hercigonja+, Nenad Drvar+

*Signum Max d.o.o., Pere Devčića 67, 10290 Zaprešić
E-mail: antonio@signummax.hr

+TOPOMATIKA d.o.o., Industrijska 3, 10431 Sveta Nedelja
E-mail: t.hercigonja@topomatika.hr, n.drvar@topomatika.hr

Keywords: component testing, 3D scanning, reverse engineering, 3D printing, DIC

1. Introduction

Finding the replacement components for products which are no longer available on the market will often pose a challenge. This paper presents a task [1] given to a student of Technical college in Bjelovar to perform the engineering task: perform the redevelopment process of a damaged plastic release button (see Figure 1) for a carry-on luggage handle by using only tools that are available to him, in this case it was the equipment available in TOPOMATIKA d.o.o. ([2] ATOS 3D scanners, reverse engineering tools, UTM Inspekt table 20 kN [3], DIC ARAMIS 3D camera and additive manufacturing technologies). The goal was to test if experiments and direct measurements on prototypes can be sufficient to develop a functional replacement that meets the mechanical requirements of the original component.

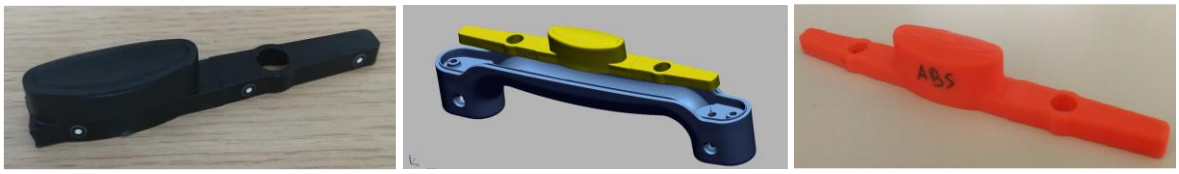


Figure 1: from left to right, original damaged part, reverse engineered part, redeveloped part [1]

2. Methods

The damaged release button of the original handle (see Figure 1) was first 3D scanned used ZEISS ATOS Q and reverse engineered using Geomagic Design X software to create a symmetric CAD model of the part. Handle was also digitized, that allowed us to virtually test if reconstructed button will again fit and to see how much space inside is left for us to work with. The reconstructed button was then 3D printed using FDM technology on a Zortrax M200 printer with three different polymer materials: Z-ABS, Z-ASA Pro, and Z-ULTRAT. A total of 18 samples were produced for testing purposes. They were first used to perform ARAMIS displacement measurement of the actual deflections (see Figure 2) during the typical usage (2-2,4 mm for Z-ULTRAT) and to see what kind of overloading (3,1 mm for Z-ULTRAT) can be performed manually in the original mechanism. Slow cycling loading in 3-point bend test (amplitude of 2,7 mm for Z-ULTRAT) was performed on the samples with original shape to determine if 3D printed parts are suitable enough or injection molding will be required to produce final parts. 600 cycles were performed, considering normal 10 times bag usage for travel within period of 3 years (20 button presses per trip were assumed). Samples were 3D scanned after cyclic tests and compared with original shape to visualize if there is significant deformation that would interfere with further usage. Those tests proved that replacements could be used without modifications, however, by performing additional static 3-point bend test together with

ARAMIS DIC strain measurements it can be seen that same area where original button broke will again be critical (see Figure 2) so additional reconstruction step was performed where two things were changed: radius 3 mm where button meets the holder and thickness of the part was increased from 1,75 mm to 2,5 mm (considering entire time that new part needs to fit back into the handle).

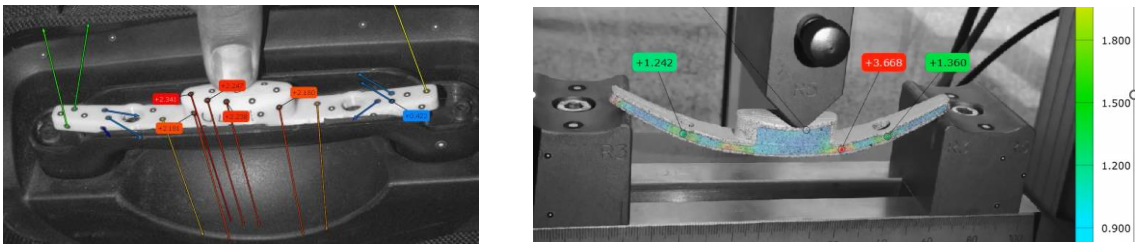


Figure 2: displacement tests in original configuration, 3-point bend test with ARAMIS DIC results [1]

3. Results

Static 3-point bend test (see Figure 3) of reconstructed button showed that local strain extreme has now moved further away from the original critical area, towards the guiding hole. By looking at Figure 3 it is clear that this happened after applying the amount of displacement that can not be done manually inside the handle. This proved that 3D printed part with applied structural changes can be successfully used as a replacement part even though it was made on a desktop Zortrax 3D printer.

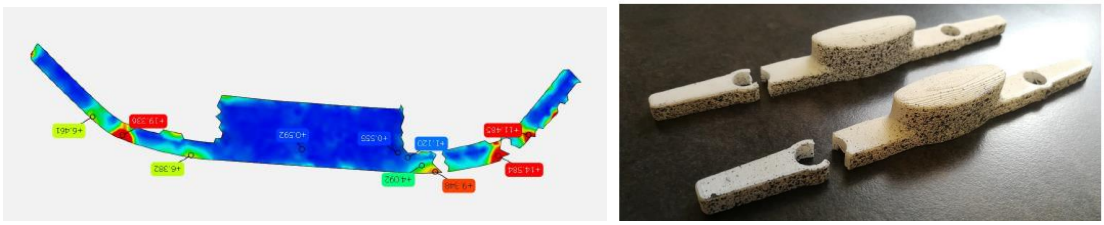


Figure 3: shifting of critical zones in DIC measurement, 3-point overloaded bend test of final part [1]

Z-ULTRAT demonstrated the best performance with the highest flexural strength (54 MPa) and Shore D hardness (73.4). The redesigned buckle made of Z-ULTRAT showed the least deformation and highest resistance to static and dynamic loads.

4. Conclusions

Performed experiments showed that by combining ATOS 3D scanning, reverse engineering, load testing, ARAMIS DIC and displacement measurements and FDM 3D print technology enabled quick and efficient reconstruction of plastic components that were no longer available on the market. The use of the ARAMIS measurement system provided critical information that helped to decide on required design change. FEM simulations were not performed, it was proven that engineering approach that included just experiments and load tests still work well together with modern shape and deformation measurement technologies. In future we plan to full-field compare strain measurements with FEM. Please note that even though we used small desktop 3D printer, we did not analyze 3D printed part shape stability, repeatability and consistency of mechanical properties, which should be also taken into account during similar reconstructions or direct additive productions.

References

[1] Antonio Horvat, *REKONSTRUKCIJA, ADITIVNA IZRADA I FUNKCIONALNO TESTIRANJE ZAMJENSKE PLASTIČNE KOMPONENTE, završni rad, Veleučilište u Bjelovaru, 2020*

[2] www.topomatika.hr

[3] www.ispitivanje.com

11th International Congress
of Croatian Society of Mechanics
September 30 – October 3 2025
Vodice, Croatia

Constitutive Modeling of Soft Materials by Deep Symbolic Regression

Mikhail Itskov*, Rasul Abdusalamov*

*Department of Continuum Mechanics, RWTH Aachen University, Eilfschornsteinstr. 18, 52062 Aachen, Germany
E-mails: {itskov,abdusalamov}@km.rwth-aachen.de

Keywords: soft materials, aerogels, hyperelasticity, Mullins effect, deep symbolic regression

1. Introduction

Symbolic regression represents a powerful tool of machine learning which can be applied to an unbiased automatized generation of constitutive models for various materials. It is based on an evolutionary procedure and starts with a population set of random mathematical expressions constructed from a user-defined list of allowed basic operators, algebraic functions, predefined independent variables and numerical constants. Then, a simple mathematical expression most accurately describing a given set of data is searched. In comparison to other data-driven methods symbolic regression reproduces a strain energy, damage or other constitutive function which can be analyzed, interpreted und easily implemented, for example into a finite element code. In the case of deep symbolic regression, a recurrent neural network is additionally applied to predict a sampling distribution of the available functions and operations through a risk-seeking policy gradient.

2. Hyperelastic Modeling of Soft Materials

In this contribution, we first focus on soft isotropic materials like for example rubbers. Deep symbolic regression can effectively be applied to formulate a strain energy function of such hyperelastic materials in terms of the principal strain invariants or principal stretches. In both cases, the so created hyperelastic model demonstrates very good agreement with experimental data from multiaxial tension tests and in this sense even outperforms many other constitutive formulations. The strain energy function in terms of the principal invariants includes as a basis the well-known Mooney-Rivlin model enhanced by some correction terms which play an important role at moderate and large deformations. Thus, the proposed procedure also grants new insights into many established and well-known material models [1-3]. Within the framework of the Valanis-Landel concept we also propose a new formulation of the strain energy function in terms of the principal stretches. It exhibits a superior performance, for example in comparison to the well-known Ogden model based on three terms and six material constants. Additionally, we study the influence of noisy data on the performance of the proposed procedure and resulting constitutive models [1].

2. Modeling of Stress Softening

Filled elastomers are often characterized by softening which appears under cyclic loading when the current stretch does not exceed its maximal value previously reached in the loading history. This type of softening referred to as the Mullins effect mostly appears in polymers, filled rubbers, hydrogels or soft biological tissues and usually accompanied by permanent set, hysteresis and other inelastic effects. Within the so-called idealized Mullins effect these inelastic effects are disregarded. In this contribution, we apply deep symbolic regression to create a damage function describing the idealized Mullins effect in elastomers. The resulting softening model shows good agreement with data both artificially created by established material models (see for example reference [4]) and resulting from cyclic tension tests with stepwise increasing amplitude.

3. Microstructural Modeling of Aerogels

Aerogels represent microporous solids with a large amount of dispersed air. Accordingly, aerogels are characterized by light weight but very high thermal and acoustic isolation properties. Microstructurally, aerogels exhibit extremely varying pore sizes with highly irregular shapes and randomized pore size distribution. In this contribution, we show how deep symbolic regression can be applied to formulate a strain energy function of an aerogel in terms of its relative volume change and microstructural parameters such as volume fraction of the solid phase and variation coefficient of the pore size distribution mentioned above. The so-obtained constitutive formulation is directly connected to synthesis parameters of the aerogel and shows good agreement with experimental data from uniaxial compression tests.

4. Conclusions

The presented results demonstrate large potential of deep symbolic regression in application to constitutive modeling of soft materials. In this way, very accurate, interpretable and unbiased material models can be formulated. The application of deep symbolic regression can further be extended to anisotropic materials and in particular to soft biological tissues. Calculation of tensor functions by deep symbolic regression also appears feasible and will be presented elsewhere.

References

[1] Abdusalamov, R., Itskov, M. Rediscovering Hyperelasticity by Deep Symbolic Regression. arXiv preprint arXiv:2503.05387

[2] Abdusalamov, R., Hillgärtner, M., Itskov, M. Automatic generation of interpretable hyperelastic material models by symbolic regression. *International Journal for Numerical Methods in Engineering*, 124 (9), 2093-2104, 2023.

[3] Abdusalamov,R., Weise, J., Itskov, M. Rediscovering the Mullins effect with deep symbolic regression. *International Journal of Plasticity*, 104037, 2024.

[4] Ogden, R.W., Roxburgh, D.G. A pseudo–elastic model for the Mullins effect in filled rubber. *Proceedings of the Royal Society of London A*, 455 (1988), 2861–2877, 1999.

11th International Congress
of Croatian Society of Mechanics
September 30 – October 3 2025
Vodice, Croatia

Phenomenological Modelling of Impact-Induced Delamination in Composite Laminates

Darko Ivančević*, Jakov Ratković*

*University of Zagreb Faculty of Mechanical Engineering and Naval Architecture, Ivana Lučića 5, 10000 Zagreb, Croatia
E-mails: {darko.ivancevic,jakov.ratkovic}@unizg.fsb.hr

Keywords: composite laminates, impact damage, failure modes, delamination

1. Introduction

Accurate and reliable simulation of impact damage in laminated composite structures is still a challenging task from a numerical point of view. The difficulties are caused by the material's anisotropy, laminated nature, imperfections and residual stresses from manufacturing. These phenomena give rise to several failure modes of the composite structure that are often interconnected and mutually dependent. Additionally, epoxy matrices, that are mostly used in the state-of-the-art composite structures, exhibit strain rate dependent mechanical properties, that are also evident in the matrix-dominated properties of the composite material in dynamic loading conditions.

The presented research is performed to improve the accuracy and reliability of impact simulations in laminated composite structures. As the strain rate dependency in composites is a complex phenomenon, the research is focused on carbon fibre reinforced epoxy matrices (CFRP). Unidirectional as well as woven fibre architectures are studied in a wide range of impact velocities.

2. Methodology

The numerical model is implemented using user material subroutines VUMAT, suitable for impact simulations in Abaqus/Explicit. The Finite Element modelling approach is shown in Figure 1. The modelling approach of the laminated composite plate can be described as a mesomechanical approach, as the individual plies are modelled using a single solid (C3D8R) element through the ply thickness. Modelling of the ply interfaces is performed using cohesive elements (COH3D8) that are placed between all plies in the plate.

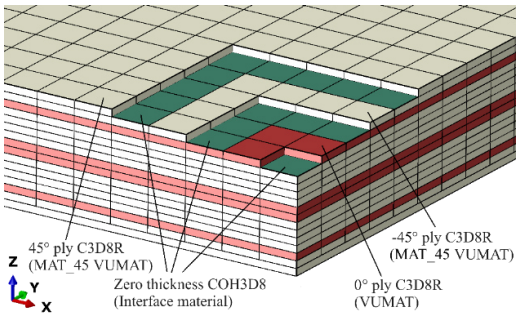


Figure 1. Example of the employed modelling approach for laminated composites

The individual strain-rate dependent damage models of the composite solid elements and the interface cohesive elements have been introduced in the previous work by the authors [1,2]. This work focuses on the connection between these two separate VUMAT subroutines, enabling phenomenological delamination initiation modelling.

To include strain rate dependency in the constitutive response of cohesive elements, dynamic increase factors were introduced to modify the affected interface mechanical property (c_{prop}).

Consequently, interface strengths, i.e. failure tractions, and fracture energies are varied based on the displacement rates using empirical logarithmic functions, as proposed by Liu et al. [3]:

$$DIF_{ij}(\dot{\delta}_{ij}) = 1 + c_{prop} \cdot \ln\left(\frac{\dot{\delta}_{ij}}{\dot{\delta}_{ref}}\right), \dot{\delta}_{\text{ref}} < \dot{\delta}_{ij} < \dot{\delta}_{\text{lim}}; i,j = 1,2,3. \quad (1)$$

The dynamic increase factors in Equation 1, and consequently the properties that they belong to, are capped below the referent ($\dot{\delta}_{\text{ref}}$) and above the limit ($\dot{\delta}_{\text{lim}}$) displacement rate values.

Figure 2 shows the results of a 15 J impact on a AS4/8552 plate with the layup [45/-45/0/45/45/-45/-45/90]$_s$. As shown, the phenomenological-based matrix damage model predicts intralaminar damage contours that are consistent in size and orientation with the C-scan results, thereby supporting the hypothesis that more accurate delamination modelling can be achieved using matrix damage as delamination initiation criterion.



Figure 2. Comparison with experimental results [4]: left-hand side image: contours of the Abaqus built-in Cohesive Zone Model, right-hand side image: matrix failure predicted by the VUMAT subroutine

3. Conclusions

As demonstrated by the initial results of this approach, two aspects of the numerical damage modelling procedure have been improved by the implemented approach. First, by using the information about matrix damage in the neighbouring plies, sizes and orientations of the predicted interface failure are better predicted compared to the Abaqus built-in cohesive model. Second, as the behaviour of cohesive elements is controlled within the VUMAT subroutine, a drop of the stable time increment caused by distorded cohesive elements is avoided by deleting interface elements connected to deleted ply solid elements, leading to increased robustness and computational efficiency.

Acknowledgements

The research is fully funded by the Croatian Science Foundation (HRZZ) within the project "COmputational modelliNg of COmposite stRuctures impact DamagE" (CONCORDE), grant number UIP-HRZZ-2020-02-9317.

References

[1] Ivančević, D., Ratković, J., Giannaros, E., Strain Rate-dependent Failure Modelling of Impact Damage in Laminated CFRP Structures, *Composite Structures*, 330, 117817, 2024.

[2] Ratković, J., Ivančević, D., Strain Rate Sensitive Delamination Modelling in Fibre Reinforced Polymer Composites, *9th European Congress on Computational Methods in Applied Sciences and Engineering,* Lisboa, PT. 2024.

[3] Liu, Y., van der Meer, F.P., Sluys, L.J., Cohesive Zone and Interfacial Thick Level Set Modeling of the Dynamic Double Cantilever Beam Test of Composite Laminate, *Theoretical and Applied Fracture Mechanics*, 96, 617-630, 2018.

[4] Falco, O., Lopes, C.S., Sommer, D.E., Thomson, D., Avila, R.L., Tijs B.H.A.H., Experimental analysis and simulation of low-velocity impact damage of composite laminates. *Composite Structures*, 287, 115278, 2022.

11th International Congress
of Croatian Society of Mechanics
September 30 – October 3 2025
Vodice, Croatia

Dynamic stall control of wind-turbine blades equipped with vortex generators and Gurney flaps

Marin Ivanković[*,+], Marvin Jentzsch[+], Anna Friederike Rahel Großmann[+], Vladimir Zimmermann[+], Marinos Manolesos[#], Christian Navid Nayeri [+], Hrvoje Kozmar[*]

[*]*Faculty of Mechanical Engineering and Naval Architecture, University of Zagreb, Ivana Lučića 5, 10000 Zagreb, Croatia, E-mails: {marin.ivankovic, hrvoje.kozmar@fsb.hr}@fsb.hr*
[+]*Hermann-Föttinger-Institut, Technische Universität Berlin, Müller-Breslau-Str. 8, 10623 Berlin, Germany, E-mails: {marvin.jentzsch, a.grossmann.1,christian.nayeri}@tu-berlin.de, vladimir.zimmermann@campus.tu-berlin.de*
[#]*School of Mechanical Engineering, National Technical University of Athens, Heroon Polytechniou 9, 15780 Zografou, Greece, E-mails: marinos@fluid.mech.ntua.gr*

Keywords: Wind turbine, Dynamic stall, Vortex generators, Gurney flaps, Wind-tunnel experiments

1. Introduction

Fluctuating loads experienced by wind-turbine blades during dynamic stall may significantly increase their fatigue loads and reduce lifetime, power production, and efficiency. These adverse effects can be mitigated by adding vortex generators (VGs) and Gurney flap (GF) to wind-turbine blades to affect the dynamic stall vortex (DSV).

VGs cause the delay of dynamic stall onset to a higher angle-of-attack (*AoA*) and increase the power production of wind turbines [1]. GFs applied at the blade trailing edge (TE) increase the lift-to-drag ratio c_L/c_D in the pre-stall regime, especially when applying very small GFs, with height less than 0.01 chord length (c) [2], [3].

Characteristics of airfoils concurrently equipped with both devices are still not sufficiently understood. The main objective of the present study is to investigate the interplay between VGs and a GF simultaneously applied to wind-turbine blades during dynamic *AoA* oscillations. Understanding the underlying flow phenomena introduced by the passive flow control devices (PFCDs) during dynamic stall conditions is important to improve the power production of future and already existing wind turbines.

2. Methodology

Experiments on a Clark Y airfoil were performed in a closed-return wind tunnel featuring an open test section at the Technische Universität Berlin, Germany. The flow is characterized by a turbulence intensity below 1%. A wing with a constant chord c = 0.14 m and an aspect ratio of AR = 2 was placed in the test section. The model was equipped with VGs and GFs of various sizes. Measurements were performed at the Reynolds number of Re = 180,000 in the $0° \leq AoA \leq 30°$ range. Dynamic tests with pitching *AoA* were conducted at reduced frequencies in the range of $0 \leq k < 0.15$.

Additional experiments on a scaled HAWT with a 3 m rotor diameter, the Berlin Research Turbine (BeRT), were performed in a closed-return wind tunnel with a closed test section. The blades of BeRT were designed with Clark Y airfoils as well. The wind-turbine model was rotated around its vertical axis to simulate yaw misalignment, but these experiments are not included here.

VGs and GFs were studied on the airfoil and wind-turbine blades. VGs with a height (h) of $0.011c \leq h \leq 0.037c$ were placed on the suction side between $0.05c$ and $0.15c$ downstream of the LE, while GFs with height of $0.0014c \leq h \leq 0.0143c$ were placed on the pressure side at the TE. Lift and drag were determined from the pressure distribution on the Clark Y airfoil. The effect of VGs and GFs on the BeRT was studied based on aerodynamic force, power, and torque coefficients.

3. Results

The results indicate the highest improvements in the static and dynamic stall and reattachment *AoA*, as well as the increase in the lift and lift-to-drag ratio, when the airfoil is simultaneously equipped with VGs with a height of 0.011*c* at 0.05*c* and a GF with a height of 0.007*c*. Figure 1 shows the static and dynamic lift coefficient (c_L) variation with *AoA* in the range of $10° \leq AoA \leq 30°$ obtained using the chord airfoil. Four configurations are shown, i.e., baseline (black), optimal VGs (red), optimal GF (dashed black), and a combination of optimal VGs and GF (green). The results in Figure 1a) are from the static tests, while the results in Figure 1b) are for the dynamic pitching case at the reduced frequency of $k = 0.15$ ($f = 6.8$ Hz).

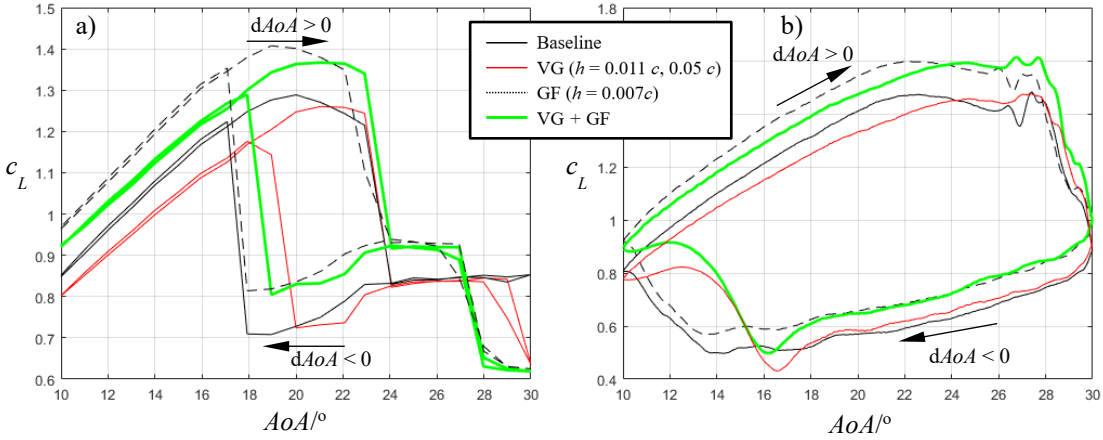


Figure 1. Lift polar of Clark Y airfoil: a) static $k = 0$ ($f = 0.0$ Hz), b) dynamic $k = 0.15$ ($f = 6.8$ Hz)

The proposed optimal VGs yield a reduced c_L in the pre-stall region, delaying the occurrence of maximal c_L to a larger *AoA,* whereas the flow reattachment for the airfoil pitching down is enhanced. The sole significant effect of the GF configuration (dashed curve) is the offset of the lift coefficient in a positive direction, but friction drag was not addressed. The concurrent application of VGs and GF (green line) combine aerodynamic enhancements of two devices, i.e., a 9% increase in the dynamic stall *AoA*, a 15% increase in the reattachment *AoA*, a 6% increase in the maximum c_L, while maintaining the same c_L/c_D ratio, and a 68% decrease in the c_L amplitude oscillations due to the DSV.

3. Conclusions

The results indicate that VGs and GF enhance airfoil performance when used alone and concurrently. A concurrent application of VGs and GF yields lift augmentation, stall delay, and a reduction of load fluctuations due to the DSV. The effects of VGs and GFs on wind-turbine blades are studied to reduce fatigue loads on wind turbines equipped with these passive flow control devices.

ACKNOWLEDGEMENTS

The support of Deutsche Forschungsgemeinschaft (DFG) Project #446073296, Deutscher Akademischer Austauschdienst (DAAD), the Erasmus+ program, COST Action CA20109 (MODENERLANDS) is gratefully acknowledged. This work was supported by the Croatian Science Foundation under the project number HRZZ-IP-2022-10-9434.

References

[1] Bak, C., Skrzypiński, W., Gaunaa, M., Villanueva, H., Brønnum, N.F. and Kruse, E.K., Full scale wind turbine test of vortex generators mounted on the entire blade. *Journal of Physics: Conference Series*, 753, 2, 022001, 1-10, 2016.

[2] Chng, L., Alber, J., Ntouras, D., Papadakis, G., Kaufmann, N., Ouro, P., Manolesos M., On the combined use of Vortex Generators and Gurney Flaps for turbine airfoils. Journal of Physics: *Conference Series*, 2265, 032040, 1-11, 2022.

[3] Yang, J., Yang, H. and Wang, X., Experimental study of turbulent inflow on the aerodynamic performance of a wind turbine with Gurney flaps. *Journal of Renewable and Sustainable Energy*, 16(3), 1-16, 2024.

11th International Congress
of Croatian Society of Mechanics
September 30 – October 3 2025
Vodice, Croatia

On the boundary conditions in meshless collocation methods for solving heat conduction problems

Boris Jalušić[+], Tomislav Jarak[†], Marin Vukovojac[*], Jurica Sorić[*], Zdenko Tonković[*]

[+]*University North*
E-mail: bjalusic@unin.hr

[†]*ITAP, School of Industrial Engineering, University of Valladolid*
E-mail: tomislav.jarak@uva.es

[*]*University in Zagreb, Faculty of Mechanical Engineering and Naval Architecture*
E-mails: {marin.vukovojac,jurica.soric,zdenko.tonkovic}@fsb.unizg.hr

Keywords: heat conduction, meshless collocation method, primal and mixed approach

1. Introduction

Meshless methods offer a flexible and efficient numerical framework for solving heat conduction problems, especially where traditional mesh-based approaches like the Finite Element Method (FEM) face geometric or structural constraints [1]. These methods use scattered nodes and smooth interpolation functions without relying on a predefined mesh [2]. Formulations can follow either strong-form (collocation) [3] or weak-form [4] approaches, with the latter often preferred for stability and convergence. However, strong-form methods are attractive due to their simplicity, lower computational cost, and avoidance of domain and boundary integration required in weak forms [5]. They are well-suited to irregular nodal distributions and adaptive refinement, as they operate directly on differential operators and require no integration domain updates [6]. Boundary conditions can be imposed directly at collocation points, eliminating the need for additional enforcement constructs such as Lagrange multipliers or penalty terms [7]. Nonetheless, strong-form methods may be sensitive to node irregularity and face challenges with discontinuities, steep gradients, and derivative boundary conditions [8], which are crucial in modeling heat flux. Thus, developing reliable strategies for imposing such conditions is key to enhancing the robustness and accuracy of meshless collocation methods.

2. Collocation methods for modelling of heat conduction

This contribution is focused on numerical modeling and solving of the steady state heat conduction problems using the Meshless Local Petrov-Galerkin (MLPG) collocation method [9]. Two contrasting approaches are considered, primal and mixed [9], and the obtained results are compared and analyzed. The steady state heat conduction problem is described by second-order elliptical partial differential equations. In the primal approach, only the temperature field is approximated using meshless functions. In the mixed approach two different formulations are used. The first one considers the approximation of temperatures and its first derivatives separately by using identical meshless functions, while the second one utilizes the approximation of the temperature field and its second derivatives. Therein, for the approximation of the unknown variables the same set of nodes is utilized, which makes the formulation simpler in comparison to ones where different sets of nodes are used [10]. In both mixed formulations, the compatibility between the approximated variables is enforced at the discretization nodes, to eliminate the nodal values of first and second derivatives of temperature from the discretized governing equations. Furthermore, for the approximation both, the standard MLS [9] and the interpolating MLS functions [11] will be considered. In the primal approach, the second-order partial derivatives need to be calculated in order

to assemble the global coefficient matrix, while in the first mixed approach only the first-order derivatives are needed. In all the formulations, different procedures for implementation of BCs will be tested. Firstly, the direct collocation method will be considered, where the Neumann condition is applied by replacing the governing PDE with its normal derivative at boundary nodes. Secondly, the penalty method will be applied. Therein, a penalty term is incorporated to enforce the derivative boundary condition by penalizing deviations from the prescribed normal derivative values [12]. The magnitude of this penalty is controlled by a user-defined parameter, which regulates the trade-off between the strictness of boundary condition enforcement and the overall numerical stability of the solution. Due to the lack of numerical integration and distinct difference in implementation of the BCs, the approaches should give contrasting results, especially near the boundary. Hence, special attention will be given to the numerical investigation of accuracy and stability dependent on the type of boundary conditions being employed. The obtained results will be presented by a set of selected heat conduction problems. In the numerical investigations, the implementation of Dirichlet, Neumann and adiabatic boundary conditions will be considered.

3. Conclusions

The application and adequate discretization of boundary conditions plays a major role in meshless collocation methods. From the authors experience with mixed meshless methods it is expected that this type of approaches should be more accurate and robust in comparison to the primal approaches for the same number of discretization nodes. This is especially the case if the derivative boundary conditions are considered in the numerical model. Therefore, the development of the mixed collocation method for application to heat conduction modeling is important since the method should be fast in achieving accurate results.

References

[1] Wang, K.X., Zhou, E.L., Wei, B.L., Wu, Y., Wang, G., An efficient and accurate numerical method for the heat conduction problems of thermal metamaterials based on edge-based smoothed finite element method, Engineering Analysis with Boundary Elements, 134, 282-297, 2022.

[2] Chen, J.S., Belytschko, T., Meshless and Meshfree Methods, Encyclopedia of Applied and Computational Mathematics, Springer, Berlin, Heidelberg, 2015.

[3] Jiang, W., Gao, X., Review of Collocation Methods and Applications in Solving Science and Engineering Problems, Computer Modeling in Engineering & Sciences, 140(1), 41-76, 2024.

[4] Xu, B.-B., Gao, X.-W., Cui, M., An efficient and accurate hybrid weak-form meshless method for transient nonlinear heterogeneous heat conduction problems. Engineering with Computers, 38, 969-984, 2022.

[5] Guan, Y., Atluri, S.N., Meshless fragile points methods based on Petrov-Galerkin weak-forms for transient heat conduction problems in complex anisotropic nonhomogeneous media, International Journal for Numerical Methods in Engineering, 122, 4055-4092, 2021.

[6] Slak, J., Gregor, K., Refined Meshless Local Strong Form solution of Cauchy–Navier equation on an irregular domain, Engineering Analysis with Boundary Elements, 100, 3-13, 2019.

[7] Rot, M., Jančič, M., Kosec, G., Spatially dependent node regularity in meshless approximation of partial differential equations, Journal of Computational Science, 79, 102306, 2024.

[8] Jalušić, B., Sorić, J., Jarak, T., Mixed meshless local Petrov–Galerkin collocation method for modeling of material discontinuity, Computational Mechanics 59, 1–19, 2017.

[9] Atluri, S.N., Liu, H., Han, Z., Meshless Local Petrov-Galerkin (MLPG) Mixed Collocation Method for Elasticity Problems, CMES: Computer Modeling in Engineering and Sciences, 14, 141-152, 2006.

[10] Wang, D., Wang, J., Wu, J., Superconvergent gradient smoothing meshfree collocation method, Computer Methods in Applied Mechanics and Engineering, 340, 728-766, 2018.

[11] Sorić, J., Jarak, T., Mixed Meshless formulation for analysis of shell-like structures, Computer Methods in Applied Mechanics and Engineering. 199, 1153-1164, 2010.

[12] Li, S., Atluri, S.N., The Mixed Collocation Method for Material Orientation and Topology Optimization of Anisotropic Solids and Structures, Computer Modeling in Engineering & Sciences, 30, 37-56, 2008.

11th International Congress
of Croatian Society of Mechanics
September 30 – October 3 2025
Vodice, Croatia

Wind-driven natural ventilation of elongated building structures

Matko Jelašić[1], Christoph Irrenfried[2], Günter Brenn[2], Hrvoje Kozmar[1]

[1] *Faculty of Mechanical Engineering and Naval Architecture, University of Zagreb, Ivana Lučića 5, 10000 Zagreb, Croatia*
matko.jelasic@fsb.unizg.hr, hrvoje.kozmar@fsb.unizg.hr

[2] *Institute of Fluid Mechanics and Heat Transfer, Graz University of Technology, Inffeldgasse 25F, 8010 Graz, Austria*
c.irrenfried@tugraz.at, guenter.brenn@tugraz.at

Keywords: natural ventilation, aerodynamics of buildings, elongated buildings

1. Introduction

Natural ventilation is the ventilation of buildings without the use of mechanical devices such as compressors and fans, which require electrical power. As a result, natural ventilation is both economically and environmentally advantageous. Natural ventilation is driven by wind forces and buoyancy effects caused by temperature differences between zones. In the present study, we focus solely on the wind-driven ventilation. The objective of this work was to assess the effects of various parameters such as freestream flow velocity, window opening angle, and wind incidence angle on the natural ventilation performance of generic elongated buildings.

2. Experiments and results

Experiments were conducted in a boundary layer wind tunnel (BLWT) at the Institute of Fluid Mechanics and Heat Transfer of the Graz University of Technology, Austria. The wind tunnel is 8 m long and features 2 m wide and 1 m high cross section. The test section of the wind tunnel, described in detail in [1], is shown in Figure 1.

The investigated building models were placed on a turntable at the end of the test section. The air change rate (ACH) was determined by using the concentration decay method, by directly measuring the decay of tracer gas (CO2) concentration within the ventilated model building. Further details on this method are provided in [2].

A Dantec Dynamics hot-wire anemometry system was used for flow velocity measurements. The hot-wire sensor was mounted on a traversing arm to measure velocity characteristics in the vertical plane at the end of the test section. The system recorded velocity data at 48 points with a sampling rate of 10 kHz for a measurement duration of 60 s.

Natural ventilation efficiency was assessed using three building models ($L = H$, $2H$, $3H$), each with windows on the flat roof. A detailed description of the models and configurations is available in [3]. In addition, variations in the freestream flow velocity, window opening angle, and flow incidence angle were analysed. The ACH for elongated buildings of various dimensions is shown in Figure 2. Flow direction (β) is plotted on the x-axis and the ACH on the y-axis. The $L = 2H$ building model (with two windows) outperformed the $L = 3H$ model (with three windows). As expected, the $L = H$ model exhibited the minimum ACH values due to only one window.

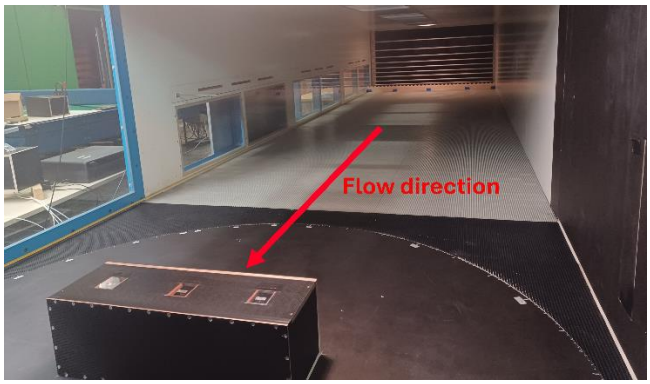


Figure 1. Wind-tunnel test section with the longest building model ($L = 3H$)

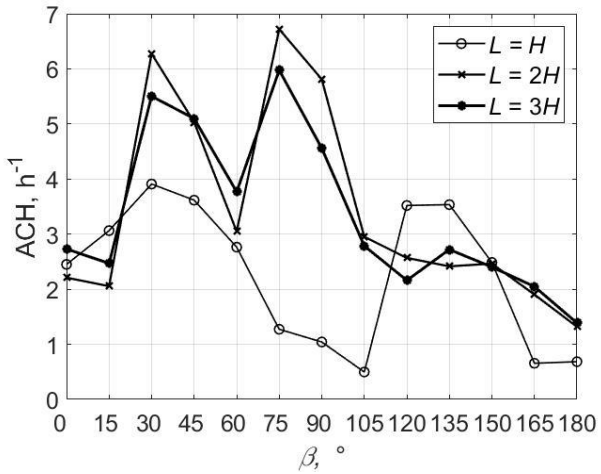


Figure 2. ACH versus incidence angle of the studied elongated buildings

3. Conclusion

The experiments were conducted in a boundary layer wind tunnel to assess the wind-driven natural ventilation of elongated building structures. Flow velocity characteristics were measured using hot-wire anemometry system. ACH of the building models was determined in various conditions regarding building design, window opening angle, wind direction, and freestream flow velocity. The skylight window shows improved natural ventilation compared to the window positioned on the cubical model's frontal wall. The $L = 2H$ building model exhibited higher ACH than the $L = 3H$ model, while the $L = H$ building model exhibited the minimum ACH. Higher ACH was achieved at larger freestream flow velocity and larger window opening angle for all building models.

Acknowledgements

This work was supported by the Croatian Science Foundation under the project number IP-2022-10-9434. The work of doctoral student Matko Jelašić has been fully supported by the "Young researchers' career development project – training of doctoral students" of the Croatian Science Foundation.

References

[1] Miše, D., Irrenfried, C., Meile, W., Brenn, G., Kozmar, H., Wind-driven natural ventilation of cubic buildings in rural and suburban areas. *Journal of Building Engineering*, 87, 1-27, 2024.

[2] Langensteiner, B., Transport processes in ventilated buildings. *PhD Thesis*, Graz University of Technology, Austria, 2014.

[3] Jelašić M., Natural ventilation of airport buildings in a rural area. *MSc Thesis*, Faculty of Mechanical Engineering and Naval Architecture, University of Zagreb, Croatia, 2023.

11th International Congress
of Croatian Society of Mechanics
September 30 – October 3 2025
Vodice, Croatia

Pure Bending of Rectangular Prism Including Anticlastic Deformation in Cosserats' Continuum – Analytical Approach

Gordan Jelenić, Dragan Ribarić

University of Rijeka, Faculty of Civil Engineering, Radmile Matejčić 3, 51000, Rijeka, Croatia
E-mails: {gordan.jelenic,dragan.ribaric}@uniri.hr

Keywords: Cosserats' (micropolar) continuum, pure bending, anticlastic deformation, hyperbolic functions

1. Introduction

Pure bending experiments on prismatic bars of rectangular cross section made of polymer foam exhibit deformation not explained by classical elasticity [1]. Instead of the bars' lateral surfaces remaining planar and only tilting as a consequence of anticlastic deformation, as predicted by the classical theory [2], certain amount of their warping is observed. A more refined theory is thus needed to capture this behaviour, the Cosserats' (micropolar) theory [3] being a possible candidate investigated here. Indeed, the theory confirms that the classical tilting of the lateral sides is only possible when the sides are appropriately loaded in addition to the usual bending moment applied. Lakes and Drugan [1] showed that Cosserats' elasticity can model the above experimentally observed warping. They assumed a 4th order polynomial warping displacement field as an approximate solution for the bar with square cross section and employed the principle of minimum potential energy to determine the coefficients of the polynomials. Good compliance of the solution with the experiments conducted was observed confirming that micropolar theory provides a good model for the anticlastic deformation observed. Here we investigate an alternative method of solution with the aim of further improving the analytical solution.

2. Problem statement

A rectangular prism is subject to a bending moment generated by applied distributed surface forces and moments as shown in Figure 1. A homogeneous isotropic centrosymmetric solid is assumed with all six Cosserats' material parameters (Young's modulus E, Poisson's ratio n, coupling number N, polar ratio, characteristic bending and torsional lengths l_b and l_t; see e.g. [4] for their definiton) known. The cross-section at x=0 is assumed to remain in the y-z plane throughout deformation. Other than the normal stress σ_{xx} and the bending couple-stress μ_{zx} acting on the crosssection, the non-zero stress and stress-couple components are assumed to exist only within the cross section, i.e. $\sigma_{xy}=\sigma_{yx}=\sigma_{zx}=\sigma_{xz}=0$, $\mu_{xx}=\mu_{yy}=\mu_{zz}=\mu_{xy}=\mu_{yx}=0$. As a result, all the unknown fields remain independent of the longitudinal co-ordinate. We further assume $\mu_{yz}=\mu_{zy}=0$ and identify the following non-trivial equilibrium and compatibility conditions:

$$\frac{2(1-N^2)}{1-2n}\frac{\partial}{\partial y}\left[(1-n)\epsilon_{yy}+n(\epsilon_{xx}+\epsilon_{zz})\right]+\frac{\partial}{\partial z}\left[\epsilon_{yz}+(1-2N^2)\epsilon_{zy}\right]=0,$$

$$\frac{\partial}{\partial y}\left[\epsilon_{zy}+(1-2N^2)\epsilon_{yz}\right]+\frac{2(1-N^2)}{1-2n}\frac{\partial}{\partial z}\left[(1-n)\epsilon_{zz}+n\epsilon_{yy}\right]=0,$$

$$\frac{\partial\omega_{xz}}{\partial z}+\frac{N^2}{2l_b^2(1-N^2)}\left(\epsilon_{zy}-\epsilon_{yz}\right)=0,\qquad \frac{\partial\epsilon_{yy}}{\partial z}=\frac{\partial\epsilon_{yz}}{\partial z},\qquad \frac{\partial\epsilon_{zz}}{\partial y}=\frac{\partial\epsilon_{zy}}{\partial z}+\omega_{xz},$$

where ω_{xz} is a change of rotation around the x axis with respect to co-ordinate z.

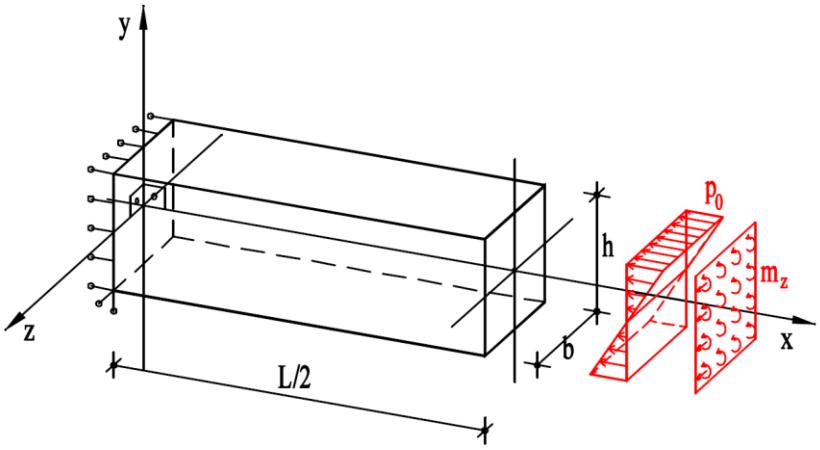


Figure 1. Please write your figure caption here

3. Analytical solution

In contrast to Lakes and Drugan [1], we consider the whole solution, rather than only the displacement contribution causing lateral bulging. Upon close examination of the properties of the governing equations, we identify the following irreducible differential equation as the starting point to the solution:

$$\frac{\partial^2 f(y,z)}{\partial y^2} + \frac{\partial^2 f(y,z)}{\partial z^2} - \frac{N^2}{l_b^2} f(y,z) = 0,$$

where function $f(y,z)$ expresses the change of difference of the in-plane shear strains acting in y and z directions: $f(y,z) = \epsilon_{yz} - \epsilon_{zy}$. A solution must satisfy the conditions $f(y,z) = 0$ at the cross-section vortices and along $z = 0$ and it may be found in a closed form involving hyperbolic functions, from where the remaining stresses and couple-stresses, as well as the strains and curvatures follow by integration.

This analytical solution is compared with Lakes and Drugan's [1] and their experimental results. In contrast to Lakes and Drugan's approximate solution, full compliance with the boundary conditions on $f(y,z)$ is achieved.

4. Conclusions

Pure Cosserats' bending of a rectangular bar gives rise to warping of lateral surfaces in addition to the usual tilt predicted by the classical theory. Cosserat's theory enables a solution that offers improvements of the currently known results.

Acknowledgement

We gratefully acknowledge the support of this research by the Croatian Science Foundation via Grant No IP-2024-05-9904 (ANEMIC PM).

References

[1] Lakes, R., W.J., Bending of a Cosserat Elastic Bar of Square Cross Section: Theory and Experiment. Journal of Applied Mechanics, Vol. 82.9, 091002(1-8), 2015.

[2] Timoshenko, S.P., Goodier, J.N., Theory of Elasticity, McGraw-Hill, New York, 1951.

[3] Nowacki, W., Theory of Micropolar Elasticity, Springler-Verlag, Vienna, 1972.

[4] Grbac, L., Jelenić, G., Ribarić, D., Grbčić Erdelj, S., Hexahedral finite elements with enhanced fixed-pole interpolation for linear static and vibration analysis of 3D micropolar continuum. International Journal for Numerical Methods in Engineering, Vo. 125.8, e7440, 2024.

11th International Congress
of Croatian Society of Mechanics
September 30 – October 3 2025
Vodice, Croatia

A Multiscale Approach to Damage Modelling in Heterogeneous Materials Using Phase-Field Method

Ante Jurčević*, Tomislav Lesičar+, Zdenko Tonković+, Jurica Sorić+

*Faculty of Forestry and Wood Technology, University of Zagreb, Svetošimunska 23
E-mail: ante.jurcevic@sumfak.unizg.hr

+Faculty of Mechanical Engineering and Naval Architecture, University of Zagreb, Ivana Lučića 5
E-mails: {tomislav.lesicar, zdenko.tonkovic, jurica.soric}@fsb.unizg.hr

Keywords: heterogeneous material, multiscale analysis, self-consistent clustering, phase-field method, damage

1 Introduction

Numerical modelling of damage and fracture in modern heterogeneous materials is a particularly attractive and demanding field of computational mechanics. Considering that heterogeneous materials represent an inevitable part of modern engineering structures, accurate and reliable prediction of damage occurrence and crack initiation becomes increasingly important.

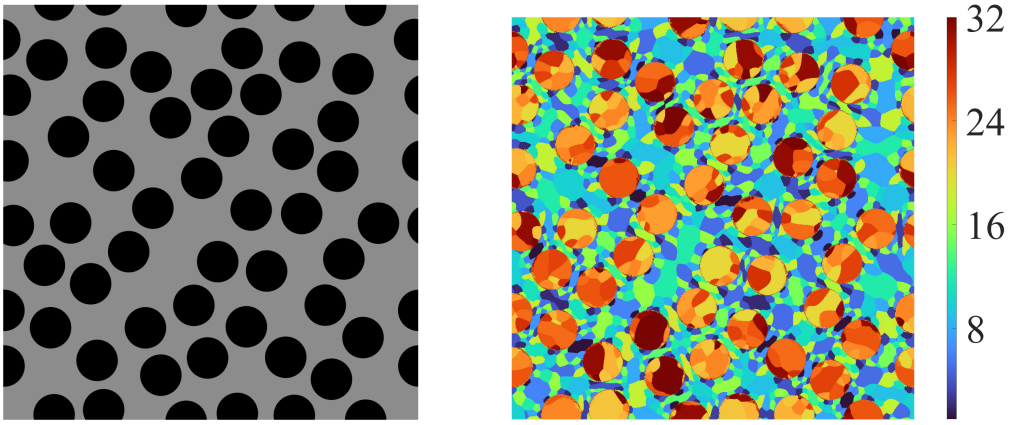
In order to numerically incorporate material's heterogeneity, which lives at its microscale, the classical phenomenological approach [1] needs to be abandoned in favour of multiscale methods [2]. With the ability to analyse material at different levels (scales), multiscale methods are a valuable tool in the field of numerical modelling of heterogeneous materials and have been in intensive development over the past two decades.

Performing a multiscale damage analysis, on any kind of heterogeneous material, represents a significant challenge from both computational and numerical standpoint. The former is related to the challenges of long computational time and high demands of computational resources, while the latter is related to problems of mesh independence, the objectivity of final results and the overall numerical stability of the analysis [2]. In order to address the major issues plaguing the numerical modelling of damage and fracture in heterogeneous materials, the proposed approach will utilise a reduced-order homogenization method called *self-consistent clustering analysis* (SCA) [3, 4] and *phase-field* (PF) fracture approach [5, 6].

2 Self-consistent clustering analysis

Self-consistent clustering analysis, or simply SCA, represents a reduced-order homogenization method which ensures computationally efficient and accurate calculation of the homogenized (macroscopic) response of the microstructure of a heterogeneous material. It achieves this by discretizing the complex microstructure into a relatively small number of material clusters (**Figure 1**), which are then analysed by means of the Lippmann-Schwinger equation [3].

Since the number of clusters is (in most cases) a double-digit number, the total amount of degrees of freedom at the microlevel is drastically reduced. This allows faster and computationally more efficient numerical analysis of the microlevel compared to direct numerical simulation (DNS) which is typically performed using finite element method (FEM) or Fast Fourier transform (FFT) based solver.



a) b)

Figure 1. Complex microstructure: a) Geometry, b) Decomposition into 32 clusters

3 Phase-field method

Although in the field of numerical modelling of fracture and damage, there exists quite a number of approaches, few have gained as much attention as the phase-field (PF) method. Characterized by simple implementation into FEM, and with the ability to simulate complicated fracture processes, including crack initiation, propagation, merging and branching PF fracture approach has *earned* its place as one of the most popular and most efficient fracture algorithms [5].

In essence, the PF method represents an enrichment of the free energy functional, where the internal part of the total potential energy is additively decomposed into bulk energy and *fracture-induces dissipating surface energy*. The modified free energy functional is then regularized, and the result of that is a set of partial differential equations that fully describe the crack's initiation and propagation.

4 Multiscale model

To achieve accurate and computationally efficient numerical modelling of damage in heterogeneous materials, this study will utilize the PF method (at the macrolevel) and SCA (at the microlevel) into a fully concurrent multiscale procedure. SCA will ensure fast and accurate calculation of the macroscopic response of the microstructure, while the presence of a non-local continuum damage model, such as PF, at the macrolevel will allow for a robust, and objective calculation of the material damage. In order to demonstrate the capabilities of the proposed algorithm, numerical examples will include both brittle and ductile fracture on a complex microstructure alongside several different geometrical samples.

References

[1] Souza de, E.A., Perić, D., Owen, D.R.J. *Computational Methods for Plasticity: Theory and Applications*. Wiley, Swansea, 2008.

[2] Jurčević, A. *Multiscale modelling of damage in ductile heterogeneous materials*. Ph.D., University of Zagreb, 2024.

[3] Liu, Z., Bessa, M.A., Liu, W.K., Self-consistent clustering analysis: An efficient multi-scale scheme for inelastic heterogeneous materials. *Computer Methods in Applied Mechanics and Engineering*, 306, 319-341, 2016.

[4] Liu, Z., Fleming, M., Liu, W.K., Microstructural material database for self-consistent clustering analysis of elastoplastic strain softening materials. *Computer Methods in Applied Mechanics and Engineering*, 330, 547-577, 2018.

[5] Seleš, K., Jurčević, A., Tonković, Z., Sorić, J., Crack propagation prediction in heterogeneous microstructure using an efficient phase-field algorithm. *Theoretical and Applied Fracture Mechanics*, 100, 2019.

[6] Lesičar, T., Polančec, T., Tonković, Z., Convergence Check Phase-Field Scheme for Modelling of Brittle and Ductile Fracture. *Applied Sciences*, 13, 2023.

11th International Congress

of Croatian Society of Mechanics

September 30 – October 3 2025

Vodice, Croatia

Numerical Structural Analysis of Steel Frames Used in Belt Conveyors

Damir Tin JURKOVIĆ, Marino BRČIĆ

University of Rijeka, Faculty of Engineering, Department of Engineering Mechanics, Vukovarska 58, HR-51000 Rijeka, Croatia

E-mails: dtjurkovic@gmail.com, marino.brcic@riteh.uniri.hr

Keywords: Structural Engineering Automation, Rule-Based Parametric Design, Genetic Algorithm

Abstract

Belt conveyors are integral components of material handling systems in mining operations, including, in this case, Direct Reduced Iron (DRI) plants [1]. Each conveyor requires a dedicated steel structure to support its weight, ensure alignment, and resist operational loads. A typical DRI facility with an annual capacity exceeding two million tons may include ten or more such conveyors, emphasizing the scale and design demand involved.

While these supporting structures are usually adapted to specific site constraints, recurring patterns in geometry and design workflow have been observed. From a structural engineering perspective, modeling each steel framework poses challenges in terms of both time and accuracy. In contrast to the standardized nature of conveyor belts themselves, the structural design process has historically lacked equivalent standardization. In an effort to formalize and automate the design process for such structures, we developed a parametric software tool that captures recurring structural patterns and engineering requirements within the commercial SAP2000 framework, which is based on the finite element method [2], using Python as the programming language for integration and control (Figure 1).

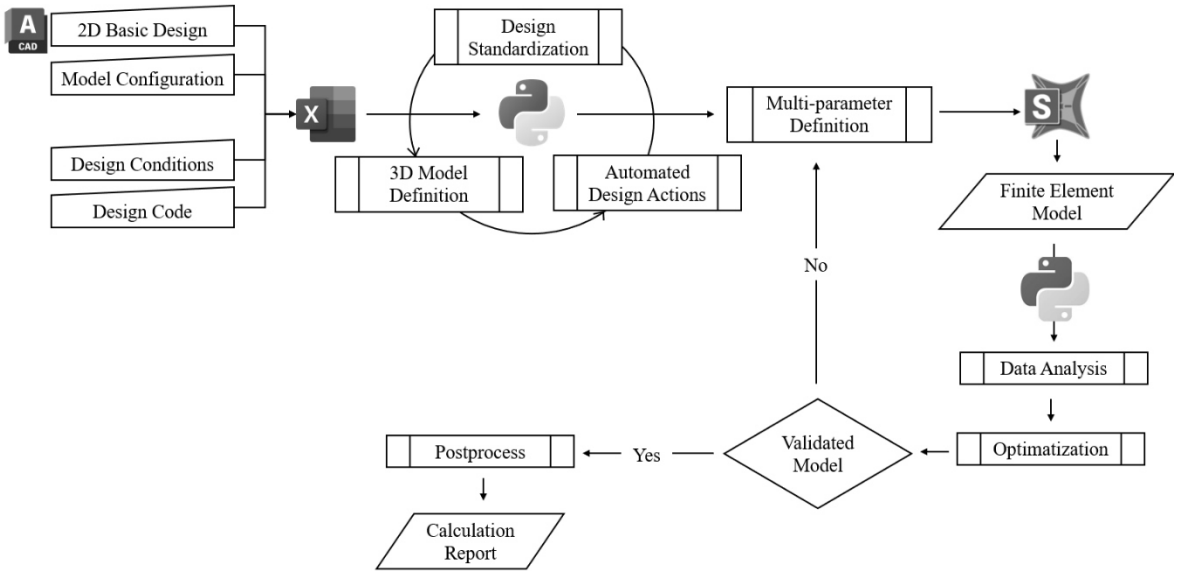


Figure 1. Simplified workflow diagram of automated structural design process.

The methodology is grounded in parametric modeling, where each structural system is defined through a multi-parameter set representing geometric, material, and loading attributes. These parameters are

governed by embedded standardization rules that ensure consistency across different configurations while maintaining compliance with engineering codes.

The parametric system also serves as a foundation for algorithmic optimization. Parameters can be compiled into a design vector and used within genetic algorithms to explore optimal solutions according to predefined performance goals. These may include structural deflection limits, stress distribution, or weight reduction. The integration of optimization routines within the design environment allows for automated generation and evaluation of design alternatives, supporting both performance-based design and early-stage decision-making [3, 4].

This work represents a key step in bridging the gap between initial routing concepts and detail design. In this intermediate phase, basic 2D layouts are discretized into 3D models with fully defined structural elements, enabling immediate use for analysis, verification, and documentation.

References

[1] Alles, R.: “Conveyor Belt System Design”, ContiTech Transportbandsysteme, Hannover, 1994.

[2] Logan, D.: “A First Course in the Finite Element Method 4th Edition”, Thomson, Wisconsin, 2007.

[3] Russel Rhinehart, R.: “Engineering Optimization: Applications, Methods and Analysis”, John Wiley & Sons Inc, Hoboken,2018.

[4] Kochenderfer, M.; Wheeler, T.: “Algorithms for Optimization”, The MIT Press, Massachusetts, 2019.

11th International Congress
of Croatian Society of Mechanics
September 30 – October 3 2025
Vodice, Croatia

Seismic Response of a Traditional Rammed Earth Sub-Assembly: Experimental and Numerical Study

Ivan Kraus*, Davide Lavorato+, Alessandro Colitta+, Petra Olić Miloš*

*Faculty of Civil Engineering and Architecture Osijek, Vladimira Preloga 3, 31000 Osijek, CROATIA
E-mails: {ikraus,policmilos}@gfos.hr

+ Roma Tre University's Department of Architecture, Largo G.B. Marzi 10, 00153 Rome, ITALY
E-mail: {davide.lavorato,ale.colitta}@uniroma3.it

Keywords: rammed earth, Croatian heritage, seismic behaviour, experimental testing, numerical modelling

1. Introduction

Traditional rammed earth (RE) houses in Croatia represent an invaluable part of the national architectural heritage [1], [2]. These structures embody authenticity and constitute a significant element of ethnographic village ensembles (Figure 1). Many of them are still in use, frequently renovated for hospitality purposes. However, the quality of these interventions is often questionable. Simultaneously, numerous earth buildings are abandoned and frequently demolished, usually due to a lack of awareness. Given Croatia's seismic activity [1], [3], the structural safety of existing and restored RE houses is a pressing concern. There is a growing need to understand their seismic vulnerability and to develop appropriate strengthening or retrofitting strategies that respect their material characteristics and architectural value. This work investigates the seismic resistance of a RE wall sub-assembly, representative of typical Croatian traditional construction. The aim is to provide experimental and numerical insights into its behaviour under seismic loading.

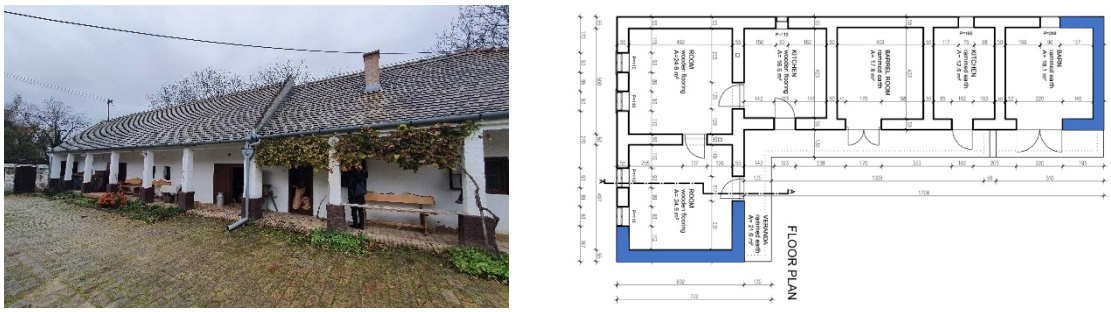


Figure 1. Traditional rammed earth house (left) and floor plan indicating C-walls (in blue) investigated in this study (right)

2. Experimental work

A reduced-scale wall specimen (1:2) was constructed at the Faculty of Civil Engineering and Architecture Osijek (Figure 2) using local soil materials [1], [4], [5], consistent with compositions observed during field investigations. The model represents a typical RE wall found in traditional Croatian buildings [2], with a prototype wall thickness of 50 cm and a storey height of approximately 250 cm. The RE technique involved compacting moist soil in layers, typically 10–15 cm thick, within a wooden formwork [2]. To simulate vertical dead load and live load, a reinforced concrete slab weighing 1150 kg was placed atop the wall specimen [1], [2]. The wall was then subjected to monotonically increasing horizontal loading to replicate seismic action. The wall was subjected to a

displacement-controlled monotonic loading protocol, where the top displacement was increased in each of 11 loading steps, without repeated cycles. The test was terminated upon the occurrence of diagonal failure across the C-wall wing. The maximum lateral force resisted by the wall was approximately 12.95 kN. Deformation measurements were performed using a combination of mechanical LVDT-s and an advanced optical tracking system (ARAMIS). Mechanical properties were also determined through tests on cubes, cylinders, and prisms, highlighting the heterogeneity and anisotropy of the material.

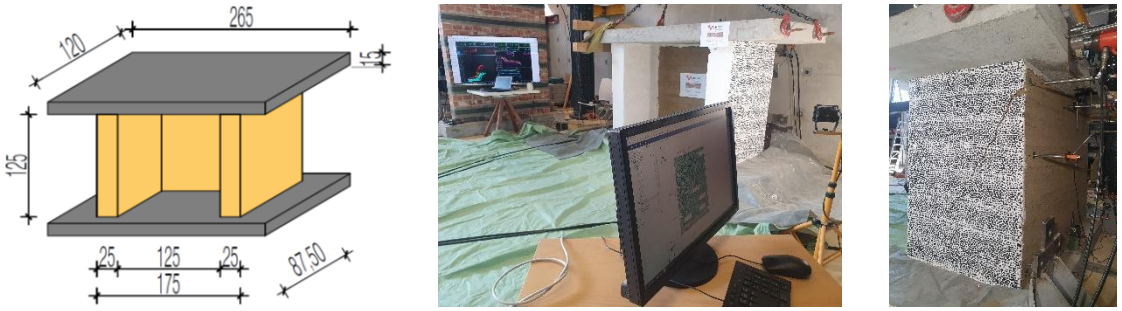


Figure 2. Schematic representation of the model (in cm) (left), experimental setup (center), and observed crack distribution on the external surface (right).

3. Numerical modelling

A detailed nonlinear finite element model of the wall was developed using advanced simulation software. The model incorporated experimentally derived material properties and boundary conditions to replicate the laboratory test setup. The calibration process focused on matching load-displacement curves and crack propagation patterns. The validated numerical model will serve as a foundation for extensive parametric studies, which will explore the influence of wall geometry, loading regimes, and soil composition on the seismic performance of similar structures. This research is intended to support the development of rational design and strengthening recommendations for earthen architecture in seismic regions.

4. Conclusions

This study underscores the structural relevance of Croatian rammed earth houses and the urgent need for informed preservation strategies. The experimental and numerical results provide a benchmark for understanding seismic vulnerability and lay the groundwork for further research into codified performance-based assessments in accordance with Eurocode 8.

Acknowledgments

This study was supported by the Croatian Science Foundation under project UIP-2020-02-7363 Rammed earth for modeling and standardization in seismically active areas—RE-forMS.

References

[1] Perić Fekete, A., Kraus, I., Grubišić, M., Dokšanović, T., In-plane seismic performance of rammed earth walls: an eastern Croatia reconnaissance based study. Bulletin of Earthquake Engineering, 22(3), 1359–1385, 2024.

[2] Brkanić Mihić, I., Kraus, I., Kaluđer, J., Perić Fekete, A., Architectural features and soil properties of traditional rammed earth houses: Eastern Croatia case study. Buildings, 14(7), 2049, 2024.

[3] Kaluđer, J., Kraus, I., Perić, A., Kraus, L., Shear strength of reproduced soil mixtures based on samples from rammed earth walls from eastern Croatia. Applied Sciences, 12(22), 11708, 2022.

[4] Kaluđer, J., Kraus, I., Perić, A., Brkanić Mihić, I., Physical properties of the soil in the walls of traditional eastern Croatia rammed earth houses. Journal of Civil Engineering, 75(11), 1067–1074, 2023.

[5] Perić Fekete, A., Augarde, C., Hughes, P., Kraus, I., Unsaturated behaviour of material from a vernacular eastern Croatia rammed earth house. In: Beckett, C., Bras, A., Fabbri, A., Keita, E., Perlot, C., Perrot, A., eds., Second RILEM International Conference on Earthen Construction, RILEM Bookseries, 52, 281–290. Springer Nature Switzerland, Cham, 2024.

11th International Congress
of Croatian Society of Mechanics
September 30 – October 3 2025
Vodice, Croatia

Dynamic Compressive Behavior of Cork Agglomerates Combined with Shear Thickening Fluids: Experimental and Computational Approaches

Lucas Lemos[*], Gabriel Serra[+], Ricardo Sousa[*] , Fábio Fernandes[+], Guilherme Sousa[*]

[*] *TEMA - Centre for Mechanical Technology and Automation, Department of Mechanical Engineering, University of Aveiro, Campo Universitário De Santiago, Aveiro, 3810-193, Portugal.*
E-mail: rsousa@ua.pt

[+] *LASI—Intelligent Systems Associate Laboratory, Portugal*

Keywords: Compression, Dynamic Behaviour, Cork, Numerical Simulation, Experimental tests

1. Introduction

Cellular materials, such as agglomerated cork, are widely utilized in engineering applications due to their exceptional properties, including fire resistance, excellent crashworthiness, low thermal conductivity, permeability, non-toxicity, and low density. This study employs finite element analysis (FEA) to model the dynamic compressive behavior of agglomerated cork, focusing on understanding the relationship between material density, stress relaxation behavior, and the influence of combining cork with shear thickening fluids (STFs). By incorporating STFs into the material matrix, as well as modeling stress relaxation and rebound effects, the study further examines and simulates the dynamic response under both initial and subsequent impacts.

Dynamic compression tests were conducted on agglomerated cork composite samples, to provide experimental data for the numerical model. The numerical model successfully replicates the response of agglomerated cork to multiple impacts, capturing both the initial dynamic compressive behavior and the material's subsequent rebound phases. The inclusion of the Mullins effect in the constitutive modeling explains the reduction in stiffness and stress softening seen after repeated loading, while the addition of STFs provides enhanced energy absorption during impacts.
This research offers a significant contribution by integrating the study of rebound phenomena and the combination of agglomerated cork with shear thickening fluids, a topic that had not been previously investigated in this group's earlier work. The findings expand the understanding of cork-STF composites in dynamic impact scenarios, with important implications for engineering applications requiring high energy absorption and resilience.

11th International Congress
of Croatian Society of Mechanics
September 30 – October 3 2025
Vodice, Croatia

Motion of the body on rough surface under random kinematic excitation

Željan Lozina*, Damir Sedlar*, Ivan Tomac*

*FESB – University of Split, R. Boskovica 32, 21000 Split, Croatia
E-mails: {zeljan.lozina, damir.sedlar, ivan.tomac}@fesb.hr

Keywords: nonlinear dynamics, Coulomb friction, nonclassical damping, random excitation, experimental verification

1. Introduction

The hardly predictable motion of the noclassicaly damped body exposed to the Coulomb friction and random kinematic is analyzed. Numerical results are aimed for experimental verification with aim to find out of influence factors establish rules for reliable assessment in generic case.

2. Mathematical models

A number of single and multi freedom degrees system have been investigated, see Figures 1 and 2. In this paper only single degree of freedom system analysis is presented.

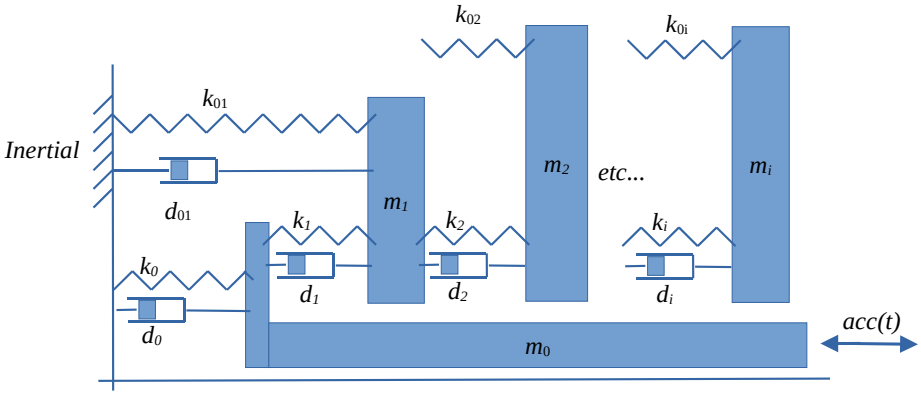


Figure 1. Generic model considered with random kinematic excitation

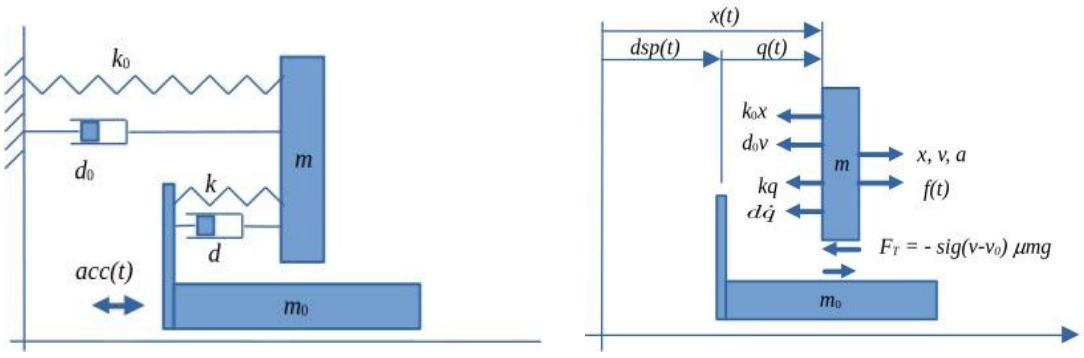


Figure 2. SDOF model under consideration

The random kinematic ground excitation due to earthquakes available in public domain is implemented, see Figure 3.

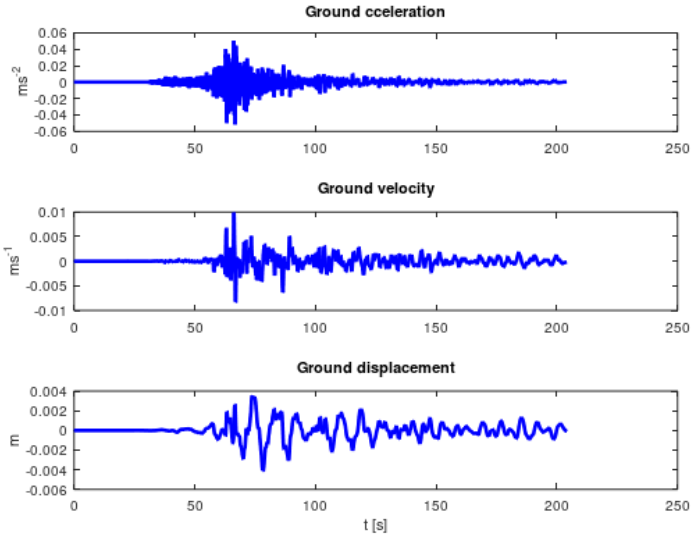


Figure 3. Kinematic horizontal ground excitation

The ground excitation are typically available as velograms and post-processing is required including PGA consideration. Typical time step of 0.01 second quite appropriate for the most applications. The ground excitation generally involves and vertical component not presented here. Treatment of vertical component posed additional challenge.
The parameters for the one of the SDOF considered models are listed in Table 1.

Table 1. Model data

SDOF parameters
• M = 500 kg • k = 190 N • d = 0 • PGA = 0.6g

The numerical integration has been performed with a number of numerical methods , [1], that all lead to the same results and therefore error of the numerical integration can be neglected. The major challenge is the efficient model and the implementation of the friction, [2], [3]. The influence of the vertical motion can be treated as energy introduction in contact that change the friction conditions.
The numerical results presented in paper are skipped here because they extensive due to high sensitivity on number of parameters such as inclination of the surface, stiffness of the supporting ground, response of the ground due to object impacts, etc. The aim of this calculations, in phase considered, is just to establish basis for the planning of the experiment.
The parameters of the experiment are basis for calibration and tuning model in update procedure.

3. Conclusions

In the paper a number of mechanical models of object subjected to Coulomb friction exposed to random kinematic excitation has been investigated in order to foreseen the object final position.

References

[1] Bathe, K.J., *Finite Elements Procedures*. Prentice Hall, New Jersey, 1998.

[2] Yaodong Lu, Vigen Arakelian, A new solution to force analysis including Coulomb friction in mechanism joints. Mechanism and Machine Theory, Volume 202, 1057-1076, 2024.

[3] Rooney G.T., Deravi P., Coulomb friction in mechanism sliding joints, Mechanism and Machine Theory, Volume 17, 297-211, 1982.

11th International Congress
of Croatian Society of Mechanics
September 30 – October 3 2025
Vodice, Croatia

Modelling of an underground quarry of dimension stone: the possibility of expanding the excavation

Tanja Mališ*, Antonia Jaguljnjak Lazarević*, Petar Hrženjak*

* *University of Zagreb, Faculty of Mining, Geology and Petroleum Engineering, Pierottijeva 6, HR-10000 Zagreb, Croatia*

E-mails: {tanja.malis, antonia.jaguljnjak-lazarevic, petar.hrzenjak}@rgn.unizg.hr

Keywords: SAP2000; numerical modelling; finite element method; underground quarry; dimension stone

1. Introduction

Numerical modelling is crucial for understanding rock behaviour and evaluating the stability of structures built on or within rock masses. Due to the complex, discontinuous nature of rock, methods like discrete and finite element modelling are used [1,2]. Underground dimension stone mining began in Croatia's "Kanfanar" quarry in 1995 [3], with initial FLAC analyses supporting design [4]. Full-scale mining using the room and pillar method began in 1997, adapting pillar placement to avoid cracked zones [5]. Stability was assessed via field/lab studies and SAP2000 modelling, which matched in-situ data and validated tributary area theory [6,7]. In [7], safety factor of 2.21 was achieved, with minimal stress changes (<10%) 20 m from the excavation, prompting further excavation analysis using SAP2000.

2. Site characteristics and geometry of the model

This study extends previous work [7], using the same input parameters. The rock mass is divided into five layers and potential future excavation is shown in red in Fig. 1.

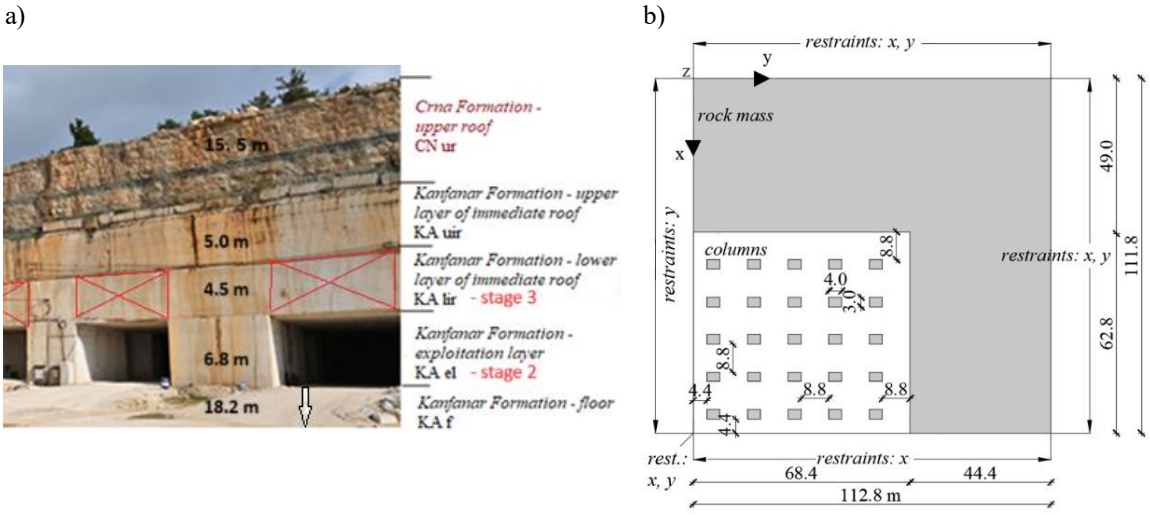


Figure 1: a) Deposit of "Kanfanar" quarry with potential further excavation expansion (in red), b) top plan at the quarter of the excavation area

3. Results for extended excavation model

For the new post-exploitation model, the highest values of vertical and horizontal compressive stresses were obtained at the edges of pillars, $\sigma_{v,max} = 9{,}88$ MPa and $\sigma_{,h,max} = 3.97$ MPa**.** The vertical stress at the centre of the most heavily loaded pillar is $\sigma_p = 6.31$ MPa. Maximum tensile stresses are 0.85 MPa and they occur along the edge of the excavation. The obtained maximum values of vertical displacements are shown in Fig. 2.

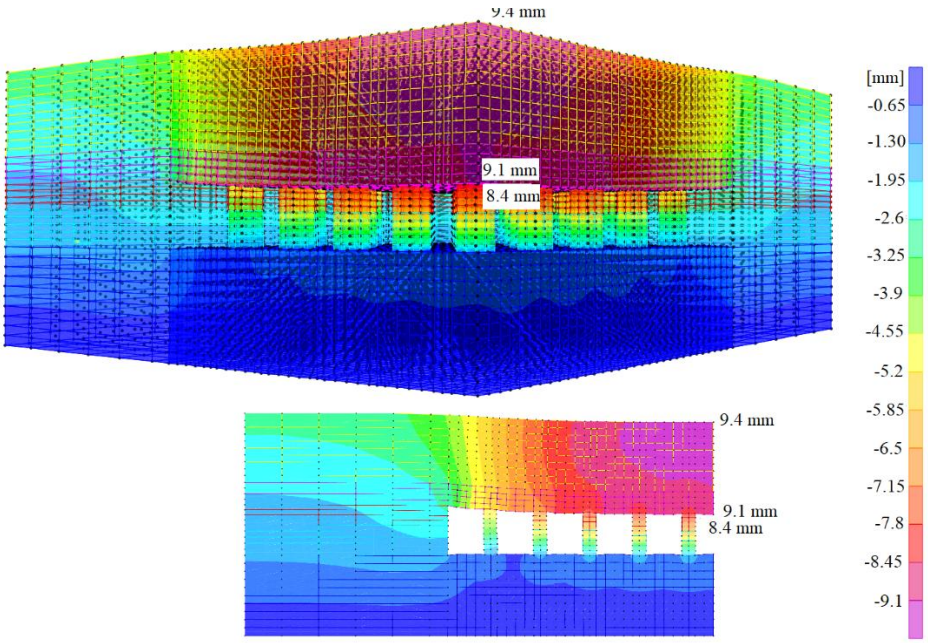


Figure 2: Stage 3: Vertical displacements of the new post-exploitation model

4. Conclusions

Comparing models with and without the KA lir layer (Stages 2 and 3) shows a decrease in roof stresses and displacements, with values remaining below the estimated strength of the KA uir layer. However, due to the weak nature of this rock, further lab and field tests are needed to confirm its strength and deformability. Pillar stresses and displacements also decrease, but pillar height increases by ~70%, requiring detailed assessment of its effect on load-bearing capacity.

.References

[1] Segalini, A., d'Attoli, M., Ferrero, A.M., Migliazza, M., Stability analysis of fractured rock mass excavation in ornamental stone quarries by mean of 3D numerical modelling. *41st U.S. Symposium on Rock Mechanics (USRMS)*: 50 Years of Rock Mechanics – Landmarks and Future Challenges. ARMA, American Rock Mechanics Association, 2006.

[2] Sari, M., Two- and three-dimensional stability analysis of underground storage caverns in soft rock (Cappadocia, Turkey) by finite element method. *Journal of Mountain Science*, 19 (4), 1182-1202, 2022.

[3] Cotman, I., Probna podzemna eksploatacija arhitektonsko-građevnog kamena u kamenolomu "Kanfanar", Istra (The trial underground exploitation of dimension stone at "Kanfanar" quarry, Istria). *Rudarsko-geološko-naftni zbornik*, 8, 81–89, 1996.

[4] Kovačević-Zelić, B., Vujec, S., Cotman, I., Numeričke analize podzemne eksploatacije arhitektonsko-građevnog kamena (Numerical analyses of the underground exploitation of dimension stone). *Rudarsko-geološko-naftni zbornik*, 8, 91–97, 1996.

[5] Cotman, I., Vujec, S., Improved method of excavation layered deposits in underground natural stone mine. In Almasi, A., & Eftekar Nezhad, J. (eds.): *20th World Mining Congress* - Mining & Sustainable Development. Geological Survey of Iran & National Geoscience Database of Iran, 2, 637-643, 1040 p, 2005.

[6] Hrženjak, P., Jaguljnjak-Lazarević, A., Uroš, M., Primjena numeričkih postupaka pri provjeri stanja naprezanja i deformacija podzemnih prostorija rudnika (Application of numerical methods for stress and strain analysis of underground mining spaces). In Šamec, E., Jaguljnjak Lazarević, A., Gidak, P., Uroš, M. (eds.): *Mini-simpozij Numerički postupci* u okviru projekta Novi, učinkoviti iteracjski postupak proračuna konstrukcija – poopćenje suvremenih postupaka, 129-137, 187 p., DOI:10.5592/CO/YODA.2019.3.2, 2019.

[7] Mališ, T., Hrženjak, P., Jaguljnjak Lazarević, A., Mikulec, M., Application of the SAP2000 computer programme in the modelling of an underground quarry of dimension stone, *Rudarsko-geološko-naftni zbornik,* Vol. 38 No. 4: No. 65, https://doi.org/10.17794/rgn.2023.4.2, 2023.

11th International Congress
of Croatian Society of Mechanics
September 30 – October 3 2025
Vodice, Croatia

Gurney Flap Effects on Savonius Turbine Performance: Aerodynamic and Structural Insights from Integrated CFD and Wind Tunnel Analysis

Ivo Marinić-Kragić*, Teo Čolović*, Marta Nekić*

*Faculty of Electrical Engineering, Mechanical Engineering and Naval Architecture, University of Split
E-mails: {imarinic, tcolov00, Marta.Nekic.00}@fesb.hr

Keywords: Gurney flap, Savonius turbine, fluid-structure interaction, wind tunnel testing

1. Introduction

Savonius-type vertical axis wind turbines (VAWTs) are valued for their self-starting capability, structural simplicity, and adaptability to turbulent flows, yet their broader adoption is limited by lower aerodynamic efficiency compared to Darrieus-type VAWTs. Gurney flaps (GFs), which enhance lift-to-drag ratios and suppress dynamic stall in Darrieus turbines [1], remain underexplored in drag-driven Savonius systems where blade-wake interactions and cyclic torque fluctuations are more pronounced. While additive manufacturing enables rapid prototyping of complex geometries [2], prior studies lack integrated assessments of aerodynamic and structural performance in GF-augmented Savonius rotors under dynamic loading. This study bridges this gap by coupling high-fidelity CFD simulations with wind tunnel experiments on 3D-printed Savonius rotors. We evaluate GF-induced torque characteristics in a low-turbulence wind tunnel and correlate transient flow with numerical and previous experimental data. Our findings provide insights for optimizing Savonius turbines that balance efficiency improvements with structural reliability.

2. Results

The experiments utilized a closed-circuit wind tunnel with a 1.3 m × 0.9 m test section, enabling wind speed modulation between 5–12 m/s. A high-resolution (0.01 Nm) torque transducer recorded dynamic torque fluctuations at 100 Hz sampling frequency. Numerical simulations employed a validated CFD model [3] previously calibrated against averaged power coefficient (c_p) measurements across tip speed ratios (TSRs). To extend validation, static torque analysis was conducted for $0° \leq \alpha \leq 180°$ wind angles in the current work, revealing persistent torque oscillations across all orientations (Figure 1). Numerical predictions showed pronounced torque coefficient (c_t) variations ranging from 0.1 to 0.8 at α=0°, diminishing near α=90°, and rising again nearly symmetrically towards α=180°—a pattern inconsistent with experimental data exhibiting sustained oscillations at all angles.

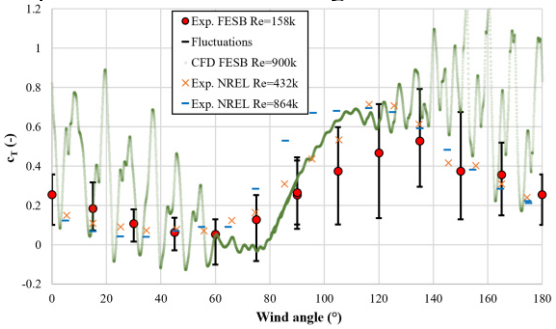


Figure 1. Static torque oscillations for conventional Savonius-type wind turbines, comparison of FESB results and NREL [4]

Discrepancies between rigid-body CFD assumptions and 3D-printed turbine behavior were identified as critical: torsional vibrations in PLA-printed rotors (despite fixed angular positioning) induced fluid-structure interactions (FSI) absent in simulations. Comparative analysis with steel-bladed NREL data [4] was attempted, and the average value agrees with our experiments (considering different Reynolds number), however the torque oscillations were not reported in [4], only the averaged coefficient was given. This underscores the necessity to increase the stiffness of the prototype design with 3D printed blades.

3. Conclusions

Experimental analysis revealed significant torsional vibrations at $\alpha \approx 90°$ wind angles in 3D-printed Savonius rotors, contrasting with numerical rigid blade and possibly the experiments with steel-blade data [4] that reported only averaged torque coefficients. This discrepancy highlights critical fluid-structure interaction (FSI) effects arising from the PLA material's flexibility - a factor not captured in rigid-body CFD simulations. While additive manufacturing enables rapid prototyping of complex geometries [2] our results demonstrate that blade compliance introduces dynamic instabilities requiring concurrent aerodynamic and structural optimization.
To address both efficiency and vibration challenges, we propose integrating Gurney flaps (Figure 2) - a solution proven to enhance Darrieus turbine performance through lift augmentation and stall suppression [1].
Preliminary wind tunnel tests with modified blades aim to quantify: Aerodynamic improvements via torque coefficient (c_t) and power coefficient (c_p) measurements across TSRs and mechanical damping effects through spectral analysis of torque oscillations. This approach will establish design guidelines for 3D-printed Savonius turbines that balance energy capture efficiency with structural reliability in turbulent flow conditions.



a) b)

Figure 2. 3D printed blades: a) placed in wind tunnel test section and b) comparison of original design and the design with added Gurney-flap.

References

[1] H. Zhu, W. Hao, C. Li, S. Luo, Q. Liu, and C. Gao, "Effect of geometric parameters of Gurney flap on performance enhancement of straight-bladed vertical axis wind turbine," *Renew. Energy*, vol. 165, pp. 464–480, Mar. 2021, doi: 10.1016/j.renene.2020.11.027.

[2] B. Deda Altan, G. Altan, and V. Kovan, "Investigation of 3D printed Savonius rotor performance," *Renew. Energy*, vol. 99, pp. 584–591, Dec. 2016, doi: 10.1016/j.renene.2016.07.043.

[3] I. Marinić-Kragić, D. Vučina, and Z. Milas, "Global optimization of Savonius-type vertical axis wind turbine with multiple circular-arc blades using validated 3D CFD model," *Energy*, vol. 241, p. 122841, Feb. 2022, doi: 10.1016/j.energy.2021.122841.

[4] R. E. Sheldahl, B. F. Blackwell, and L. V. Feltz, "Wind tunnel performance data for two- and three-bucket Savonius rotors," *J. Energy*, vol. 2, no. 3, pp. 160–164, May 1978, doi: 10.2514/3.47966.

11th International Congress
of Croatian Society of Mechanics
September 30 – October 3 2025
Vodice, Croatia

Experimental analysis of marine environment effects on the additively manufactured stainless steel AISI 316L

Benjamin Mihaljec*, Goran Vukelić+

University of Rijeka, Faculty of Maritime Studies, Marine Engineering Department, Studentska 2, 51000 Rijeka, Croatia
**E-mail: benjamin.mihaljec@uniri.hr*

+E-mail: goran.vukelic@pfri.uniri.hr

Keywords: stainless steel, AISI 316L, corrosion, marine environment

1. Introduction

To meet the increasing demand for lightweight, complex, and high-performance parts, the maritime and offshore industries are turning more frequently to advanced manufacturing technologies, notably additive manufacturing (AM) [1]. However, marine conditions create challenges for engineering structures [2], primarily due to extreme corrosion risks, which can compromise offshore infrastructure and marine vessels. AM-produced stainless steels may behave differently under these conditions compared to conventionally manufactured steels due to variations in surface roughness, composition and internal stress distribution [3].

In this paper, an experimental study is conducted on the effects of the marine environment on the properties of the additively manufactured AISI 316L stainless steel specimens. One group of the specimens was immersed in the Adriatic Sea, while the second group was exposed to tidal conditions for periods of one, three, and six months. After extraction, specimens have been examined, cleaned, and weighed to determine their mass loss. In addition, tensile tests were conducted on the specimens to determine the change in tensile strength.

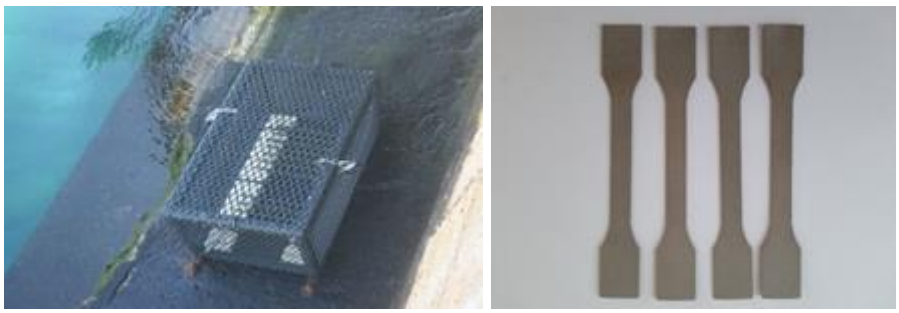
2. Materials and methods

Additively manufactured specimens of the stainless steel AISI 316L were exposed to a marine environment for periods of 1, 3 and 6 months to investigate the influence of corrosion behaviour on the specimens. Specimens have been separated into two groups, one group was immersed in sea water, while the other group was exposed to the tidal conditions, Figure 1 (a). An additional group was kept in a room atmosphere for reference. When extracted, the change in mass was measured. In addition, standardized tests were carried out on the universal testing machine to obtain stress-strain diagrams for inspection of changes in tensile strength.

AM specimens were printed with Laser PBF (Powder Bed Fusion) technology on the EOS M280 3D printing machine, Figure 1 (b). The size range of the material powder particles is between 10 and 40 µm. The 3D printing machine operating parameters were wavelength of 1030 nm, output power of 200 W, and layer thickness of 30 µm. Surface finish used on the specimens was shot-peening, while plates were flat-oriented for printing. Inert gas used in the process for preventing powder oxidation was argon, which was continuously supplied at a pressure of 12 mbar and a flow rate of 7.5 L/min. Printing parameters were chosen based on previous studies [1].

The experimental location was in the northern part of the Adriatic Sea in Croatia, near the city of Rijeka. The first group was immersed 10 meters below the seawater surface from July 2024 to January 2025. The second group was fixed on the stone platform of the pier for tidal conditions exposure. In addition, one group of specimens was kept in a dry atmosphere at room temperature as a reference. Extracted specimens were cleaned from rust with a soft brush, washed in distilled water,

and dried at room temperature prior to tensile testing, following standardized procedures [4]. Universal testing machine Hegewald-Peschke Inspekt Table 20 kN was used for tensile tests.

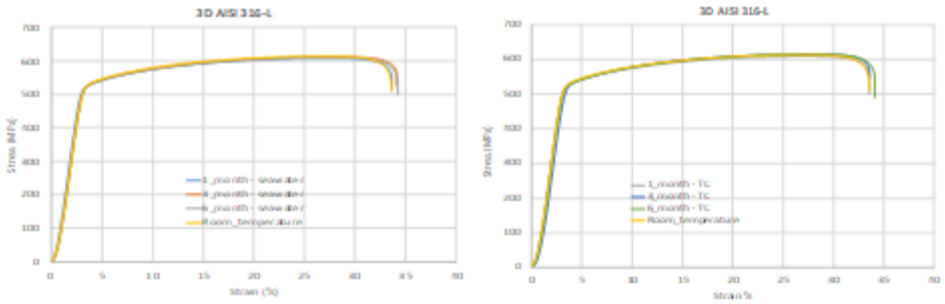


(a) (b)

Figure 1. (a) Test exposure site. (b) AM specimens.

3. Results and conclusions

The effect of the marine environment on the tensile strength of the AM stainless steel AISI 316L is represented on stress-strain diagrams, Figure 2.



(a) (b)

Figure 2. Engineering stress-strain diagrams for AM AISI 316L exposed: (a) under seawater, (b) to tidal conditions.

Generally, a reduction in the tensile strength can be noticed due to prolonged exposure to the marine environment when compared with the reference material. Also, tidal conditions tend to have a stronger influence on the tensile strength when compared to simple submergence under the sea. There are some exceptions, like the specimens exposed for 6 months, which indicate higher values of tensile strength, marking the need for additional research.

References

[1] G. Vukelic, B. Mihaljec, and Š. Ivošević, 'Marine Environment Effect on Welded Additively Manufactured Stainless Steel AISI 316L', *J. Mar. Sci. Eng.*, vol. 13, no. 3, p. 459, Feb. 2025, doi: 10.3390/jmse13030459.

[2] D. Pastorcic, G. Vukelic, J. Parunov, and Z. Bozic, 'Fatigue life estimation of corroded welded steel joint using probabilistic approach', *Int. J. Fatigue*, vol. 182, p. 108195, May 2024, doi: 10.1016/j.ijfatigue.2024.108195.

[3] P. Renner, Y. Chen, M. Li, C. Ma, D. Parkinson, and H. Liang, 'Corrosive Behavior of 3D-Printed 316L Stainless Steel', *Mater. Perform. Charact.*, vol. 10, no. 1, pp. 74–86, 2021, doi: 10.1520/MPC20200082.

[4] G. Vukelic, G. Vizentin, S. Ivosevic, and Z. Bozic, 'Analysis of prolonged marine exposure on properties of AH36 steel', *Eng. Fail. Anal.*, vol. 135, p. 106132, May 2022, doi: 10.1016/j.engfailanal.2022.106132.

11th International Congress
of Croatian Society of Mechanics
September 30 – October 3 2025
Vodice, Croatia

Comparison of analytical and numerical calculations of the steel shell silo reinforced with thin rings

Ivan Morosavljević*, Dražan Kozak*, Janko Morosavljević*, Pejo Konjatić*

* *University of Slavonski Brod, Mechanical Engineering Faculty, Slavonski Brod, Croatia*
E-mails: imorosavljevic@unisb.hr
jmorosavljevic@unisb.hr
dkozak@unisb.hr
pkonjatic@unisb.hr

Keywords: analytical calculations; numerical calculations; steel silo; thin-walled structure; ring reinforcement

1. Introduction

Silos are essential structures in both industry and agriculture, serving purposes such as storing, preserving, receiving, transporting, and drying agricultural products and other materials. Typically, silos are slender, thin-walled constructions where the wall thickness is significantly smaller than the diameter. This paper presents a numerical and analytical comparison of a cylindrical silo designed for storing hydrated lime, constructed from SPH265 steel.

2. Materials and methods

The silo has a radius of 2450 mm, a height of 13000 mm, a constant wall thickness of 8 mm, and a total volume of 270 m^3. It is filled with fine lime precipitate with a grain size of less than 100 μm, a density of 2121 kg/m^3, and a specific gravity of 20.81 kN/m^3. The cone at the base of the silo is made from the same material and has the same wall thickness as the cylindrical section, featuring a discharge diameter of 1000 mm and a height of 3300 mm. The structure is reinforced with nine steel rings measuring 60 x 20 mm, except for the lower ring, which measures 60 x 40 mm because of the way silo is supported.

2.1. Analytical calculation

A silo that is under internal pressure comprises several structural elements: a cylindrical shell, a ring, and the connections between the cylinder, cone, and ring. Each of these components experiences internal hydrostatic pressure, which results in transverse forces (Q) and bending moments (M) at their connection points. Additionally, the shell elements are subjected to membrane forces, both circular and longitudinal. [1]

The intensity of hydrostatic pressure increases with depth, leading to a linear increase in the hydrostatic pressure load on the ring towards its lower edge.[2-4] However, due to the negligible height of the ring compared to the overall height of the silo, it is assumed that the hydrostatic force acts at the midpoint (the center of gravity) of the ring, and that the external load is uniformly distributed across its upper and lower edges.

In accordance with ring theory, certain assumptions are made during the calculation process that are dictated by the ring's geometry and the loads it experiences. These assumptions include [5]:

1. The transverse dimensions of the ring are of similar magnitude.
2. The ring is axisymmetric, subjected to axisymmetric loading, and is fixed in place.

Taking these conditions into account, the analysis of stresses and deformations assumes that:

3. The shape of the ring's cross-section remains unchanged during deformation, effectively moving as a rigid body.

4. An approximately uniaxial state of stress prevails within the ring, meaning that the axial and radial stresses are negligibly small compared to the circumferential stress.

2.1. Numerical calculation

The 3D model was developed using the DS SolidWorks 2022 software, following the designated design specifications. The preparation for finite element method (FEM) analysis was conducted using Spaceclaim software. Due to the significantly smaller wall thickness of the silo relative to its diameter, two-dimensional second-order shell elements, known as Quad8, were employed for the FEM analysis. These elements are formulated by combining a 2D membrane element with a plate element based on Reissner-Mindlin plate theory. [6]

For the 3D model, the mesh consisted of 135747 Quad8 elements for the shell surfaces, 13902 Hex20 elements for the rings, and 32669 Tet10 elements for the silo supports, resulting in a total of 182318 finite elements and 572453 nodes. To facilitate a comparison between analytical and numerical results, deflection probes were placed at each individual ring.

To ensure the application of shell finite elements, all shell silo structures were reduced to a mid-surface using the mid-surface tool in the Spaceclaim software.

3. Conclusions

By using rings instead of variable wall thickness, while simultaneously reducing the amount of material used to make silos, it is possible to partially achieve product modularity in silo production because the hydrostatic pressure caused by liquid or fine precipitate increases linearly with increasing silo height.

Considering the mathematical complexity involved in the analytical calculation of the shell structure and the various compatibility conditions required to address the analytical problem, it is noteworthy that the average discrepancy between the results of numerical and analytical calculations is 4.56% or less. This discrepancy is even lower when excluding the lower ring, for which we do not account for the silo supports that further reinforce the structure around the bottom ring.

Table 1. Comparison of numerical and analytical ring total deflection results

Position	Numerical deflection, mm	Analytical deflection, mm	Discrepancy, %
Ring 1	0,00943	0,0087	7,74
Ring 2	0,1759	0,17	3,35
Ring 3	0,276	0,26	5,80
Ring 4	0,361	0,35	3,05
Ring 5	0,463	0,44	4,97
Ring 6	0,524	0,52	0,76
Ring 7	0,592	0,61	-3,04
Ring 8	0,7252	0,72	0,72
Ring 9	0,215	0,19	11,63

References

[1] Inženjerski priručnik IP1; Temelji inženjerskih znanja; 1. izdanje; Zagreb; Školska knjiga; 1996.-XVI., 1094p; ISBN: 953-0-31662-3

[2] Čantrak S., Benišek M., Pavlović M., Marjanović P., Crnojević C., Petković Z.; REŠENI ZADACI IZ MEHANIKE FLUIDA SA IZVODIMA IZ TEORIJE, IRO, Beograd, 1985.

[3] I. Alfirefić; Nauka o čvrstoći II; Fakultet strojarstva i brodogradnje, Zagreb, 1999., ISBN: 953-6168-85-5

[4] S. Timošenko; S. Vojnovski-Kriger: TEORIJA PLOČA I LJUSKI, Građevinska knjiga, Beograd, 1962., McGraw-Hill Book Company inc., 1959., 2. Izdanje

[5] I. Alfirefić; LINEARNA ANALIZA KONSTRUKCIJA, Fakultet strojarstava i brodogradnje, Zagreb 2011., 3. Izdanje, 413p, ISBN: 978-953-6313-57-0

[6] Hoang, Trung & Ádány, Sándor. (2022). Constrained finite element method with displacement mapping. Thin-Walled Structures. 181. 110120. 10.1016/j.tws.2022.110120

11th International Congress
of Croatian Society of Mechanics
September 30 – October 3 2025
Vodice, Croatia

Embedded discontinuity dynamic fracture model and Bayesian identification of parameters

Mijo Nikolić[1], Andjelka Stanic[2], Noemi Friedman[3], Hermann G. Matthies[4]

[1]*University of Split, Faculty of Civil Engineering, Architecture and Geodesy, 21000 Split, Croatia*
E-mail: mijo.nikolic@gradst.hr

[2]*Faculty of Engineering Technology, University of Twente, Drienerlolaan 5, 7522 NB Enschede, The Netherlands*
E-mail: andjelka.stanic@gmail.com

[3]*HUN-REN Institute for Computer Science and Control (SZTAKI), Kende u. 13-17, 1111 Budapest, Hungary*
E-mail: noemi@friedmango.net

[4]*Institute of Scientific Computing, Technische Universit¨at Braunschweig, 38092 Braunschweig, Germany*
E-mail: h.matthies@tu-bs.de.hr

Keywords: dynamic fracture propagation, Kalthoff test, Bayesian identification procedure

1. Introduction

A Bayesian probabilistic approach [1-2] is employed for the identification of material and fracture parameters governing dynamic crack propagation. This methodology enables a robust framework for calibrating models against experimental observations. The focus of this study is the Kalthoff test (Figure 1.), a benchmark dynamic fracture experiment involving impact loading, where stress waves generated by the impact initiate and drive crack propagation in a brittle material specimen. The test is simulated using an embedded strong discontinuity model, which captures the initiation and evolution of cracks through a localized displacement jump embedded within the finite element formulation [3].

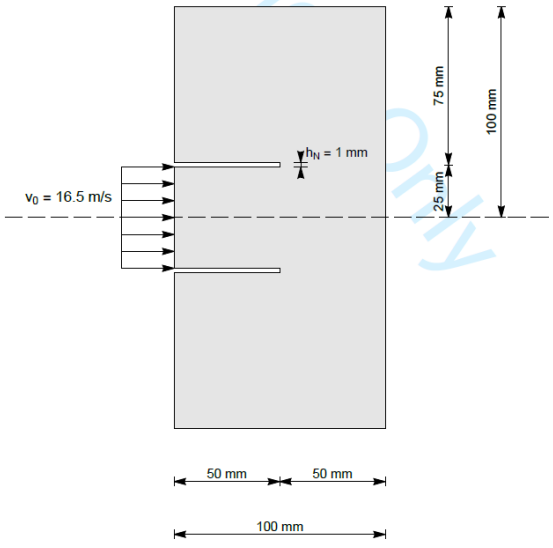
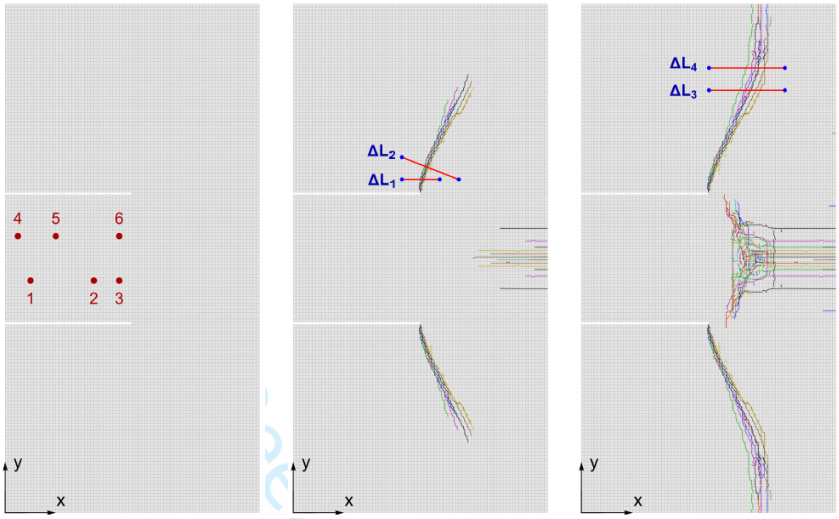


Figure 1. Kalthoff's test setting

2. Identification procedure



(a) Phase 1 (b) Phase 2 (c) Phase 3

Figure 2. The three phases of identification: a) elastic, b) first fracture phase, c) second fracture phase

The identification of material parameters is conducted in three phases (Figure 2.), aiming at a specific set of mechanical properties relevant to different stages of the dynamic fracture process. In the first phase, the elastic parameters, bulk modulus K and shear modulus G, are identified by analyzing the velocity of stress wave propagation through the specimen after the impact, relating the wave speed and elastic material response. The second phase corresponds to the initial fracture stage, where the onset of crack initiation is used to identify the ultimate tensile strength and tensile fracture energy. These parameters are inferred from measurements of crack opening displacement captured during the early stages of crack formation. In the final phase, when the crack changes direction, identification of shear strength and shear fracture energy is achieved through analysis of crack opening behavior associated with mixed-mode loading conditions, where shear effects become dominant.

3. Conclusions

The probabilistic approach based on Bayesian inference proved to be capable for the identification of the complete set of material parameters governing the failure behavior in dynamic crack propagation. It enabled a systematic calibration process while also accounting for uncertainties. The embedded strong discontinuity model demonstrated its effectiveness in capturing the complex fracture processes and offered computational efficiency, making it particularly suitable for multiple simulations required in the probabilistic identification framework.

Acknowledgement
This research has been supported by the project 'Parameter estimation framework for fracture propagation problems under extreme mechanical loads' (HRZZ-UIP-2020-02-6693), funded by the Croatian Science Foundation.

References

[1] Matthies, H.G., Zander, E., Rosic, B., Litvinenko, A., Pajonk, O. Inverse Problems in a Bayesian Setting. *In: Computational Methods for Solids and Fluids*, 41, 245-286, 2016.

[2] Šodan, M., Urbanics, A., Friedman, N., Stanić, A., Nikolić, M. Comparison of machine learning and gpc-based proxy solutions for an efficient bayesian identification of fracture parameters. *Computer Methods in Applied Mechanics and Engineering*, 436, 117686, 2025.

[3] Šodan, M., Stanić, A., Nikolić, M. Enhanced solid element model with embedded strong discontinuity for representation of mesoscale quasi-brittle failure. *Int J Fract*, 248, 1-25, 2024.

11th International Congress
of Croatian Society of Mechanics
September 30 – October 3 2025
Vodice, Croatia

Assessing Additively Manufactured TPMS Structures Under High-Speed Loading

Nejc Novak*, Oraib Al-Ketan+, Anja Mauko*, Matej Vesenjak*, Zoran Ren*

*Faculty of Mechanical Engineering, University of Maribor, Slovenia
E-mails: n.novak@um.si, anja.mauko@um.si, matej.vesenjak@um.si, zoran.ren@um.si

+Core Technology Platform, New York University Abu Dhabi, United Arab Emirates
E-mail: oga2@nyu.edu

Keywords: TPMS, Metamaterials, Impact, High-strain rate, Mechanical properties

1. Introduction

TPMS cellular metamaterials exhibit superior mechanical properties through their mathematically optimised porous architectures [1,2]. These engineered structures demonstrate remarkable deformation capacity and strain-rate adaptability, with sheet-based designs outperforming conventional strut-based lattices [3]. Our study advances understanding of their dynamic behaviour by integrating high-speed experimental characterisation with multi-scale computational modelling across loading regimes.

The research specifically examines implicit-based TPMS structures under high strain-rate conditions, employing innovative testing methods, including Hopkinson bar techniques. Computational models bridge microstructural response with macroscopic performance, enabling accurate prediction of impact behaviour. Beyond their mechanical advantages, these lightweight metamaterials offer sustainable solutions through material-efficient designs that maintain structural integrity while reducing mass.

Findings provide critical insights for engineering applications where energy absorption is paramount. This work establishes a framework for developing optimised TPMS metamaterials tailored to specific loading conditions. Understanding the dynamic performance of these materials is critical for their application in crashworthiness, blast mitigation, and ballistic protection systems [3,4]. By elucidating their behaviour under extreme loading conditions, this research aims to pave the way for next-generation safety solutions in aerospace, automotive, and defence engineering.

2. Materials and methods

The TPMS-based lattice structures were designed using our in-house software MSLattice [5], which generated uniform test specimens from four distinct unit cell geometries: Schoen Gyroid, Schwarz Diamond, Schoen IWP, and Schwarz Primitive. We also created hybrid specimens by strategically combining Gyroid and Diamond unit cells along the sample's vertical axis to study how topological arrangements influence mechanical performance. The samples were fabricated using additive manufacturing technologies.

A multi-rate testing approach was employed for mechanical characterisation to capture the full spectrum of material behaviour. Quasi-static compression tests were conducted at 0.1 mm/s using an INSTRON 8801 servo-hydraulic universal testing machine, while low dynamic tests employed the same system at 284 mm/s to examine rate-dependent effects at moderate strain rates. To investigate high-strain-rate behaviour, we utilised our innovative Direct Impact Hopkinson Bar (DIHB) system, developed explicitly for cellular metamaterials, which allowed precise dynamic characterisation at strain rates around 1,000 s^{-1}. For even more extreme loading conditions approaching 11,000 s^{-1}, we implemented a one-stage powder gun setup where controlled detonation of gunpowder propelled a projectile-mounted specimen into a rigid wall, simulating ultra-high-velocity impact scenarios.

3. Results

Figure 1a presents deformation patterns observed in physical tests and simulations, revealing consistent failure modes and collapse mechanisms across different loading velocities. The computational models accurately captured the progressive buckling and layer-by-layer collapse characteristics observed experimentally in Gyroid TPMS structures. Energy absorption performance (Specific Energy Absorption - SEA) shows significant variation among different cellular geometries (Figure 1b). The Gyroid architecture demonstrates superior energy dissipation capabilities compared to other TPMS topologies, particularly at intermediate strain rates between 10^2 and 10^3 s^{-1}. This enhanced performance correlates with the observed deformation mechanics, where the Gyroid's interconnected curvature promotes more uniform stress distribution during collapse.

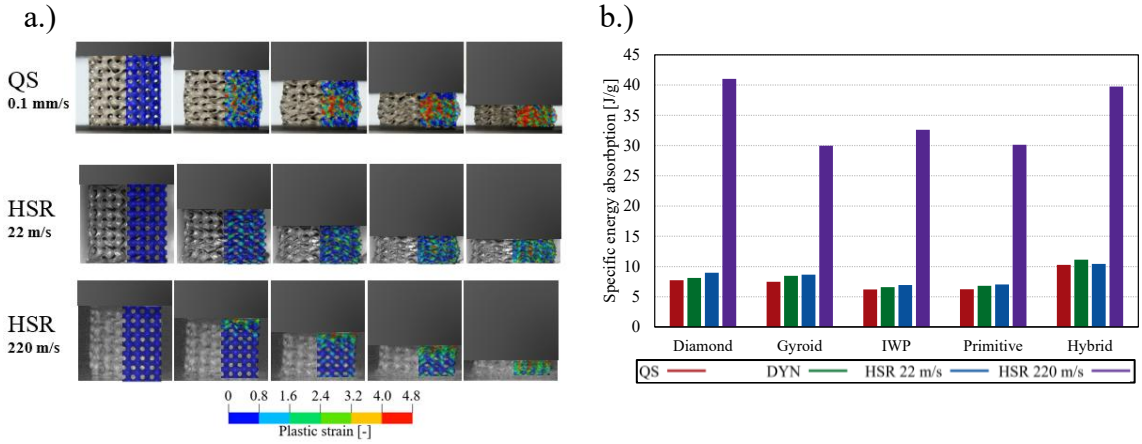


Figure 1. Comparative analysis of TPMS lattice performance: (a) Deformation pattern correlation between experiments (left) and simulations (right) of Gyroid TPMS structures, and (b) Specific Energy Absorption (SEA) for different TPMS topologies across the tested strain rate regime.

4. Conclusions

This study reveals how TPMS lattices transition from moderate strain hardening at low rates (<1,000 s^{-1}) to dramatic performance shifts under extreme loading (>10,000 s^{-1}). Diamond and IWP structures showed 5 times greater energy absorption at high rates due to shock deformation [6], while hybrid designs demonstrated tuneable rate sensitivity. These findings enable targeted metamaterial design for applications ranging from impact protection to lightweight structures, with geometric hybridisation emerging as a key strategy for controlling dynamic performance.

References

[1] L.J. Gibson, M.F. Ashby, Cellular solids: structure and properties, Cambridge University Press, 1999.

[2] M. Benedetti, A. du Plessis, R.O. Ritchie, M. Dallago, S.M.J. Razavi, F. Berto, Architected cellular materials: A review on their mechanical properties towards fatigue-tolerant design and fabrication, Mater. Sci. Eng. R Reports. 144 (2021) 100606. https://doi.org/10.1016/j.mser.2021.100606.

[3] O. Al-Ketan, R. Rowshan, R.K.R. Abu Al-Rub, Topology-mechanical property relationship of 3D printed strut, skeletal, and sheet based periodic metallic cellular materials, Addit. Manuf. 19 (2018) 167–183. https://doi.org/10.1016/j.addma.2017.12.006.

[4] Y. Sun, Q.M. Li, Dynamic compressive behaviour of cellular materials: A review of phenomenon, mechanism and modelling, Int. J. Impact Eng. 112 (2018) 74–115. https://doi.org/10.1016/j.ijimpeng.2017.10.006.

[5] O. Al-Ketan, R.K.R.K. Abu Al-Rub, O. Al-Ketan, R.K.K. Abu Al-Rub, MSLattice: A free software for generating uniform and graded lattices based on triply periodic minimal surfaces, 3 1–10. https://doi.org/10.1002/mdp2.205.

[6] N. Novak, S. Tanaka, K. Hokamoto, A. Mauko, Y. Emre, High strain rate mechanical behaviour of uniform and hybrid metallic TPMS cellular structures, Thin-Walled Struct. 191 (2023) 111109. https://doi.org/10.1016/j.tws.2023.111109.

11th International Congress
of Croatian Society of Mechanics
September 30 – October 3 2025
Vodice, Croatia

On the use of sparse regression for experimental joint identification in frequency-based substructuring

Domen Ocepek*, Jure Korbar*, Gregor Čepon*

*University of Ljubljana
E-mails: domen.ocepek@fs.uni-lj.si, jure.korbar@fs.uni-lj.si, gregor.cepon@fs.uni-lj.si

Keywords: frequency-based substructuring, joint parametrization, sparse regression

1 Introduction

Assembly dynamics can be estimated by combining dynamic models of the individual components through the compatibility of connecting interface displacements and the equilibrium of interface forces, known as dynamic substructuring (DS). However, connections within real structures rely on connecting elements that may not strictly satisfy these idealized constraints. This makes DS predictions inaccurate, especially in cases where resilient elements are used to connect individual substructures.

The dynamic properties of the interface connections can be identified separately in what is known as joint identification, where the connections between substructures are referred to as joints. Instead of assuming idealized rigid joints, the identified dynamic properties of the joints are used to indirectly couple the individual substructures. Joint identification strategies generally rely on measuring the assembly dynamics and isolating the joint by removing the effects of the individual substructures [1].

This study focuses on obtaining a physical-domain representation of the joint, also known as joint parametrization. To address the issues associated with measurement inaccuracies, sparsity of the joint model is promoted by applying the least absolute shrinkage and selection operator (LASSO) [2]. While the significance of some parameters in the traditional least-squares (LS) procedure may be caused by measurement errors, the aim of applying LASSO is to neglect such terms.

2 Joint parametrization

Writing the joint impedance $\mathbf{Z}^{\mathrm{J}}$ in terms of the system matrices leads to the joint parametrization:

$$\mathbf{Z}^{\mathrm{J}} = -\omega^2\mathbf{M}^{\mathrm{J}} + \mathrm{j}\omega\mathbf{C}^{\mathrm{J}} + \mathrm{j}\mathbf{D}^{\mathrm{J}} + \mathbf{K}, \tag{1}$$

where $\mathbf{M}^{\mathrm{J}}$, $\mathbf{C}^{\mathrm{J}}$, $\mathbf{D}^{\mathrm{J}}$, and $\mathbf{K}^{\mathrm{J}}$ are the mass, viscous damping, structural damping, and stiffness matrices, while ω denotes the angular frequency. Obtaining the unknown parameters in system matrices from the experimental joint data can be formulated as:

$$\mathbf{A}\boldsymbol{p} = \boldsymbol{y}, \tag{2}$$

where the definition of $\mathbf{A}$ can be found in [3], $\boldsymbol{p}$ is a single set of unknown variables (Eq. (3)), while $\boldsymbol{y}$ is a vectorized difference of the coupled admittance matrix $\mathbf{Y}^{\mathrm{AJB}}$ (Joint J connecting the substructures A and B; assembly of AJB) and the block-diagonal admittance of the substructures $\mathbf{Y}^{\mathrm{A|B}}$ (Eq. (4)):

$$\boldsymbol{p} = \begin{bmatrix} \boldsymbol{m}^{\mathrm{J}} \\ \boldsymbol{c}^{\mathrm{J}} \\ \boldsymbol{d}^{\mathrm{J}} \\ \boldsymbol{k}^{\mathrm{J}} \end{bmatrix} = \begin{bmatrix} \mathrm{vech}\left(\mathbf{M}^{\mathrm{J}}\right) \\ \mathrm{vech}\left(\mathbf{C}^{\mathrm{J}}\right) \\ \mathrm{vech}\left(\mathbf{D}^{\mathrm{J}}\right) \\ \mathrm{vech}\left(\mathbf{K}^{\mathrm{J}}\right) \end{bmatrix}, \tag{3}$$

$$\boldsymbol{y} = -\mathrm{vec}\left(\mathbf{Y}^{\mathrm{AJB}} - \mathbf{Y}^{\mathrm{A|B}}\right). \tag{4}$$

The LS solution of Eq. (2) can be prone to overfitting [1], as it can recognize some parameters as significant only to reduce the difference between the uncoupled and the coupled response models

in $\boldsymbol{y}$. Therefore, it can be beneficial to perform sparse regression to eliminate some of the terms in the system matrices, which may be present due to inaccurate measurements. This work considers LASSO as the sparse regression method of choice. Considering a system of linear equations $\mathbf{X}\boldsymbol{\beta} = \boldsymbol{y}$, the LASSO solution is found by solving Eq. (5):

$$\hat{\boldsymbol{\beta}} = \underset{\beta}{\operatorname{argmin}} \left(\|\boldsymbol{y} - \mathbf{X}\boldsymbol{\beta}\|_2^2 + \lambda \|\boldsymbol{\beta}\|_1 \right) \tag{5}$$

where $\lambda \|\boldsymbol{\beta}\|_1$ is the penalty term responsible for variable selection, with λ determining the penalty strength. Applying LASSO to the set of all variables $\boldsymbol{p}$ can, however, be problematic, as FRFs are sensitive to damping only at frequencies in the vicinity of resonance peaks. Therefore, LASSO tends to remove the majority of the damping parameters, leading to underestimated joint damping. It is therefore more beneficial to search for a sparse solution only among the mass and stiffness parameters $\boldsymbol{m}^{\mathrm{J}}$ and $\boldsymbol{k}^{\mathrm{J}}$:

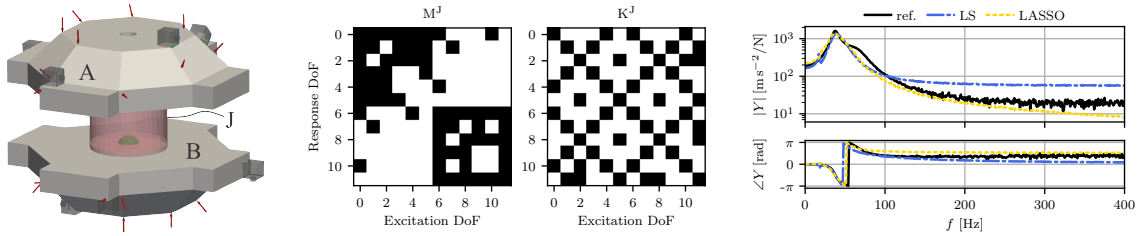
$$\hat{\boldsymbol{p}}_{\mathrm{mk}},\ \hat{\boldsymbol{p}}_{\mathrm{cd}} = \underset{\boldsymbol{p}_{\mathrm{mk}},\ \boldsymbol{p}_{\mathrm{cd}}}{\operatorname{argmin}} \left(\|\boldsymbol{y} - \mathbf{A}_{\mathrm{mk}}\boldsymbol{p}_{\mathrm{mk}} - \mathbf{A}_{\mathrm{cd}}\boldsymbol{p}_{\mathrm{cd}}\|_2^2 + \lambda \|\boldsymbol{p}_{\mathrm{mk}}\|_1 \right) \tag{6}$$

where LASSO is applied only to a subset $\boldsymbol{p}_{\mathrm{mk}}$ of all variables for what the Eq. (2) is rearranged as:

$$\begin{bmatrix} \mathbf{A}_{\mathrm{mk}} & \mathbf{A}_{\mathrm{cd}} \end{bmatrix} \begin{bmatrix} \boldsymbol{p}_{\mathrm{mk}} \\ \boldsymbol{p}_{\mathrm{cd}} \end{bmatrix} = \boldsymbol{y}, \quad \text{with} \quad \boldsymbol{p}_{\mathrm{mk}} = \begin{bmatrix} \boldsymbol{m}^{\mathrm{J}} \\ \boldsymbol{k}^{\mathrm{J}} \end{bmatrix} \quad \text{and} \quad \boldsymbol{p}_{\mathrm{cd}} = \begin{bmatrix} \boldsymbol{c}^{\mathrm{J}} \\ \boldsymbol{d}^{\mathrm{J}} \end{bmatrix}. \tag{7}$$

2.1. Numerical validation

Joint parametrization using the proposed approach is demonstrated on a numerical case study, depicted in Fig. 1a. While solution from LS approach is dense, LASSO gives us sparse mass and stiffness matrices (Fig. 1b). Reconstructing frequency response from the identified parameters for both LASSO and LS models demonstrates the difference between the two (Fig. 1c).



(a) **(b)** **(c)**

Figure 1. (a) Substructures AJB within joint identification; (b) sparsity promoting effect of LASSO on the identified mass and stiffness matrices; (c) comparison of LS and LASSO on estimated off-diagonal FRFs.

3 Conclusion

Performing joint identification in the form of model parametrization is often required for the purposes of subsequent experimental or numerical substructure assembly; therefore, obtaining a valid joint model is essential. Sparse regression promotes sparsity in the joint's system matrices and thus removes terms sensitive to measurement errors, where the LS approach may be prone to overfitting. In this work, LASSO is considered as the sparse regression method of choice. A numerical study demonstrates that sparse systems matrices are obtained from the proposed parametrization approach.

References

[1] Kreutz, M., Trainotti, F., Gimpl, V. and Rixen, D.J., On the robust experimental multi-degree-of-freedom identification of bolted joints using frequency-based substructuring. *Mechanical Systems and Signal Processing*, 203, 110626, 2023.

[2] Tibshirani, R., Regression shrinkage and selection via the lasso. *Journal of the Royal Statistical Society Series B: Statistical Methodology*, 58(1), 267-288, 1996.

[3] Korbar, J., Ocepek, D., Pogačar, M. and Čepon, G., Towards an Improved Experimental Joint Identification in Frequency-Based Substructuring. *In submission*, 2025.

11th International Congress
of Croatian Society of Mechanics
September 30 – October 3 2025
Vodice, Croatia

Numerical analysis of the influence of pipe support stiffness in pipeline systems

Domagoj Opačak*, Darko Damjanović*, Dražan Kozak*, Nenad Gubeljak+

*Name and Address of Institute
E-mails: {dopacak,ddamjanovic, dkozak}@unisb.hr

+University of Maribor, Faculty of Mechanical Engineering, Smetanova 17, SI-2000 Maribor, Slovenia
E-mail: nenad.gubeljak@um.si

Keywords: Pipe, Stiffness, Stress, Rohr2

1. Introduction

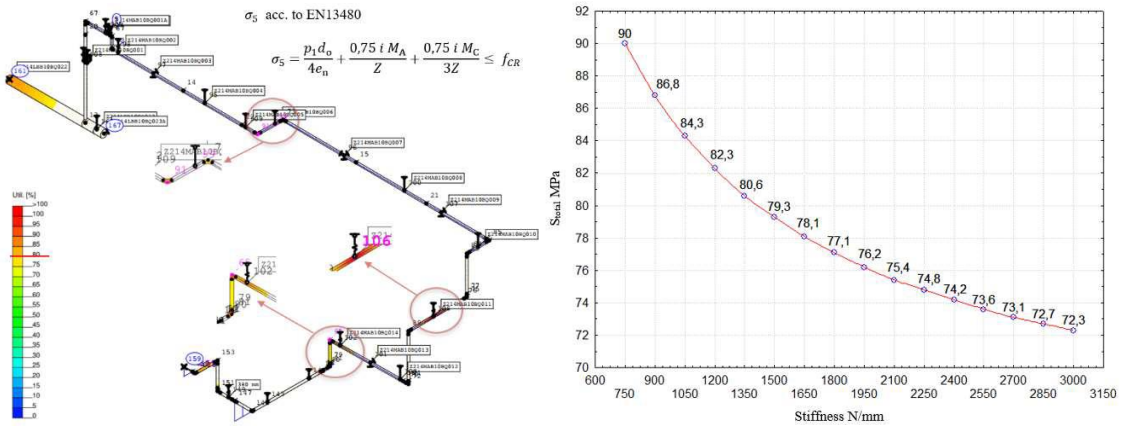
The pipeline MAB (part of LBB- hot reheat piping system) analysed by this paper will spend its life cycle inside the combined cycle thermal power plant. The LBB pipeline function is to reheat steam for turbine also used to start a medium pressure steam turbine. Additionally, this study examines how variations in support stiffness affect the output values of the pipeline stress analysis. Understanding the influence of support stiffness is crucial for ensuring structural integrity and preventing excessive loads under operational conditions. Pipe support stiffness is a critical factor in the design and analysis of piping systems, as it affects the stress distribution, deflection, and overall stability of the pipes.

2. Modelling

The structure analysis was performed within the Rohr2 software package. Material P92 acc. DIN 1.4901 is used for pipe and pipe components on LBB system where pipe OD = 168,3 mm and Wt = 8,0 mm. Work pressure p_w = 34 bar, work temperature t_w = 565 °C , calc. pressure p_c = 43,4 bar and calc. temperature t_c = 570,5 °C. On one end, the pipeline LBB is connected to the LBA piping system, while on the other end, it is connected to another pipe that is part of the equipment, with a known boundary conditions and geometry. Since more analyses have been performed with different support stiffness and different load cases only results for operation load case (self-weight and temp.) with creep will be shown. Pipe support stiffness ranging from 750 N/mm to 3000 N/mm. Figure 1(a) shows stress utilization. The stress utilization for this load case takes into account the load due to self-weight and temperature. It also considers creep as the operating temp. is 570,5 °C. From the Figure 1(a), it is $S_{total} > S_{allow}$ on node 106 for stiffness off supports 750 N/mm. The allowable stress is 80,2 MPa. Certain points of the pipeline (node 106) do not meet the stress requirements.

From Figure 1(b) it is evident that as stiffness increases, the stress values decrease. For a stiffness of 750 N/mm, the ratio Stotal/Sallow, expressed in percentages, is 112,2%. As explained the total stress exceeds the allowable limit, meaning the pipeline supported in this manner does not meet the requirements. It can be concluded from *Figure 1(b)* that by transitioning from the region of low support stiffness to the region of medium stiffness ($k \geq 3000$ N/mm), the pipeline satisfies the stress criteria according to EN13480-3.

Figure 2(a) shows variations in the support forces due to changes in the support stiffness. It is evident that there are certain significant changes in the support force with variations in the support stiffness. On some supports, the force changes within a range of 0,5 kN to over 2 kN, representing a change of more than 75%. F*igure 2(b)* show displacement values of every pipe support node in z direction with variations in the support stiffness.



Section	S1	S(M)	Sa	Sb	St	Stotal	Salow. MPa	Sutl
89-106(v)	87,7	2,3	0	2,0	0,5	90,0	80,2	112,2%
106-76(m)	87,7	2,3	0	2,0	0,5	90,0	80,2	112,2%

Figure 1. (a) Stress utilization for operation load case and (b) Variation of stress depending on the stiffness of supports (node 106)

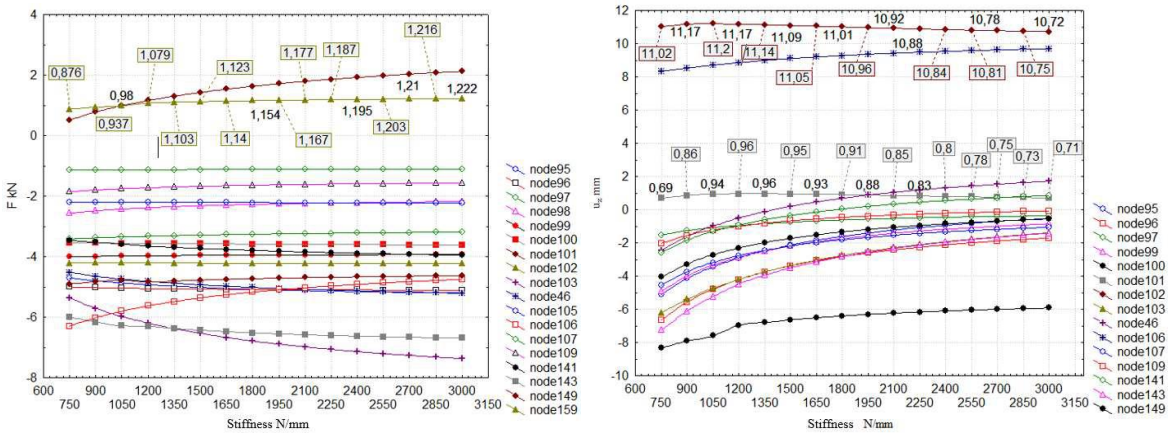


Figure 2. (a) Forces F on supports in z direction for operation load case (b) Displacement in z direction on nodes for operation load case.

3. Conclusions

Analysis of the results presented in this work shows that changes in support stiffness can lead to stresses in the pipeline that exceed allowable limits. From Figure 1(b), it is evident that as the stiffness of the supports increases, the stress on a specific segment of the pipeline (node 106) decreases. It can be concluded that stiffness of supports is crucial for determining load distribution and system flexibility. Neglecting it may result in underestimating localized stresses or inaccurately predicting displacements. Therefore, it is essential to account for the stiffness of supports in the analysis, particularly in critical applications, to ensure precision and adherence to the requirements of relevant standards.

References

[1] SIGMA Rohr 2 34.1, 2025, SIGMA Ingenieurgesellschaft mbH

[2] BS EN 13480-3:2012, Metallic industrial piping - Design and calculation, 2012, British Standards Institution

[3] VDI 3842, Vibrations in piping systems, June 2004, Engl. VDI-Gesellschaft Produkt- und Prozessgestaltung

[4] STATISTICA V8., 202, TIBCO Software Inc.

Acknowledgments and Funding: The authors would like to acknowledge the EU Research Project (NPOO.C3.2.R3-I1.04.0117) financed from The Recovery and Resilience Facility (NextGenerationEU).

11th International Congress
of Croatian Society of Mechanics
September 30 – October 3 2025
Vodice, Croatia

Bayesian approach for identifying elastic parameters and coefficients for lattice element models

Duje Pavić*, Matej Šodan*, Noemi Friedman+, Mijo Nikolić*

*University of Split, Faculty of Civil Engineering, Architecture and Geodesy, Matice hrvatske 15, 21000 Split, Croatia
E-mails: {dpavic, msodan, mnikolic}@gradst.hr

+HUN-REN Institute for Computer Science and Control (SZTAKI), Kende u.13-17, Budapest, 1111, Hungary
E-mail: n.friedman@ilab.sztaki.hu

Keywords: Lattice model, Bayesian inference, Markov Chain Monte Carlo, parameter identification, Polynomial chaos method

This paper introduces a Bayesian framework for identifying elastic parameters and coefficients in lattice models of Timoshenko beams. Timoshenko beams are used as cohesive links, and Voronoi cells represent the beam cross-sections (see Figure 1) [1-4].

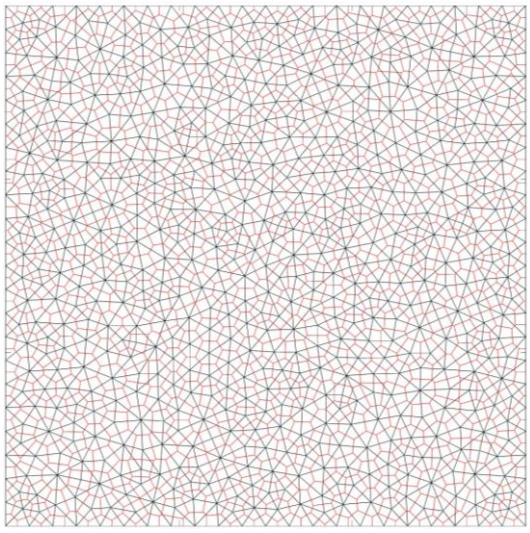


Figure 1. 2D irregular lattice domain with Voronoi tesselation

The model is based on a discrete lattice representation of the domain, the premise is that the elastic modulus and Poisson's ratio of the model differ from those of the Timoshenko beams. This discrepancy necessitates the determination of the coefficients for longitudinal (k_k), shear (k_s), and bending (k_i) stiffness of Timoshenko beams. Bayesian inference, utilizing Markov Chain Monte Carlo (MCMC) methods, is employed to estimate the posterior distributions of these stiffness coefficients, providing a robust, probabilistic approach for model calibration [5]. To enhance the computational efficiency of the MCMC procedure, a polynomial chaos expansion (PCE) model is incorporated, reducing computational costs without compromising accuracy (see Figure 2). By determining the appropriate stiffness coefficients, we aim to ensure that the lattice model exhibits the same elastic properties as the Timoshenoko beam. The proposed approach is tested on various shapes of the model domain and standard mechanical loading scenarious (tension, bending and

shear) to assess its accuracy and generalization. The ultimate goal is to determine the coefficients enabling a domain composed of 1D beams to behave like a continuum. This framework not only facilitates parameter identification but also deepens the understanding of the relationship between beam properties and macroscopic continuum behavior. The results highlight the effectiveness of combining Bayesian inference with surrogate modeling techniques to handle high-dimensional uncertainty quantification problems.

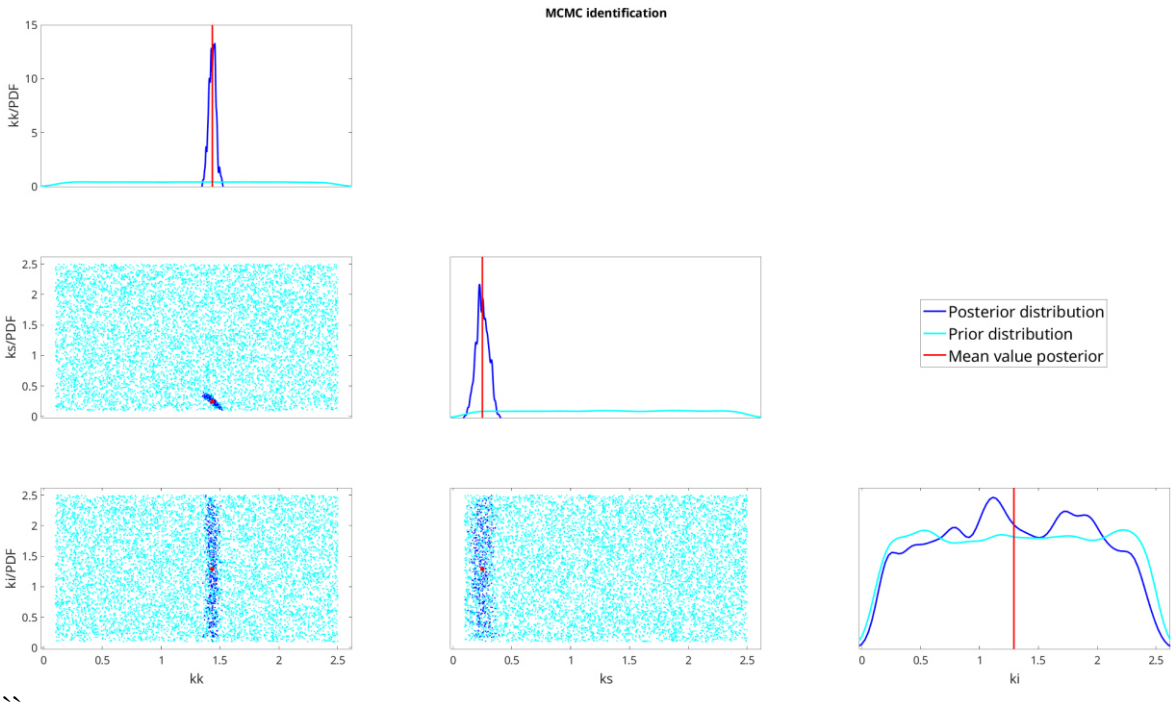


Figure 2. Posterior distributions of the stiffness coefficients

Acknowledgments

This research has been supported by the project ‘Parameter estimation framework for fracture propagation problems under extreme mechanical loads’ (HRZZ-UIP-2020-02-6693), and the project 'Young Researchers’ Career Development Project – Training New Doctoral Students' (DOK-NPOO-2023-10-8014), funded by the Croatian Science Foundation

References

[1] M. Nikolic, E. Karavelic, A. Ibrahimbegovic, P.Miscevic. Lattice element models and their peculiarities. Arch. Computat. Methods in Engrg., 25 (3): 753-784, 2018

[2] M. Nikolic, A. Ibrahimbegovic, Rock mechanics model capable of representing initial heterogeneities and full set of 3D failure mechanisms, Comput. Methods Appl. Mech. Engrg., 290: 209-227, 2015

[3] M. Nikolic, Discrete element model for the failure analysis of partially saturated porous media with propagating cracks represented with embedded strong discontinuities, Comput. Methods Appl. Mech. Engrg. 390: 114482, 2022

[4] Mijo Nikolić, Xuan Khanh Do, Adnan Ibrahimbegovic, Željana Nikolić. Crack propagation in dynamicsby embedded strong discontinuity approach: Enhanced solid versus discrete lattice model. Computer Methods in Applied Mechanics and Engineering, 2018, 340, pp.480-499. _x005F_xffff_10.1016/j.cma.2018.06.012_x005F_xffff_. hal-01996636_x005F_xffff_

[5] Matej Šodan, András Urbanics, Noémi Friedman, Andjelka Stanic, Mijo Nikolić, Comparison of Machine Learning and gPC-based proxy solutions for an efficient Bayesian identification of fracture parameters, Computer Methods in Applied Mechanics and Engineering, Volume 436, 2025, 117686, ISSN 0045-7825.

11th International Congress
of Croatian Society of Mechanics
September 30 – October 3 2025
Vodice, Croatia

Design of Helical Springs for Vibratory Sorter Mounting

Pavel Polach*, Michal Hajžman*, Luboš Smolík*

*Research and Testing Institute Plzen
Tylova 1581/46, 301 00 Plzen, Czech Republic
E-mails: {polach,hajzman,smolik}@vzuplzen.cz

Keywords: helical spring, vibratory sorter, computer simulations, optimal design

1. Introduction

The presented work falls into the field of applied research, focuses on designing optimal helical springs for mounting the vibratory sorter. It presents a computational model to estimate the maximum forces transmitted by the helical springs during both the startup and operation of the sorter. Based on the evaluation of results obtained for helical springs with varying parameters, an optimal design is proposed, considering the transmitted forces and the spatial constraints of the structure.

2. Computational model of the vibratory sorter and its validation

A computational model of the vibratory sorter was developed to realistically estimate the forces transmitted by the helical springs and to facilitate parametric analyses for qualitatively assessing spring loads based on their characteristics. Considering the nature of its motion and operating excitation frequencies, the sorter's main body was assumed to be ideally rigid. The body is supported by four helical springs directly attached to a fixed frame. In the actual setup, these springs connect to a movable damping frame, which is mounted onto the fixed frame through GERB-type damping elements. However, the damping frame and GERB elements were not included in the computational model, resulting in a more conservative estimation of transmitted forces. A well-constructed computational model enables detailed analysis of the machine's support reactions and allows for various numerical simulations to aid in designing an optimized mounting system. The preferred tool for creating this computational model is software based on multibody system analysis; specifically, the SIMPACK software was utilized. A visualization of the model is shown in Figure 1; the displayed geometry serves solely for motion visualization and does not detail the sorter's construction.

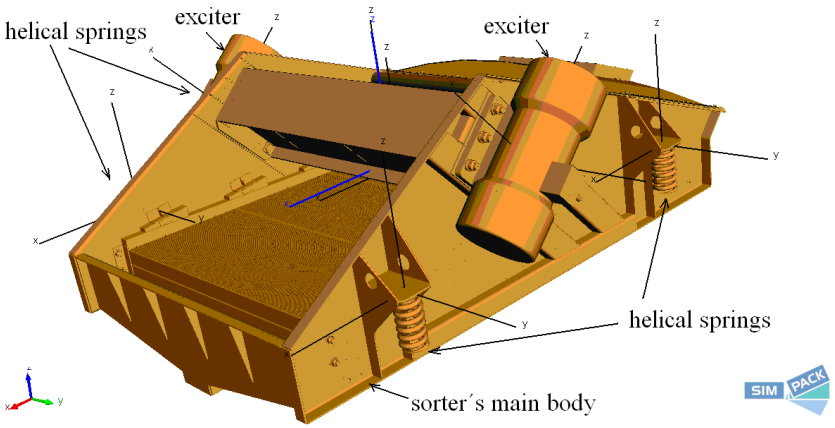


Figure 1. Visualization of the sorter model in the SIMPACK software (with defined markers)

During operation, the vibratory sorter is excited by two exciters generating directed forces due to unbalanced masses. These excitation forces were applied at specific markers corresponding to the exciters' positions.

Each computational model must be validated to ensure it accurately reflects the real-world behavior of the system under investigation. The vibratory sorter underwent extensive experimental analyses and measurements [1, 2], providing sufficient data for this validation process.

The validation involved:

1. Verifying the symmetrical motion of the sorter.
2. Comparing the natural frequencies and mode shapes obtained from the model with those estimated from experimental measurements.
3. Assessing the agreement between measured and calculated acceleration amplitudes and displacements during steady-state operation.

3. Results of numerical simulations

The validated computational model was employed to analyze the forces exerted on the helical springs under various stiffness scenarios. Simulations encompassed the startup phase, accelerating from zero to operational exciter speed, followed by a sufficiently long steady-state operation to ensure motion stabilization.

During the startup of the vibratory sorter, springs with different stiffnesses experience varying force amplitudes. Therefore, specific load effects corresponding to each spring's stiffness were defined for each set of springs. The following load conditions were examined:

- Nominal operation: Operation of the sorter at a working frequency of 980 rpm with a maximum allowable deformation amplitude of 4.4 mm.
- Startup: Acceleration of the sorter from 0 rpm to 980 rpm.
- Overload: Triple the force amplitudes experienced during nominal operation.

Four preliminary spring designs were evaluated: three springs with the same wire diameter (d19, d20, and d21), the d20 spring with a reduced number of active coils, the original d19 design, and an alternative d20 spring.

In each case, the excitation was configured to maintain a consistent technological displacement of the sorter. All calculations were performed in accordance with the UNE-EN 13906-1:2013 European standard “Cylindrical helical springs made from round wire and bar”, which specifies methods for the design and calculation of metal springs subjected to dynamic forces, including:

- Safety of springs against buckling.
- Safety of springs against resonance.
- Safety against fatigue limit state.
- Safety against yield limit.

4. Conclusions

The objective of this work was to design springs ensuring the reliable long-term operation of the vibratory sorter. To achieve this, a multibody model of the device was developed and validated, enabling the calculation of forces acting on the springs during the sorter's startup. Based on the calculations carried out, the spring design option that best met the operational requirements of the classifier was selected from the six evaluated alternatives.

Acknowledgements

This research was supported by the project CZ.02.01.01/00/23_021/0009165 “Development of digital twins of structural components with support for online monitoring of their operating loads and simulations in laboratory conditions”. The project is funded by the Johannes Amos Comenius Programme (P JAC) under the cross-sector cooperation program for ITI.

References

[1] Smolík, L., *Technological Procedure: Measurement of Operational Vibrations of the Delta 150.250.1 Sorter at Construction Site 1625, Technological Report No. VZU-TGZ-47/24/002r1*. Research and Testing Institute Plzen, Plzen 2024.

[2] Pašek, R., Smolík, L., Houdek, V., *Measurement of Operational Vibrations of the Sorter, Type Delta 150.250.1, Test Protocol No. VZU-2433P-0191-01Nr1,* Research and Testing Institute Plzen, Plzen, 2024.

11th International Congress
of Croatian Society of Mechanics
September 30 – October 3 2025
Vodice, Croatia

Thymos - A Compact, Open-Hardware Testing Frame for Small-Scale Mechanical Experiments

Matěj Porubský*, Jan Havelka*, Pavel Rychnovský*, Jan Novák*

*CTU in Prage, Faculty of Civil Engineering
E-mails: matej.porubsky@fsv.cvut.cz, jnhavelka@gmail.com, pavelrych@gmail.com, novakja@fsv.cvut.cz

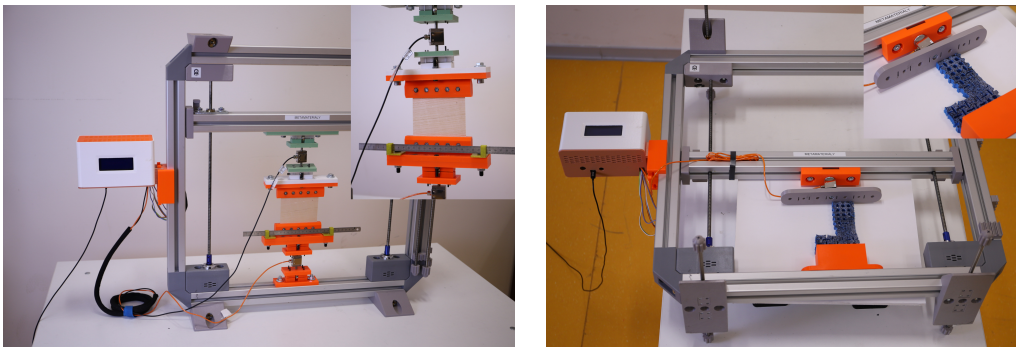
Keywords: Mechanical Testing, Open Hardware, Portability, 3D printing

1 Introduction

This contribution presents an Open Hardware-based high-precision testing frame for small-to-medium-sized samples under loads up to 500N (tested up to 1000N), with support for contactless Digital Image Correlation (DIC) observations. A key feature is its adjustable orientation, allowing use in vertical, horizontal, or arbitrary planes to control gravitational effects on the specimen. The frame has been employed for testing soft silicone (meta)materials, PCB solder joints in miniaturized electronics, and various 3D-printed prototypes. For educational use, a limited 50N load capacity ensures safe student handling without special safety measures. A commercial version is envisioned as a proof-of-concept tool for refining complex experiments in academic and R&D settings.

2 Design features

The frame is an adjustable and modular system. All parts can be tailored. The symmmetric chassis comprises off-the-shelf modular high-strength anodized extruded aluminium profile beams, with T-slot rails for universal mountings or guides. The frame design allows the specimen daylight (compression/tension space), beeing adjustable in dimensions. All plastic parts are FDM (Fused Deposition Modeling) 3D printed. The lenths of T-slot beams for main frame i.e. guide columns is customized to 596mm, top beam and base beam are both customized to 331mm. All beams are manufactured from ASKMT Profile 10 45x45L - System 45. Length of the crosshead beam is customized to 450mm and is made up of ASKMT Profile 8 30x30 - System 45. Thanks to its multi-axis symetry, Thymos may be operated also in horizontal setting, Figure 1(b).



(a) (b)

Figure 1. Thymos testing frame, a) Vertical setup, b) Horizontal setup

3 Control system

The Thymos testing frame is powered by the ESP32-S3-MINI-1U-N4R2 microcontroller, chosen for its processing capabilities and peripheral support. It features 4 MB Flash storage, 512 KB

internal SRAM, and 2 MB external PSRAM. Designed for precise measurement, motor control, and safe operation, the system supports USB connectivity, with future Wi-Fi and Bluetooth integration via the ESP32's second core. The measurement system includes up to three load cells interfaced through a 24-bit differential ADS1256 ADC, with noise reduction via a 7.66 kHz differential filter. Several I^2C sensors support monitoring and orientation recognition, including an LSM6DS3TR-C 6-axis IMU for motion tracking, an INA3221AIRGVR for load cell voltage and current monitoring, and an INA228AQDGSRQ1 for overall power consumption. Non-volatile FRAM memory (MB85RC256VPNF) stores key state variables such as calibration data, motor positions, and load cell presets. Motion control is managed by hybrid servo motors (steppers with encoders) driven by external motor drivers. Each motor connects via an RJ45 cable, transmitting power, control signals, alarm feedback, and dual endstop signals for precise positioning and safety. The system operates on a 24V to 48V power supply, requiring at least 150W for reliable performance. For connectivity, Thymos includes a 3.5mm jack for DSLR camera control, a PWM-controlled 5V fan for cooling, and a microSD card slot for local storage. An I^2C extension connector allows additional sensors or peripherals, while dual USB-C ports support PC connection and external display integration via UART. Dual RJ45 connectors handle motor control and safety feedback. Comprehensive safety features ensure reliable operation, with forceful (immediate stop) and graceful (controlled stop) mechanisms. Built-in endstops prevent over-travel, while an auxiliary endstop enables early stopping. A motor alarm state disables faulty motors, while overcurrent and over/under-voltage protection prevent electrical damage. Machine overload monitoring halts operation under excessive mechanical load, and independent load cell overload protection preserves calibration data. Additional safeguards include a USB connection check to prevent unintended motion and a watchdog system for continuous monitoring. Currently, control is USB-based, with future plans for wireless operation.

4 Software

The Thymos test frame is powered by an open-source software solution built in HTML and JavaScript, ensuring cross-platform compatibility on Windows, Linux, macOS, and mobile devices. Running directly in a web browser, it requires no installation and provides seamless updates, while also supporting offline use or local server hosting. The software enables full test frame control, firmware updates, and USB connectivity, with future plans for Bluetooth, Wi-Fi, and cloud-based remote operation, data storage, and profile sharing. The dynamic GUI allows real-time monitoring, customizable test sequences, and integrated Digital Image Correlation (DIC) for both visualization and machine control. DIC analysis, available in real-time and post-processing modes, supports contact less strain-controll based experiments, with computation options both locally and in the cloud. Fully open-source, the system fosters adaptability, innovation, and customization within the users community.

5 Conclusions

The Thymos testing frame combines modularity, portability, and adaptability. Its structure is built from high-strength anodized extruded aluminum (EN-AW 6060) with T-slot rails, allowing flexible mounting and guidance. Designed for small-scale, adjustable testing, it operates with gentle loads, making it suitable for educational use without specific safety concerns. As an open hardware and software solution, Thymos can be customized to meet specific needs, unlike most commercial alternatives. Control is managed via HTML GUI, with an option for software-as-a-service functionality, ensuring accessibility and continuous updates.

Acknowledgement

This work was co-funded by the European Union under the project ROBOPROX - Robotics and Advanced Industrial Production (reg. no. CZ.02.01.01/00/22_008/0004590).

References

[1] Jan Havelka, et al., A Ligth Portable Frame for Mechanical Testing. *Submitted to HardwareX*, 2025.

11th International Congress
of Croatian Society of Mechanics
September 30 – October 3 2025
Vodice, Croatia

On the stabilization of a low-order polytopal mixed displacement-pressure finite element formulation

Bjorn Sauren*, Sven Klinkel*

*Chair of Structural Analysis and Dynamics, RWTH Aachen University, Germany
E-mails: sauren@lbb.rwth-aachen.de , klinkel@lbb.rwth-aachen.de

Keywords: polyhedral finite elements, nonlinear analysis, inf-sup, spurious modes, SBFEM

1. Introduction

The contribution is concerned with a mixed formulation based on the scaled boundary parameterization for the analysis of nearly-incompressible, hyperelastic materials at finite strains. The element domain is parameterized in both the boundary and scaling directions and necessitates the definition of a scaling center. Interpolation functions are introduced in both directions, which allow for an application to physically and geometrically nonlinear problems. This is an extension to the original scaled boundary finite element method (SBFEM), in which an analytical solution in the scaling direction is employed. Whereas the SBFEM approach is restricted to star-convex element geometries, the present approach allows for non-star-convex polygonal element shapes, see [1]. A mixed displacement-pressure formulation is proposed to alleviate volumetric locking, which typically occurs in case of nearly-incompressible material behavior. In the 2D case the formulation leads to a polygonal element with an arbitrary number of edges, see [2]; in the 3D case a polyhedral element of lowest order is derived, see [3]. The contribution aims on the exclusion of spurious pressure modes from the solution *a priori* based on the mesh. By employing polyhedral/polygonal finite element formulations on Voronoi tessellations, we show that the discrete kernel of the linearized mixed bilinear form only consists of the hydrostatic pressure mode. A spurious pressure mode is automatically suppressed due to the vertex-to-element ratio in the finite element mesh. Several numerical examples demonstrate excellent behavior in terms of computational efficiency compared to standard quadrilateral elements and to the virtual element method (VEM). The ability of the present formulation to alleviate volumetric locking is shown and it is demonstrated that a higher accuracy can be reached on Voronoi meshes compared to quadrilateral/hexahedral discretizations.

2. Numerical example

Although the lid-driven cavity problem is classically used in fluid mechanics, we treat the same problem by solid elements. A square domain as shown in Figure 1(A) with width $b = 1$ and height $h = 1$ is fully constrained on its left, right, and bottom edges. The vertical displacements on the top edge are fixed, while displacements $u_x(x)$ are prescribed according to the function

$$\bar{u}_x(x) = 0.1\sin(\pi x).$$

The polygonal finite element with linear displacement interpolation and constant element-wise pressure is applied to two quadrilateral and Voronoi meshes and the pressures are determined. The pressure distribution in the domain is depicted in Figure 1(B) and (C). The quadrilateral mesh produces extreme checkerboarding throughout the domain, while the Voronoi discretization retains a stable pressure field in accordance with the expected distribution. By increasing Poisson's ratio from $\nu = 0.4999$ to $\nu = 0.49999$, the pressure oscillations in Figure 1(B) become even more extreme. On the contrary, the Voronoi mesh can represent the minimal change in pressure due to the increase in Poisson's ratio accurately. This becomes evident from Figure 2, in which the pressure

distribution $p(y)$ at $x = 0$ is plotted. Here, one can recognize the almost negligible change in pressure due to the increase in ν on the Voronoi discretization. The pressure determined on the quadrilateral mesh oscillates about the Voronoi solution. Overall, the small increase in Poisson's ratio increases the amplitude of the checkerboard mode on the quadrilateral mesh by a factor 10, while the pressure field obtained on the Voronoi mesh remains unaffected.

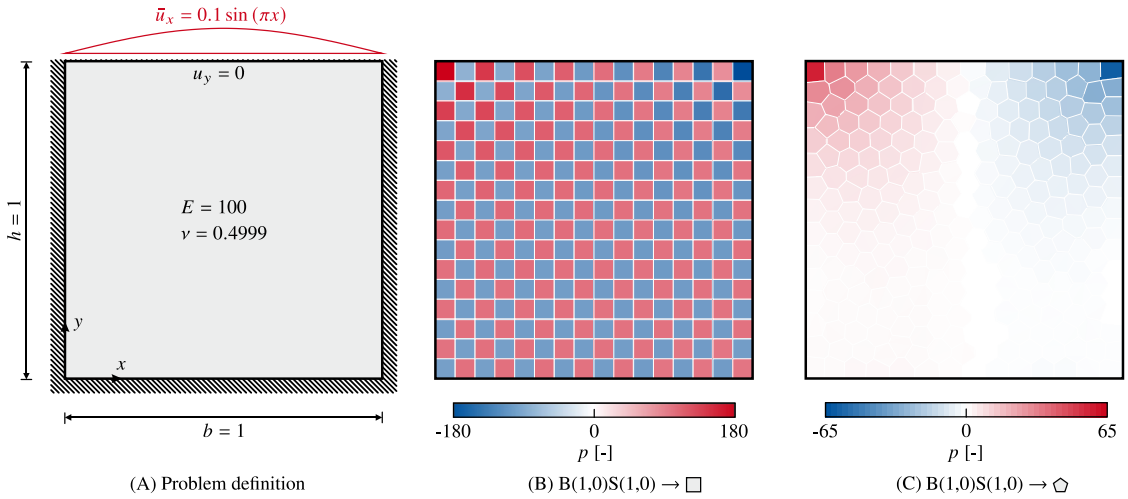


Figure 1. Lid driven cavity. Pressure plots obtained on quadrilateral and Voronoi meshes.

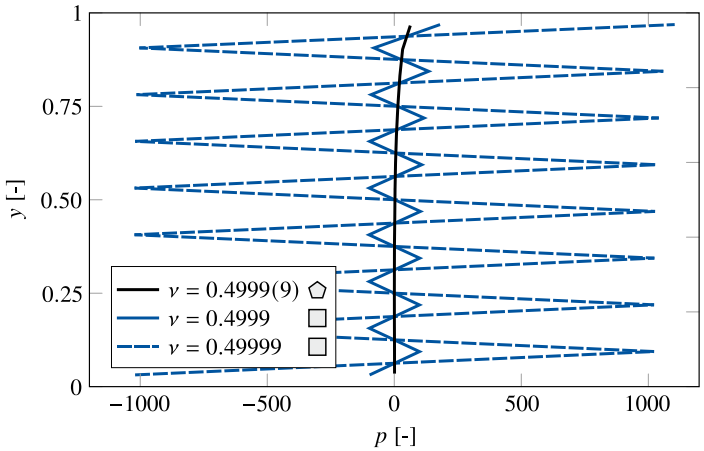


Figure 2. Pressure solution $p(y)$ at $x = 0$ for $\nu = 0.4999$ and $\nu = 0.49999$. Data points correspond to the center of the element edge. The black line represents both $\nu = 0.4999$ and $\nu = 0.49999$.

3. Conclusions

On structured quadrilateral discretizations, two pressure modes can occur. Whereas the hydrostatic pressure mode is generally suppressed, the occurrence of a spurious checkerboard mode is inevitable. By choosing a Voronoi discretization, the hydrostatic pressure mode is the only mode possible. It is shown that a checkerboard mode cannot occur.

References

[1] Sauren, B., Klarmann, S., Kobbelt, L., & Klinkel, S., A mixed polygonal finite element formulation for nearly-incompressible finite elasticity. *Comp. Meth. in Appl. Mech. and Eng.*, *403*, 115656, 2023

[2] Sauren, B., & Klinkel, S.. On the stability of mixed polygonal finite element formulations in nonlinear analysis. *International Journal for Numerical Methods in Engineering*, *125*(9), e7358, 2024

[3] Sauren, B., & Klinkel, S., Mesh topology-based spurious pressure stabilization in 3D finite elasticity using Voronoi tessellations. *Computational Mechanics*, 1-19, 2024

11th International Congress
of Croatian Society of Mechanics
September 30 – October 3 2025
Vodice, Croatia

Characterization of early-age creep behavior and strength of low carbon cement pastes and multiscale strength modeling

Sophie J. Schmid*, Alexandre Ouzia+, Markus Königsberger*, Bernhard Pichler*

*Institute for Mechanics of Materials and Structures, TU Wien, Karlsplatz 13, 1040 Vienna, Austria
E-mails: sophie.schmid@tuwien.ac.at, markus.koenigsberger@tuwien.ac.at, bernhard.pichler@tuwien.ac.at

+Heidelberg Technology Center, Heidelberg Materials, Oberklam 2-4, 69181 Leimen, Germany
E-mail: alexandre.ouzia@heidelbergmaterials.com

Keywords: limestone, calcined clay, creep, multiscale strength modeling

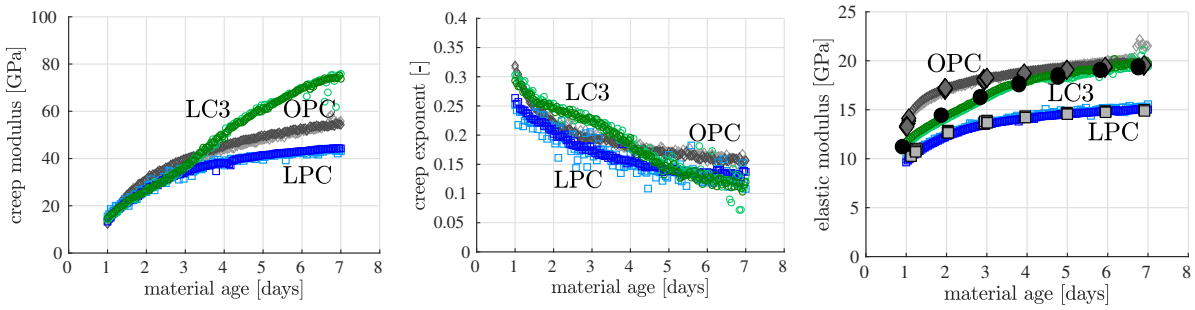
1 Introduction

Around four billion tons of ordinary Portland cement (OPC) are produced each year. OPC production is carbon-intensive. This provides the motivation to develop eco-friendly alternatives. One strategy is to partially replace OPC with supplementary cementitious materials, such as limestone and calcined clay. In this contribution we investigate the early-age creep behavior and model the strength evolution of limestone Portland cement (LPC) and limestone calcined clay cement (LC3) pastes. We show that LC3 paste creeps less than OPC paste, and that OPC hydration plays a governing role for the early-age strength development of blended cements.

2 Materials, Methods, and Results

Three types of binders are investigated: one OPC, one LPC, and one LC3 binder. For the blended binders, the cement replacement ratio amounts to 30%, and the limestone-to-calcined clay ratio is equal to 1. Cement pastes are produced at an initial water-to-solid mass ratio equal to 0.45.

A multi-technique characterization study is performed between 1 and 7 days after paste production. Isothermal calorimetry testing provides the hydration kinetics. Uniaxial compressive strength test results are used as input for hourly minute-long creep tests. The latter allow for monitoring the early-age evolution of viscoelastic properties in cementitious materials. To characterize *linear* creep behavior, the loading imposed on the specimen during three-minute creep testing is limited to 15% of the strength of the material. Each of the 870 performed creep tests is evaluated individually applying a two-step evaluation method which enables the efficient and reliable quantification of the elastic modulus, the creep modulus, and the creep exponent without constraining assumptions, see [1] and Fig. 1. Ultrasound pulse velocimetry measurements reproduce the elastic modulus quantified from creep tests, underlining the reliability of results. The multiscale mechanics interpretation of the creep test results allow for discussing microstructure-macroproperty relationships.



(a) creep modulus (b) creep exponent (c) elastic modulus

Figure 1. Evolution of viscoelastic properties of OPC, LPC, and LC3 pastes, after [1]; results of the elastic modulus are reproduced by ultrasound pulse velocimetry measurements.

A multiscale strength study investigates to which extent the OPC hydration contributes to the early-age strength evolution of LPC and LC3 pastes, respectively. For this, an OPC-validated multiscale strength model is adapted to consider limestone and calcined clay as inert material phases. The model is used to compute the strength evolutions of the LPC and LC3 pastes under the assumptions that neither limestone nor calcined clay would affect the chemistry of the OPC hydration, that the OPC hydration would follow the kinetics measured in calorimetry testing of the LPC and LC3 pastes, and that the microstructural organization of the LPC and LC3 pastes is similar to that of the OPC paste. The volume fractions are computed using Powers' hydration model. Elastic phase properties are taken from the literature. Model-computed strength values are available as a function of the hydration degree.

3 Discussion and Conclusions

For accurate quantification of the creep modulus and the creep exponent from a minutes-long creep test, it is important to account for the fact that *both* elastic and time-dependent creep strains develop during fast load application. The qualitative and quantitative differences between the OPC and the LC3 paste are led back to the pozzolanic reaction [1]. The LC3 paste creeps less than the OPC paste, already some 3.5 days after material production. This is a result of (i) space filling due to precipitation of C-A-S-H phases which creep less than C-S-H, and (ii) the precipitation of AFm phases in nanoscopic slit pores between C-S-H structures, which glues formerly viscous interfaces.

The comparison of model-computed and experimental strength values requires a link between the degree of hydration used in the model and the material age noted in the experiments. For OPC pastes, the multiplication of the hydration degree by the latent heat (here 500 J/g) allows for showing model-computed strength values as a function of the cumulative heat. Assuming limestone and calcined clay as inert material phases allows for applying the approach also to LPC and LC3 pastes, see the solid lines in Fig. 2. Isothermal calorimetry results enable the assignment of cumulative heat release values

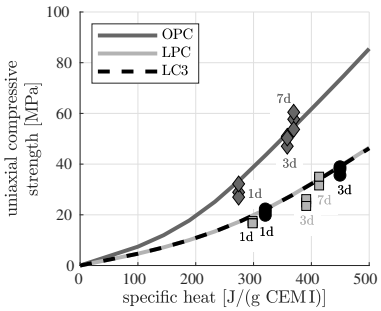


Figure 2. Model-computed (solid lines) and experimental (symbols) uniaxial compressive strength of the OPC, LPC, and LC3 pastes, as a function of the cumulative heat release per gram OPC in the binder [2].

to the material age. Then, the strength test results can be plotted over these values, see the symbols in Fig. 2. The model-predicted strength values agree well with the experimental strength values. The extended multiscale strength model provides a good estimate of early-age strength development also for binary and ternary blended cement pastes, at least for the here investigated materials. This indicates that the OPC hydration plays a governing role for the early-age strength development of limestone- and calcined clay-blended cement pastes. One of the next steps is to incorporate the pozzolanic reaction into the modeling of LC3 pastes.

References

[1] Schmid, S.J., Zelaya, L., Lahayne, O., Peyerl, M., and Pichler, B., Hourly three-minute creep testing of an LC3 paste at early ages: Advanced test evaluation and the effects of the pozzolanic reaction on shrinkage, elastic stiffness, and creep. *Cement and Concrete Research*, 187, 107705, 2025.

[2] Schmid, S.J., Königsberger, M., and Pichler, B., Early-age strength developments of cement pastes made of CEM I, limestone, and calcined clay: The governing role of OPC hydration. In: B.L.A. Pichler, Ch. Hellmich, P. Preinstorfer (Eds.), 12th *International Conference on Fracture Mechanics of Concrete and Concrete Structures*, Vienna, 2025.

Acknowledgments

Financial support through the MatCHMaker project which has received funding from the European Union's Horizon Europe research and innovation programme under grant agreement N° 101091687 is gratefully acknowledged.

11th International Congress
of Croatian Society of Mechanics
September 30 – October 3 2025
Vodice, Croatia

Integration scheme with modal analysis and modal superposition for non-linear problems

Damir Sedlar*, Zeljan Lozina*, Ivan Tomac*

*University of Split, Faculty of Electrical Engineering, Mechanical Engineering and Naval Architecture, Rudjera Boskovica 32, 21000 Split, Croatia
E-mails: {dsedlar, lozina, itomac}@fesb.hr

Keywords: modal superposition, modal analysis, non-linear dynamics, time integration,

1. Introduction

When analyzing dynamic systems and designing different structures, it is often necessary to consider various non-linearities in addition to the linear response, [1] and [2]. In contrast to linear analysis, which is well researched and much simpler for dynamic analysis, the analysis of nonlinear dynamic systems is much more complex and depends on several factors, especially the type of nonlinearity. The choice of an efficient and accurate method of nonlinear dynamic analysis is therefore crucial, and these two conditions, efficient and accurate, are usually on opposite sides and the fulfilment of one condition worsens the other condition. Existing methods for dynamic analysis and integration such as the Newmark method, [3], are used for linear and nonlinear problems. However, it is not possible to apply these methods to all types of nonlinearity, nor to all requirements that are made today. Normally, the integration time step is one tenth of the period of the highest natural frequency of interest. Depending on the nature of the problem or the non-linearity, it is sometimes necessary to adaptively change the integration time step.

The introduction of modal analysis and the use of modal superposition considerably simplifies time integration and the need for computing resources. For non-linear dynamic systems, especially for systems with non-classical damping, methods with state space are typically used. The application of methods from the state-space spectrum can successfully solve nonlinear dynamic problems, but the simplicity and physical interpretation of classical modal analysis and other parameters is lost in their application. This paper will present a method for solving a dynamic system with non-classical damping using modal analysis and modal superposition, without losing the physical interpretation of the problem itself. Some of the methods that use a similar concept can be found in [4] and [5].

2. Theoretical background of the method

A typical governing equation for a dynamic system with multiple degrees of freedom including damping is as follows:

$$\mathbf{M}\ddot{\mathbf{q}} + \mathbf{D}\dot{\mathbf{q}} + \mathbf{K}\mathbf{q} = \mathbf{F} \tag{1}$$

where:
M - n x n mass matrix,
D - n x n damping matrix,
K - n x n stiffness matrix,
F - n x 1 force vector,
q - n x 1 displacement vector,
where n is the number of degrees of freedom of the dynamic system. A simple dynamic system of this type is shown in Figure 1.

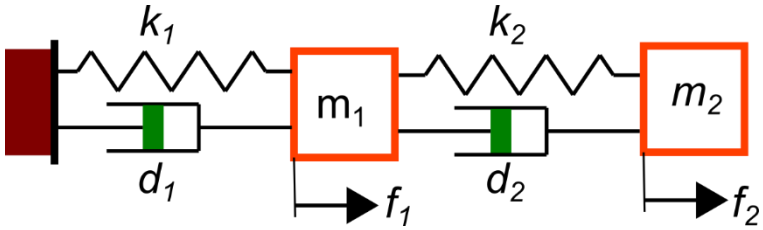


Figure 1. The dynamic system in the analysis.

If the damping is non- classical, it can be divided into two parts. One is the linear part of the damping $\mathbf{D}_L$, the other is the non-linear part $\mathbf{D}_{NL}$. The governing equation (1) can now be expressed as follows:

$$\mathbf{M}\ddot{\mathbf{q}} + \mathbf{D}_L\dot{\mathbf{q}} + \mathbf{K}\mathbf{q} = \mathbf{F} - \mathbf{D}_{NL}\dot{\mathbf{q}} \tag{2}$$

Once the mode shapes of the undamped system $\boldsymbol{\phi}$ and the natural frequency $\boldsymbol{\Lambda}$ have been found, it is now possible to represent equation (2) as a system of uncoupled differential equations:

$$\ddot{\mathbf{s}} + \boldsymbol{\phi}^{\mathrm{T}}\mathbf{D}_L\boldsymbol{\phi}\dot{\mathbf{s}} + \boldsymbol{\Lambda}\mathbf{s} = \boldsymbol{\phi}^{\mathrm{T}}\mathbf{F} - \boldsymbol{\phi}^{\mathrm{T}}\mathbf{D}_{NL}\dot{\mathbf{s}} \tag{3}$$

where the symbol $\mathbf{s}$ denotes the vector of modal coordinates. In this case, a diagonal matrix is obtained by multiplying $\boldsymbol{\phi}^{\mathrm{T}}\mathbf{D}_L\boldsymbol{\phi}$. The resulting system in equation (3) is decoupled on the left-hand side. This allows a simple solution of the system. In such analyses, the right-hand side of equation (3) is considered known. However, since a velocity component occurs on this side, it is necessary to insert an additional loop in the solution algorithm that resolves the nonlinearity until convergence is achieved. It has been shown that convergence is achieved very quickly in this additional loop, which does not significantly increase the computational requirements, and that only the modes that are needed can be included in the solution of the system. This approach can be useful in some special calculation cases where an analysis for individual modes is required or perhaps the motion of a rigid body is to be excluded from the calculation.

3. Conclusions

This article presents one of the possibilities to solve the numerical time integration of systems with non-classical damping without losing the physical meaning of all terms of the equation of motion. This method shows its potential especially in cases where it is necessary to use modal analysis and modal superposition to obtain the final solution.

References

[1] Zhao, M., Li, H., Cao, S. and Du, X., An explicit time integration algorithm for linear and non-linear finite element analyses of dynamic and wave problems, *Engineering Computations*, 36(1),161-177, 2019.

[2] Wang, M-F., Wang, Z-H., Time-domain integration methods of exponentially damped linear systems. International Journal for Numerical Methods in Engineering, 114, 347–374, 2018.

[3] Newmark, N.M., A Method of Computation for Structural Dynamics, *Journal of the Engineering Mechanics Division*, 85(3), 67-94, 1959.

[4] Paneer, M., Bašić, J., Sedlar, D., Lozina, Ž., Degiuli, N., Peng, C. Fluid Structure Interaction Using Modal Superposition and Lagrangian CFD. *Journal of Marine Science and Engineering*, 12(2), 318, 2024.

[5] Wang, M., Zhou, X., On precise time integration method for non-classically damped MDOF systems. *Earthquake Engineering and Engineering Vibration*, 5, 79–85, 2006.

11th International Congress
of Croatian Society of Mechanics
September 30 – October 3 2025
Vodice, Croatia

A Hybrid Computational Framework for Phase-Field Brittle Fracture Modelling

Ana Marija Šegon, Tomislav Lesičar

Faculty of Mechanical Engineering and Naval Architecture, I. Lučića 5, 10000 Zagreb
E-mails: {ana.marija.segon,tomislav.lesicar}@fsb.unizg.hr

Keywords: machine learning, neural networks, heterogeneous materials, brittle fracture, phase field

1. Introduction

The constitutive behaviour of materials has traditionally been described using analytical models based on costly experiments. While effective for classical engineering, these models fall short for advanced, heterogeneous materials that require more accurate descriptions. As most materials show heterogeneity at various scales, recent research has shifted towards numerical modelling to better capture the complex effects of microstructural interactions.

2. Neural networks

One of the primary advantages of neural network-based material models lies in their ability to capture complex mechanical behaviour without relying on classical constitutive laws or *a priori* assumptions regarding the material model or microstructural effects. This characteristic is particularly beneficial when dealing with novel or highly complex materials for which no analytical constitutive models currently exist. The accurate prediction of material behaviour using neural networks depends solely on the availability of a large dataset, typically generated through numerical simulations. Furthermore, once developed, these models can be refined and enhanced with additional simulation data or experimental observations.

Neural networks are composed of interconnected processing units or neurons, organized into layers. The input layer receives raw data, the output layer produces the final predictions, while the intermediate hidden layers facilitate nonlinear transformations of the input. One of the most widely used architectures is the feedforward neural network (FNN), in which neurons are fully connected and information flows unidirectionally from the input to the output layer. An illustrative representation of this architecture is provided in Figure 1.

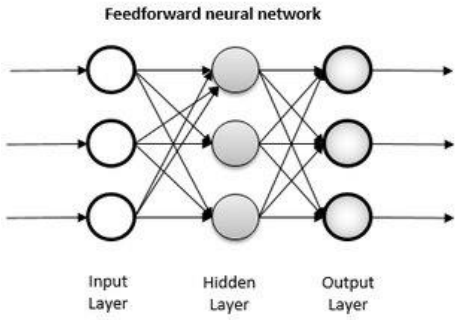


Figure 1. Schematic representation of feedforward neural network architecture [1]

In the given architecture, connections between neurons are characterized by adjustable weights and biases. Training is typically performed using the backpropagation algorithm in conjunction with optimization techniques such as stochastic gradient descent. The objective of the training process is to iteratively adjust the weights to minimize the error between the predicted and known output values

[2]. In this study, a database was constructed to enable a neural network to learn the behaviour of the yield surface. The model consists of two separate networks, one for learning the shape of the yield surface, and the other for learning the gradient of the yield surface, which arises during plastic flow. This approach allows more accurate modelling of complex material behaviour through the decoupled learning of the yield function and its gradient [3]. The input data consist of stress values expressed in cylindrical coordinates, where p is the hydrostatic pressure, ρ is the Lode radius, and θ is the Lode angle. In this manner, the yield surface is interpreted as a geometric object in Euclidean space. To generate stress points which do not lie on the yield surface, the Level Set method is employed [4]. The points are distributed so that they are located both inside the yield surface, within the elastic regime, and outside the yield surface, representing inadmissible stress states. If the material is in the elastic region, the yield function takes negative values, whereas if plastic yielding has occurred, the function must be equal to zero.

3. Phase field method

The phase-field method has recently gained significant attention in fracture modelling due to its capability to capture both crack initiation and propagation without the need for additional empirical criteria. In this approach, the crack geometry is represented by a continuous scalar field by introducing an additional scalar variable ϕ, which takes the value 1 in regions corresponding to a fully developed crack and 0 in undamaged material. In the context of solid mechanics, phase-field models originate from Griffith's fracture theory, which minimizes the internal energy functional Ψ:

$$\Psi = \Psi^b + \Psi^s = \int_{\Omega/\Gamma} \Psi_e(\varepsilon) d\Omega + \int_{\Gamma} G_c d\Gamma, \tag{1}$$

where Ψ^b denotes the elastic deformation energy, while Ψ^s represents the dissipated fracture surface energy, ε is the small strain tensor, and G_c represents the material's fracture toughness [5]. This modelling strategy has become widely adopted for both brittle and ductile fracture scenarios.

4. Integrating neural networks into brittle fracture models

In this work, a neural network-based material model is coupled with a phase-field algorithm to simulate brittle damage. The neural network learns the material behaviour, including the shape and gradient of the yield surface, from a generated dataset using open-source libraries (e.g. PyTorch) in Python. This data-driven model is then integrated into a phase-field framework to capture brittle fracture processes, such as crack initiation and propagation, through the implementation of UMAT and UEL subroutines within the software package ABAQUS. The proposed approach is validated by comparing its results to a reference simulation governed by classical constitutive model embedded into the phase-field algorithm. This comparison aims to assess the performance and accuracy of the neural network-enhanced model relative to the conventional analytical approach within the context of brittle damage modelling. Although the focus of this study is on brittle fracture, this represents only the first stage of the research. Future work will extend the methodology to ductile materials and fracture, leveraging the neural network's capacity to model elastoplastic behaviour already established in this study.

References

[1] Pekel, E., Kara, S., A comprehensive review for artificial neural network application to public transportation, *Sigma J Eng & Nat Sci*, 35, 157-179, 2017.

[2] Hagan, M. T., Demuth, H. B., Beale, M. H., De Jesus, O., *Neural network design 2nd edition*, 2014.

[3] Suh, H.S., Kweon, C., Lester, B., Kramer, S., Sun, W., A publicly available PyTorch-ABAQUS UMAT deep-learning framework for level-set plasticity, *Mechanics of Materials*, vol 184, 2023.

[4] Vlassis, N.N., Sun W.C., Sobolev training of thermodynamic-informed neural networks for interpretable elasto-plasticity models with level set hardening, *Comput Methods Appl Mech Eng*., vol 377, 2021.

[5] Francfort, G.A., Marigo, J.J., Revisiting brittle fracture as an energy minimization problem. *J Mech Phys Solids*, vol 46., pp. 1319-42, 1998.

11th International Congress
of Croatian Society of Mechanics
September 30 – October 3 2025
Vodice, Croatia

Simulation of Adhesive Debonding in Fracture-Mechanics Tests Using a Novel Hybrid Analytical-Numerical Model

Leo Škec*, Damjan Jurković*, Giulio Alfano+

*Univeristy of Rijeka, Faculty of Civil Engineering, Radmile Matejčić 3, 51000 Rijeka, Croatia
E-mails: leo.skec@gradri.uniri.hr, damjan.jurkovic@gradri.uniri.hr

+Department of Mechanical and Aerospace Engineering, Brunel University London, Kingston Lane, Uxbridge UB8 3PH, UK
E-mail: giulio.alfano@brunel.ac.uk

Keywords: adhesive joints, debonding, delamination, cohesive-zone model, analytical solution

1 Introduction

Adhesively bonded joints are widely used in automotive, aerospace and civil engineering due to their structural and manufacturing advantages. However, their design must account for potential failure by debonding, a critical mode in which the adhesive bond between components is lost. To characterise this behaviour, standard fracture mechanics tests are performed to extract material parameters for design and verification. With the growing reliance on bonded structures in demanding applications, there is a strong need for numerical models that can simulate debonding both accurately and efficiently. Such models support experimental interpretation, design optimisation and virtual testing. In particular, efficient modelling of the fracture process zone and crack growth is essential for reducing computational cost while maintaining predictive capability.

2 Hybrid analytical-numerical model

In this work, we propose a novel hybrid analytical–numerical model for the simulation of adhesive debonding in standard fracture mechanics tests, such as the Double Cantilever Beam (DCB), End-Notch Flexure (ENF) and Mixed-Mode Bending (MMB) configurations. The DCB test (Figure 1(a)) is designed to evaluate Mode I (opening mode) fracture resistance by applying symmetrical tensile loads at the ends of two bonded beams (arms), causing the crack to propagate in pure opening. The ENF test (Figure 1(b)) targets Mode II (sliding mode) failure by applying a three-point bending load to a specimen with a pre-crack located at the interface between the two bonded beams. The MMB test (Figure 1(c)) combines the DCB and ENF setups to produce a controlled mix of Mode I and Mode II loading by applying loads through a lever arm system, allowing investigation of mixed-mode fracture behaviour. In these tests, the region ahead of the crack tip is referred to as the damage process zone (DPZ), where the adhesive undergoes material softening prior to complete failure. The remainder of the specimen (including the fully separated arms and the bonded region that remains undamaged) exhibits linear-elastic behaviour.

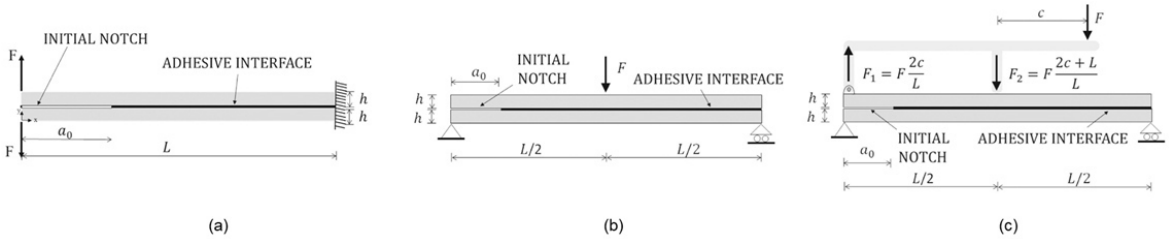


Figure 1. Standard fracture mechanics tests: (a) DCB, (b) ENF and (c) MMB.

The concept behind the hybrid model is to combine exact analytical solutions [1, 2], applied to the fully separated and undamaged parts of the specimen, with finite element (FE) solutions in the damage process zone (DPZ) [3]. This approach enables a substantial reduction in the total number of degrees of freedom compared to conventional fully-meshed FE models, resulting in significantly lower computational cost. The method is applicable not only to bilinear and trilinear (or trapezoidal) traction–separation laws (TSLs), but also to nonlinear TSLs, such as exponential or power-law formulations, for which closed-form analytical solutions are not available. For each displacement or time increment, a stack of finite elements is placed in the DPZ and moves with it as the crack propagates, while the remainder of the specimen (whether it consists of an intact interface, a fully debonded interface or an initial crack) is represented analytically.

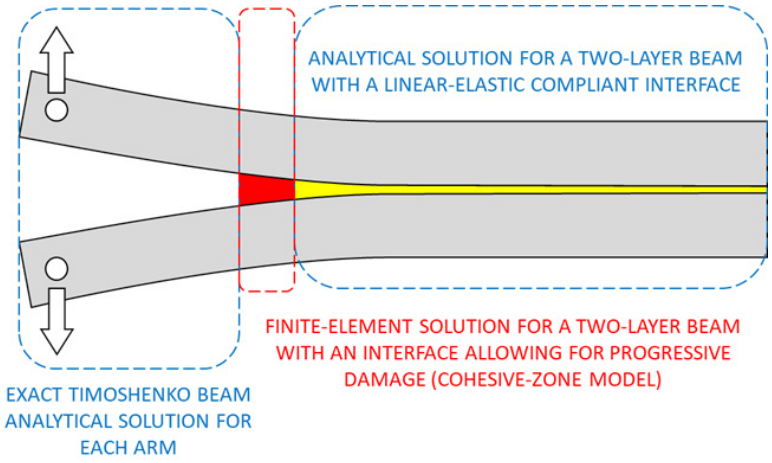


Figure 2. The concept of the hybrid analytical-numerical model.

This hybrid framework is particularly well suited for efficiently simulating the rate-dependent debonding of adhesive joints. In the rate-dependent cohesive zone model (CZM) [4], the adhesive response in compression (which governs most of the undamaged region) is considered rate-independent and can therefore be captured using analytical solutions. Consequently, the FE formulation developed in [4] can be restricted to the narrow zone ahead of the crack tip. The rate-dependent CZM is based on fractional viscoelasticity, which provides a compact yet accurate framework for modelling the rate sensitivity of polymers and elastomers across a broad range of strain rates, using far fewer parameters than classical models based on exponential kernels.

3 Conclusion

The proposed hybrid analytical–numerical model offers an efficient and accurate framework for simulating adhesive debonding in standard fracture mechanics tests. By coupling closed-form analytical solutions in the linear-elastic regions with finite element analysis confined to the damage process zone, the model significantly reduces computational cost while retaining fidelity in the prediction of crack propagation. The approach holds strong potential for integration into design and analysis tools aimed at characterising and optimising the performance of adhesively bonded structures.

References

[1] Siciliano, A.F., Škec, L., Jelenić, G., Closed-form solutions for modelling the rotational stiffness of continuous and discontinuous compliant interfaces in two-layer Timoshenko beams, *Acta Mechanica*, 232, 2793–2824, 2021.

[2] Siciliano, A.F., Škec, L., Jelenić, G., Closed-form solutions for two-layer Timoshenko beams with interlayer slip, uplift and rotation compliance, *Meccanica*, 58, 893–918, 2023.

[3] Ranjbar, M., Škec, L., Jelenić, G., Ribarić, D., Mixed-mode delamination of layered structures modeled as Timoshenko beams with linked interpolation, *International Journal for Numerical Methods in Engineering*, 124(8), 1773–1797, 2023.

[4] Škec, L., Alfano, G., Experimental and numerical study of rate-dependent mode-I failure of a structural adhesive, *The Journal of Adhesion*, 99(8), 1323–1355, 2022.

11th International Congress
of Croatian Society of Mechanics
September 30 – October 3 2025
Vodice, Croatia

Numerical Simulations of Hydraulic Transients in HPP Zakučac

Jerko Škifić*, Zoran Čarija*

*Tehnički fakultet, Sveučilište u Rijeci, Vukovarska 58, 51000 rijeka
E-mails: jerko.skific@uniri.hr, zoran.carija@riteh.uniri.hr

Keywords: hydraulic transients, numerical simulations, hydraulic power plant, hyperbolic PDE

1 Introduction

Hydraulic transients refer to sudden pressure changes caused by variations in fluid velocity. These rapid changes can lead to significant damage to the conveyance systems of high-pressure hydropower facilities. To mitigate the adverse effects of hydraulic transients on hydraulic system components, this phenomenon has been the focus of extensive research efforts.

During numerical simulations of hydraulic transients, energy losses due to friction are typically approximated using formulations derived for steady or quasi-steady flow conditions. However, such simplifications fail to adequately capture the dissipation and oscillatory behavior of water hammer phenomena.

This study employs an unsteady friction model based on an extended version of Brunone's formulation, expressed in a conservative form with nonconservative product. The resulting numerical model is solved using a second-order flux-limited numerical method. This approach offers a balance of computational speed, accuracy, and stability across a wide range of spatial and temporal resolutions.

The stability of numerical simulations largely depends on the correct implementation of boundary conditions, particularly those involving the surge tank.

The developed model is validated by comparing numerical results with measured data from the observed system.

2 Description of HPP Zakučac

HPP Zakucac is the most important part of a multipurpose system for utilization of the Cetina river watershed. Two intake structures are located at the Prančevići reservoir, providing daily discharge regulation of the Cetina river, one for each pressure tunnels. Both concrete tunnels with diameters of 6,1 and 6,5 m respectively, a length of about 9.650 m lead to two surge chambers, one for each tunnel, which share a common overspill basin Gata. Furthermore, both pressure tunnels are connected to one shared surge tank approximately 230 m downstream of the first surge tank and approximately 50 m upstream of the valve chamber. Pressure tunnels are connected to two penstocks each, which are equipped with butterfly valves of 3,5 m and 3,75 m in diameter at the first and second stage penstocks, respectively. Four penstocks are 289 m long vertical concrete lined steel pipes. Spherical valves of 2,4 m and 2,6 m are installed in front of four vertical Francis turbines with synchronous generators generating units.

3 Mathematical and numerical model

Pressure tunnels are modelled by using the unsteady one dimensional Allievi model written as hyperbolic PDEs taking into an account head losses cause by steady and unsteady friction. The numerical model is solved using a second-order flux-limited finite volume scheme.

Considering boundary conditions, the Prančevići reservoir with the intake structure is modelled as a simple reservoir boundary condition, one for each pressure line. Surge tanks connected to the Gata basin are modelled as orifice surge tanks with custom spillway expressions tailored to model the inflow and outflow from the abovementioned Gata basin. A shared surge tank is modelled as an orifice tank. In the numerical model, the four turbines are represented with the Dirichlet boundary conditions of known discharge values.

4 Numerical results

The developed numerical model is tested against the three conducted measurements:

- Operation with units A and B only through the right inlet tunnel
- Operation with units C and D only through the left inlet tunnel
- Operation with all four units through both inlet tunnels

The separation of the tunnels during the first two tests was not fully implemented, as the gates at the intake structures and the gates at the junction between the Gata basin and the first surge tanks remained open, as indicated by the recorded water levels at the intake structures. This partial isolation introduced additional complexity to the numerical analyses, making accurate modeling and interpretation of the hydraulic behavior more challenging. The results of the numerical simulations show very good agreement with the measured values. The oscillations of the piezometric head are successfully reconstructed, both in amplitude and frequency, as seen in Figure 1.

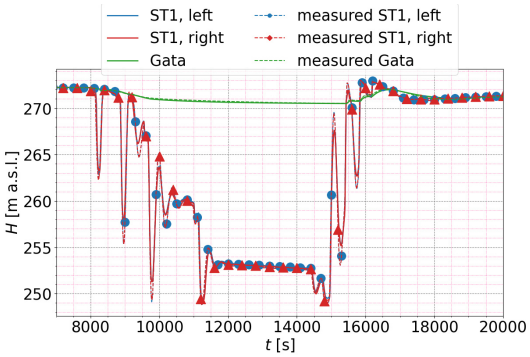


Figure 1. Comparison of numerical results and measurements for the measurements with all four units through both inlet tunnels

5 Conclusion

The conducted numerical analysis of the HPP Zakučac demonstrates a high level of accuracy in simulating the unsteady flow conditions across various operational scenarios. Despite partial tunnel separation during the first two tests—introducing additional complexity to the flow dynamics,the model successfully captured key hydraulic responses, both in amplitude and frequency of the piezometric head. The developed mathematical and numerical model, along with detailed boundary condition modeling, proved effective in replicating real system behavior. These results confirm the robustness and reliability of the developed model for future operational analysis and optimization of the HPP Zakučac.

References

[1] Bergant, A., Simpson, A., Vitkovsky, J. A. R.: *Developments in unsteady pipe flow friction modelling*, J. Hydraul. Res., 39, 3, 249–258. 2001.

[2] Brunone, B., Ferrante, M., Cacciamani, M: *Decay of pressure and energy dissipation in laminar transient flow*, J. Fluids Eng., 126, 928-934. 2004.

[3] Bouazza, Z., Brunelle, P. E.: *A new friction model for transient pipe flows development of the frequency dependence approach of Brunone*, Proc., 9th Int. Conf. on Pressure Surges, BHR, Chester, U.K., 391-404. 2004.

[4] Škifić, J., Maćešić, S., Črnjarić-Žic, N.: *Nonconservative Formulation of Unsteady Pipe Flow*, Journal of Hydraulic Engineering - ASCE, 136, 8, 483-492. 2010.

[5] Wan, W.,Zhang, B., Chen, X., Lian, J.: *Water Hammer Control Analysis of an Intelligent Surge Tank with Spring Self-Adaptive Auxiliary Control System*, Energies, 12, 2527, 2019.

[6] Ling Zhou, L., Li, Y., Karney,B., Cheng, Y., Liu, D., *Godunov-Type Solutions for Transient Pipe Flow Implicitly Incorporating Brunone Unsteady Friction*, Journal of Hydraulic Engineering 147(7), 2021.

11th International Congress
of Croatian Society of Mechanics
September 30 – October 3 2025
Vodice, Croatia

Numerical strategies for finding roots of transcendental characteristic equations

Ante Skoblar*, Goranka Štimac Rončević*, Roberto Žigulić*, Marko Čanađija*

* *University of Rijeka Faculty of Engineering*
E-mails: ante.skoblar@riteh.uniri.hr, goranka.stimac@riteh.uniri.hr, roberto.zigulic@riteh.uniri.hr, marko.canadija@riteh.uniri.hr

Keywords: natural frequency, roots of transcendental characteristic equation, matrix singular values

1. Introduction

The calculation of natural frequencies and mode shapes is a fundamental step in the analysis of free vibrations. By applying the boundary conditions to the equations of motion of the given vibration system, a system of equations is obtained whose nontrivial solutions correspond to the roots of the determinant of the characteristic equation of the matrix. Often, this equation does not have an analytical solution, so numerical methods are used to find the roots.

2. Typing area

This paper presents an example of axial vibrations of a rod (see Figure 1), which is connected at both ends to the ground with two linear axial springs of equal stiffness. The example is chosen because the characteristic matrix is of size 2x2, allowing the eigenvectors to be visualized as vectors in a plane, and it is asymmetric, as its eigenvalues can be complex numbers.

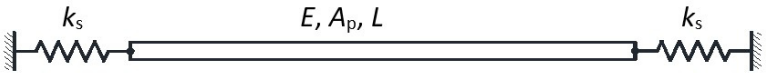


Figure 1. Model of axial vibrations of a rod supported by two linear axial springs of equal stiffness

The general form of mode shapes, defined after separation from the general solution of the differential equation of motion, is given as follows [1]:

$$U(x) = A\cos(kx) + B\sin(kx), \tag{1}$$

where k is the wave number, and A and B are constants. The unknown constants are determined by applying the boundary conditions to the general solution of the equation of motion. The result of this approach is a system of equations that can be defined as the product of the characteristic matrix and the vector of constants

$$f(x) = ax + b, \tag{1}$$

where ks is the stiffness of the axial spring, E is the modulus of elasticity of the beam, A_p is the crosssectional area of the beam, and L is the length of the beam. From the expression of the characteristic matrix, it is evident that the matrix elements are transcendental functions, and therefore its determinant is also a transcendental function. At the natural frequencies of the system, the determinant of the characteristic matrix is equal to zero. Since the characteristic functions are often complex expressions without analytical solutions, finding its roots requires numerical solving. To define the discretization of the wave number domain, the roots of the element functions are determined first, as these may correspond to the roots of the characteristic equation. Then, the

characteristic matrix elements functions that may cause discontinuities (such as cot(k), tan(k), 1/sin(k), 1/β, etc.) were checked, as they cause the discontinuities of the determinant function. Such points should not be searched, as they certainly do not represent roots of the determinant and will cause the code to break. Between these points, the determinant function is continuous, since the functions of the matrix elements are also continuous, and it is possible to begin the search for its roots. However, a root of the determinant function coincides with a root of at least one eigenvalue and at least one singular value of the characteristic matrix. Since the computation of singular values is generally faster than that of eigenvalues and the determinant, especially for large and asymmetric matrices, it is recommended to use singular value functions to identify the roots. Moreover, the eigenvalues of an asymmetric matrix are often complex numbers, while the singular values are always positive real numbers, which makes the numerical computation more stable. The choice of discretization density in the wave number domain is based on the known roots of the matrix element functions. It is recommended to calculate an approximate greatest common divisor of all known roots of the matrix element functions (in the example, it was calculated with a precision of 0.001). This value is then linearly divided into six parts (recommended), assuming that all zeros of the matrix element functions are also zeros of the determinant. This level of discretization is sufficient for visualizing the peaks of the function of the lowest singular values of the matrix (see Figure 2).

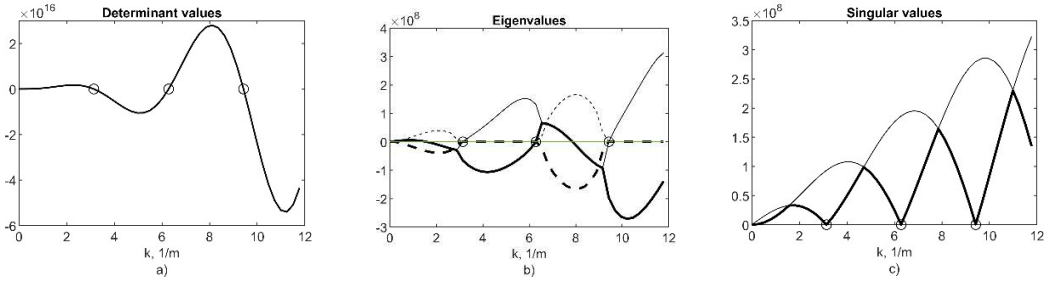


Figure 2. Function of a) determinant values, b) eigenvalues, and c) singular values, along with the wave number values "O" at which the determinant equals zero

In this example, the zeros of the matrix element functions coincide with the zeros of the transcendental characteristic equation and are thus confirmed using the described discretization. However, the values of the natural frequencies can be validated because analytical solutions are known for this case. If it is uncertain whether all roots have been identified, the analysis should be continued using an adaptive approach [2] on the singular value curve or the condition number curve, where variations are even more pronounced. After completing the root-finding procedure, it is necessary to verify that each identified root of the determinant corresponds to a root eigenvalue and the appropriate direction of the eigenvector, thereby confirming that they represent the system's natural frequencies. In the case of geometrically simple systems (rod, beam, plate), verification that all natural frequencies have been identified can be performed by visualizing the mode shapes, where the number of nodal points increases with each successive higher natural frequency.

3. Conclusions

This paper presents a numerical procedure for determining the roots of a transcendental characteristic equation based on the functions of the elements of the characteristic matrix. The use of singular value functions for root searching is recommended, as they are numerically stable and fast to compute.

Acknowledgements: This work was supported by University of Rijeka under the project number uniri-iskusni-tehnic-23-112 and the project number uniri-iskusni-tehnic-23-37.

References

[1] Rao, S.S., *Vibration of Continuous Systems*. John Wiley & Sons, Hoboken, New Jersey, USA, 2007.

[2] Boyd, John., *Solving Transcendental Equations: The Chebyshev Polynomial Proxy and Other Numerical Rootfinders, Perturbation Series, and Oracles*. SIAM, Philadelphia, Pennsylvania, USA, 2014.

11th International Congress
of Croatian Society of Mechanics
September 30 – October 3 2025
Vodice, Croatia

Constitutive Modelling of FDM Printed Continuous Fibre Composites

Ivica Smojver*, Darko Ivančević *, Fran Ušurić *

*University of Zagreb, Faculty of Mechanical Engineering and Naval Architecture
E-mails: {ivica.smojver,darko.ivancevic,fran.usuric}@fsb.hr

Keywords: additive manufacturing, continuous fibre co-extrusion, numerical constitutive modelling

1. Introduction

Fibre-reinforced polymers manufactured via additive techniques, especially continuous fibre 3D printing, have gained significant attention due to their lightweight structure, tailored anisotropy, and process-driven performance. However, their mechanical behaviour is complex and highly dependent on the printing parameters, including fibre raster angle, infill density, presence of voids, nozzle and heating device adjustments — an inherent challenge in Fused Deposition Modelling (FDM). (Xiaoyong et al., 2022) The objective of this work is twofold: to analyse the mechanical properties of 3D printed continuous fibre-reinforced polymers under varying print configurations, and to develop a numerical model capturing the microstructural features of the printed parts using Abaqus finite element software. This approach enables the validation of the developed numerical model as well as prediction of mechanical behaviour with greater fidelity for future designs. In this analysis, special features of Abaqus, such as User Subroutines, have been employed to tackle the specifics of constitutive modelling of these material systems, as well as 3D printed morphology.

2. Numerical model

To capture the heterogeneous nature of 3D printed fibre-reinforced polymers, a detailed mesoscale Representative Volume Element (RVE) was developed, consisting of fibres embedded in matrix layers with voids observed during the printing process (Somireddy, Czekanski, 2021). The matrix was modelled as a homogeneous isotropic material with linear elastic behaviour, while the fibres were orthotropic, aligned with the printing paths. Void geometry and morphology were based on microscopic cross-sectional analysis. These voids, primarily resulting from incomplete resin impregnation (Xiaoyong et al., 2022), were introduced as elliptical inclusions at the fibre–matrix interfaces to simulate filament deposition imperfections (Polyzos et al., 2020). Modelled as physical holes, voids are typically aligned longitudinally, making the material susceptible to transverse cracking under load, significantly reducing the stiffness and strength of 3D printed carbon fibre composites (Hou et al., 2020).

The mesh was generated using structured hexahedral elements (C3D8R) and tetrahedral elements (C3D10), with refined meshing around the voids and fibre edges to accurately capture local stress gradients. The element size was chosen based on a mesh convergence study to balance accuracy and computational efficiency.

Boundary conditions were applied to replicate the uniaxial tensile tests performed experimentally. One face of the model was fully constrained while a displacement load was applied on the opposite face to induce uniform strain. Periodic boundary conditions were used for higher-fidelity homogenization cases.

Material properties for the carbon fibres and nylon matrix used in the development of the numerical model have been adopted from the manufacturer's specifications. The manufacturer of the carbon fibre material is Anisoprint®, and the material is delivered as a spool with the length of 750 m. Nylon polymer matrix has been modelled as an isotropic material with Young's modulus of E =

1.2 GPa and Poisson's ratio $\nu = 0.35$ as stated by the manufacturer Polymaker®. Carbon fibre material properties have been provided by the manufacturer Anisoprint®.

Table 1 Carbon fibre material properties as stated by manufacturer Anisoprint®

Effective diameter	Elastic modulus	Tensile strength	Max. printing temperature	Volume fraction
0.35 mm	149 GPa	2206 MPa	270 °C	60%

Simulation outputs, including stress–strain curves and local stress concentrations, were compared to analytical methods (Rule of Mixtures, Concentric Cylinder Method) and validated against experiments. Test specimens were manufactured using an Anisoprint® Composer A3 printer, with careful cooling to avoid fibre/matrix de-bonding (Heidari-Rarani et al., 2019). The printer offers a build volume of 460 × 297 × 210 mm, minimum layer thickness of 60 μm, enabling the fabrication of medium-sized components. Print speed for Continuous Fiber Co-extrusion (CFC) is 1 – 10 mm/s and the processing temperature is up to 270 ◦C. Tensile testing followed ASTM D3039 standards (Chacon et al., 2019). While the mesoscale model predicted composite behaviour, mechanical properties remained highly sensitive to printing parameters. Future work will focus on the effects of process parameters on porosity and mechanical performance.

3. Conclusions

The mesoscale model demonstrated a capability to predict the mechanical behaviour of the additively manufactured composite material. However, significant variability introduced by printing parameters had a strong impact on the microstructure and, consequently, on the material properties. Additionally, the actual microstructure of the fabricated specimens differed morphologically from the one assumed in the numerical model, which may have contributed to the observed discrepancies. Future work will focus on investigating the influence of process parameters on porosity and mechanical performance, as well as refining the numerical model to more accurately represent the real microstructural morphology.

Acknowledgements

The research is fully funded by the Croatian Science Foundation (HRZZ) within the project "Development of Numerical Methods in Modelling New Generation of Advanced Composite Structures" (DENNGA), grant number IP-2022-10-8845.

References

[1] Xiaoyong, T., et al., 3D Printing of Continuous Fiber Reinforced Polymer Composites: Development, Application, and Prospective, *Chinese Journal of Mechanical Engineering: Additive Manufacturing Frontiers*, 1, 2022

[2] Somireddy, D., Czekanski, A., Computational modeling of constitutive behaviour of 3D printed composite structures, *Journal of Materials Research and Technology*, 11, 2021

[3] Polyzos, E., et al., A multi-scale analytical methodology for the prediction of mechanical properties of 3D-printed materials with continuous fibres, *Additive Manufacturing*, Vol. 36, 2020

[4] Hou, Z., et al., A constitutive model for 3D printed continuous fiber reinforced composite structures with variable fiber content, *Composites Part B: Engineering*, 189, 2020

[5] Heidari-Rarani, M., Rafiee-Afarani, M., Zahedi, A. M., Mechanical characterization of FDM 3D printing of continuous carbon fiber reinforced PLA composites, *Composites Part B: Engineering*, 175, 2019

[6] Chacon, J., et al., Additive manufacturing of continuous fibre reinforced thermoplastic composites using fused deposition modelling: Effect of process parameters on mechanical properties, *Composites Science and Technology*, 181, 2019

11th International Congress
of Croatian Society of Mechanics
September 30 – October 3 2025
Vodice, Croatia

Bayesian parameter identification of non-standard aluminum specimens using simple laboratory measurements

Matej Šodan[*], Vladimir Divić[*], Noémi Friedman[+], Mijo Nikolić[*],

[*] *University of Split, Faculty of Civil Engineering, Architecture and Geodesy, Matice hrvatske 15, 21000 Split, Croatia*
E-mail: matej.sodan@gradst.hr

[+] *HUN-REN Institute for Computer Science and Control (SZTAKI), Kende u.13-17, Budapest, 1111, Hungary*

Keywords: Bayesian identification; embedded strong discontinuity; laboratory measurements, material parameters, non-standard specimen

1. Introduction

Numerical models are essential tools in engineering, as they allow for the simulation of complex physical behaviours, including nonlinearities and failure mechanisms. However, their accuracy depends on how well they represent real-world phenomena through appropriate formulations and material parameters. Material parameters are typically determined through standardized laboratory tests, especially for simpler responses such as elastic. In contrast, non-standard tests are used to investigate localized effects and nonlinear behaviour. However, the results of such tests are often influenced by specimen geometry and size effects, which can complicate interpretation and limit the general applicability of the obtained parameter values [1].

This work focuses on the identification of parameters governing the elastic, plastic hardening, and failure mechanisms in aluminum specimens through tensile tests. A Bayesian inverse method, combined with an embedded strong discontinuity model, is applied to identify material parameters based on simple laboratory measurements. This approach enables parameter identification even when ideal testing conditions or standard specimen geometries are not available.

2. Methodology

The process of determining parameter values that align numerical model results with experimental data is known as parameter identification. The Bayesian inverse method is a probabilistic approach to parameter identification, where parameters are treated as random variables described by probability distributions. The initial knowledge about the parameter values are represented by prior distributions. These priors are then updated using experimental data obtained from tested specimens or structures. One of the key advantages of this approach is that the required parameters do not need to be measured directly. Instead, combinations of simpler experimental measurements can provide valuable indirect information for parameter estimation [2].

The numerical model employed to simulate material behaviour and used to identify elastic, plastic, and fracture parameters is a 2D solid quadrilateral finite element, enhanced with the embedded strong discontinuity method [3]. In this model, each finite element initially follows linear elastic law, defined by Young's modulus (E) and Poisson's ratio (ν). As loading increases, the element undergoes plastic hardening, characterized by the yield strength (σ_0) and the hardening modulus (H). When the stress values exceeds the material strength, a crack is introduced. Crack initiation and propagation are simulated using the embedded strong discontinuity method, governed by two fracture parameters: material strength (σ_n) and fracture energy (G_{fn}).

3. Test design and experimental setup

An aluminium 6060 alloy with unknown material properties was selected for parameter identification. Two different specimen geometries were used (see Figure 1). The rectangular

specimen was employed for the identification of elastic parameters, while the single-notched specimen was used for identifying plastic and fracture parameters.

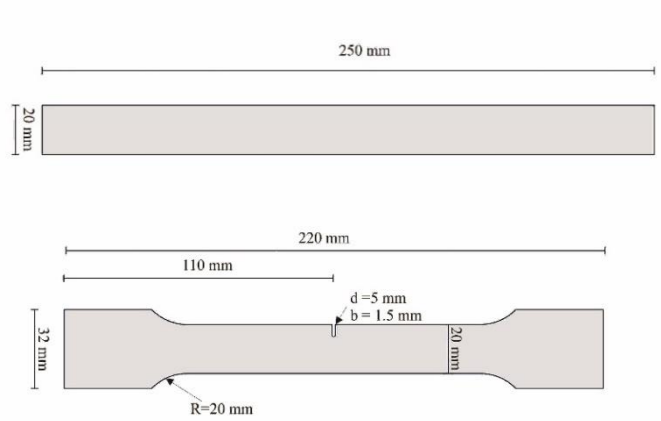
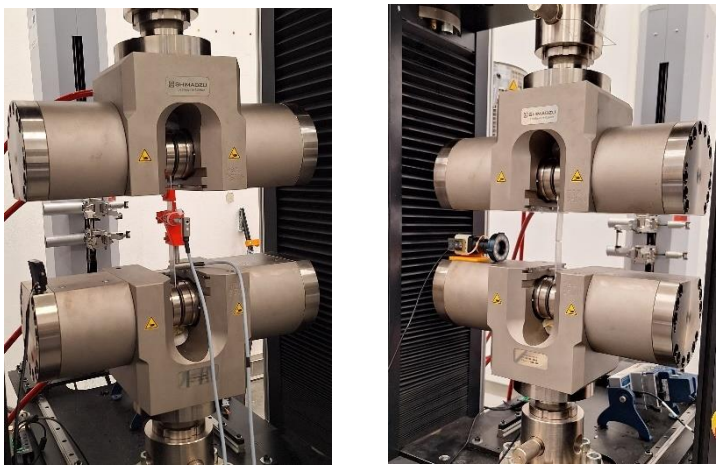


Figure 1. Aluminium alloy specimens: Rectangular and single-notched dogbone

The specimens were manufactured using a CNC milling machine, ensuring consistent and accurate dimensions. The experimental setup included a Universal Testing Machine (UTM), optical measurement equipment, and LVDT sensors (see Figure 2).



a) **b)**

Figure 2. Laboratory setup: a) UTM and LVDT b) UTM and optical equipment

Acknowledgements

This work has been supported through the project 'Parameter estimation framework for fracture propagation problems under extreme mechanical loads' (UIP-2020-02-6693), funded by the Croatian Science Foundation.

References

[1] H. G. Matthies, E. Zander, B. V. Rosič, A. Litvinenko, and O. Pajonk, "Inverse problems in a bayesian setting," in Computational Methods for Solids and Fluids: Multiscale Analysis, Probability Aspects and Model Reduction. Springer International Publishing, 2016, pp. 245–286. DOI: 10.1007/978-3-319-27996-1_10.

[2] M. Šodan, A. Urbanics, N. Friedman, A. Stanic, and M. Nikolić, "Comparison of machine learning and gpc-based proxy solutions for an efficient bayesian identification of fracture parameters," Computer Methods in Applied Mechanics and Engineering, vol. 436, p. 117 686, 2025. DOI: 10.1016/j.cma.2024.117686.

[3] M. Šodan, A. Stanic, and M. Nikolić, "Enhanced solid element model with embedded strong discontinuity for representation of mesoscale quasi-brittle failure," International Journal of Fracture, vol. 248, pp. 1–25, 2024. DOI: 10.1007/s10704-024-00797-0.

11th International Congress
of Croatian Society of Mechanics
September 30 – October 3 2025
Vodice, Croatia

Environmental loads on offshore engineering structures

Ivan Sokol, Ivan Ćatipović[+], Neven Hadžić[+], Hrvoje Kozmar[+]

E-mail: isokolzg@gmail.com

[+]*Name and Address of Institute*
E-mails: {ivan.catipovic,neven.hadzic,hrvoje.kozmar}@fsb.unizg.hr

Keywords: Offshore engineering structures, environmental loads, wind turbines, wave energy converters, tidal turbines

1. Introduction

Offshore renewable energy structures are complex engineering objects gaining attention as the world increasingly relies on renewable energy. Major drawbacks of the current recommendations provided in international standards and codes regarding offshore engineering structures are outlined here. In these standards, the wind effects are currently simplified and calculated based on the average wind velocity with a correction factor to account for atmospheric turbulence. These conditions do not adequately represent atmospheric wind conditions, where the standard deviation of the wind velocity fluctuations due to turbulence can be up to 40% of the average wind velocity. It is therefore required, when designing offshore renewable energy structures, to take into account realistic atmospheric wind conditions, i.e., integral turbulence length scales, turbulence intensity, Reynolds shear stress and power spectral density of wind velocity fluctuations, given the fact that aerodynamic loads on structures may be up to 70% of the total environmental loads. It is also crucial to consider the effects of both the synoptic and non-synoptic winds. Neglecting atmospheric turbulence and non-synoptic wind effects may likely yield substantial errors in the structural design of offshore engineering structures.

1.1. Wind turbines

The offshore wind potential is present globally. For example, the available wind potential in Europe is ~350 GW, while the US potential is larger than 2000 GW. Offshore wind resource in China is ~500 GW for water depths less than 50 m, while the east and west Indian coasts have an offshore wind potential of 6.7 GW and 4.4 GW, respectively, [1].

1.2. Wave energy converters

Wave energy converters (WEC) can produce electricity using ocean waves. These devices have been developed to extract energy from shallow and deep waters. In general, wave energy conversion is characterized by low environmental impact compared to other renewable energy sources, high utilization factor and high-power density, [2].

1.3. Tidal turbines

Tidal energy can be created using technologies such as tidal barges, fences, and turbines. Tidal barges utilize energy created by the height between high and low tides. Tidal fences operate like large turnstiles while using the gravitational interaction between the Earth, Moon, and Sun while tidal turbines can harness kinetic energy from tidal currents, [3].

1.4. Solar panels

The most prevalent application of solar energy is through photovoltaic (PV) systems, which transform sunlight into electricity. A particularly promising variant is the floating photovoltaic (FPV) system, which boasts greater efficiency than traditional ground-mounted PV systems and helps minimize water evaporation from reservoirs. It is estimated that by covering just 1% of natural basin areas with FPV panels, approximately 25% of the global electrical energy demand could be satisfied, [4].

2. Environmental loads on offshore engineering structures

In general, the loads acting on offshore engineering structures may be considered in three groups i.e., permanent, live, and environmental loads. The environmental loads will be explained in more detail.

2.1. Wind loads

When wind impinges on wind turbines, it exerts a lateral thrust force on both the rotor and the tower. The aerodynamic forces exerted on the rotor nacelle assembly (RNA) are transmitted to the tower as a concentrated lateral load, [5]. Until now, most numerical and experimental studies of offshore wind turbines have relied on uniform wind flow, thus the oversimplified aerodynamic modelling. However, actual wind fields are turbulent rather than uniform, and they change not only over time but also across various locations, [6].

2.2. Wave loads

Stationary objects, such as floating or submerged substructures, experience significant first-order wave forces and moments when exposed to irregular waves. These forces are linearly related to wave height and share the same frequencies as the waves. The second-order forces are distinguished by their lower frequencies, which can be calculated as the differences between the frequencies of the incoming waves, [7].

2.3. Sea current loads

Sea current acts as a load exerted by the movement of water particles. The current load decreases with an increase in depth, while it reaches its maximum value at the free surface. This load may cause scour if the current is not zero at the seabed.

2. Offshore and naval engineering standards and codes

In total, three standards were considered in the present study, i.e., Det Norske Veritas (DNV), [8], the American Bureau of Shipping (ABS), [9], and Bureau Veritas (BV), [10]. The shortcomings were identified, and recommendations were provided for further code development.

Table 1 Overview of shortcomings regarding wind load assessment in major offshore and marine engineering standards and the recommendations for improvements

Offshore and naval engineering standard	Wind load assessment according to standards	Recommendation for improvement
DNV	Standard-oriented method	Realistic wind flow data
	Mean wind velocity profile based on the power law	Non-synoptic wind profile
ABS	Synoptic winds	Non-synoptic winds
BV	Turbulence intensity $I_u(z)$	Turbulence intensity $I_u(z), I_v(z), I_w(z)$ Integral turbulence length scales $L_{u,x}(z)$ Reynolds shear stress τ Power spectral density $S_u(f)$

3. Conclusions

There is an urgent requirement for improvements and a comprehensive review of offshore engineering standards and codes to provide accurate recommendations for offshore structures. A notable knowledge gap exists in understanding the simultaneous load effects of wind, waves, and current on these complex structures. Creating an effective simulation method to tackle the non-stationary stochastic vibration caused by nonlinear, coupled, and transient aerodynamic loads during intense non-synoptic thunderstorms is a key topic for the future. It is therefore suggested, when designing offshore renewable energy structures, to consider the parameters characteristic of the atmospheric wind conditions, i.e., turbulence intensity, turbulence length scales, Reynolds shear stress, power spectral density of wind velocity fluctuations, given the fact that aerodynamic loads on structures may be up to 70% of the total environmental loads. It is furthermore crucial to consider

the effects of non-synoptic winds as well, e.g., hurricane, tornado, downburst, bora, etc., in addition to the standard synoptic winds.

Acknowledgements

This work was supported by the Croatian Science Foundation under the project numbers UIP-2019-04-6573, IP-2022-10-4408, IP-2022-10-9434. The COST Action CA20109 MODENERLANDS support by COST (European Cooperation in Science and Technology) is gratefully acknowledged.

References

[1] A. Fernández-Guillamón, K. Das, N. A. Cutululis and Á. Molina-García, "Offshore Wind Power Integration into Future Power Systems: Overview and Trends," Marine Science and Engineering, p. 23, 10 october 2019.

[2] M.Fadaeenejad, R.Shamsipour, S.D.Rokni and C.Gomes, "New approaches in harnessing wave energy: With special attention to small islands," Renewable and Sustainable Energy Reviews, vol. 29, pp. 345-354, 2014.

[3] W.-H. Lam and A. Bhatia, "Folding tidal turbine as an innovative concept toward the new era of turbines," Renewable and Sustainable Energy Reviews, pp. 463-473, 2013.

[4] P. Ranjbaran, H. Yousefi, G. Gharehpetian and F. R. Astaraei, "A review on floating photovoltaic (FPV) power generation units," Renewable and Sustainable Energy Reviews, no. 110, pp. 332-347, 2019.

[5] V. K. Harikrishnan, S. Annamalai, S. Sampath and S. Paramasivam, "A time-performance improvement model with optimal ergonomic risk level using genetic algorithm," Transactions of Famena, p. 20, 2023

[6] L. Li, Y. Liu, Z. Yuan and Y. Gao, "Dynamic and structural performances of offshore floating wind turbines in turbulent wind flow," Ocean Engineering, Vols. 92-103, p. 12, 2019.

[7] I. Ćatipović, K. Martić, N. Alujević and S. Rudan, "Hydrodinamic Forces and Reactions of Two Floating Bodies in Close Proximity," Pomorski zbornik, vol. 62, pp. 57-74, 2022.

[8] Det Norske Veritas, "Loads and site conditions for wind turbines," DNV-ST-0437, 2021.

[9] American Bureau of Shipping, "Bottom-founded offshore wind turbine instalations," New York, 2018.

[10] Bureau Veritas, "Classification and Certification of Floating Offshore Wind Turbines," Marine & Offshore, France, 2019.

11th International Congress
of Croatian Society of Mechanics
September 30 – October 3 2025
Vodice, Croatia

Regression-based machine learning for predicting natural frequencies of thin beams supported by translational springs

Goranka Štimac Rončević*, Ante Skoblar*, Sanjin Braut*, Roberto Žigulić*, Goran Turkalj*

*University of Rijeka Faculty of Engineering
E-mails: goranka.stimac@riteh.uniri.hr, ante.skoblar@riteh.uniri.hr, sanjin.braut@riteh.uniri.hr, roberto.zigulic@riteh.uniri.hr, goran.turkalj@riteh.uniri.hr

Keywords: regression-based machine learning, natural frequency, thin beams, translational springs

1 Introduction

Beams are fundamental structural elements widely used in various engineering applications. The study of beams subjected to transverse vibrations remains a central topic in structural dynamics, as these vibrations have a significant impact on the performance and safety of engineering structures. In recent decades, extensive research has focused on identifying the natural frequencies of beams with added lumped elements, such as translational and rotational springs, masses, and inertias. These studies have employed various mathematical approaches to address the complexity of these systems.

This study builds upon the authors' previous work [1], which highlighted the challenges associated with solving the frequency equation and determining the natural frequencies of beams supported by a large number of translational springs. As the number of beam segments and supporting elements increases, the size of the system matrix grows accordingly, resulting in significant computational complexity. To overcome these challenges, machine learning techniques offer a compelling alternative, delivering not only accurate results but also efficient solutions to problems that are otherwise computationally intensive and time-consuming. Paper [2] explores prediction of natural frequencies in aluminum and steel beams of varying thickness. To further demonstrate the advantages of machine learning, this study focuses on predicting the first non-dimensional natural frequency of an Euler–Bernoulli beam supported by n equally spaced translational springs. The prediction is carried out using several regression-based machine learning approaches: Linear Regression (LR), Random Forest (RF), Support Vector Regression (SVR) and Neural Network (NN).

2 Preparation of the dataset

The dataset used for training and evaluation is obtained from an analytical model of an Euler–Bernoulli beam supported by n equally spaced translational springs (Figure 1).

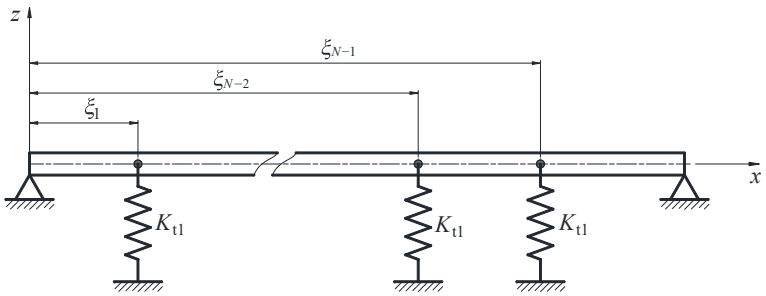


Figure 1. Pinned-pinned Euler-Bernoulli beam supported with translational springs

The model is developed using the dynamic stiffness matrix method, the derivation and detailed formulation of which are thoroughly presented in [3]. The resulting transcendental eigenvalue problem, which governs the determination of natural frequencies, is solved using the Wittrick–Williams algorithm. A total of 300 experiments are conducted to generate the dataset. The value ranges for the

two input parameters are: number of springs, n, from 1 to 40, and their corresponding non-dimensional stiffness values, K_{t1}, from 1 to 2000. The calculated output is the first natural frequency. To avoid overfitting and ensure robust model evaluation, a 5-fold cross-validation approach is employed instead of a standard train–test split. Z-score standardization is applied to normalize the input data for both SVR and NN algorithms, ensuring a mean of zero and a standard deviation of one. This prevents the dominance of features with larger scales during training and enhances model convergence.

3 Performance evaluation results

The model's performance is evaluated using the correlation coefficient (R^2), mean absolute error (MAE) and root mean square error (RMSE). Figure 2 illustrates the fitting of the predicted non-dimensional natural frequencies against the actual values from the test set for the LR, RF, SVR, and NN algorithms. The NN algorithm yields the highest correlation coefficient, along with the lowest MAE and RMSE values, indicating the best performance among the models.

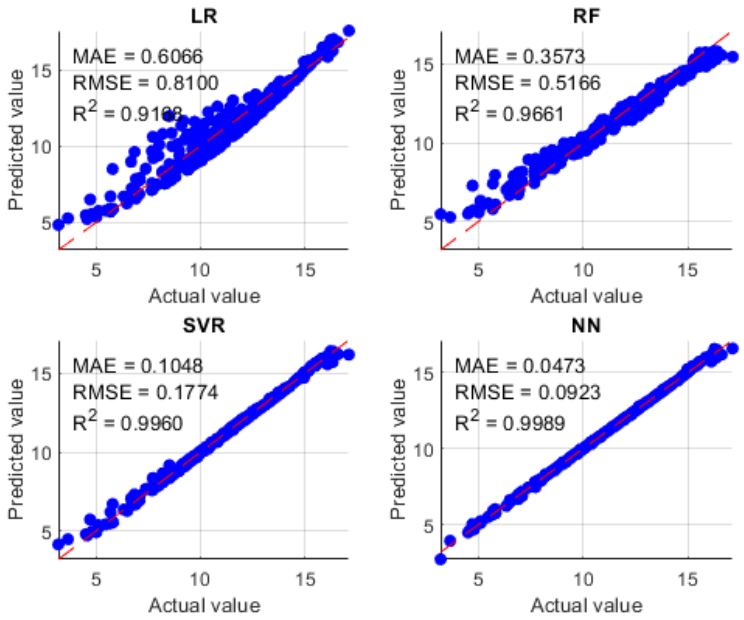


Figure 2. Scatter plot for comparing predicted and actual first non-dimensional natural frequency

4 Conclusion

To exploit the potential of machine learning in structural dynamics, this study investigates the prediction of the non-dimensional natural frequency of an Euler–Bernoulli beam supported by translational springs using regression-based techniques, including LR, RF, SVR, and NN. Among these, the NN delivers the best performance, and its superiority is discussed. This approach provides an efficient solution to problems that would otherwise be computationally intensive and time-consuming.

Acknowledgements: This work was supported by University of Rijeka under the project number uniri-iskusni-tehnic-23-112 and Croatian Science Foundation under the project number HRZZ-IP-2024-05-6868.

References

[1] Štimac Rončević, G., Rončević, B., Skoblar, A., Žigulić, R., Closed form solutions for frequency equation and mode shapes of elastically suported Euler-Bernoulli beams. *Journal of Sound and vibration*, 457, 118-138, 2019.

[2] Das, O., Prediction of the natural frequencies of various beams using regression machine learning models. *Sigma Journal of Engineering and Natural Sciences*, 41, 302-321, 2023.

[3] Banerjee, J. R., Dynamic stiffness formulation and its application for a combined beam and a two degree-of-freedom system. *Journal of Sound and vibration*, 125, 351-358, 2003.

11th International Congress
of Croatian Society of Mechanics
September 30 – October 3 2025
Vodice, Croatia

Tensile Testing of Welded Joints Using Small-Scale Specimens

Damir Tomerlin*, Dražan Kozak*, Nenad Gubeljak+, Darko Damjanović*

*University of Slavonski Brod, Mechanical Engineering Faculty in Slavonski Brod, Trg Ivane Brlić Mažuranić 2, HR-35000 Slavonski Brod, Croatia
E-mails: {dtomerlin,dkozak,ddamjanovic}@unisb.hr

+University of Maribor, Faculty of Mechanical Engineering, Smetanova 17, SI-2000 Maribor, Slovenia
E-mail: nenad.gubeljak@um.si

Keywords: experimental testing, mini tensile specimens, small scale specimen, welded joints, heterogeneity

1. Introduction

Welded joints are inherently heterogeneous structures, characterized by their main segments: the base metal (BM), heat-affected zone (HAZ), and weld metal (WM). The HAZ, which typically spans a few millimeters in fusion welding processes, is further divided into several distinct regions that differ in grain microstructure and size [1]. This microstructural heterogeneity leads to mechanical properties differences across the welded joint. Tensile testing of such small material volumes is very difficult or impossible using the conventional size specimens. Even the subsize tensile specimens are very difficult to properly position and extract from the narrow HAZ regions of the weld.

This study examines a fusion welded X joint made of S690QL1 high-strength steel (HSS), welded with slightly overmatching filler metal. The tensile properties of the welded joint material are assessed using the small-scale specimens methodology. This include the ASTM E8 subsize round tensile specimens and mini tensile specimens (MTS) in flat sheet dogbone shape [2].

2. Materials and methods

The steel BM used in this study is HSS S690QL1, a fine-grained steel, according to EN10025-6, intended for demanding structural welded applications. For 40 mm thick plate, it has declared yield strength $R_{p0.2} \geq 690$ MPa, with tensile strength $R_m = 770$ to 940 MPa. The WM filler metal Mn3Ni1CrMo (ER110S-G) has $R_{p0.2} = 800$ MPa and $R_m = 900$ MPa. WM to BM mismatch factor M = 1.16.

The first small-scale method used is tensile testing with ASTM E8 subsize round specimens. The method is used for tensile testing in longitudinal direction, and can determine stress–strain (σ–ε) material curves with characteristic parameters: yield strength $R_{p0.2}$, tensile strength R_m, percentage elongation after fracture A_5, and Young's modulus E. This method is suitable for assessing welded joint material properties on a general scale, within a diameter of $Ø = 2.5$ mm. This method enables testing of BM, HAZ, and WM segments of welded joint only, as can be seen on the example of X welded joint half section, in Figure 1a.

Thes MTS method can also determine the material parameters $R_{p0.2}$, R_m, percentage total elongation at maximum force A_{gt}, and E. The method is very significant for determination of stress–strain properties along the welded joint cross sectional transverse line, having the possibility to distinguish between general scale segments BM and WM, and individual HAZ subregions, as shown in Figure 1b. For application in welded joints testing, it provides excellent results and provides significant insight into the behavior of the complete welded joint. It is very important to place the MTS specimen in the correct location in regard to specific material region to be tested. The MTS specimens are extracted from welded joint using the electrical discharge wire cutting (EDWC).

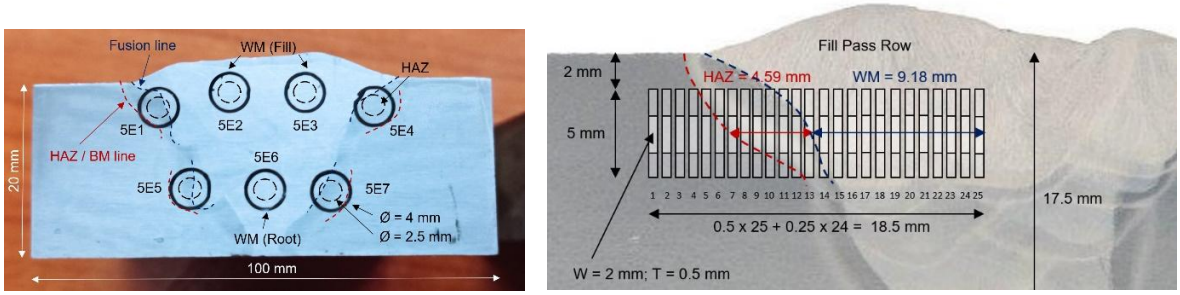


Figure 1. Small-scale specimens tensile testing methods: a) ASTM E8, b) MTS

3. Results

Tensile testing according to ASTM E8 determined the material parameters $R_{p0.2}$ and R_m for BM, HAZ and WM (Figure 2a). Strength testing of BM material determined the average $R_{p0.2}$ = 736.6 MPa and R_m = 810.3 MPa, with statistical deviations SD = 66.5/46.0 MPa, respectively. WM testing determined the average $R_{p0.2}$ = 779.0 MPa and R_m = 902.4 MPa, with SD = 56.9/25.2 MPa. HAZ average $R_{p0.2}$ = 859.9 MPa and R_m = 937.6 MPa, with SD = 109.2/74.0 MPa. This method is unable to distinguish between specific HAZ subregions and can determine the HAZ properties on a general material level only, which in turn leads to substantial $R_{p0.2}$/ R_m deviations.

In case of MTS testing (Figure 2b), for BM material the average $R_{p0.2}$ = 734.0MPa and R_m = 822.0 MPa, with SD = 5.7/ 16.4 MPa, respectively. The WM average $R_{p0.2}$ = 783.8 MPa and R_m = 865.6 MPa with SD = 29.7/ 21.0 MPa. The HAZ average $R_{p0.2}$ = 782.4 MPa and R_m = 865.6 MPa with SD = 70.0/ 58.7 MPa. Overall MTS results deviations for BM and WM are relatively low, and significantly lower as compared to ASTM E8 round specimens testing method. The HAZ shows greater deviations, which can be attributed to the anticipated variations in the material's properties.

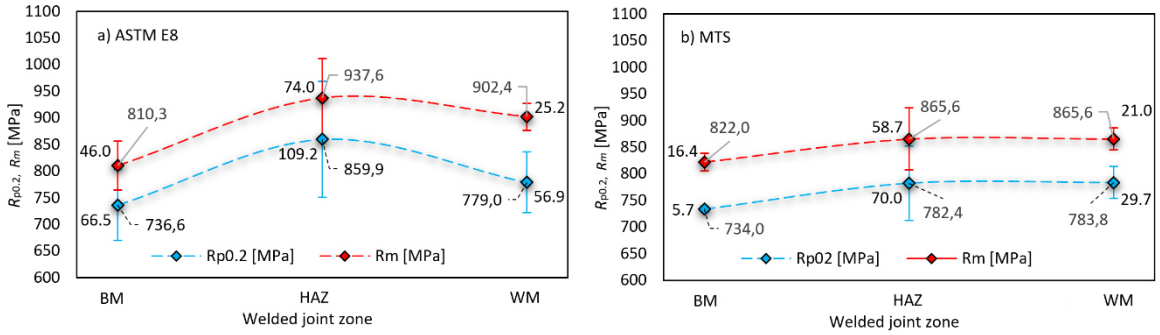


Figure 2. Tensile testing $R_{p0.2}$ and R_m values for BM, HAZ and WM: a) ASTM E8, b) MTS testing

4. Conclusions

The ASTM E8 round tensile subsize specimen method is suitable for general-scale testing of welded joints and can effectively assess the tensile properties of primary segments BM, HAZ, and WM. Specimen diameter of $Ø$ = 2.5 mm, result in a circular test area of 4.909 mm². Since the method cannot differentiate between HAZ subregions, the $R_{p0.2}$/ R_m for HAZ show significant deviations. MTS method is applicable of complete linear characterization of heterogeneous weld material, being able to distinguish between general scale segments BM and WM, as well as individual HAZ subregions. The specimen has rectangular test area (W = 2 mm x T = 0.5 mm), resulting in a rectangular test area of 1 mm^2.

References

[1] Nippes, E. F., The weld heat-affected zone. *Weld. J*, vol. 38, pp. 1–17, 1959.

[2] Tomerlin, D., Kozak, D., Gubeljak, N., Pentek, I., Tensile testing of S690QL1 HSS welded joint heterogeneous zones using small scale specimens and indentation methods. *Materials Testing*, vol. 66, no. 10, pp. 1600-1619, 2024. https://doi.org/10.1515/mt-2024-0136

11th International Congress
of Croatian Society of Mechanics
September 30 – October 3 2025
Vodice, Croatia

DVC analysis of failure modes in glass plain-weave fabric composites under on- and off-axis loading

Zvonimir Tomičević[*], Andrija Zaplatić[*], Benjamin Smaniotto[+], François Hild[+]

[*] *Faculty of mechanical engineering and naval architecture, Ivana Lučića 5, 10 000 Zagreb*
E-mails: {zvonimir.tomicevic,andrija.zaplatic}@fsb.unizg.hr

[+] *Université Paris-Saclay, CentraleSupélec, ENS Paris-Saclay, CNRS, LMPS - Laboratoire de Mécanique Paris-Saclay, 91190 Gif-sur-Yvette, France*
E-mail: {francois.hild,benjamin.smaniotto}@ens-paris-saclay.fr

Keywords: woven composite, X-Ray Computed Tomography, Digital Volume Correlation, strain localization, failure modes

1. Introduction

Composites with woven fibre (WF) architectures and thermoplastic matrices are widely used in industries such as aerospace, automotive, and energy due to their lightweight properties and rapid thermoformability. However, the complexity of structural part geometries often results in loading paths that are misaligned with the weave directions [1]. In addition, these components frequently incorporate geometrical singularities (*i.e.*, notches, holes, or abrupt changes in geometry) to accommodate assembly and functional requirements [2]. These factors, combined with the mesoscale intricacy of multi-ply woven structures, lead to complex deformation and failure modes that vary with loading direction and material architecture. Accurate performance prediction under such conditions requires a multiscale understanding of both the global response and the formation of localized damage. Full-field measurement techniques, particularly X-ray Computed Tomography (XCT) combined with Digital Volume Correlation (DVC), have proven effective for *in-situ* tracking of internal deformation and damage evolution across multiple length scales.

This study investigates strain localization and failure modes in a glass fiber/vinyl ester composite subjected to on- and off-axis uniaxial loading, using single-notched specimens. An XCT and FE-based DVC framework is employed to capture strain localization and internal damage progression during cyclic loading [3]. The findings improve the understanding of load path effects linked to different fiber orientations and support more accurate predictions of the influence of geometric discontinuities. This is crucial for the reliable modelling and simulation of damage in multi-layered textile composites.

2. Experimental protocol and DVC measurements

The experimental study was conducted on a glass plain-woven fabric reinforced vinyl ester resin composite manufactured via vacuum infusion. Dogbone-shaped specimens with a rectangular notch were extracted from a 5.2 mm thick GFRP plate using water jet cutting technology. The two specimens were oriented at 0°/90° (on-axis) and 45° (off-axis) relative to the weave direction (Fig. 1(a) and (b)). The central region of each specimen was thinned with a 39 mm radius, and the notch had a depth of 1.1 mm and a width of 1 mm. The specimens were subjected to cyclic tensile loading (see Fig. 1. c)) using an in-situ TTC Deben testing machine integrated within the X50+ CT scanner (NSI) at LMPS. The *in-situ* mechanical test was performed under displacement control with a stroke velocity of 4 µm/s. The on-axis specimen was loaded through five cycles, reaching 25%, 55%, 65%, 78%, and 88% of the ultimate tensile strength. For the off-axis specimen, eight loading cycles were applied, corresponding to 30%, 60%, 80%, 85%, 90%, 95%, 100%, and 93% of the ultimate tensile strength (Fig. 1(c)). The uniaxial force measurements revealed noticeable relaxation effects during

CT scanning at constant displacement levels. The region of interest (ROI), adapted to the thinned ligament of the dogbone specimen, measured 421 × 588 × 1200 voxels, with a voxel size of 15.1 µm. A global DVC analysis was carried out using the Correli 3.0 framework [4], employing a first-order tetrahedral discretization of the ROI.

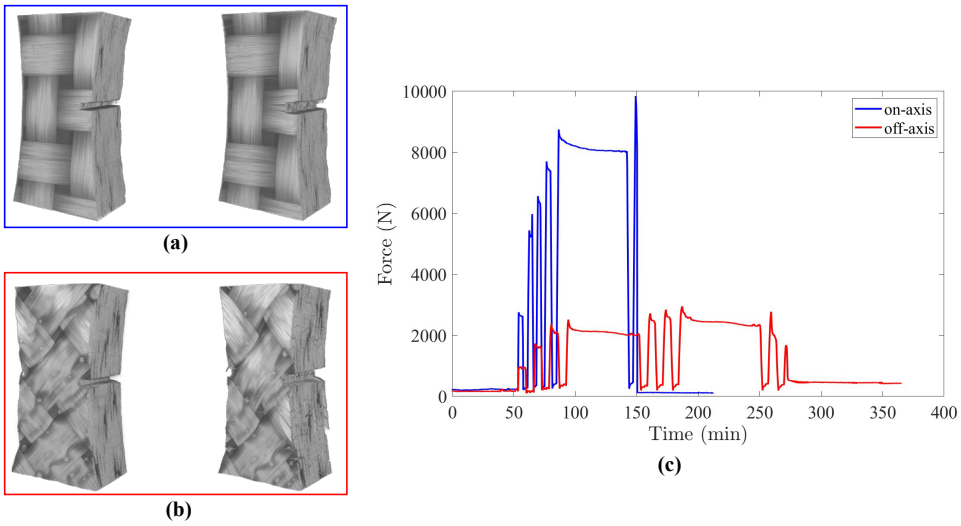


Figure 1. 3D renderings of the reference and deformed single-notched tensile specimens with (a) on- and (b) off-axis woven fabric orientations. (c) Loading histories of the in-situ cyclic experiments.

3. Conclusions

Calculated strain maps and virtual gauge data revealed permanent strain accumulation within the analyzed ROI throughout the imposed loading history. Correlation residual maps from both experiments were used to characterize mesoscale damage mechanisms within the bulk of the material that led to final failure. In the on-axis specimen, cracks oriented orthogonally to the loading direction were observed both on the surface and within the ROI. The dominant damage mechanism was identified as matrix–yarn debonding. As expected, strain concentration developed at the notch tip, accompanied by the formation of strain bands that originate within the notch and progressively propagate parallel to the loading axis. In the off-axis specimen, damage initiated at the lateral surfaces of the ligament and gradually propagated inward. The major principal strains were observed outside the geometrical discontinuity of the specimen, indicating that the failure was driven by the material architecture rather than the imposed singularity. The dominant damage mechanism in this case was identified as intra-yarn debonding. This study demonstrates the capability of global DVC to capture complex kinematics, including the formation and evolution of strain bands, as well as the underlying failure modes associated with different woven fabric orientations.

Acknowledgements

This work was performed within the GENKON project supported by the European Union and National Recovery and Resilience Plan (NPOO.C3.2.R3-I1.04.0121 Grant).

References

[1] Holmes, J., Sommacal, S., Das, R., Stachurski, Z., Compston, P., Characterisation of off-axis tensile behaviour and mesoscale deformation of woven carbon-fibre/PEEK using digital image correlation and X-ray computed tomography. *Composites Part B: Engineering*, 229, 109448, 2022.

[2] Vrgoč, A., Tomičević, Z., Smaniotto, B., Hild, F., Characterization of glass fiber reinforced polymer via Digital Volume Correlation: Investigation of notch sensitivity. *Mechanics of Materials*, 177, 104552, 2023.

[3] Vrgoč, A., Tomičević, Z., Smaniotto, B., Hild. F. Characterization of glass fiber reinforced polymer via digital volume correlation: Quantification of strain activity and damage growth. *Composites Science and Technology*, 234, 109932, 2023.

[4] Leclerc, H. et al. Correli 3.0. Agence pour la Protection des Programmes, Paris (France), IDDN.FR.001.520008.000.S.P.2015.000.31500, 2015.

11th International Congress
of Croatian Society of Mechanics
September 30 – October 3 2025
Vodice, Croatia

Mixed *hp*-finite element framework for modeling laser pulse heating processes in irreversible thermodynamics

Balázs Tóth

Institute of Applied Mechanics, University of Miskolc, Hungary, H-3515 Miskolc-Egyetemváros
E-mail: balazs.toth@uni-miskolc.hu

Keywords: Mixed hp-FE technology, Ballistic-conductive model, Maxwell–Cattaneo–Vernotte model, Guyer–Krumhansl model, Laser-pulse heating processes

1 Introduction

In this presentation, new multi-field variational formulations are implemented for solving the following thermodynamic models: (i) ballistic-conductive system, (ii) the Guyer–Krumhansl heat conduction model and (iii) the Maxwell–Cattaneo–Vernotte model as some models of the extended irreversible thermodynamic, treating the temperature, the heat flux and the current density of heat flux as independent field variables. Based on these variational approaches as theoretical background, a family of mixed *hp*-version finite element methods, which is capable of reliably and efficiently modeling the temperature responses, is developed.

In the conference the solutions provided by the constructed *hp*-FE framework will be illustrated for the following two heat pulse experiments as benchmark problems: (1) sinusoid laser pulse heating process and (2) rectangular (step-like) laser pulse train. It is numerically verified that stable, oscillation-free temperature response functions can be obtained not only for the ballistic-conductive system and the Maxwell–Cattaneo–Vernotte model but also for the under-diffuse and the over-diffuse parameter settings of the Guyer–Krumhansl heat conduction model.

2 Variational approaches as theoretical backgrounds

The mathematical background associated with the previously-mentioned topic can be found in the papers [1, 2], within which the joint partial differential equation system of the ballistic-conductive model, the Guyer–Krumhansl heat cunductivity model, and the Maxwell–Cattaneo–Vernotte model, as well as the related initial and boundary conditions are detailed in non-dimensionalized form.

Accordingly, a three-field variational formulation can be obtained for the ballistic-conductive thermodynamic system that reads for homogeneous materials as follows: we seek the variable triplet $[T(t,.)], Q(t,.)] \in H^1(\Omega)$ and $q(t,.) \in L^2(\Omega)$ as trial functions satisfying *a priori* the temperature boundary condition and the initial conditions in such a way that the variational equations

$$\lambda \int_\Omega \dot{T}\, u \,\mathrm{d}\Omega - \int_\Omega q\, u' \,\mathrm{d}\Omega = \tilde{q}\, u(0) \quad \forall u \in H^1(\Omega)\,,$$

$$\frac{\tau_q}{\lambda} \int_\Omega \dot{q}\, v \,\mathrm{d}\Omega + \frac{1}{\lambda} \int_\Omega q\, v \,\mathrm{d}\Omega + \int_\Omega T'\, v \,\mathrm{d}\Omega + \frac{\kappa}{\lambda} \int_\Omega Q'\, v \,\mathrm{d}\Omega = 0 \quad \forall v \in L^2(\Omega)\,,$$

$$\frac{\tau_Q}{\lambda} \int_\Omega \dot{Q}\, w \,\mathrm{d}\Omega + \frac{1}{\lambda} \int_\Omega Q\, w \,\mathrm{d}\Omega - \frac{\kappa}{\lambda} \int_\Omega q\, w' \,\mathrm{d}\Omega = \frac{\kappa}{\lambda}\, q(0)\, w(0) - \frac{\kappa}{\lambda}\, q(\ell)\, w(\ell) \quad \forall w \in H^1(\Omega)$$

hold true enforcing the homogeneous form of the temperature boundary condition on the test function $u(x)$ at the right-hand-sided boundary $x = \ell$, namely, $u(\ell) = 0$, yielding a unified three-field variational framework for the ballistic-conductive system including both the Guyer–Krumhansl- and the Maxwell–Cattaneo–Vernotte system as part- or sub-cases. Here, λ, τ_q, τ_Q and κ are the dimensionless Fourier-type heat conductivity coefficient, the relaxation times and a diffusivity material parameter, while $T(x,t)$, $q(x,t)$ and $Q(x,t)$ are the temperature, the heat flux and the current density of heat flux as field variables, as well as $\Omega \in [0,1]$ is the non-dimensionalized space domain.

The variational equation system of the ballistic-conductive model becomes the variational equation system of Guyer–Krumhansl if $\tau_Q = 0$, resulting in the three-field system

$$\lambda \int_\Omega \dot{T}\, u \,\mathrm{d}\Omega - \int_\Omega q\, u' \,\mathrm{d}\Omega = \tilde{q}\, u(0) \quad \forall u \in H^1(\Omega)\,,$$

$$\frac{\tau_q}{\lambda} \int_\Omega \dot{q}\, v \,\mathrm{d}\Omega + \frac{1}{\lambda} \int_\Omega q\, v \,\mathrm{d}\Omega + \int_\Omega T'\, v \,\mathrm{d}\Omega + \frac{\kappa}{\lambda} \int_\Omega Q'\, v \,\mathrm{d}\Omega = 0 \quad \forall v \in L^2(\Omega)\,,$$

$$\frac{1}{\lambda} \int_\Omega Q\, w \,\mathrm{d}\Omega - \frac{\kappa}{\lambda} \int_\Omega q\, w' \,\mathrm{d}\Omega = \frac{\kappa}{\lambda}\, q(0)\, w(0) - \frac{\kappa}{\lambda}\, q(\ell)\, w(\ell) \quad \forall w \in H^1(\Omega)\,,$$

where the third variational integral does not contain the time derivative of any field variable at all, i.e., this is not a differential equation with respect to the time coordinate; while if both $\tau_Q = 0$ and $\kappa = 0$ simultaneously, the two-field variational equation system of the Maxwell–Cattaneo–Vernotte heat conductivity model is obtained:

$$\lambda \int_\Omega \dot{T}\, u \,\mathrm{d}\Omega - \int_\Omega q\, u' \,\mathrm{d}\Omega = \tilde{q}\, u(0) \quad \forall u \in H^1(\Omega)\,,$$

$$\frac{\tau_q}{\lambda} \int_\Omega \dot{q}\, v \,\mathrm{d}\Omega + \frac{1}{\lambda} \int_\Omega q\, v \,\mathrm{d}\Omega + \int_\Omega T'\, v \,\mathrm{d}\Omega = 0 \quad \forall v \in L^2(\Omega)\,.$$

This variational framework provides as a strong mathematical basis for the development of a stable mixed *hp*-FE code [2, 3]. The higher-order space discretization scheme will be tested on the two typical benchmark problems mentioned in the Introduction.

3 Conclusion

It will be presented in the conference that the solutions reproduce the desired characteristics in each case, contrary to COMSOL Multiphysics, see the results in [4]. That is a very important consequence since the low-order, mesh refinement-based FE approaches do not work satisfactorily in each case, and it is not worth treating the temperature as a single-field variable. The benefits of the unified multi-field *hp*-FE framework are collected as follows [2, 3]:

1. Since the derived variational formulations and the related FE framework are multi-field ones, we obtain numerical results directly for each field variable, i.e., the temperature field, the heat flux and the internal variable, thereby *requiring low computational cost and shorter time of the postprocessing*.

2. The developed *hp*-FE framework gives oscillation-free simulation results, thereby producing stable FE solutions for the temperature response functions.

References

[1] Kovács, R., Ván, P., Generalized heat conduction in heat pulse experiments. *International Journal of Heat and Mass Transfer*, Vol. 83, Pages 613-620, 2015.

[2] Tóth, B., A unified mixed *hp*-finite element framework for modeling laser pulse heating processes in the refined thermodynamics. *International Journal of Heat and Mass Transfer*, Vol. 238, Paper ID: 126456, 2025.

[3] Tóth, B., Three-field mixed *hp*-finite element method for the solution of the Guyer–Krumhansl heat conduction model. *International Journal of Heat and Mass Transfer*, Vol. 217, Paper ID: 124663, 2023.

[4] Rieth, A., Kovács, R., Fülöp, T., Implicit numerical schemes for generalized heat conduction equations. *International Journal of Heat and Mass Transfer*, Vol. 126, Part B, Pages 1177-1182, 2018.

11th International Congress
of Croatian Society of Mechanics
September 30 – October 3 2025
Vodice, Croatia

Stress and Displacement Analysis of a Thin-walled Curved Beam Subjected to the Eccentric Uniformly Distributed Line Load

Vukasović Marko*, Kustura Dražen+, Vlak Frane*, Pavazza Radoslav*, Matić Tomislav+

* *Faculty of Electrical Engineering, Mechanical Engineering and Naval Architecture, University of Split, Ruđera Boškovića 32, Split, Croatia*
E-mails: {mvukasov, fvlak, rpavazza}@fsb.hr

+ *Faculty of Science, University of Split, Ruđera Boškovića 33, Split, Croatia*
E-mail: {dkustura, tmatic}@pmfst.hr

Keywords: thin-walled curved beam, doubly symmetric H cross-section, closed-form solutions, eccentric distributed line loads, coupled in-plane and out-of-plane static linear analysis

1. Introduction

Coupling effect of displacements and internal forces is practically inevitable feature in the analysis of thin-walled curved beams [1, 2]. These effects are less pronounced when the analyzed cross-section is doubly symmetric, and they are more pronounced when the distributed line load is acting outside of the centroid line. The aim of this study is to analyze the effect of the skewed eccentric uniformly distributed line load on the centroid displacements and the circumferential normal stresses of the thin-walled curved beam with a doubly symmetric H-shaped cross-section. The closed-form solutions of this approach [3, 4], that are based on the assumptions of Vlasov [5] and where the Maclaurin series expansion is used to obtain geometric properties, are compared with the results obtained with the shell finite element model.

2. Analysis parameters

The middle-surface of a thin-walled curved beam with a doubly symmetric H-shaped cross-section is shown in Fig. 1.a, while the cross-section of the analysed beam loaded with an eccentric uniformly distributed skewed line load is shown in Fig. 1.b. The cylindrical coordinate system $O\rho\phi Z$ and the curvilinear coordinate system $Cxyz$ were used in this analysis, where: R is the undeformed centroid line radius with length L, q is the magnitude of the uniformly distributed skewed line load acting on the outer web-flange junction line, α is the angle of the distributed line load with respect to the curvature plane $O\rho\phi$, and b, h, t are the width, height and thickness of the cross-section.

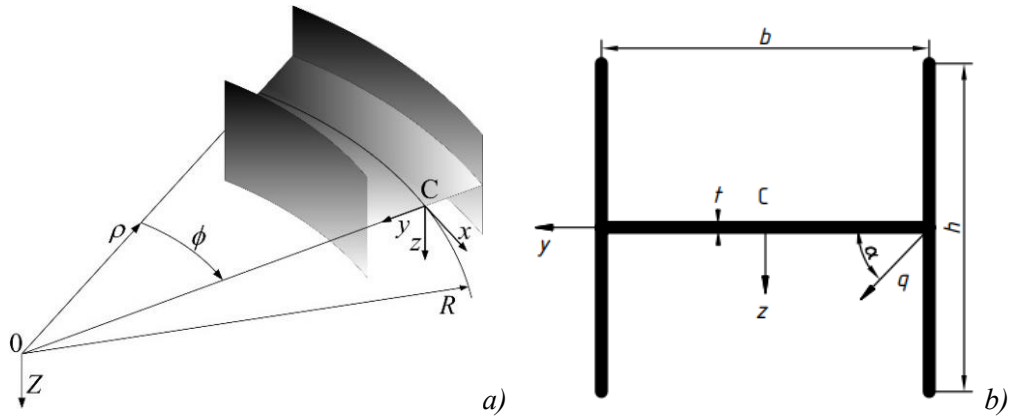


Figure 1. Thin-walled curved beam: a) middle surface [3] and b) cross-section dimensions

For this problem, the governing equations for the out-of-plane [3] and in-plane [4] analyses as well as their closed-form solutions and boundary conditions are omitted in this paper due to its extensiveness. According to the Fig 1.b, the centroid line loads are defined as:

$$q_y = q\frac{R+b/2}{R}\cos\alpha\,, \qquad q_z = q\frac{R+b/2}{R}\sin\alpha\,, \qquad m_{\mathrm{P}} = -q\frac{b}{2}\frac{R+b/2}{R}\sin\alpha, \tag{1}$$

where q_y and q_z are uniformly distributed centroid line loads with respect to the y- and z- axis, and m_{P} is a uniformly distributed torsional load. The analysed beam is clamped at both ends and the symmetry with respect to the beam mid-span is considered in all models. The analysed beam parameters are: $t = 5$ mm, $h/t = 10$, $b/t = 20$, $L/b = 20$, $q = 20$ N/mm, $\alpha = \pi/6$, with Poisson's ratio $\nu = 0.3$ and modulus of elasticity $E = 73$ GPa. The relative errors are used in this study to compare the obtained analytical (A) and numerical (N) results and are defined as follows:

$$\delta u = 100\frac{u_{\mathrm{C}}^{\mathrm{A}} - u_{\mathrm{C}}^{\mathrm{N}}}{u_{\mathrm{C}}^{\mathrm{N}}}, \delta v = 100\frac{v_{\mathrm{C}}^{\mathrm{A}} - v_{\mathrm{C}}^{\mathrm{N}}}{v_{\mathrm{C}}^{\mathrm{N}}}, \delta w = 100\frac{w_{\mathrm{C}}^{\mathrm{A}} - w_{\mathrm{C}}^{\mathrm{N}}}{w_{\mathrm{C}}^{\mathrm{N}}}, \delta\sigma = 100\frac{\sigma_x^{\mathrm{A}} - \sigma_x^{\mathrm{N}}}{\sigma_x^{\mathrm{N}}}, \tag{2}$$

where u_{C}, v_{C} and w_{C} are centroid displacements in the directions of the x-, y- and z- axis and σ_x is the circumferential normal stress. The relative errors of the maximum stress σ_x and the displacements v_{C} and w_{C} at the beam mid-span are listed in Table 1 for four different radii R (ratios R/b). The relative errors of the displacement u_{C} at the beam quarter-span are shown also.

Table 1. Relative errors of the centroid displacements and the circumferential normal stress

R/b	δu (%)	δv (%)	δw (%)	$\delta\sigma$ (%)
8	3.28	1.05	-9.17	6.32
10	3.51	1.11	-5.79	4.04
12.5	3.42	0.91	-3.53	2.71
15	3.12	0.55	-2.3	2.03

The results in Table 1 show a good agreement between the results of the proposed approach and the numerical results, especially for the beams with small curvature ($R/b \geq 10$). The proposed approach slightly overestimates the results of the in-plane displacements u_{C} and v_{C}, as well as the circumferential normal stress σ_x, but underestimates the results of the out-of-plane displacement w_{C}. It should be noted that the maximum normal stress for the cross-section under consideration is appearing at the outer flange and its value is significantly higher than the value of the normal stress at the inner flange.

3. Conclusions

According to the results and the investigations previously carried out by the authors, this approach shows good agreement with the numerical results. The relative errors generally increase with decreasing radius, so the curvature effect should be fully considered in future studies. Different types of cross-sections with a more pronounced coupling effect should also be analysed in future studies.

References

[1] Tong, G., Xu, Q., An exact theory for curved beams with any thin-walled open sections. *Advances in Structural Engineering*, 5(4), 195–209, 2002.

[2] Yang, Y., Kuo, S., Static stability of curved thin-walled beams. *Journal of Engineering Mechanics*, 112(8), 821–841, 1986.

[3] Kustura, D., Vlak, F., Matić, T., Vukasović, M., The out-of-plane static analysis of thin-walled curved H-beams. *Transactions of FAMENA*, 47(3), 61–78, 2023.

[4] Kustura, D., Vlak, F., Matić, T., Vukasović, M., Analysis of Thin-walled Curved Beams with a Doubly Symmetric I- and H- Shaped Cross-sections Loaded with Uniformly Distributed In-plane Line Loads. In: Buljan, B., Miletić, D., eds., *Contemporary Issues in Economy and Technology - CIET 2024 - conference proceedings*, 234-244. University of Split, University Department of Professional Studies, Split, 2024.

[5] Vlasov, V. Z, *Thin-walled elastic beams*. Israel program for scientific translations, 1961.

11th International Congress
of Croatian Society of Mechanics
September 30 – October 3 2025
Vodice, Croatia

Finite Element Modelling of Residual Stress Development and Damage Progression in Welded Components

Marin Vukovojac*, Boris Jalušić+, Tomislav Lesičar*, Ivica Skozrit*, Zdenko Tonković*

*University in Zagreb, Faculty of Mechanical Engineering and Naval Architecture
E-mails: {marin.vukovojac,tomislav.lesicar,ivica.skozrit,zdenko.tonkovic}@fsb.hr

+University North
E-mail: bjalusic@unin.hr

Keywords: welding, post-welding heat treatment, damage

1. Introduction

Fusion welding is still very relevant in modern manufacturing. It enables the production of complex structures across a wide range of engineering applications, including heavy-duty machinery, shipbuilding, energy, and industry. In recent years, researchers are putting a lot of effort into improving the efficiency of existing welding processes and developing new ones. The efficiency of the welding process is measured by the deposition rate of molten metal per unit of time. Welding in multiple passes is usually used for the welding of thick plates. Because of the reheating of the welding beads through multiple passing, residual stresses are decreasing – just as in post-weld heat treatment for reduction of residual stress. For more efficient welding of thick plates, it is necessary to achieve greater heat input, which in return decreases the number of welding passes. Baba et al. [1] developed a novel modified gas metal arc welding process, the buried arc, by increasing the level of welding current and placing the tip of the electrode under the surface level of the molten metal. Buried-arc welding enables welding of 20-mm-thick plates in a single pass. Perić et al. [2] further investigated the buried arc welding by conducting experimental and numerical research.

As known, welding is characterised by localised heating and melting, and subsequent cooling and solidification of molten material. The high thermal gradients and rapid cooling rates associated with fusion welding introduce significant microstructural and residual stress heterogeneities, which can adversely affect the mechanical integrity of the welded joint. Also, high tensile residual stresses favour the formation of cracks and their propagation. A lot of effort has been put into the experimental and numerical investigation of the initiation and propagation of cracks in welded structures subjected to service conditions. The phase-field method (PFM) has recently emerged as a widely adopted framework for simulating damage phenomena in both brittle [3, 4] and ductile [3, 4] materials. Jalušić et al. [5] implemented the PFM to investigate damage and fracture behaviour in welded joints.

To achieve higher levels of mechanical properties and lower levels of tensile residual stresses in the welded joint, post-weld heat treatment (PWHT) is widely applied as a mitigation strategy to alleviate residual stresses and enhance the overall mechanical performance of welded joints. As such, a comprehensive understanding of the interplay between welding-induced damage mechanisms and heat treatment responses is crucial for enhancing the weld design and ensuring long-term structural integrity. Liu et al. [6] experimentally and numerically studied the influence of PWHT and ultrasonic impact treatment (UIT) on residual stresses in GMAW butt-welded 40-mm thick plates made of Q390B low-carbon steel. It was found that UIT mainly affects the residual stresses only within the boundaries of the treated region, while the PWHT had a much larger effect on the surface stress distribution.

2. Numerical modelling of welding and PWHT

Numerical modelling of welding is usually done by thermo-mechanical elastoplastic finite element analysis. This is accomplished by sequential calculation of the temperature field and displacement field, which are obtained during thermal analysis and structural analysis, respectively. Since welding is a transient and highly nonlinear process, obtaining a transient temperature field is essential for the calculation of temperature-dependant mechanical properties. All three modes of heat transfer should be taken into consideration: conduction, convection and radiation. Residual stresses and plastic strains obtained in the structural analysis are very important for further steps in the assessment of damage initiation and propagation.

Numerical modelling of post-weld heat treatment is usually done by thermo-mechanical elastic-plastic-creep finite element analysis. This is also accomplished by simultaneous or sequential calculation of the temperature field and displacement field. Here, temperature field and time are of great importance because the calculation of creep strain is essential for reduction of residual stresses. All three modes of heat transfer should be taken into consideration: conduction, convection and radiation, but sometimes this can be simplified by assigning a boundary condition to materials surface which represents a transient temperature profile.

By obtaining the following fields: displacement, residual stress, plastic strain, and possibly creep strain, it is possible to predict damage initiation and propagation by implementing phase-field method into finite element method. This requires two layers of finite element mesh for calculating displacement field and phase-field, and one finite element of special purpose, which drives the global convergence of the model. Because of that, the staggered phase field algorithm is used.

4. Conclusions

This work is focused on achieving the highest possible levels of mechanical properties of the welded joint, minimal levels of residual stresses and angular distortion of the welded joint and structural integrity of the welded joint. Numerical examples shown in this work give insight into the methods and procedures necessary for obtaining welding induced residual stresses and plastic strains, reduction of residual stress by post-weld heat treatment, and the difference in damage initiation and propagation for welded and nonwelded specimens.

Acknowledgement

This work has been supported and co-funded by the European Union through the European Regional Development Fund, Operational Programme “Competitiveness and Cohesion” 2014 – 2020 of the Republic of Croatia, project “Improvement of high-efficiency welding technology” (ImproWE, KK.01.1.1.07.0076).

References

[1] H. Baba, T. Era, T. Ueyama, M. Tanaka, Single pass full penetration joining for heavy plate steel using high current GMA process, Weld. World. 61, 963–969, 2017.

[2] M. Perić, I. Garašić, Z. Tonković, T. Vuherer, S. Nižetić, and H. Dedić-Jandrek, Numerical prediction and experimental validation of temperature and residual stress distributions in buried-arc welded thick plates, Int. J. Energy Res., 8, 3590–3600, 2019.

[3] K. Seleš, F. Aldakheel, Z. Tonković, J. Sorić, and P. Wriggers, A general phase-field model for fatigue failure in brittle and ductile solids, Comput. Mech., 5, 1431–1452, 2021.

[4] T. Lesičar, T. Polančec, and Z. Tonković, Convergence Check Phase-Field Scheme for Modelling of Brittle and Ductile Fractures, Appl. Sci., 13, 7776, 2023.

[5] B. Jalušić, M. Vukovojac, T. Lesičar, M. Perić, I. Skozrit, and Z. Tonković, Modelling of crack propagation in welded structure using a separated phase-field approach, in 7th International Conference on Smart and Sustainable Technologies (SpliTech), 2022, 6.

[6] C. Liu, J.B. Shen, J.L. Yan, Q.L. Chu, J.X. Wang, Y. Zhao, Experimental Investigations on Welding Stress Distribution in Thick Specimens After Post-Weld Heat Treatment and Ultrasonic Impact Treatment, J. Mater. Eng. Perform., 29, 1820–1829, 2020.

11th International Congress
of Croatian Society of Mechanics
September 30 – October 3 2025
Vodice, Croatia

Recovering isotropic energies with Mullins-type damage using physics-augmented neural networks

Martin Zlatić*, Marko Čanađija*,

*Faculty of Engineering, University of Rijeka
E-mails: martin.zlatic@riteh.uniri.hr, marko.canadija@riteh.uniri.hr

Keywords: hyperelasticity, neural networks, physical constraints

1 Introduction

Modelling of materials using neural networks has existed as an area of research for a long time [1] but has gathered significant interest in the recent decade as computational capabilities have increased. The appearance of open-source machine learning libraries, such as TensorFlow [2], has increased the ease with which machine learning can be adopted and applied to a multitude of problems. Neural network in particular have been applied to modelling hyperelastic materials where the neural network takes the form of the strain energy function that defines the material, as opposed to using the conventional analytical forms such as the Neo-Hookean, Mooney-Rivlin or Ogden model. More specifically, physics-augmented neural networks (PANNs) are specialised NNs which take into consideration physical constraints to improve the general behaviour of the NN [3, 4, 5, 6, 7]. In this paper the results of applying PANNs to hyperelastic behaviour with Mullins-type damage are presented.

2 Training Data and Neural Network Architecture

The material data on which the NN is trained on is generated artificially using the three term Ogden model for which the strain energy ψ_0 is defined using the principal stretches λ_a $(a = 1,2,3)$ as

$$\psi_0(\lambda_1,\lambda_2,\lambda_3) = \sum_{p=1}^{3} \frac{\mu_p}{\alpha_p}\left(\lambda_1^{\alpha_p} + \lambda_2^{\alpha_p} + \lambda_3^{\alpha_p} - 3\right), \tag{1}$$

with the values of the shear moduli μ_p and dimensionless constants α_p are given in Table 1.

Table 1: Ogden model parameter values.

μ [MPa]	0.63	0.0012	-0.01
α [-]	1.3	5	-2

The Mullins effect is considered which is an isotropic damage behaviour where the material first follows a primary loading path and upon unloading a secondary path. When the material is loaded again it first follows the secondary path until the point where it was previously unloaded and then continues following the primary loading path. The isotropic Mullins damage is added using the expressions

$$\psi_{\text{Mullins}} = (1-\zeta(\gamma))\,\psi_0, \quad \zeta(\gamma) = \zeta_\infty\left(1-\exp\left(-\frac{\gamma}{\iota}\right)\right), \quad \gamma = \max_{s\in[0,t]}\psi_0(s), \tag{2}$$

where ψ_{Mullins} is the damaged strain energy, $\zeta(\gamma)$ is the damage parameter, and γ is the maximum historical values of the undamaged strain energy during the analysis. The parameter ζ_∞ is the maximum possible damage and ι is called the saturation parameters. They were taken as $\zeta_\infty = 0.8$ and $\iota = 1$.

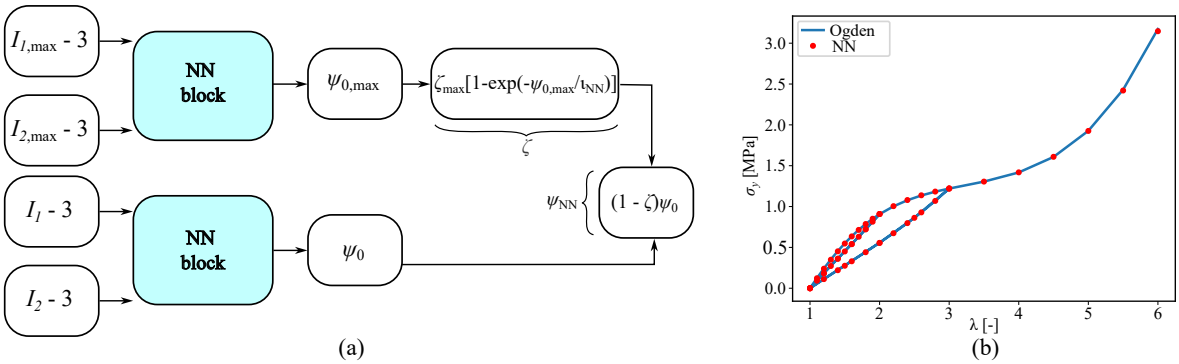


Figure 1. Proposed NN architecture on the left and results of a uniaxial test performed in Abaqus with NN used as a material model.

The proposed NN takes the invariants of the right Cauchy-Green deformation tensor as inputs, denoted as I_1 and I_2, and takes two sets of inputs, one set for the current state of deformation, and another state marking the state where the undamaged strain energy reached its maximum. The architecture is shown in Fig. 1a. Although the NN predicts the strain energy it was trained on the second Piola-Kirchhoff stress using TensorFlows built-in auto-differentiation tool.

The NN was trained on simple tests assuming plane stress conditions, namely on uniaxial, equibiaxial and planar tension. A loading/unloading test was performed for each type of test with three loading and two unloading cycles, with a total of 200 data points per test giving a total number of 600 training samples.

The results are presented for a uniaxial test performed using the finite element software Abaqus in Fig. 1b. The test was performed with 3 loading and 2 unloading cycles.

3 Conclusion

The proposed NN model can successfully capture isotropic Mullins damage and can be applied to a variety of analysis types even though it was trained assuming plane stress conditions. Additionally, even though only three simple tests were performed for generating the training data, the model can be applied to more complex loading scenarios. Physics-augmented neural networks have shown to be me a perfect fit for this application and enable the description of complex materials using an effective generalised approach.

References

[1] Yagawa, G., Okuda, H., Neural networks in computational mechanics. Archives of Computational Methods in Engineering, Vol. 3, No. 4, p. 435-512, 1996.

[2] Abadi, M., et al., TensorFlow: A system for large-scale machine learning. 12th USENIX Symposium on Operating Systems Design and Implementation (OSDI 16), p. 265-283, 2016.

[3] Linka, K., et al., Constitutive artificial neural networks: A fast and general approach to predictive data-driven constitutive modeling by deep learning. Journal of Computational Physics, Vol. 429, 110010, 2021.

[4] Linka, K., Kuhl, E., A new family of Constitutive Artificial Neural Networks towards automated model discovery. Computer Methods in Applied Mechanics and Engineering, Vol. 403, 115731, 2023.

[5] Linden, L., et al., Neural networks meet hyperelasticity: A guide to enforcing physics. Journal of the Mechanics and Physics of Solids, Vol. 179, 105363, 2023.

[6] Kalina, K., et al., Neural network-based multiscale modeling of finite strain magneto-elasticity with relaxed convexity criteria. Computer Methods in Applied Mechanics and Engineering, Vol. 421, 116739, 2024.

[7] Zlatić, M., Čanađija, M., Recovering Mullins damage hyperelastic behaviour with physics augmented neural networks. Journal of the Mechanics and Physics of Solids, Vol. 193, 105839, 2024.

CSM
CROATIAN SOCIETY OF MECHANICS
ZAGREB - OSIJEK - RIJEKA - SL. BROD - SPLIT

Author Index

A

Abdusalamov, R. 113
Adamec, T. 69
Adamović, P. 71
Alfano, G. 59, 165
Al-Ketan, O. 145
Amendola, A. 33
Ammendolea, D. 27
Andrade, D.G. 73

B

Bagavac, P. 75
Ban, D. 77, 79
Banić, D. 81
Barlat, F. 83
Barle, J. 79
Barretta, R. 31, 35, 49, 51
Belšak, A. 85
Blocken, B. 3
Bonada Bo, J. 33
Borovinšek, M. 85
Braut, S. 179
Brčić, M. 127
Brenn, G. 121
Buljac, A. 87
Burlon, A. 15

C

Čanađija, M. 29, 35, 89, 169, 191
Caporale, A. 31
Caracoglia, L. 89
Cardoso, C. 91
Čarija, Z. 167
Carpentieri, G. 33
Ćatipović, I. 175
Čeh, N. 57, 61
Čepon, G. 147
Chapetti, M.D. 93
Charandabi, R.N. 33
Cima, V. 31
Colitta, A. 129
Čolović, T. 137
Cvitanić, V. 73

D

Damjanović, D. 149, 181
Das, B. 35
De Angelis, F. 37
de Castro Motta, J. 33
De Lorenzis, L. 5
Deur, J. 109
Diaco, M. 49
Divić, V. 103, 173
Domel, G. 7
Drvar, N. 111

E

Erice, B. 61

F

Fabbrocino, F. 47
Failla, G. 15, 17
Fantuzzi, N. 53
Feo, L. 39, 43
Fernandes, F. 91, 131
Fraternali, F. 33
Friedman, N. 143, 151, 173

G

Galić, M. 103
Gáspár, C. 95
Glodež, S. 65, 85
Gotovac, H. 97
Grbac, L. 99
Grbčić Erdelj, S. 101
Grebo, A. 75

Greco, F. 27
Großmann, A.F.R. 117
Grozdanić, G. 103
Gubeljak, N. 93, 149, 181
Guo, J. 7

H

Hadžalić, E. 107
Hadžić, N. 175
Hajžman, M. 153
Haramina, K. 109
Havelka, J. 155
Hercigonja, T. 111
Hild, F. 183
Hoić, M. 109
Horvat, A. 111
Hrženjak, P. 135

I

Ibrahimbegović, A. 101, 107
Ignatijev, A. 85
Irrenfried, C. 121
Itskov, M. 113
Ivančević, D. 115, 171
Ivanković, M. 117
Ivić, S. 29

J

Jaguljnjak Lazarević, A. 135
Jalušić, B. 119, 189
Janković, A. 57
Jarak, T. 119
Jelašić, M. 121
Jelenić, G. 99, 101, 123
Jentzsch, M. 117
Jurčević, A. 125
Jurković, D. 59, 165
Jurković, D.T. 127

K

Kareem, A. 87
Klinkel, S. 157
Kodvanj, J. 71
Königsberger, M. 159
Konjatić, P. 141
Korbar, J. 147
Kozak, D. 19, 141, 149, 181
Kozmar, H. 87, 117, 121, 175
Kranjčević, N. 109
Kraus, I. 129
Krstulović-Opara, L. 75
Kustura, D. 187

L

Lambiase, A. 43
Lanc, D. 81
Landi, G. 43
Lavorato, D. 129
Le Barbenchon, L. 61
Lee, J. 61
Lemos, L. 131
Leonetti, L. 27
Lesičar, T. 125, 163, 189
Li, W. 19
Lißner, M. 61
Liu, W.K. 7
Lo Iacono, F. 15
Logo, J. 63
Lonetti, P. 27
Lovisi, G. 39, 43
Lozina, Z. 133
Lozina, Ž. 161
Luciano, R. 31, 47, 51, 53

M

Mališ, T. 135
Manolesos, M. 117
Marinić-Kragić, I. 137
Marotti de Sciarra, F. 51
Matić, T. 187
Matoc, L. 71
Matthies, H.G. 143
Mauko, A. 145

Medvidović, A. 75
Merczel, D.B. 63
Mihaljec, B. 139
Misra, A. 47
Morosavljević, I. 19, 141
Morosavljević, J. 19, 141

N

Navarra, G. 15
Nayeri, C.N. 117
Nečemer, B. 21, 65
Nekić, M. 137
Nikolić, M. 143, 151, 173
Nikolić, Ž. 75
Novak, J. 155
Novak, N. 65, 145

O

Ocepek, D. 147
Olić Miloš, P. 129
Opačak, D. 149
Ouzia, A. 159

P

Park, C. 7
Pascuzzo, A. 27
Pavazza, R. 187
Pavić, D. 151
Penna, R. 39, 43
Perišić, S. 79
Petruska, J. 69
Pichler, B. 159
Placidi, L. 47
Polach, P. 153
Porubsky, M. 155

R

Ratković, J. 115
Ren, Z. 145
Ribarić, D. 123
Rikić, A. 21
Rodrigues, D.M. 73
Romano, G. 49
Ruškan, I. 109
Russillo, A.F. 17
Rychnovsky, P. 155

S

Sabalić, S. 71
Sauren, B. 157
Schmid, S.J. 159
Schröder, J. 9
Sebek, F. 69
Sedlar, D. 133, 161
Šegon, A.M. 163
Serra, G. 131
Servadei, R. 23
Silva, A. 91
Simões da Silva, L. 73
Sindičić, I. 57
Škec, L. 57, 59, 107, 165
Škifić, J. 167
Skoblar, A. 169, 179
Skozrit, I. 189
Škvorc, P. 87
Smaniotto, B. 183
Smojver, I. 171
Smolík, L. 153
Šodan, M. 151, 173
Sokol, I. 175
Sorić, J. 119, 125
Sousa, G. 131
Sousa, R. 91, 131
Stanic, A. 143
Štimac Rončević, G. 169, 179

T

Tantawi, M. 63
Tomac, I. 133, 161
Tomerlin, D. 181
Tomičević, Z. 183
Tonković, Z. 119, 125, 189
Tóth, B. 185

Turkalj, G. 81, 179

U

Ušurić, F. 171

V

Vaccaro, M.S. 31, 51
Vescovini, R. 53
Vesenjak, M. 145
Vlak, F. 187
Vorwerk, M. 9
Vukasović, M. 187
Vukelić, G. 139
Vukovojac, M. 119, 189

Y

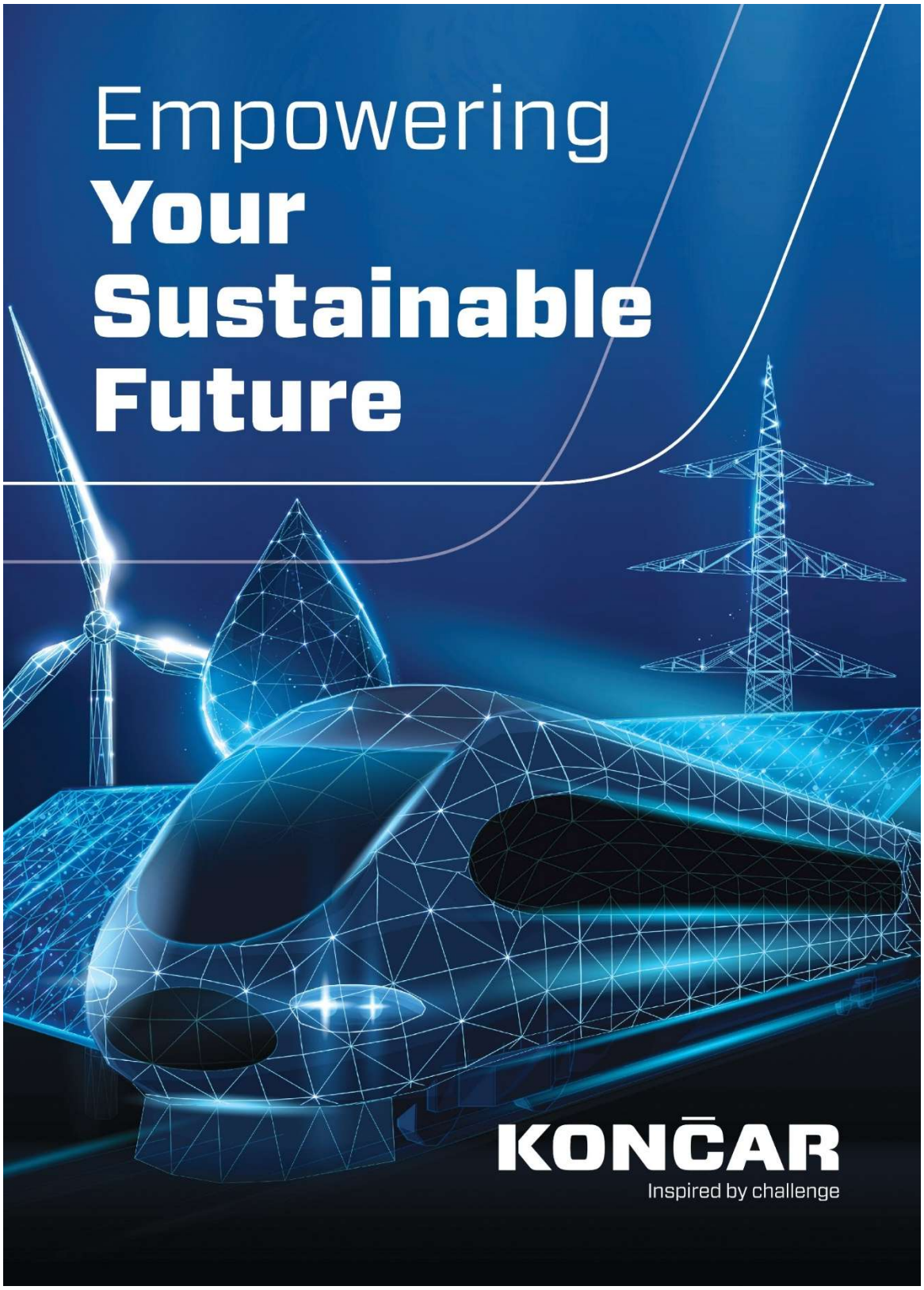
Yan, C.A. 53
Yang, W. 87

Z

Zaplatić, A. 183
Zelenika, M. 97
Zhang, H. 7
Žigulić, R. 169, 179
Zimmermann, V. 117
Zlatić, M. 191
Žnidarič, Ž. 65

CSM
CROATIAN SOCIETY OF MECHANICS
ZAGREB - OSIJEK - RIJEKA - SL. BROD - SPLIT

Sponsors


Empowering
Your
Sustainable
Future
KONČAR
Inspired by challenge

FEM
NVH
MULTIBODY ANALYSIS
MULTIDISCIPLINARY ANALYSIS
RIJEKA,CROATIA
Tel +385 91 542 04 69
Email: goran@east.hr

EAST d.o.o.

SUHA GRADNJA
RIGIPS, KNAUF
SERILIA
d.o.o.
mail: info@serilia.de
www.serilia.de
I OSTALI SISTEMI
mob.: +385 99 7330 214 • tel.: +49 160 9196 0875

Our Services

Drywall Installation – precise and durable wall solutions
Spray Painting & Wall Finishing – fast, flawless, and smooth results
Professional Plastering – perfect surfaces, ready for painting
Firestop Sealing Solutions – certified protection and safety

Quality workmanship, reliable service, and lasting results

Contact

Serilia d.o.o., Brestovice 18b, 51215 Kastav, Croatia
e-mail: info@serilia.de, phone: ++385 99 7330 214

TOPOMATIKA

Precizno industrijsko 3D mjeriteljstvo

ZEISS Certified Metrology Partner

- Optičko 3D skeniranje i mjerenje



- Ispitivanje materijala i mjerenje pomaka i deformacija



- CT mjerenje i unutarnja inspekcija



TOPOMATIKA d.o.o.
Industrijska ulica 3, Novaki, HR-10431 Sveta Nedelja
info@topomatika.hr; Tel: +385 1 3496 010

www.topomatika.hr

Croatian Society of Mechanics is especially grateful to our sponsors:

Silver sponsor

KONČAR

KONČAR, Fallerovo šetalište 22, 10000 Zagreb, Croatia

Bronze sponsors

EAST d.o.o.

EAST d.o.o, Ivana Matrljana 39, 51000 Rijeka, Croatia

SUHA GRADNJA
RIGIPS, KNAUF
SERILIA
D.O.O.
mail: info@serilia.de
www.serilia.de
I OSTALI SISTEMI
mob.: +385 99 7330 214 • tel.: +49 160 9196 0875

SERILIA d.o.o., Brestovice 18 b, 51215 Kastav, Croatia

TOPOMATIKA

TOPOMATIKA d. o. o., Industrijska ulica 3, Novaki, 10431 Sveta Nedelja, Croatia

csm.hr/iccsm2025

iccsm2025@csm.hr

ISSN 2584-7716

Under the Auspices of
Central European Association
for Computational Mechanics

ECCOMAS
Special Interest Conference

CSM
CROATIAN SOCIETY OF MECHANICS
ZAGREB – OSIJEK – RIJEKA – SL. BROD – SPLIT